UNIVERSITY OF CALIFORNIA
SANTA CRUZ

SYNTHESIS OF CATIONIC EXTENDED FRAMEWORKS FOR ANION-BASED APPLICATIONS

A dissertation submitted in partial satisfaction
of the requirements for the degree of

DOCTOR OF PHILOSOPHY

in

CHEMISTRY

by

Honghan Fei

September 2012

The Dissertation of Honghan Fei
is approved:

_____
Professor Scott R. J. Oliver

_____
Professor Jin Z. Zhang

_____
Professor Yat Li

_____
Tyrus Miller
Vice Provost and Dean of Graduate Studies

Table of Contents

Chapter 10. Polymer Templated Nanospider TiO_2 Thin Films for Efficient Photoelectrochemical Water Splitting

Chapter 11. Solid-State Dye-Sensitized Solar Cells from Polymer Templated TiO_2 Bilayer Thin Films

List of Figures

List of Tables

Abstract

Synthesis of Cationic Extended Frameworks for Anion-Based Applications

by

Honghan Fei

Many of the metal pollutants listed as priorities by the EPA (U.S. Environmental Protection Agency) occur in water as their oxo-hydroxo anionic forms (e.g. perchlorate, chromate, selenite, etc.). Radioactive technetium (Tc-99) in the form of soluble pertechnetate (TcO_4^-) is highly problematic in low-activity waste (LAW) to separate the nuclear waste into primary solids. Its easy leakage from glass after vitrification does not meet long-term storage performance assessment requirements. LAW also contains other non-radioactive inorganic and organic species [e.g. carbonate (CO_3^{2-}), nitrate (NO_3^-), etc.] that may interfere with immobilizing radioactive species in solid-state ion-exchange materials. Chromate is another problematic anion for vitrification because it weakens the integrity of the waste glass by forming spinels; such particles can also obstruct the glass flow within the melter during vitrification.

There is an extensive class of purely inorganic extended materials and hybrid inorganic-organic extended frameworks. However, the majority of this group of materials occurs to bear a neutral or negative charge on their extended framework (e.g. zeolites). Layered double hydroxides (LDHs) are a class of well-studied

isostructural cationic materials, and have been extensively studied in anion exchange. This group of materials, however, has limited capacity as evidenced by adsorption titration and isotherms. They also display low selectivity towards anion pollutants, especially in the presence of carbonate.

Exploration of transition metals and lower *p* block metals lead to synthesis of cationic inorganic materials and cationic metal-organic frameworks (MOFs). Ag(I) based cationic extended frameworks with α,ω-alkanedisulfonate as anionic SDAs has successfully been synthesized with the formula as following, $Ag_2(4,4'\text{-bipy})_2(O_3SCH_2CH_2SO_3)\cdot 4H_2O$ (SLUG-21). The unbound ethanedisulfonate anions display effective anion pollutant trapping on permanganate (MnO_4^-) and perrhenate (ReO_4^-) with high adsorption capacity and selectivity. These two anions are chosen for anion exchange study owing to the same group as pertechnetate (TcO_4^-). SLUG-21 displayed its adsorption capacity in record levels over all previous materials with 292 mg/g and 602 mg/g, respectively, for permanganate and perrhenate. These values are over five times compared to the conventional layered double hydroxides (LDHs) under the same condition. We further investigated the mechanism of these exceptional high adsorption capacities in view of crystallography. In addition to exceptional high adsorption capacity, SLUG-21 displayed excellent selectivity towards anionic pollutants over non-toxic anions. One hundred fold excess of nitrate or carbonate do not interfere with SLUG-21 trapping permanganate and perrhenate. The favorable trend of anions to be intercalated in SLUG-21 is as following: $MnO_4^- > ReO_4^- > ClO_4^- > CrO_4^{2-} > NO_3^- > CO_3^{2-}$, with the toxic pollutants topping the list.

We are also successful in the synthesis of cationic inorganic layered materials, which displayed higher thermal and chemical stability than cationic MOFs. Our approach focuses on the use of anionic SDAs and excluding any potential cationic SDAs. The first copper-based cationic layered extended framework $Cu_4(OH)_6(O_3SCH_2CH_2SO_3)\cdot 2H_2O$ (SLUG-26) was hydrothermally synthesized. Inorganic connectivity (Cu-O-Cu) construct a cationic 2-D extended layer $[Cu_4(OH)_6]^{2+}$ with ethanedisulfonate weakly bounding between adjacent layers. This material display rich intercalation chemistry with different α,ω-alkanedicarboxylate anions. The *d*-spacing between cationic cuprate layer can be tuned from 7.6 Å with intercalating malonate ($^{-}O_2CCH_2CO_2^{-}$) to 11.1 Å with glutarate ($^{-}O_2C(CH_2)_3CO_2^{-}$) separating layers. Besides organic anions, SLUG-26 also showed exchange capabilities upon inorganic anion pollutants, exhibiting five times higher adsorption capacity for permanganate than LDHs.

The complete exchange of the interlamellar anions of a 2-D cationic inorganic material was demonstrated. The α,ω-alkanedisulfonates were exchanged for α,ω-alkanedicarboxylates, leading to two new cationic materials with the same $[Pb_2F_2]^{2+}$ layered architecture. Both were solved by single crystal X-ray diffraction and the transformation also followed by *in-situ* optical microscopy and *ex-situ* powder X-ray diffraction. This report represents a rare example of metal-organic framework displaying highly efficient and complete replacement of its anionic organic linker while retaining the original extended inorganic layer. It also opens up further

possibilities for introducing other anions or abatement of problematic anions such as pharmaceuticals and their metabolites.

A rare example of an extended nickel oxide open framework with succinate capping the channels was synthesized. A honeycomb-like layer of 14-membered rings centered in the (-111) plane are connected by vertex-sharing NiO_6 octahedra and water resides in the channels. The structure is the second example of an extended hybrid containing 3-D Ni-O-Ni connectivity and was structurally characterized by single-crystal and powder X-ray diffraction. The material displays excellent chemical stability in aqueous solution from pH ~ 1 to 13 and thermal stability to ~ 375 °C as evidenced by thermogravimetic analysis coupled mass spectroscopy. The Ni^{2+} ions order ferromagnetically order below T_c = 5.1 K, and anisotropic exchange interactions lead to a field-induced metamagnetic transition and spin-glass-like dependence on cooling conditions in magnetic field.

$[Sb_6O_7][(SO_4)_2]$ (SLUG-34) consists of a very unusual 1-D antimony oxide chain four Sb atoms wide, with unprotonated sulfate between the chains. The material can be synthesized in high yield and pure phase and was characterized by both powder and single-crystal X-ray diffraction. The entirely inorganic nature of SLUG-34 along with infinite 1-D Sb-O-Sb connectivity results in high thermal stability and chemical resistance. SLUG-34 is thermally stable to *ca.* 500 °C as evidenced by *in-situ* variable temperature thermodiffraction as well as thermogravimetric analysis. Unlike the basic nature of layered double hydroxides (which are the only well-studied class of cationic inorganic materials), SLUG-34 is

chemically stable in aqueous acidic conditions. This opens up the possibility for synthesis of other non-LDH type cationic inorganic materials with potential host-guest applications based on their extraframework anions.

A facile and inexpensive approach to fabricate "nanospider" TiO_2 thin films was demonstrated with not only an amazing morphology but highly efficient water splitting to produce hydrogen. Our method employs benzene-swollen poly(ethylene glycol) as a sacrificial organic polymer to template the semiconductor thin film. The synthesized TiO_2 thin films are highly crystalline with optimized particle and channel size to enhance the liquid-semiconductor junction interaction. This enhanced contact area leads to more than twice the water splitting performance than conventional P25 thin films. In addition, the nanospider thin films also outperform P25 films in the photodegradation of toxic organics.

An inexpensive method using solvent-swollen poly(methyl methacrylate) as a sacrificial template for mesoporous titanium oxide thin films was investigated with tunable meso/nano morphology. The conversion efficiency reaches 4.2 % despite using a solid state electrolyte, which circumvents the longevity issues of liquid electrolytes. The cells show a large short-circuit photocurrent density of 7.98 mA, open-circuit voltage of 0.78 V and maximum conversion efficiency of 4.2 % under air-mass 1.5 global illumination. At higher titania precursor ratios, nanodisk particles are formed, increasing light scattering and doubling the efficiency over our previous reports. The tunability of the semiconductor morphology and all solid-state nature of the cells makes the method a viable alternative to existing solar cell technology.

Dedication

This thesis is dedicated to my wife

Han Zhang for all of your love and support.

It is also dedicated to my parents,

Weimei Li and Yuexing Fei,

who have been supported me all the way

since the beginning of my studies.

Acknowledgements

I would like to express my deepest appreciation to my thesis advisor, Professor Scott R. J. Oliver. His convincingly and continually encouraging guidance, encouragement and support make graduate research of chemistry fun for me. Without his persistent help, this dissertation would not have been possible.

I would like to acknowledge Professor Pradip K. Mascharak and the rest of my committee members, Professor Stacey I. Zones, Professor Jin Z. Zhang, and Professor Yat Li for their insightful discussions, questions and advices.

In addition, my sincere thanks to my labmates in Scott Oliver research group: Dr. Xiaojuan Fan, Dr. Claudia Swanson, Dr. David Rogow, Marc Bresler, Yashar Abdollahian, Jessica St. Johns, Jeremy Robins, Latisha Paw U, Catherine Pham, Yucheng Yang, Cari Han, Kevin Sergo, Howard Han for numerous days we work together during the last five years. I would also like to thank Professor Arthur Ramirez, Dr. Andrew LaForge, Dr. Allen Oliver, Dr. Wei Chen, Dr. Debraj Ghosh, Dr. Guangmei Zhai, Gongming Wang, Xiongwu Kang, Yichuan Ling for their contribution in this thesis.

Financial support was provided by NSF Grant DMR-0506279, CHE-0521569, DMR-1126845, a Chancellor's Dissertation Year Fellowship from UC Santa Cruz Graduate Division, and two Ludo Frevel Crystallography Scholarships by the International Center for Diffraction Data (ICDD).

Chapter 1

Cationic Extended Materials for Anion-Based Applications

Abstract

The majority of inorganic extended materials or hybrid inorganic-organic materials possess an overall neutral or anionic charge (e.g. zeolites and clays), despite their enormous applications in molecular separation, catalysis and water purification. However, many EPA priority pollutants are in the oxo-hydroxo anionic form. The trapping, immobilization and recognition of both inorganic and organic anionic species (e.g. DNA polyanions, pharmaceutical pollutants and their metabolites) are important in both biological and environmental systems. Layered double hydroxides are a rare group of materials bearing a positive charge on the extended layered host. This chapter describes current examples of inorganic or metal-organic materials that adopt a positive charge on their frameworks. These materials display anion-based host-guest interactions, which are not possible with as-synthesized neutral or anionic materials. Their inorganic nature allows advantages of higher thermal and chemical stability over the conventional ion-exchange resins.

1.1 Layered Double Hydroxides

1.1.1 Synthesis and Structures

There is an extensive class of hybrid inorganic-organic materials and purely inorganic materials which are based on extended arrays such as one-dimensional (1-D) chains, two-dimensional (2-D) sheets, and three-dimensional (3-D) networks.[1] The majority of this group of materials bears a neutral or negative charge on their extended framework. All zeolites, one of the most intriguing sub-class of these materials, possess a neutral or negative charge and employed in catalysis, separations, water purification, etc.[2-5] However, investigations into rational synthesis of cationic inorganic extended materials and cationic hybrid inorganic-organic materials are

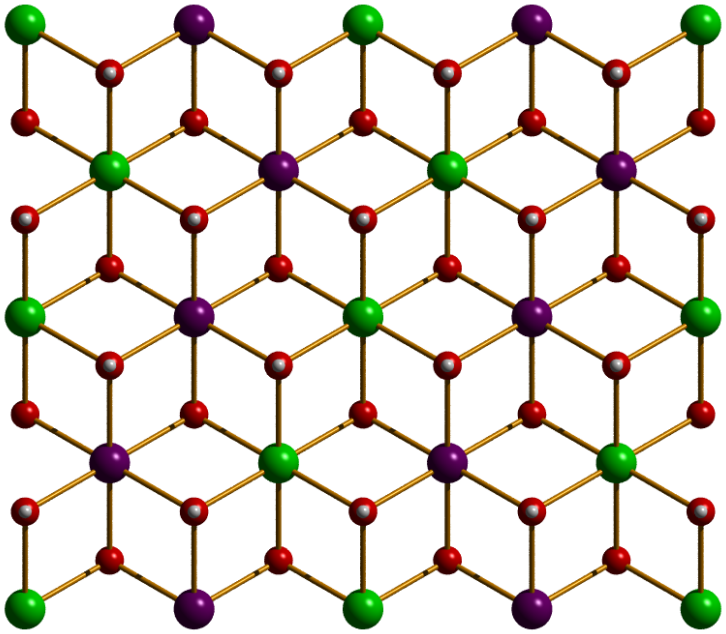

Figure 1.1 Crystallographic view of one cationic layer of layered double hydroxides (trivalent metal: green, divalent metal: violet, oxygen: red, hydrogen: white).

limited.[6]

Layered double hydroxides (LDHs) are a widely studied and occurring group of cationic mineral with general formula $[M^{2+}_{1-x}M^{3+}_{x}(OH)_2][A^{n-}_{x/n} \cdot mH_2O]$, where M^{2+} and M^{3+} are a range of metals (e.g. Mg^{2+} and Al^{3+}), x is the ratio of $M^{3+}/(M^{2+}+M^{3+})$, and A^{n-} are n-valent interlamellar anions (e.g. CO_3^{2-}, HCO_3^-, NO_3^-).[7-9] The composition of LDHs can be diverse as displayed by their formula

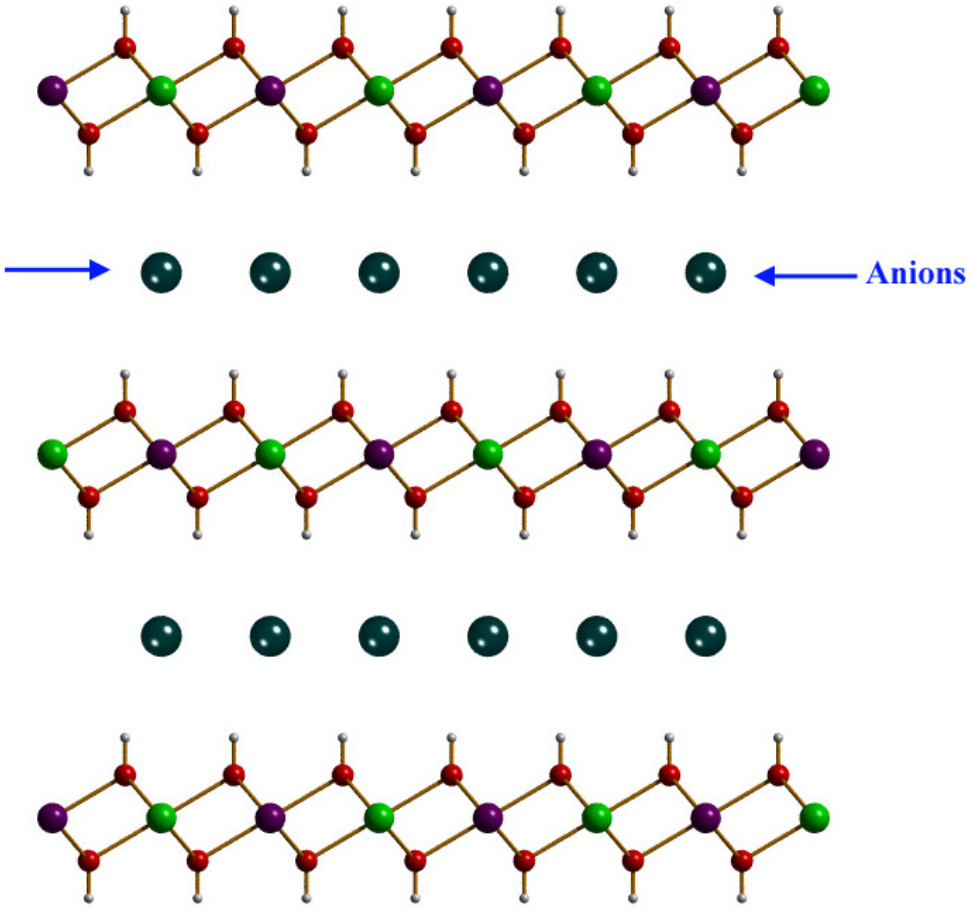

Figure 1.2 Crystallographic view of layered double hydroxides presenting the intercalation of counter anions between cationic layers (trivalent metal: green, divalent metal: violet, oxygen: red, hydrogen: white, cyan: intercalated anions).

with various metals, metal ratio, and counter anions. However, they are a class of isostructural materials, shown in Figure 1.1 and 1.2. Each cationic layer derives from brucite $Mg(OH)_2$, with edge-sharing $M(OH)_6$ forming an infinite layer (Figure 1.1). Unlike brucite [$Mg(OH)_2$] forming a neutral layer with all the metal centers divalent, LDHs contain partial substitution of divalent metal centers (M^{2+}) to trivalent counterparts (M^{3+}) in the same lattice to define a positively charged inorganic extended sheet. Charge-balancing counter anions are intercalated between adjacent cationic layers, and water molecules are also co-intercalated to form hydrogen bonds to hydroxyls in the host layers or intercalated counter anions (Figure 1.2).

LDHs occur naturally as hydrotalcites, which can also been synthesized by the co-precipitation method. Typically, two metal salts aqueous solutions are combined under alkaline condition with addition of sodium hydroxide to maintain a constant pH.[10-12] Hydrothermal reactions as well as hydrolysis of urea are also employed to control the crystallinity and particle morphology of the synthetic product.[13,14] Powder X-ray diffraction (PXRD) is the most common characterization method to determine the *d*-spacing of LDHs, which is normally the distance between adjacent metal hydroxide layers. Thermogravimetric analysis (TGA) and Fourier transform infrared spectroscopy (FTIR) are used to study the intercalated anionic species between cationic inorganic layers. This group of cationic minerals exhibits a wide range of applications, including ion exchange, drug delivery, catalysis, interlayer polymerization, etc.[15-19]

1.1.2 LDH Applications in Anion Exchange

Many inorganic pollutants in the form of metal oxo-hydroxo anions [e.g. arsenite (AsO_3^{3-}), arsenate (AsO_4^{3-}), chromate (CrO_4^{2-}), selenite (SeO_3^{2-}), selenate (SeO_4^{2-}), borate (BO_3^{3-}) and perchlorate (ClO_4^-)] are listed as EPA (U.S. Environmental Protection Agency) priority pollutants.[20] EPA set a national limit for perchlorate in drinking water recently and will set for chromate in the near future,[21] while the prior is known to be a widespread anion occurring from spent rocket fuel, fireworks and other sources.[22] Pertechnetate (TcO_4^-) is also a problematic monomeric oxo-anion in radioactive waste vitrification.[23-25] Its trapping in the solid-state is highly necessary before the vitrification of low-activity waste since leakage out of glass occurs due to its high mobility in aqueous solution.[24] Besides metal oxo-anions, some monoatomic anions [e.g. fluoride (F^-), chloride (Cl^-), bromide (Br^-), iodide (I^-)] in aqueous solution are also inorganic contaminants that need to be ion exchanged. Meanwhile, many organic anionic pollutants at neutral pH have gained increasing attention due to pharmaceuticals and their metabolites [e.g. salicylate (metabolite of Aspirin), carbamazepine, clofibrate, ibuprofen, etc.].[26] Indeed, the current treatment process of chlorination often leads to even more toxic compounds such as monohalogenated and/or oxidized by-products.[27,28] The need for materials which can trap anionic pollutants in both inorganic and organic form will have widespread applications.

LDHs are considered plausible alternatives to ion-exchange resins, not only due to their reversible anion exchange for many inorganic and organic anions but

their facile synthesis, cost effectiveness, and being the most widely studied class of materials in anion exchange. Solid solution LDHs with formula represented as $[M^{2+}_{1-x}M^{3+}_{x}(OH)_2][A^{n-}_{x/n} \cdot mH_2O]$ have a large range of anion guest species that can be exchanged into the interlamellar regions since a wide range of layer charges can be derived from different x values ($0.1 \leq x \leq 0.5$). Figure 1.3 displays a crystallographic structure view of LDHs after partial anion exchange with tartrate, which is used as the example for intercalated organic linker.[29] The variation of x and its consequent layer charge also induce the anion selectivity and capacity towards anions. LDHs with the composition of $[Mg^{2+}_{1-x}Al^{3+}_{x}(OH)_2][(NO_3^-)_x]$ have a higher tendency for chromate trapping with Al content of 33 % than that of 25 %.[30] The latter's adsorption capacity for chromate is only 58 mol. % as Al content 33% $[Mg^{2+}_{1-x}Al^{3+}_{x}(OH)_2][NO_3^-{}_x]$, since

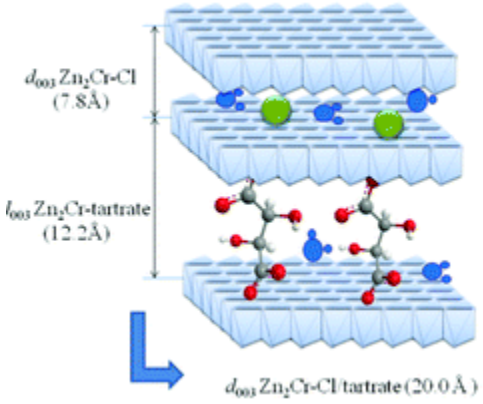

Figure 1.3 Schematic representation of the structure of Zn_2Cr–Cl/tartrate second-stage intermediate with alternate interlayers occupied by tartrate and Cl^- anions.[29]

its occupying higher NO_3^- symmetry limits the insertion of other anions into the framework. PXRD is one of the most common methods to monitor the anion exchange process with the appearance of a series of new higher order (00*l*) diffractions while retaining its original *d*-spacing peaks. Figure 1.4 shows anion exchange between Zn/Al-CO_3^{2-} LDH (Zn^{2+}/Al^{3+} based LDH with CO_3^{2-} as intercalated counter anion) and *p*-hydroxybenzoic (PHBA) anion.[31] Besides the appearance of the original *d*-spacing of 7.6 Å (2θ=11.6°), a new basal *d*-spacing of 15.2 Å (2θ=5.8°) is observed after anion exchange, corresponding to partially inserted PHBA LDHs.

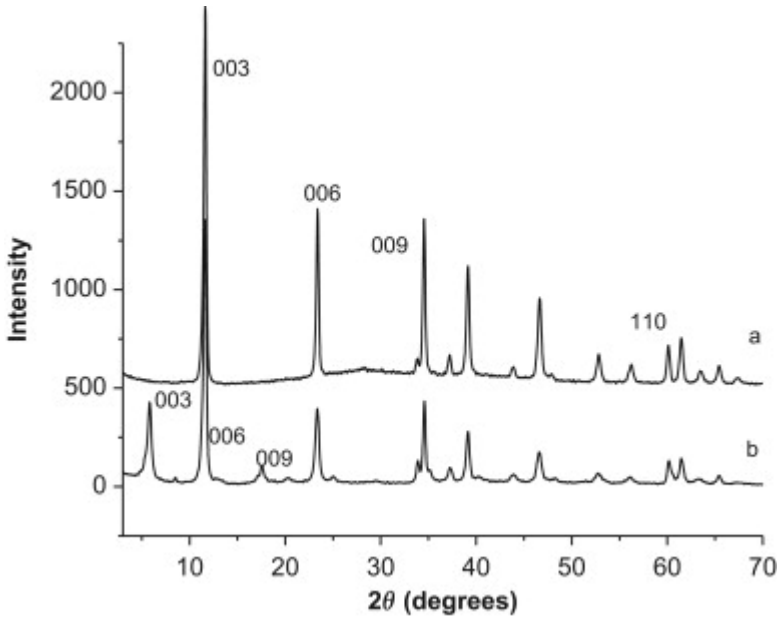

Figure 1.4 PXRD patterns of (a) original Zn/Al-LDH with CO_3^- as counter anion, and (b) Zn/Al-LDH after anion exchange with PHBA.[31]

Though the LDHs' equilibrium-driven anion exchange was once considered an ideal anion pollutant trapping process, several factors limits its wide industrial application. First, their high selectivity towards carbonate and/or bicarbonate as intercalated anions limits their adsorption capacities and thus potential application in anion pollutant trapping. There are many published reports on the effect of competitive anions on targeted anion pollutant adsorption by LDHs, and their anion selectivity and/or capacity.[32-37] The anion affinity towards the cationic layers in LDHs obeys the following order:[38]

$$CO_3^{2-} > SO_4^{2-} > OH^- > F^- > Cl^- > Br^- > NO_3^- > I^-$$

Selectivity has been a long-term problem for LDHs with the presence of both anion pollutants and carbonate in solution, and the latter is always present in water from atmospheric CO_2. Anion adsorption capacity, another equally important property of the anion exchanger selectivity, is also greatly influenced by this competitive anion interference (Table 1.1).[39] Indeed, LDHs, especially the commercialized carbonate or hydrocarbonate form, often require calcination pretreatment before anion exchange.

Table 1.1 Adsorption Capacity of Various Oxyanions with LDHs.[39]

Anion	Types of LDHs	Ads. Capacity (mg/g)
Arsenite	Uncalcined chloride-LDHs	0.086
Arsenite	Calcined Mg-Fe LDHs	87.5
Arsenate	Uncalcined Mg-Al LDHs	32.6
Arsenate	Calcined Mg-Al LDHs	202
Chromate	Uncalcined Mg-Al LDHs	5-40
Chromate	Calcined Mg-Al LDHs	120
Phosphate	Uncalcined Mg-Al LDHs	28.8
Phosphate	Calcined Mg-Al LDHs	81.6
Borate	Uncalcined Mg-Al LDHs	14

Calcination partially removes the intercalated anions in LDHs and therefore the possibility to enhance its adsorption capacity, as shown in Table 1.1. In this equilibrium-driven manner, it is never possible to remove all anions and/or introduce complete selectivity, limiting the adsorption capacity for oxyanions in the range of 15~120 mg/g. Moreover, LDHs require calcination pretreatment up to 450 °C within 24 hours before anion exchange due to the memory effect, where the layers rehydrate and reintercalate unwanted anions into the interlayer.[40] They also display difficulty in recovery and reusability after ion exchange, owing to basic nature of cationic hydroxide layers limiting their chemical stability in aqueous acidic condition, thus in applications in corrosive wastewater.[39] Indeed, most of LDHs remain only partial heterogeneity in neutral acidic solution, and require *ca.* 30 min centrifuge to separate them from aqueous media.

1.2 Cationic Inorganic Frameworks

1.2.1 Synthesis Strategies

Most inorganic extended structures, such as zeolites (nanoprous silicates/aluminosilicates), are either neutral or anionic in charge. Conventional neutral or cationic structural directing agents (SDAs), such as organic ammoniums or alkali metals, reside in the pore and/or interlamellar regions of the host, templating the formation of a particular inorganic extended framework. Relatively fewer attempts were made towards the synthesis of inorganic extended frameworks bearing a positive charge using anionic molecule templates. Cationic inorganic frameworks

can basically be synthesized by employing anionic templates coupled with suitable choice of metals to construct 2-D or 3-D extended architecture bearing a positive charge. During the general synthetic procedure, metal salts react with anionic species under modified pH at solvothermal/hydrothermal conditions or by room temperature homogeneous precipitation, and the latter is also one of the conventional approaches in LDHs synthesis.[41-43]

Anionic templates based on coordination strength in ascending order are classified as following proposed by Brisse and coworkers, with slight modification:[44] (i) mainly non-coordinating anions (BF_4^-, PF_6^-, SbF_6^-, Cl^-, etc.); (ii) weakly coordinating anions (ClO_4^- and etc.); (iii) fairly coordinating anions (NO_3^-, SO_4^{2-}, and etc.); (iv) moderately coordinating anions (triflate $CF_3SO_3^-$, ethanesulfonate $CH_2SO_3^-$, 1,2-ethanedisulfonate $^-O_3S\text{-}C_2H_4\text{-}SO_3^-$, 2,6-naphthalenedisulfonate $^-O_3S\text{-}C_{10}H_6\text{-}SO_3^-$, and other organosulfonate anions); (v) strongly coordinating carboxylate-containing anions (succinate $^-O_2C\text{-}C_2H_4\text{-}CO_2^-$, glutarate $^-O_2C\text{-}C_3H_6\text{-}CO_2^-$, sebacate $^-O_2C\text{-}C_8H_{16}\text{-}CO_2^-$, 1,4-benzenedicarboxylate $^-O_2C\text{-}C_6H_4\text{-}CO_2^-$, and other organocarboxylate anions).

Custelcean and co-workers classified the role of anions into four groups from a structural point of view.[45] In extended frameworks, interaction between anionic guest molecules and cationic host is also strongly related to coordination strength of metal and/or metal clusters. Moreover, they may also play decisive roles in determining the overall charge of consequent structures (Table 1.2). (i) Anions function as mere charge balancing counter ion, named as *spectator*. This situation is

an ideal model for cationic inorganic frameworks with no structural interaction between cationic hosts and intercalated anionic guests. These species, often crystallographically disordered in pore channels, are non-coordinating anions as classified above. One typical example is a cationic (4,4)-connected net topology [e.g. $Cu(H_2O)_2$(4,4'-bipy)] with BF_4^- or PF_6^- as charge-balancing anions residing in channels of open grid.[46] Custelcean *et al.* discovered a cationic metal-organic framework $[CuCl(BNA)_2]\cdot Cl(H_2O)_4$ (BNA= binicotinic acid), with Cl^- as counter anion.[47] (ii) Anions play a relatively important role in structure formation to indirectly construct the framework. They are called *structure-directing*, which is the most common role of organoammonium cations in the pore of zeolites. This group of anions, derived from weakly coordinating or fairly coordinating anions, participate in constructing majority of the cationic inorganic materials. Layered rare earth hydroxides are a widely studied group of materials among them.[48] Our group reported synthesis of cationic layered lead fluoride materials with perchlorate as structure-directing agents to non-covalently template the structure.[49] (iii) Anions directly participate in formation of cationic structures, though not the components of the framework. This group of anions is moderately-coordinating anions, often result in building up cationic hybrid inorganic-organic frameworks. Examples of materials with this behavior of anion incorporation are commonly include organosulfonate, e.g. RPF-14 $[Y(1,5\text{-nds})(OH)(H_2O)]$.[50] (iv) Anions are a central component of the structure. This group of *building unit* anions forms covalent bonds with metal-centered building blocks, consequently directing structures of coordination polymers

and/or metal-organic frameworks (MOFs). The most common group of these materials is 3-D highly porous MOFs (e.g. MOF-5,[51] MIL-101[52]).

Synthesis of cationic inorganic frameworks employs anionic species with coordination strength classified from group (i) to group (iv) to template cationic inorganic extended frameworks with suitable a source of metal. In most cases, group (v) strongly coordinating anions preferably form traditional neutral extended frameworks.

1.2.2 Structural Diversity

Most efforts in development of cationic inorganic frameworks to date lead to low dimensionality of inorganic connectivity (0-D, 1-D, 2-D), while recent investigations also discover a few cationic extended structures containing 3-D inorganic counterparts. Based on the length of this section, structural features on

Table 1.2 Relationship between Structure Charge and Coordination Strength and Role of Anion Templates

Anion Example	Coordi-nation	Anion Role	Structure Charge	Examples
BF_4^-, PF_6^-, Cl^-, Br^-	non coordinating	Spectator	Cationic	$Cu(4,4'\text{-bipy})(PF_6)_2$[46] $[CuCl(BNA)_2]\cdot Cl$[47]
ClO_4^-	weakly coordinating	Structure-Directing	Cationic	$[Pb_9F_{16}][(ClO_4)_2]$[49]
NO_3^-, SO_4^{2-}	fairly coordinating	Structure-Directing	Cationic	LRHs[48]
Organosulfonate	moderately coordinating	Building Unit	Cationic/ Neutral	LRHs,[48] RPF-12~14[50]
Organocarboxylate	strongly coordinating	Building Unit	Neutral	MOF-5,[51] MIL-101[52]

cationic inorganic layers (2-D) and cationic 3-D inorganic extended structures are discussed in detail.

1.2.2 (a) 2-D Structures with *f*-Block Metal

Cationic layered inorganic frameworks based on rare earth metals are the most developed group of materials in this class, representing the majority of cationic layered frameworks reported to date. Layers of $[M_2(OH)_5]^+$ are successfully synthesized by high charge of *f*-block metals cations (e.g. M^{3+}) along with their large

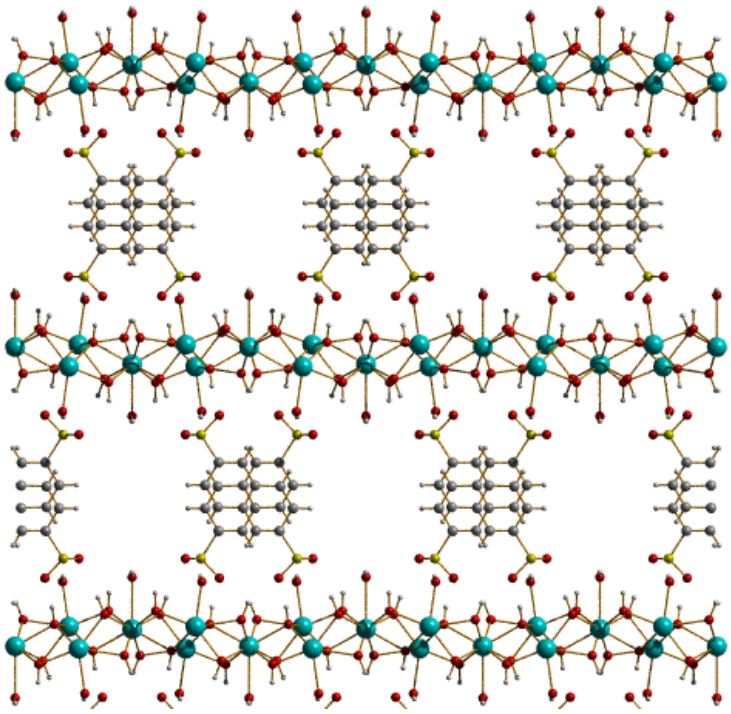

Figure 1.5 Crystallographic view of $[Y_4(OH)_{10}][O_3S\text{-}C_{10}H_6\text{-}SO_3]$ along the *c*-axis (Y-turquoise, O-red, S-yellow, C-gray, H-light gray).

number and flexible coordination behavior, where M is rare earth metals. The first structurally characterized examples of cationic inorganic framework based on *f*-block metal were reported in 2006 by Monge and co-workers.[53] They utilized organosulfonates [2,6-naphelenedisulfonate (NDS^{2-}) , 2,6-anthraquinonedisulfonate (ADS^{2-})] to template pillared isostructural cationic layered frameworks based on trivalent rare earth metals, including Yb^{3+}, Y^{3+}, Dy^{3+}, and Ho^{3+}. Though only two structures based on Yb^{3+} and Y^{3+} are structurally characterized by single-crystal X-ray diffraction (Figure 1.5), other isostructural examples are supported by powder diffraction patterns. This family of layered rare earth hydroxides consists of cationic inorganic layers $[M_4(OH)_{10}]^{2+}$ (M= Yb^{3+}, Y^{3+}, Dy^{3+}, and Ho^{3+}) with NDS^{2-} or ADS^{2-} residing in the interlamellar regions. Eight and nine-coordinate trivalent metal centers bridged by μ_3-hydroxl groups form the extended layer with non-coordinating organosulfonate anions compensating the overall charge of the framework. However, slight modification of hydrothermal synthetic conditions with different metal/template/solvent ratio and/or pH modifier led to another phase RPF-5 $[M_2(OH)_2][(ADS)_2]$, which is 0-D metal clusters $[M_2(OH)_2]^{2+}$ covalently binding with organosulfonates and lack of a 2-D pillared feature.[54]

Besides moderately coordinating organosulfonates as classified in Table 1.2, non coordinating, weakly coordinating and fairly coordinating inorganic anions were also discovered to template cationic rare earth frameworks. Fogg and co-workers discovered a new series of layered rare earth hydroxide materials employing a similar *f*-block group of trivalent metals (Y^{3+}, Yb^{3+}, Dy^{3+} and Er^{3+}) templated by non-coordinating halide anions (Figure 1.6).[55] The cationic $[M_2(OH)_5]^+$ layers have two crystallographic independent metal centers with eight or nine coordination, respectively. Chloride anions are non-coordinating anions electrostatically charge-

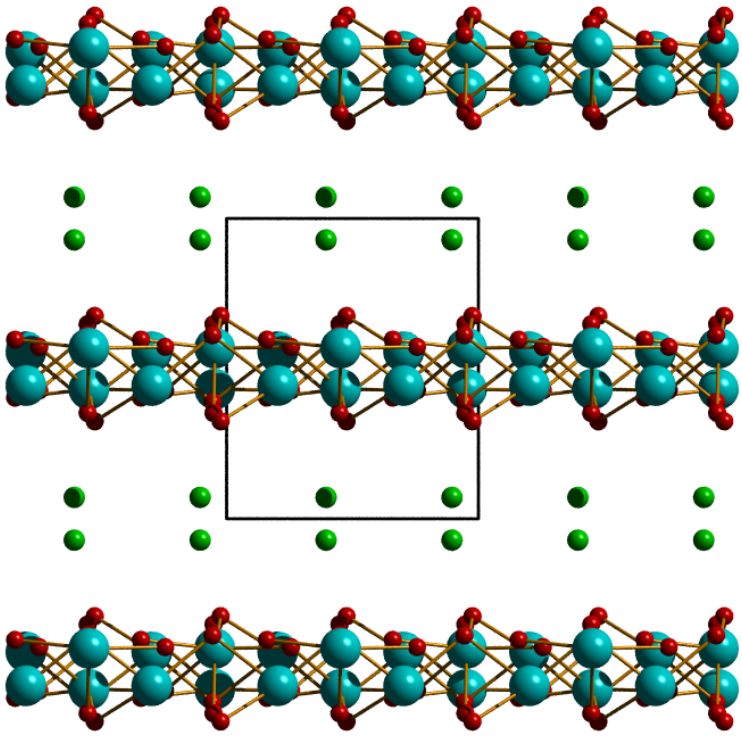

Figure 1.6 Crystallographic view of $[Y_2(OH)_5]Cl$ along the *b*-axis (Y-turquoise, O-red, Cl-green). Solvent water and hydrogen atoms are omitted for clarity.

balancing the positively charged inorganic sheets. Indeed, cationic inorganic sheet $[M_2(OH)_5]^+$ occupy similar inorganic connectivity to the rare earth hydroxide layer of earlier reported organosulfonate templated $[M_4(OH)_{10}][O_3S\text{-}C_{10}H_6\text{-}SO_3]$. The dimension along the plane of cationic layer of $[Y_2(OH)_5]Cl$ is 12.5108(10) Å × 7.0438(10) Å, while that of $[Y_4(OH)_{10}][O_3S\text{-}C_{10}H_6\text{-}SO_3]$ is 12.6388(10) Å ×

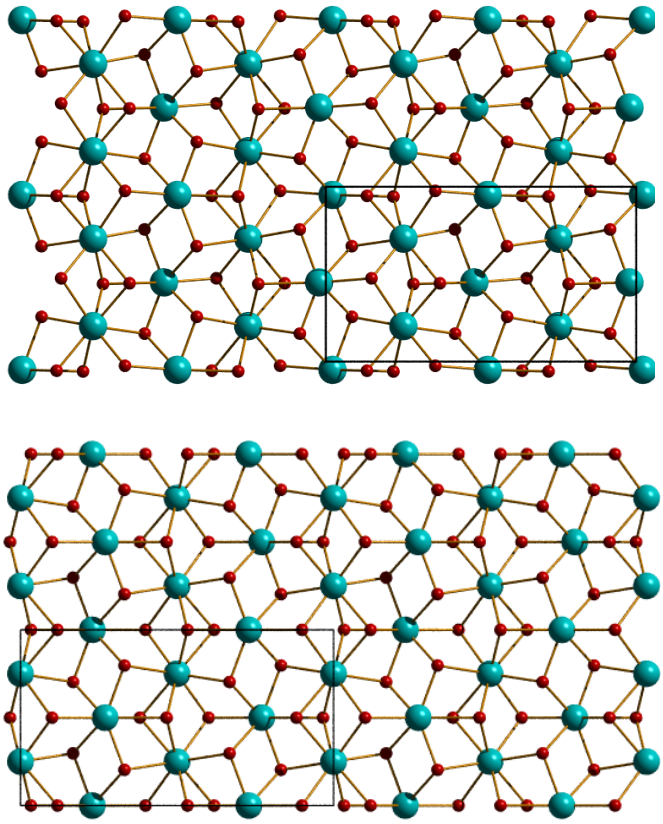

Figure 1.7 Crystallographic view of one single $[Y_4(OH)_{10}]^{2+}$ layer of $[Y_4(OH)_{10}]$ $[O_3S\text{-}C_{10}H_6\text{-}SO_3]$ (top) and one single $[Y_2(OH)_5]^+$ layer of $[Y_4(OH)_{10}]Cl$ (bottom) (Y-turquoise, O-red). Hydrogen atoms are omitted for clarity.

7.1348(6) Å with only 1.01 % and 1.26 % elongation along *a*-axis and *c*-axis, respectively (Figure 1.7). This class of layered rare earth hydroxide chloride also displays a structural evolution with linearly decreasing in-plane lattice parameter (along the single layer as in Figure 1.7) corresponding with lanthanide contraction of increasing atomic number.[56] Synchrotron Rietveld refinement also indicates a lower number of hydration water molecules for decreasing rare earth metal size.

Another family of 2-D cationic inorganic frameworks based on *f*-block with determined crystal structures is layered rare earth hydroxide sulfates $M_2(OH)_4SO_4$ (M = Pr^{3+}, Nd^{3+}, Sm^{3+}, Eu^{3+}, Gd^{3+}, Tb^{3+}).[57] The crystal structures were determined by

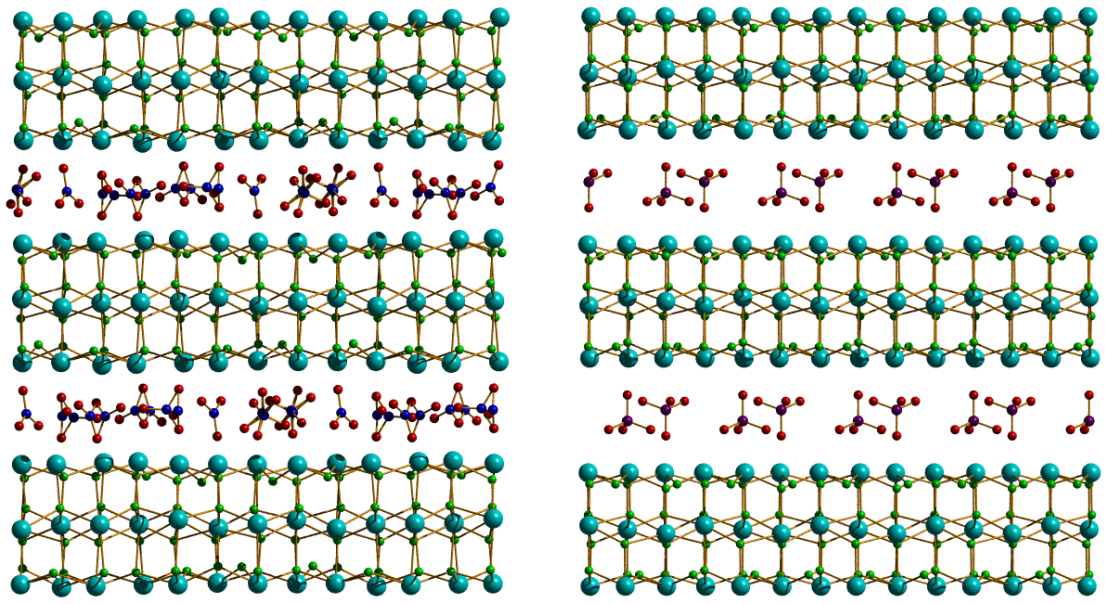

Figure 1.8 Crystallographic views of BING-5 [$(Pb_3F_5)(NO_3)$] (left) along *b*-axis and SLUG-10 [$(Pb_9F_{16})(ClO_4)$] along *b*-axis (right) (Pb-turquoise, F-green, O-red, N-blue, Cl-purple).

Rietveld refinement of synchrotron powder diffraction data. The pillared framework consists of $[M_2(OH)_4]^{2+}$ layers with sulfate as counter anion in the interlamellar region, bidentate weakly coordinated towards metal centers in adjacent layers. Other rare earth cationic inorganic frameworks possibly based on $[M_2(OH)_5]^{+}$ or $[M_2(OH)_4]^{2+}$ (where M is rare earth metals) positively charged sheets were reported, templated by nitrate or sulfate and structurally monitored by PXRD, elemental analysis and electron diffraction.[58-64] However, no related crystal structure was reported by single-crystal X-ray diffraction or Rietveld profile.

1.2.2 (b) 2-D Structures with *p* Block Metals

Heavy *p* block metals are known to have high and multiple oxidation states, e.g. Pb^{2+}/Pb^{4+}, In^{+}/In^{3+}, etc, contributing to their possibility for pillared frameworks possessing cationic inorganic layers. Lower oxidation states are relatively stable in the coordination chemistry of lower *p* block metals. However, the inert pair effect is observed on the metal center with a full s-shell of valance electrons, which are two outermost s electrons to remain unionized or unshared. This phenomenon is observed mostly in heavy post transition metals, and contributes to stability of cationic layers. Heavy *p* block metal cations with inert pairs are more likely to occupy umbrella-like unsaturated coordination geometry and possibly give overall positively charged framework, such as Pb^{2+}, Sb^{3+}, and Bi^{3+}.

Our group has reported the structural feature of cationic layered inorganic frameworks based on this series of main group metals, especially Pb^{2+}.[6] BING-5

$[(Pb_3F_5)(NO_3)]$ possess cationic inorganic triple layers $[Pb_3F_5]^+$ with partially disordered nitrate as counter anion as structure-directing agents (SDAs) in the interlamellar region (Figure 1.8 left).[65] Each triple layer consists of a neutral Pb_2F_4 central layer with six-coordinated octahedral metal centers and two cationic $[Pb_2F_3]^+$ outer layers with an inert pair and five-coordinated square pyramid lead pointing towards the interlamellar region. Another example of lead fluoride layered material SLUG-10 $[(Pb_9F_{16})(ClO_4)]$ also possesses a cationic triple layer with perchlorate as charge-balancing anion between adjacent layers (Figure 1.8 right).[49] The triple layer

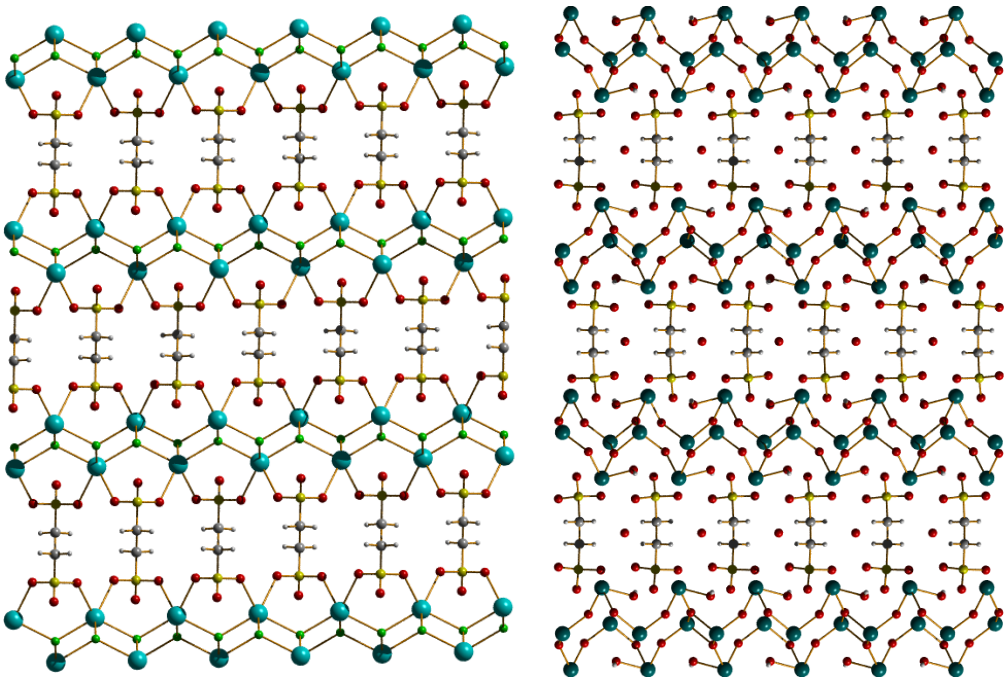

Figure 1.9 Crystallographic views of SLUG-6 $[Pb_2F_2][O_3S\text{-}C_2H_4\text{-}SO_3]$ (left) along *b*-axis and SLUG-5 $[(Sb_4O_4(OH)_2][O_3S\text{-}C_2H_4\text{-}SO_3]$ (right) along *b*-axis (Pb-turquoise, F-green, O-red, N-blue, Cl-purple).

of SLUG-10 contains the same neutral Pb_2F_4 middle layer as BING-5 and two cationic $[Pb_5F_8]^{2+}$ outer layers.

Besides weakly coordinating inorganic anions, anions with higher coordination strength (e.g. organosulfonates) also construct cationic layered frameworks with a lead fluoride cationic layered framework. SLUG-6 $[(Pb_2F_2)(O_3S\text{-}C_2H_4\text{-}SO_3)]$ contains cationic $[Pb_2F_2]^{2+}$ layers pillared by 1,2-ethanedisulfonate in perpendicular manner, and two of three oxygens at each sulfonate end are covalently

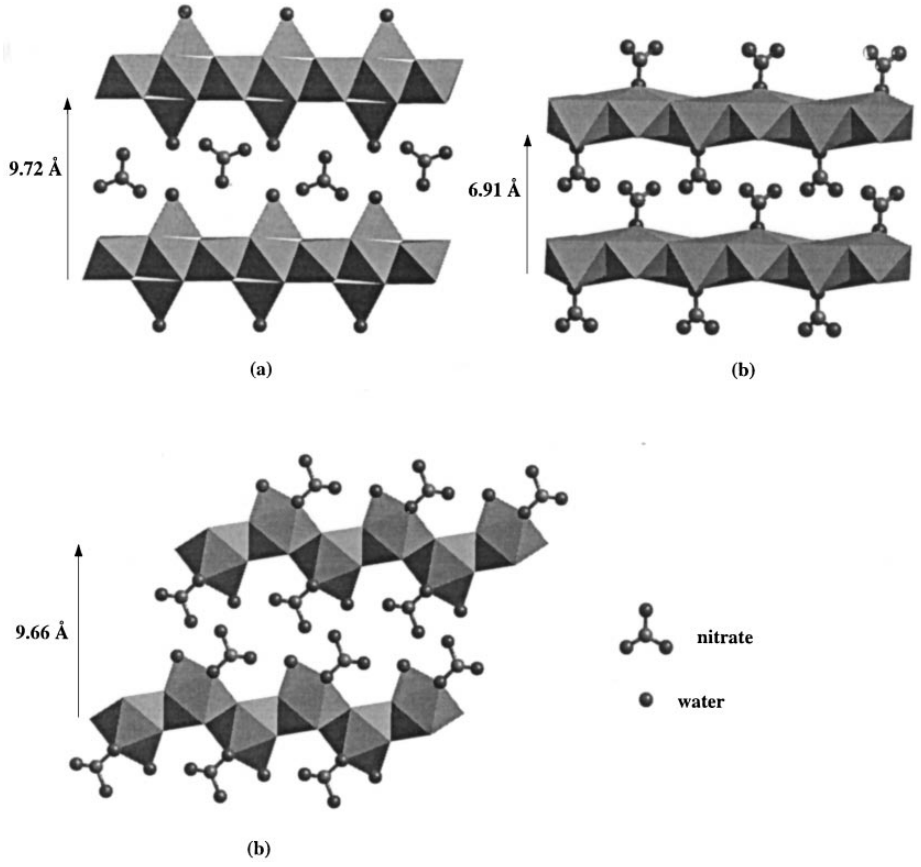

Figure 1.10 Crystallographic view of the structures of (a) $Zn_5(OH)_8(NO_3)_2 \cdot 2H_2O$, (b) $Cu_2(OH)_3NO_3$, and (c) $La(OH)_2(NO_3) \cdot H_2O$.

coordinated to two different lead centers (Figure 1.9 left).[66] Two other isoreticular frameworks with the same $[Pb_2F_2]^{2+}$ layers have been discovered with 1,3-propanedisulfonate and 1,4-butanedisulfonate, increasing the distance between adjacent inorganic sheets to 12.08 Å and 13.23 Å, respectively.[49] Unlike α,ω-alkanesulfonates covalently bonding with cationic lead fluoride layers, we also reported another example of a layered material, SLUG-5 $[(Sb_4O_4(OH)_2(O_3S\text{-}C_2H_4\text{-}SO_3)]$ with α,ω-alkanedisulfonate weak coordination towards the antimony centers.[67] 1,2-ethanedisulfonate is located in the interlamellar region of adjacent $[(Sb_4O_4(OH)_2]^{2+}$ layers by electrostatic interaction, and the distance between antimony and oxygen of sulfonate is 2.451(2) Å, well beyond the accepted Sb-O covalent bond range between 1.9 Å and 2.2 Å (Figure 1.9 right). Other heavy *p*-block metals, such as Bi^{3+}, display their potential for cationic layered inorganic frameworks by achieving hexanuclear and nonanuclear bismuthate clusters bridged by organosulfonate and triflate, respectively.[68]

1.2.2 (c) 2-D Structures with *d* Block Metals

A few transition metal hydroxide-based layered frameworks possess a non-LDH type positively charged layered architecture. One example includes transition metal-based hydroxyl salts containing only divalent metal layered hydroxide salt, which is called hydroxyl double salts (HDSs).[69] Unlike LDHs containing both M^{3+} and M^{2+} with general formula of $M^{2+}_{1-x}M^{3+}_x(OH)_2][A^{n-}_{x/n} \cdot mH_2O]$, HDSs are constructed with only a divalent metal ion M^{2+} and typical formula presented as $[(M_1,$

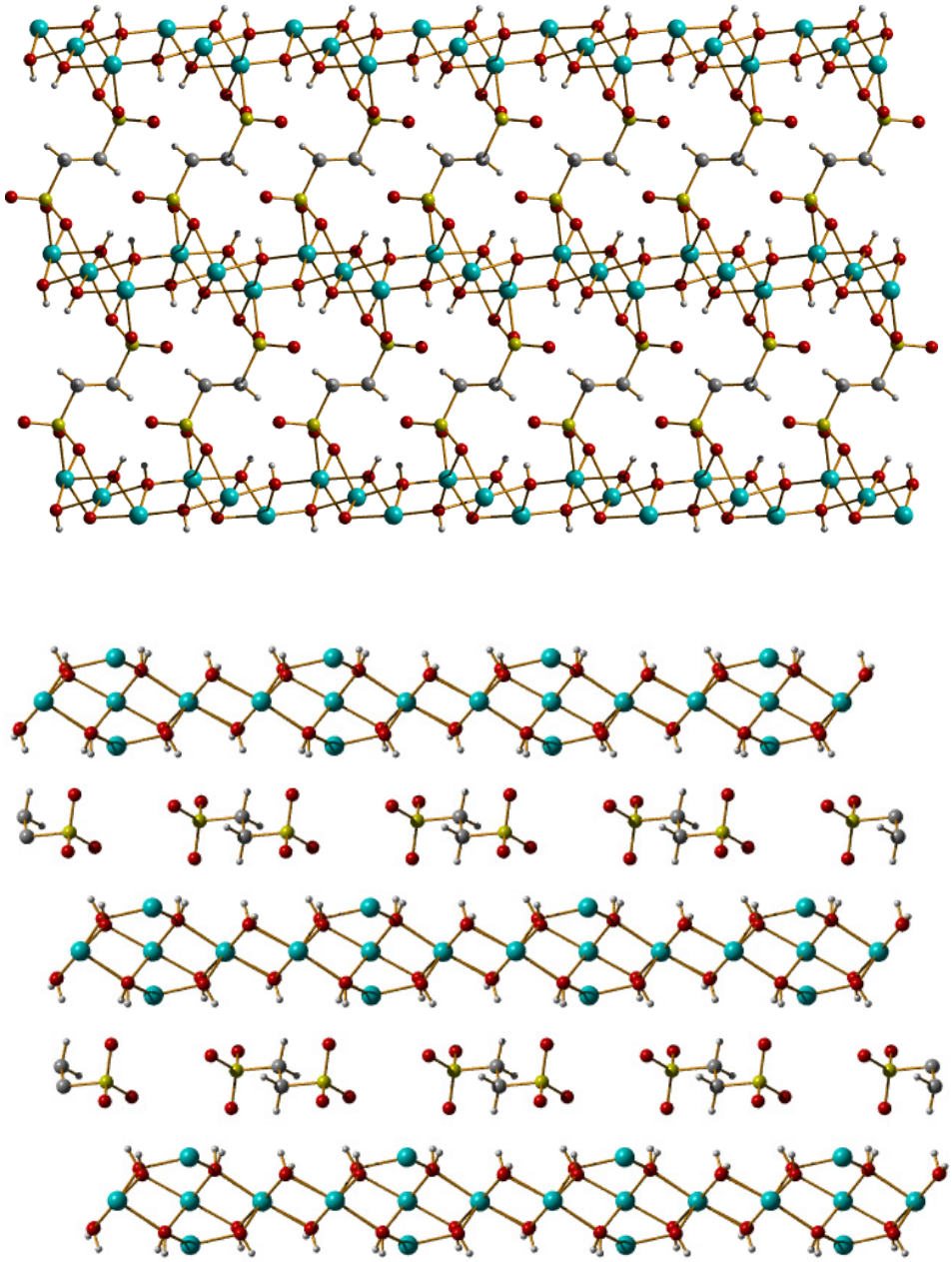

Figure 1.11 Crystallographic view of the structures of $Co_3(OH)_4(O_3S\text{-}C_2H_4\text{-}SO_3)$ (top) and $Co_7(OH)_{12}(O_3S\text{-}C_2H_4\text{-}SO_3)$ (bottom) (Co-turquoise, O-red, H-blue, S-yellow).

$M_2)_2(OH)_3(A^{n-})_{1/n}]$, where M_1 and M_2 are a range of divalent transition metals (e.g. Co^{2+}, Ni^{2+} Cu^{2+}, and Zn^{2+}), and A^- is *n*-valent interlamellar anions. The synthesis of

this group of materials involves the combination of a metal oxide (e.g. CuO) solids and aqueous nitrate solution of another metal source [e.g. $Ni(NO_3)_2$]. Slow evaporation for six days leads to the HDS product. Though unsuccessful in obtaining crystal structures from single-crystal X-ray diffraction (SC-XRD), powder X-ray patterns display strong and sharp (00*l*) diffractions and no peaks from metal oxide precursors, indicating its layered feature and phase purity, respectively.

Single transition metal hydroxide layered frameworks have been also reported by Newman and Jones.[70] Similar to synthesis of LDHs *via* the co-precipitation method, preparation of single-metal hydroxide involves the precipitation of metal nitrate solution with slow addition of sodium hydroxide solution to a certain pH. The crystal structure of $Zn_5(OH)_8(NO_3)_2$ was determined by SC-XRD that one-fourth of the coordination positions located at Zn^{2+}-centered octahedra are vacant (Figure 1.10 a), leading to positively charged sheets with nitrate electrostatically bound in the interlamellar regions.[71] $Cu_2(OH)_3NO_3$ has one-fourth of oxygens at the corner of Cu octahedra substituted with nitrate, which is perpendicular to the layer and located in the interlayer regions (Figure 1.10 b).[72] $La(OH)_2(NO_3)$ was structurally characterized by Rietveld refinement with part of the nine-coordination La centers connected with nitrate (Figure 1.10 c).[73] Two cationic cobalt hydroxide layered inorganic materials have been reported by Cheetham and co-workers.[74, 75] One structure is constructed with $[Co_3O_4]^{2+}$ cationic sheets pillared by 1,2-ethanedisulfonate with two oxygens of each sulfonate end covalently bonding to two adjacent Co centers (Figure 1.11 top). The other structure contains $[Co_7O_{12}]^{2+}$ positively charged layers with non-

coordinating alkanedisulfonates parallel to the layers in the interlamellar region (Figure 1.11 bottom). Fogg and co-workers also reported a series of two-dimensional inorganic mixed-metal oxide layers pillared by inorganic dianions. The cationic layers with a general formula of $[Ln(H_2O)MO_4]^+$ ($Ln=La^{3+}/Nd^{3+}$, $M=Mo^{6+}/W^{6+}$) consist of bilayered frameworks with edge-sharing metal-centered polyhedra.[76] Organodisulfonates or organodicarboxylates are covalently coordinating to the rare earth metals to form pillared inorganic extended structures.

1.2.2 (d) 2-D Structures with *s* Block Metals

Alkali and alkaline earth metals are relatively less investigated in the field of cationic inorganic structures, most likely due to their lower oxidation states and

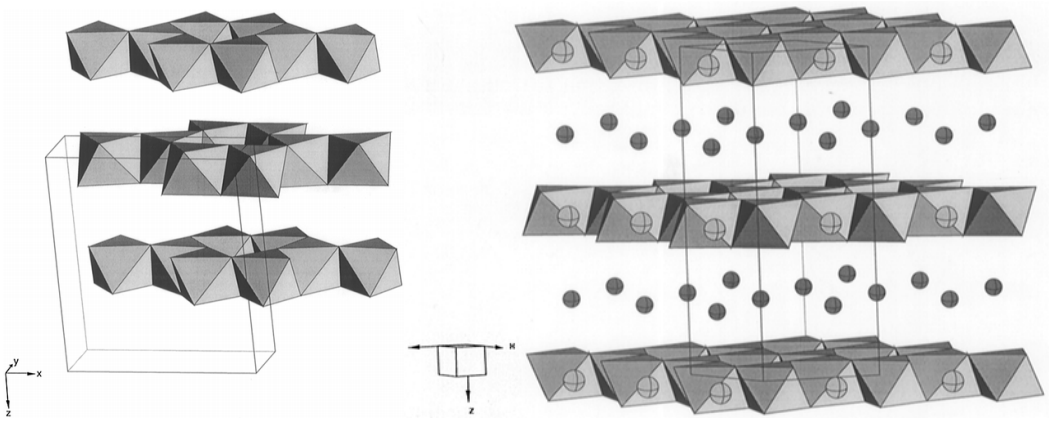

Figure 1.12 Crystallographic view of gibbsite (γ-$Al(OH)_3$) (left) and lithium chloride intercalated gibbsite $LiAl_2(OH)_6Cl$ (right).

tendency to form ionic bonding. Among the limited number of *s* block examples, one typical mixed-metal cationic inorganic material is treatment of gibbsite [γ-$Al(OH)_3$] with lithium halide.[77] Intercalation of counter anions is achieved by stirring the gibbsite mineral powder in an aqueous solution of lithium halide (LiCl, LiBr) or lithium nitrate. The filtrated and dried product is characterized by synchrotron X-ray diffraction and neutron powder diffraction to determine its structure. The neutral layered gibbsite mineral structure (Figure 1.12 left) expands into a new extended structure containing both Li^+ and Al^{3+} centers with halide anions charge-balancing the positively charged sheets (Figure 1.12 right). Our group has successfully employed a monovalent bridging anion to achieve $[Ba_2F_2]^{2+}$ positively charged sheets. 1,2-ethanedisulfoante in the interlamellar region covalently pillars adjacent layers to give the overall formula of $[Ba_2F_2][O_3S\text{-}C_2H_4\text{-}SO_3]$ (Figure 1.13). Other *s* block metals also achieve pillared structure with α,ω-alkanedisulfonates, however without cationic 2-D layered feature.[78]

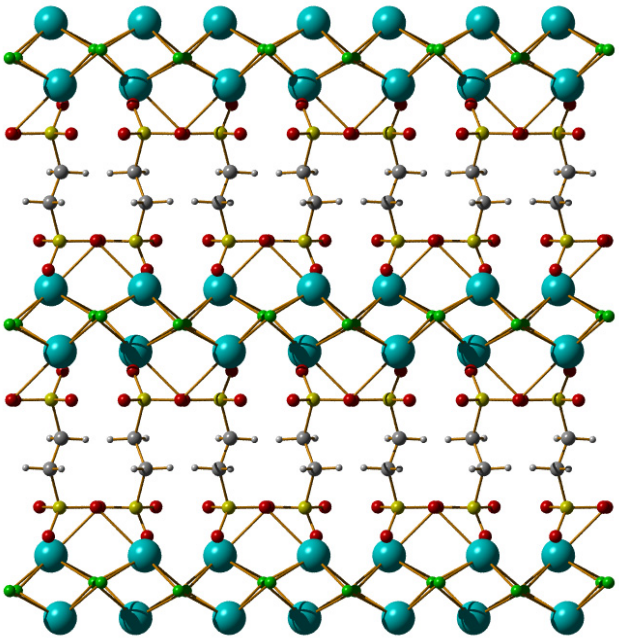

Figure 1.13 Crystallographic view of the structures of $[Ba_2F_2][O_3S\text{-}C_2H_4\text{-}SO_3]$ along *c*-axis (Ba-turquoise, O-red, H-blue, S-yellow).

1.2.2 (e) 3-D Structures

Though two-dimensional layered inorganic materials are well studied, 3-D zeotype cationic inorganic extended structures are much rarer and are primarily limited to francisite $Cu_3Bi(SeO_3)O_2X$ (X=Cl, Br and I).[79] However, its high dimensionality is questionable based on the long distance between bismuth and oxygen of SeO_3, which is also evidenced by collapse of the entire framework upon removal of the halide anions. Wang *et al.* discovered a solvothermal approach with molten borates as both SDA and solvent to achieve the first 3-D cationic inorganic

material $[ThB_5O_6(OH)_6][BO(OH)_2]\cdot 2.5H_2O$ based on Th^{4+}.[80] The supertetrahedral framework contains secondary building blocks of borates (BO_3 and BO_4) decorating twelve-coordinate thorium centers, giving an unusual cationic thorium borate framework $[ThB_5O_6(OH)_6]^+$ (Figure 1.14 left). Crown-like $[BO(OH)_2]^-$ charge-balancing anions and water molecules reside in the 1-D zigzag channel along the [110] direction. Another 3-D cationic inorganic material based on ytterbium was also discovered recently by Fogg and co-workers.[81] This 3-D inorganic oxide hydroxide framework consists of $[Yb_3O(OH)_6]^+$ with open aperture dimension of 7.6 × 4.8 Å with disordered chloride and water in the 1-D channel, which occupies the 30.3% solvent-accessible void space (Figure 1.14 right). The presence of

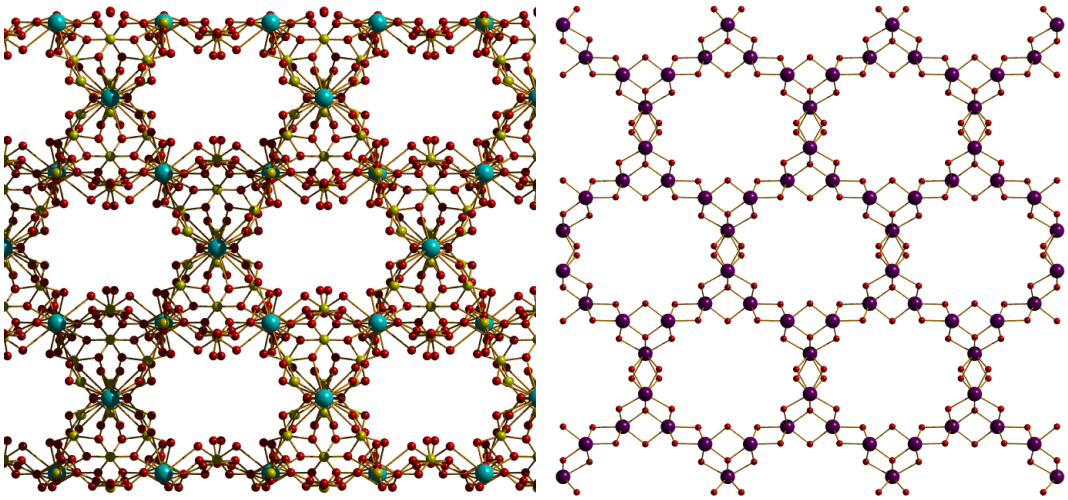

Figure 1.14. Crystallographic view of the structures of $[ThB_5O_6(OH)_6][BO(OH)_2] \cdot 2.5H_2O$ (left) along [110] direction and $Yb_3O(OH)_6Cl\cdot 2H_2O$ (right) along *c*-axis (Th-turquoise, Yb-purple, B-yellow, O-red). The disordered anion, solvent water and hydrogen atoms have been omitted for clarity.

unprotonated bridging oxygens in $Yb_3O(OH)_6Cl{\cdot}2H_2O$ acts as nodes between rare earth hydroxide layers. This connectivity feature avoids formation of the conventional layered hydroxide frameworks, allowing formation of 3-D architecture.

1.2.3 Intercalation Chemistry

The standard anion exchanger is the organic resin column, which is of limited thermal and chemical stability. LDHs as a plausible alternative to anion-exchange resins require calcination pre-treatment but have limited adsorption capacity/selectivity. Cationic inorganic frameworks are a series of promising anion exchangers, undergoing an equilibrium-driven exchange mechanism. Their solid-state exchange reactions take place by simply placing and stirring the as-synthesized solids in an aqueous solution of targeted anion in sodium salt form with 2-fold or 3-fold excess concentration.

Unlike LDHs which partially dissolve in the solution containing the anionic species to form a paste, synthetic cationic inorganic materials remain heterogeneous in the bottom of the aqueous solution and can be easily recovered and reused. Layered rare earth hydroxides with $[M_2(OH)_5]^+$ layers and halide or nitrate as counter anion display efficient anion exchange with different inorganic and organic anions, including halide, nitrate, sulfate, maleate, fumarate, phthalate, terephthalate, malonate, succinate, glutarate, suberate, decylsufonate, NDS, 2,6-anthraquinonedisulfonate.[60,62,82] The completeness of the exchange processes is monitored by a host of analytical techniques, such as FTIR, PXRD, and elemental

analysis, to determine *d*-spacing and the ratio of organic linkers present in the interlamellar region (Figure 1.15).[62] Anion exchange of layered hydroxide structures with decylsulfonate, followed by formamide treatment, led to exfoliation of the layered structure into rare earth hydroxide nanosheets. These nanoscale lamellar materials open up other applications, such as catalysis, and optical devices. Partial

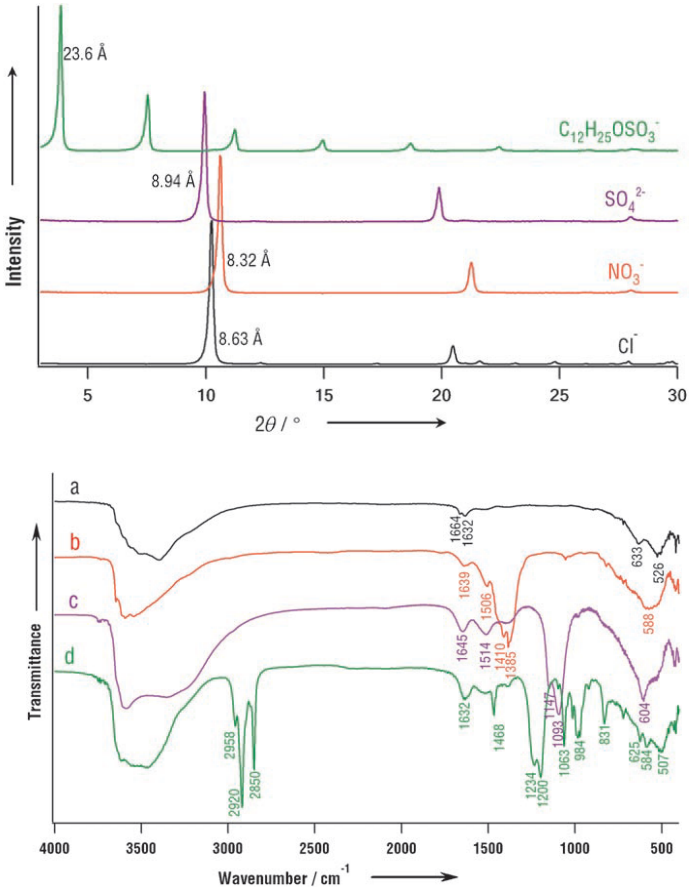

Figure 1.15 PXRD (left) and FTIR (right) of chloride-intercalated layered rare earth hydroxides (a) and their anion exchange product with NO_3^- (b), SO_4^{2-} (c), and $C_{12}H_{25}OSO_3^-$ (d).

decomposition of inorganic layers has also been observed for $[(Pb_9F_{16})(ClO_4)]$ and $[(Pb_3F_5)(NO_3)]$ anion exchange with chromate and dichromate, producing α-PbF_2 and $PbCr_2O_7$ as phases after anion exchange, respectively.[49,65] Compared with non-coordinating or weakly coordinating anions, attempts to exchange moderately coordinated organosulfonate intercalated cationic inorganic frameworks were not successful based on limited literature to date.

Metal anions in oxo-hydroxo form, such as CrO_4^{2-}, $Cr_2O_7^{2-}$, MnO_4^-, and ReO_4^-, are anions that would be beneficial to trap in solid-state materials from solution. Efficient single-crystal to single-crystal transformations have been observed for the 3-D thorium borate inorganic framework $[ThB_5O_6(OH)_6][BO(OH)_2]\cdot 2.5H_2O$.[80] Optical microscopy demonstrates that borate in its channels are partially or fully exchanged with metal oxo-hydroxo anions with retention of framework. This high-dimensional cationic material also displays efficient TcO_4^- removal up to 72 %. Initial studies of anion exchange on the other 3-D cationic inorganic framework $[Yb_3O(OH)_6]Cl$ exhibit its anion exchangeability with smaller anions such as carbonate, succinate, oxalate with survival of the high-dimensional topology.[81]

1.3 Cationic Metal-Organic Frameworks

Metal–organic frameworks (MOFs) are an emerging class of inorganic–organic hybrid materials attracting much attention due to not only the vast array of possible topologies but potential applications in gas storage/separation, size-selective catalysis and chemical sensors.[83-87] As a sub-class of MOFs, cationic MOFs occur when the positive charge on the metal ions outnumber the negative or neutral charge

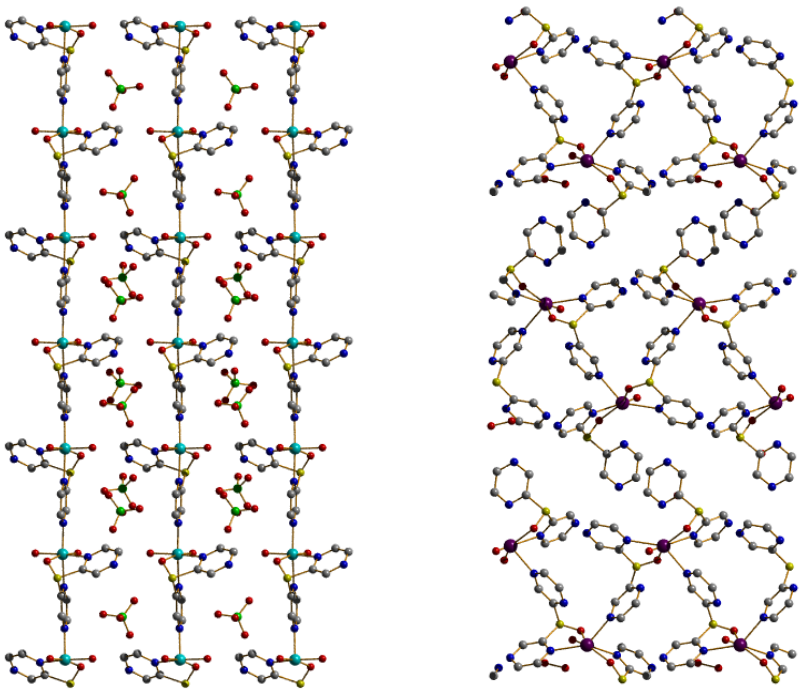

Figure 1.16 Crystallographic view of $[Zn(pyz_2SO)(H_2O)_2](ClO_4)_2$ (left) and $Cd(pyz_2SO)_2(H_2O)](ClO_4)_2 \cdot H_2O$ (right) (Zn- turquoise, Cd-purple, S-yellow, O-red, Cl green, N-blue, C-grey). Hydrogen atoms and perchlorate anions in right figure have been eliminated for clarity.

on the organic linkers. The synthesis and crystal engineering within this field involves many variable conformations, especially the following factors: metal coordinations, ligands, solvents, and counter anions.

1.3.1 Synthesis and Structural Diversity

1.3.1 (a) Metals

Metal coordination preferences play an important role in formation of cationic frameworks. In most cases, the framework dimensions increase accordingly with increasing coordination number around the metal and metal clusters. One example contains one of two transition metals with the same d^{10} electronic configuration (Zn^{2+} and Cd^{2+}) and organic linker dipyrazinyl sulfoxide [(pyrazinyl-SO-pyrazinyl), pyz_2SO] and counter anion perchlorate (ClO_4^-).[88] In Zn(II)-based structure, zinc centers are surrounded by two water molecules, one tridentate dipyrzinyl sulfoxide (two nitrogen and one oxygen on sulfoxide), and one nitrogen end of the other dipyrzinyl sulfoxide, giving an overall ZnN_3O_3 octahedral coordination environment (Figure 1.16 left). One pyrzinyl of each dipyrzinyl sulfoxide linker linearly bridges two adjacent Zn centers to form a straight infinite 1-D chain. Perchlorate anions are intercalated between adjacent chains. However, Cd is surrounded by one aqua ligand and three different dipyrzinyl sulfoxide linker (two bidentate and one bridging). The larger ionic radius of Cd(II) compared with Zn(II) is likely to induce each Cd center to covalent bond with one more linker than Zn, producing infinite zigzag chains with perchlorate encapsulated in the π-pockets surrounded by pyrzinyne rings (Figure 1.16

right). Another study revealed that metals in +2 oxidation states (e.g. Co^{2+} Ni^{2+}, Cd^{2+}) are more likely to produce a more π-acidic ring than Ag(I) due to their stronger Lewis acidity.[89] These acidic rings have a tendency to form a high degree of anion-π interaction. Indeed, the polarizing effect of the metal ion is also important in anion binding when using less π-acidic heterocyclic rings such as pyrazine. Two metal center Co^{2+} and Cd^{2+} with different coordination geometry also give helical polymeric chains and 2-D zigzag networks, using the same α,α′-bis(pyrazolyl)-*m*-xylene linker and chloride counter anion.[90]

1.3.3 (b) Ligands

In most cases, pyridine-based N-donor organic linkers are chosen to bridge adjacent metal or metal cluster centers to construct cationic extended frameworks. The framework bears overall positive charge and non-coordinating or weakly coordinating extraframework anions reside in 1-D channels or 0-D pockets, which have the potential to be exchanged for other anionic species. Organic linkers containing a urea proton donor are conventionally recognized as ideal ligands with anion-binding groups, since amine fragments on urea form strong hydrogen bonding interactions with the oxygens of anions.[91]

Anionic organic linkers could also achieve cationic MOFs with the overall positive charge on the metal ions exceeding the negative charge on the organic linkers. One example is the first cationic barium organosulfonate structure with 3-D extended framework [Ba_2(1,3,5-tris(sulfomethyl)-benzene)-$(H_2O)_5$]Cl and extraframework chloride anions residing in the 1-D channels.[92] Other examples show successful synthesis employing a metal center with high oxidation state either as discrete atoms or in a secondary building block with high positive charge, and outnumber the negative charge of the carboxylate-based organic linker. Yaghi and co-workers reported an iron(III)-based cationic MOF with $[Fe_3O]^{7+}$ secondary

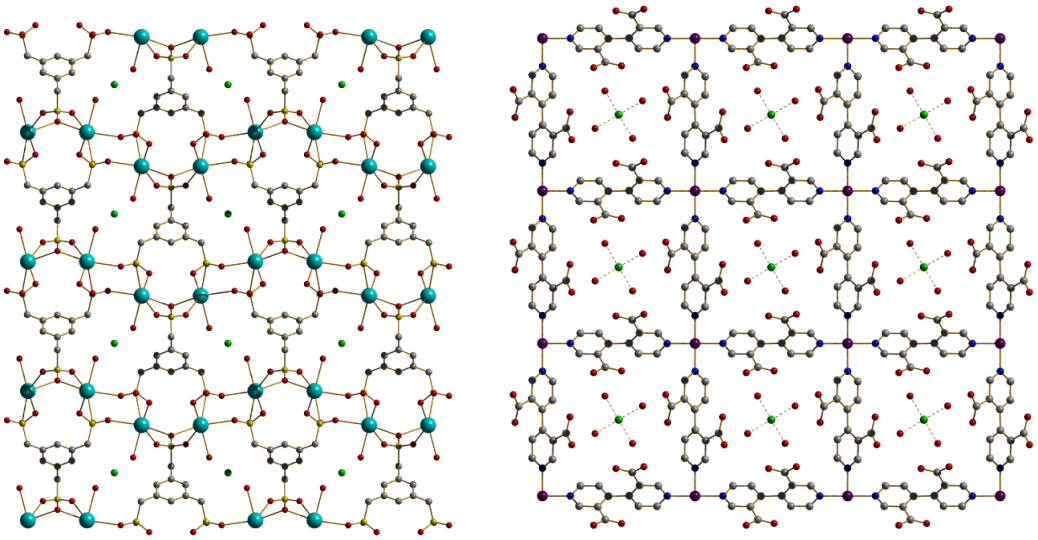

Figure 1.17 Crystallographic view of [Ba_2(1,3,5-tris(sulfomethyl)-benzene)-$(H_2O)_5$]Cl (left) and [$CuCl(BNA)_2$]·$Cl(H_2O)_4$ (right) (Ba- turquoise, Cu-purple, S-yellow, O-red, Cl green, N-blue, C-grey). Hydrogen atoms are omitted for clarity.

building block. The SBUs are connected with 1,4-benzenedicarboxylate in a high symmetry **acs** topology to give an overall formula of $[Fe_3O(1,4\text{-}BDC)_3(DMF)_3][FeCl_4]\cdot(DMF)_3$, with $[FeCl_4]^-$ located in hexagonal pores of the cationic framework.[93] Custelcean *et al.* discovered a cationic metal-organic framework $[CuCl(BNA)_2]\cdot Cl(H_2O)_4$ (BNA= binicotinic acid), and the neutral N-donor containing a free –COOH functional group acts as a binding group for the $[Cl(H_2O)_4]^-$ counter anion.[47]

Postsynthetic modifications of MOFs show the possibility of introducing a positive charge to the framework along with counter anions. Hupp and co-workers investigated postsynthetic treatment of a MOF containing alcohol functionality with magnesium alkoxides.[94] Stoichiometric incorporation of Mg^{2+} to hydroxyl functional groups resulted in a positively charged framework with retention of the same topology and permanent porosity, and methoxide anions are newly present as charge-balancing anions during the modification process.

1.3.3 (c) Anions

In most cationic MOFs, anions play the role of not only charge balancing counter ion, but dominating factor to template the extended structure. Noro *et al.* investigated the Jahn Teller distorted Cu(II) and 4,4'-bipyridine frameworks templated by various inorganic anions, including SiF_6^{2-}, GeF_6^{2-}, PF_6^-, ClO_4^- and SO_4^{2-}.[46] The resultant coordination polymers occupy a host of porous frameworks, ranging from 2-D layers (e.g. 2-D grid, 2-D interpenetrated framework and 2-D double layer) to 3-D grids (e.g. 3-D regulate grid and 3-D undulated grid). Homochiral 3-D frameworks were also assembled by linearly coordinated Ag(I) and chiral 3,3′-bipyridine-5,5′,6,6′-tetramethyl-2,2′-dimethoxy-1,1′-biphenyl ligands. Nitrate (NO_3^-), perchlorate (ClO_4^-) and hexafluorophosphate (PF_6^-) direct the polymeric strand into 2_1, 3_1, and 4_1 helices.[95] Many inorganic and organic anions,

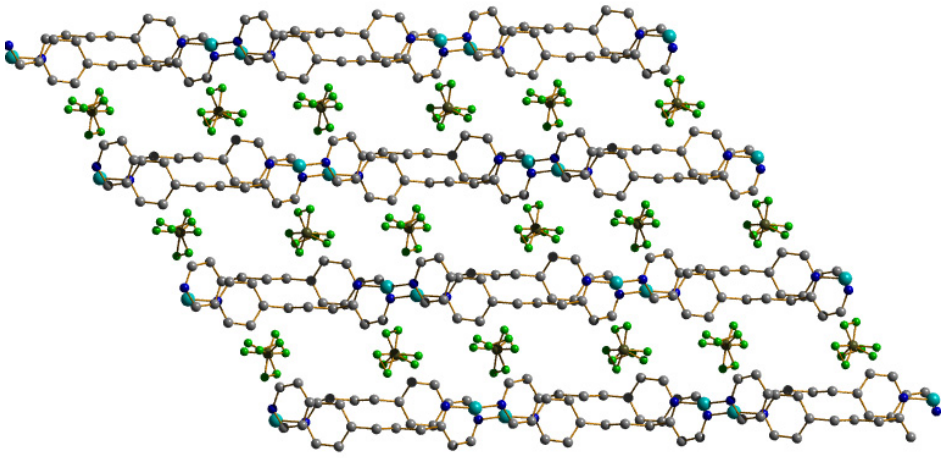

Figure 1.18 Crystallographic view of $[Cu(bpp)]BF_4$ (Cu-turquoise, O-red, Cl green, N-blue, C-grey, B-dark yellow). Hydrogen atoms are omitted for clarity.

including halides, acetate, triflate, sulfate, nitrate, perchlorate, organocarboxylates, also direct structure formation with other transition metals and flexible N-donor ligands.[96-99]

Synthesis with ionic liquids containing structure-directing anions is a plausible alternative to reach cationic MOFs.[100] Ionic liquids present as bifunctional reagents of both anion and solvent, and cationic frameworks with ionic liquids crystallize under solvothermal and/or slow diffusion conditions. One example is employing the ionic liquid [bmim][BF_4] (bmim=1-butyl-3-methylimidozolium) as counter anion and solvent, resulting in a 2-D metal-organic framework [Cu(bpp)]BF_4 [bpp=1,3-bis(4-pyridyl)propane] by a solvothermal reaction.[101] Infinite wave-like Cu(I)-bpp chains stack into cationic 2-D layers by edge-to-edge π-π stacking and a metal-to-metal weak interaction, while BF_4^- anions are disordered residing in the interlamellar region. Other anions in ionic liquids, such as bis(trifluoromethanesulfonyl)imide [$(NTf_2)^-$] and hexafluorophosphate (PF_6^-), can also be synthesized and included in the cationic MOFs by the same manner. Presence of another co-solvent other than ionic liquids facilitates crystallization of extended frameworks containing both anionic species in ionic liquid and co-solvent residing in the 1-D channel or 0-D pocket.[102-104]

1.3.2 Anion-Based Applications

The major problem of cationic MOFs and hydrogen-bonded frameworks for application in anion pollutant trapping is their relatively lower thermal and chemical stability, especially in the harsh chemical environment of wastewater. The stability of MOFs directly influences their practical applications in the field of anion separation. Some of highly porous MOFs are not chemically stable under water or other solvents, while others can survive in pH ~ 4 to 10 buffered aqueous solution and common organic solvents.[105] These relatively chemically stable MOFs display rich chemistry in anion-based applications under neutral aqueous condition, including anion exchange, anion separation, anion pollutant trapping and anion sensing.[91]

Many environmental pollutants that are anionic species are present with a vast array of non-toxic anions. One typical example is pertechnetate (TcO_4^-) in low-activity nuclear wastewater, which also contain non-radioactive anions, $Al(OH)_4^-$, Cl^-, F^-, NO_3^-, NO_2^-, OH^-, CO_3^{2-}, and organics.[23] The requirement of an ion exchanger to selectively trap pertechnetate into solid-state materials is necessary to prepare immobilized low-activity waste (LAW) glass that meets performance assessment requirements. After Frank Hofmeister established the ordering of anions in the ability of forming a salt to precipitate egg-white globulin, Hofmeister selectivity has been extended to hydration Gibbs free energy.[106] The decreasing hydration energy of anion species is in the same order as its charge and extractability from aqueous solution. Microscopy studies (atomic force microscopy and transmission electron microscopy) revealed the one-dimensional MOFs display a

solvent-mediated process anion exchange process involving dissolution of metal, ligand and anion and competitive recrystallization of metal, ligand and the other anion.[107] The Hofmeister series is a classification of anions in order of their ability to forming salt with cations. The selectivity for anions in aqueous media in this anion separation involves Hofmeister effects, giving the order of increasing hydration energy:[108-110]

$$PO_4^{3-} < CO_3^{2-} < SO_4^{2-} < CrO_4^{2-} < F^- < Cl^- < NO_3^-$$

$$< CF_3SO_3^- < TcO_4^- < ClO_4^- < Ph_4B^-$$

The majority of this selectivity trend is promising since anion pollutants (TcO_4^- and ClO_4^-) have higher hydration energy than non-toxic anions (CO_3^{2-}). Our group has successfully synthesized a cationic metal-organic framework Ag_2(4,4'-bipy)$_2$($O_3SCH_2CH_2SO_3$)·$4H_2O$, consisting of a cationic layer of π-π stacked Ag-bipy infinite chains with 1,2-ethanedisulfonate anions residing in the interlamellar regions.[111] Compared to LDHs, this material reached over five times adsorption capacity of 292 and 602 mg/g for permanganate and perrhenate, respectively.[111-113] Both anionic species were chosen as surrogates for pertechnetate. This material displays high selectivity in the order of following with anionic pollutants topping the list:[113]

$$CO_3^{2-} < NO_3^- < CrO_4^{2-} < ClO_4^- < ReO_4^- < MnO_4^-$$

The general trend is in the same order as Hofmeister effect with slight exceptions of anti-Hofmeister bias, which is a selectivity of anionic species not strictly according to hydrophobicity and hydrophilicity. This is most likely due to the geometry and

coordination behavior of anionic species, and their coordination towards cationic framework. The anti-Hofmeister effect has also been observed for cationic MOFs containing hydrogen-bonds (–NH and –OH) and active anion-binding sites. Urea-functionalized organic linker can selectively trap specific anions (e.g. sulfate) through hydrogen-bonded network, though presence of other anions.[114] One example is one-dimensional metal-organic frameworks of Zn^{2+} and N,N'-bis(*m*-pyridyl)urea.[115] This group of cationic frameworks displays selective crystallization with a host of anions, including Cl^-, Br^-, I^-, ClO_4^-, NO_3^- and SO_4^{2-}. In the presence of metal and a urea-based ligand, Cl^-, Br^-, I^- and SO_4^{2-} form an extended framework, while ClO_4^- and NO_3^- only forms discrete cluster. This anti-Hofmeister selectivity is induced by strong hydrogen bonding provided by urea (-NH groups) for selective anion-binding sites along with higher halide coordination number with respect to metal centers.

There have also been recent sustained research on anion binding sites, specifically for anionic compound sensing. This growth is mainly attributed to the importance of anions in biological (e.g. DNA polyanions) and environmental system (e.g. perchlorate, chromate, pharmaceuticals and their metabolites).[116] The discovery of Tb(btc) (btc=1,3,5-benzenetricarboxylate) framework has been investigated for anion sensing *via* photoluminescence in a methanol solution of sodium halide.[117] The unsaturated rare earth coordination center displays adsorption towards sodium halide salts, while fluoride binding offers the largest enhancement of photoluminescence intensity. Another Tb-based MOF, $Tb_2(OOC\text{-}[CH(OH)]_4\text{-}COO)_3$, displays similar

photoluminescence-responsive anion recognition for CO_3^{2-} and NO_3^-, attributed to hydrogen bonding between anions and mucicate $^-OOC\text{-}[CH(OH)]_4\text{-}COO^-$ linker.[118]

1.4 Concluding Remarks

Cationic inorganic frameworks and MOFs are two classes of positively charged materials having multiple anion-based applications. Cationic inorganic frameworks contain either 2-D or 3-D extended inorganic connectivity, with high thermal, chemical and framework stability for anion pollutant trapping applications. The majority of these materials undergo an equilibrium-driven anion exchange process, showing a vast array of advantages (e.g. heterogeneity, no memory effect, high capacity/selectivity, etc.) over conventional LDHs/hydrotalcite clays. The recent discovery of two 3-D cationic inorganic materials and their studies in anion exchange further enhance the possible cationic framework stability and applications. The rich intercalation chemistry of cationic layered inorganic materials introduces possible delamination into nanosheets, opening up other possible applications, including catalysis, solid state batteries, and biomedical applications. Cationic MOFs also display intriguing anion separation and sensing properties, despite their stability problem. Their underlying anion separation is in the order of Hofmeister effect with possible modifications, which were achieved by ligand choices with specific anion-binding sites. With all that has already been learned in the field of cationic materials, the ultimate goal is the rational design of specific anion trapping or recognition materials with high-dimensionality and thus high framework stability.

1.5 References

1. Cheetham, A. K.; Rao, C. N. R.; Feller, R. K., *Chem. Commun.* **2006**, 4780-4795.

2. Davis, M. E., *Nature* **2002,** *417*, 813-821.

3. Weitkamp, J., *Solid State Ionics* **2000,** *131*, 175-188.

4. Thomas, J. M., *Sci. Am.* **1992,** *1992*, 112-115.

5. Corma, A., *J. Catal.* **2003,** *216*, 298-312.

6. Oliver, S. R. J., *Chem. Soc. Rev.* **2009,** *38*, 1868-1881.

7. Rives, V., *LDHs: Layered Double Hydroxides: Present and Future*. Nova Science Publishers Inc., Hauppauge, New York, USA: 2001.

8. Slade, D. G. E. a. R. C. T., *Layered Double Hydroxides*. X. Duan and D. G. Evans ed.; Springer-Verlag, New York, NY, USA: 2006; p 1-87.

9. Boclair, J. W.; Braterman, P. S.; Brister, B. D.; Yarberry, F., *Chem. Mater.* **1999,** *11*, 2199-2204.

10. Liu, Z.; Ma, R.; Ebina, Y.; Iyi, N.; Takada, K.; Sasaki, T., *Langmuir* **2007,** *23*, 861-867.

11. Cho, S.; Jung, S. H.; Jang, J. W.; Oh, E.; Lee, K. H., *Cryst. Growth Des.* **2008,** *8*, 4553-4558.

12. Valente, J. S.; Lima, E.; Toledo-Antonio, J. A.; Cortes-Jacome, M. A.; Lartundo-Rojas, L.; Montiel, R.; Prince, J., *J. Phys. Chem. C* **2010,** *114*, 2089-2099.

13. Liang, J.; Ma, R.; Iyi, N.; Ebina, Y.; Takada, K.; Sasaki, T., *Chem. Mater.* **2010,** *22*, 371-378.

14. Ma, R.; Liu, Z.; Takada, K.; Iyi, N.; Bando, Y.; Sasaki, T., *J. Am. Chem. Soc.* **2007,** *129*, 5257-5263.

15. Meyn, M.; Beneke, K.; Lagaly, G., *Inorg. Chem.* **1990,** *29*, 5201-5207.

16. Li, B.; He, J.; Evans, D. G.; Duan, X., *App. Caly Sci.* **2004,** *27*, 199-207.

17. Choudary, B. M.; Jaya, V. S.; Reddy, B. R.; Kantam, M. L.; Rao, M. M.; Madhavendra, S. S., *Chem. Mater.* **2005,** *17*, 2740-1743.

18. Jin, L.; Liu, Q.; Sun, Z.; Ni, X.; Wei, M., *Ind. Eng. Chem. Res* **2010,** *49*, 11176-11181.

19. Depege, C.; Metoui, F. E.; Forano, C.; Roy, A.; Dupuis, J.; Besse, J. P., *Chem. Mater.* **1996,** *8*, 952-960.

20. Keith, L. H.; Teillard, W. A., *Environ. Sci. Technol.* **1979,** *13*, 416.

21. Hogue, C., *Chemical & Engineering News* **2011,** *89*, 6.

22. *Perchlorate environmental contamination: toxicological review and risk characterization*. Second external review draft, NCEA-1-0503; U.S. EPA, Office of Research and Development, National Center for Environmental Assessment, U.S. Government Printing Office: Washington, DC, 2002.

23. Darab, J. G.; Amonette, A. B.; Burke, D. S. D.; Orr, R. D.; Ponder, S. M.; Schrick, B.; Mallouk, T. M.; Lukens, W. W.; Caulder, D. L.; Shuh, D. K., *Chem. Mater.* **2007,** *19* (5703-5713).

24. Darab, J. G.; Smith, P. A., *Chem. Mater.* **1996,** *8*, 1004-1021.

25. Wang, Y.; Bryan, C.; Gao, H.; Phol, P. I.; Brinker, C. J.; Yu, K.; Xu, H.; Yang, Y.; Braterman, P. S.; Xu, Z., *Sandia Report (Potential Applications of*

Nanostructured Materials in Nuclear Waste Management **2003,** *SAND2003-3313*, 1-95.

26. Wu, M.; Janssen, S., *Environ. Sci. Technol.* **2011,** *45*, 366-367.

27. Mark, R.; Findley, W. N., *Polym. Eng. Sci.* **1978,** *18*, 6-15.

28. Bedner, M.; Maccrehan, W. A., *Environ. Sci. Technol.* **2006,** *40*, 516-522.

29. Taviot-Gueho, C.; Feng, Y.; Faour, A.; Leroux, F., *Dalton Trans.* **2010,** *39*, 5994-6005.

30. Prasanna, S. V.; Kamath, P. V., *Solid State Sci.* **2007,** *10*, 260-266.

31. Hu, G. J.; Wang, H. X.; Yan, L. L.; Pu, M.; He, J.; Evans, D. G., *J. Phys. Chem. Solids* **2010,** *71*, 1290-1294.

32. Yang, L.; Shahrivari, Z.; Liu, P. K. T.; Sahimi, M.; Tsotsis, T. T., *Ind. Eng. Chem. Res* **2005,** *44*, 6804-6815.

33. Das, J.; Patra, B. S.; Baliarsingh, N.; Parida, K. M., *App. Caly Sci.* **2006,** *32*, 252-260.

34. Das, J.; Das, D.; Dash, G. P.; Das, D. P.; Parida, K. M., *Int. J. Environ. Stud.* **2004,** *61* 605-616.

35. You, Y. W.; Vance, G. F.; Zhao, H. T., *App. Caly Sci.* **2001,** *20*, 13-25.

36. Goswamee, R. L.; Sengupta, P.; Bhattacharyya, K. G.; Dutta, D. K., *Appl. Clay Sci.* **1998,** *13*, 21-34.

37. You, Y. W.; Zhao, H. T.; Vance, G. F., *Environ. Technol.* **2001,** *22*, 1447-1457.

38. Miyata, S., *Clays Clay Miner.* **1983,** *31*, 305-311.

39. Goh, K. H.; Lim, T. T.; Dong, Z., *Water Res.* **2008,** *42*, 1343-1368.

40. Li, F.; Duan, X., *Struct. Bond.* **2005,** *119*, 193-223.

41. Iyi, N.; Matsumoto, T.; Kaneko, Y.; Kitamura, K., *Chem. Lett.* **2004,** *33*, 1122-1123.

42. Liu, Z.; Ma, R.; Osada, M.; Iyi, N.; Ebina, Y.; Takada, K.; Sasaki, T., *J. Am. Chem. Soc.* **2006,** *128*, 4872-4880.

43. Constantino, V. R. L.; Pinnavaia, T. J., *Inorg. Chem.* **1995,** *34*, 883-892.

44. Awaleh, M. O.; Badia, A.; Brisse, F., *Cryst. Growth Des.* **2006,** *6*, 2674-2685.

45. Custelcean, R., *Chem. Soc. Rev.* **2010,** *39*, 3675-3685.

46. Noro, S.; Kitaura, R.; Kondo, M.; Kitagawa, S.; Ishii, T.; Matsuzaka, H.; Yamashita, M., *J. Am. Chem. Soc.* **2002,** *124*, 2568-2583.

47. Custelcean, R.; Gorbunova, M. G., *J. Am. Chem. Soc.* **2005,** *127*, 16362-16363.

48. Geng, F.; Ma, R.; Sasaki, T., *Acc. Chem. Res.* **2010,** *43*, 1177-1185.

49. Rogow, D. L.; Russell, M. P.; Wayman, L. M.; Swanson, C. H.; Oliver, A. G.; J., O. S. R., *Crystal Growth & Design* **2010,** *10*, 823-829.

50. Perles, J.; Snejko, N.; Iglesia, M.; Monge, M. A., *J. Mater. Chem.* **2009,** *19*, 6504-6511.

51. Li, H.; Eddaoudi, M.; O'Keeffe, M.; Yaghi, O. M., *Nature* **1999,** *402*, 276-279.

52. Ferey, G.; Mellot, C. D.; Serre, C.; Millange, F.; Dutour, J.; Surble, S.; Margiolaki, I., *Science* **2005,** *309*, 2040-2042.

53. Gandara, F.; Perles, J.; Snejko, N.; Iglesia, M.; Gomez-Lor, B.; Gutierrez-puebla, R.; Monge, M. A., *Angew. Chem. Int. Ed.* **2006,** *45*, 7998-8001.

54. Gandara, F.; Puebla, E. G.; Iglesia, M.; Proserpio, D. M.; Snejko, N.; Monge, M. A., *Chem. Mater.* **2009,** *21*, 655-661.

55. Poudret, L.; Prior, T. J.; McIntyre, L. J.; Fogg, A. M., *Chem. Mater.* **2008,** *20*, 7447-7453.

56. Geng, F.; Matsushida, Y.; Ma, R.; Xin, H.; Tanaka, M.; Izumi, F.; Lyi, N.; Sasaki, T., *J. Am. Chem. Soc.* **2008,** *130*, 16344-16350.

57. Geng, F.; Ma, R.; Matsushida, Y.; Liang, J.; Michiue, Y.; Sasaki, T., *Inorg. Chem.* **2011,** *50*, 6667-6672.

58. Lee, K. H.; Byeon, S. H., *Eur. J. Inorg. Chem.* **2009**, 926-936.

59. McIntyre, L. J.; Jackson, L. K.; Fogg, A. M., *J. Phys. Chem. Solids* **2008,** *69*, 1070-1074.

60. McIntyre, L. J.; Jackson, L. K.; Fogg, A. M., *Chem. Mater.* **2008,** *20*, 335-340.

61. Hindocha, S. A.; McIntyre, L. J.; Fogg, A. M., *Inorg. Chem.* **2009,** *48*, 6724-6730.

62. Geng, F.; Xin, H.; Matsushida, Y.; Ma, R.; Tanaka, M.; Izumi, F.; Lyi, N.; Sasaki, T., *Chem. Eur. J.* **2008,** *14*, 9255-9260.

63. Geng, F.; Matsushida, Y.; Ma, R.; Xin, H.; Tanaka, M.; Iyi, N.; Sasaki, T., *Inorg. Chem.* **2009,** *48*, 6724-6730.

64. Liang, J.; Ma, R.; Geng, F.; Ebina, Y.; Sasaki, T., *Chem. Mater.* **2010,** *22*, 6001-6007.

65. Tran, D. T.; Zavalij, P. Y.; Oliver, S. R. J., *J. Am. Chem. Soc.* **2002,** *124*, 3966-3969.

66. Rogow, D. L.; Zapata, G.; Swanson, C. H.; Fan, X.; Campana, C. F.; Oliver, A. G.; Oliver, S. R. J., *Chem. Mater.* **2007,** *19*, 4658-4662.

67. Swanson, C. H.; Shaikh, H. A.; Rogow, D. L.; Oliver, A. G.; Campana, C. F.; Oliver, S. R. J., *J. Am. Chem. Soc.* **2008,** *130*, 11737-11741.

68. Rogow, D. L.; Fei, H.; Brennan, D. P.; Ikehata, M.; Zavalij, P. Y.; Oliver, A. G.; Oliver, S. R. J., *Inorg. Chem.* **2010,** *49*, 5619-5624.

69. Meyn, M.; Beneke, K.; Lagaly, G., *Inorg. Chem.* **1993,** *32*, 1209-1215.

70. Newman, S. P.; Jones, W., *J. Solid State Chem* **1999,** *148*, 26-40.

71. Stahlin, W.; Oswald, H. R., *Acta Cryst. B* **1970,** *26*, 860-861.

72. Nowacki, W.; Scheidegger, R., *Helv. Chim. Acta.* **1952**, 375-376.

73. Louer, M.; Louer, D.; Delgado, A. L.; Martinez, O. G., *Eur. J. Solid State Inorg. Chem.* **1989,** *26*, 241-245.

74. Forster, P. M.; Tafoya, M. M.; Cheetham, A. K., *J. Phys. Chem. Solids* **2004,** *65*, 11-15.

75. Feller, R. K.; Melot, B. C.; Forster, P. M.; Cheetham, A. K., *J. Mater. Chem.* **2009,** *19* 2604-2609.

76. Nicholls, J. L.; Hulse, S. E.; Callear, S. K.; Tizzard, G. J.; Stephenson, R. A.; Hursthouse, M. B.; Clegg, W.; Harrington, R. W.; Fogg, A. M., *Inorg. Chem.* **2010,** *49*, 8545-8551.

77. Besserguenev, A. V.; Fogg, A. M.; Francis, R. J.; Price, S. J.; O'Hare, D.; Isupov, V. P.; Tolochko, B. P., *Chem. Mater.* **1997,** *9*, 241-247.

78. Salami, T. O.; Patterson, S. N.; Jones, V. D.; Masello, A.; Abboud, K. A., *Inorg. Chem. Comm.* **2009,** *12*, 1150-1153.

79. Millet, P.; Bastide, B.; Pashchenko, V.; Gnatchenko, S.; Gapon, V.; Ksari, Y.; Stepanov, A., *J. Mater. Chem.* **2001,** *11*, 1152.

80. Wang, S.; Alekseev, E. V.; Diwu, J. C.; W. H.; Phillips; B. L.; Depmeier, W.; Albrecht-Schmitt, T. E., *Angew. Chem. Int. Ed.* **2010,** *49*, 1057-1060.

81. Goulding, H. V.; Hulse, S. E.; Clegg, W.; Harrington, R. W.; Playford, H. Y.; Walton, R. I.; Fogg, A. M., *J. Am. Chem. Soc.* **2010,** *132*, 13618-13620.

82. Hindocha, S. A.; McIntyre, L. J.; Fogg, A. M., *J. Solid State Chem* **2009,** *182*, 1070-1074.

83. Long, J. R.; Yaghi, O. M., *Chem. Soc. Rev.* **2009,** *38*, 1213-1214.

84. Ni, Z.; O'Keeffe; M.; Yaghi, O. M., *Angew. Chem. Int. Ed.* **2008,** *47*, 5136-5147.

85. Ferey, G., *Chem. Soc. Rev.* **2008,** *37*, 191-214.

86. Kitagawa, S.; Kitaura, R.; Noro, S., *Angew. Chem. Int. Ed.* **2004,** *43*, 2334-2375.

87. Horike, S.; Dinca, M.; Tamaki, K.; Long, J. R., *J. Am. Chem. Soc.* **2008,** *130*, 5854-5855.

88. Wan, C.; Zhao, L.; Mak, T. C. W., *Inorg. Chem.* **2010,** *49*, 97-107.

89. Black, C. A.; Hanton, L. R.; Spicer, M. D., *Inorg. Chem.* **2007,** *46*, 3669-3679.

90. Balamurugan, V.; Mukherjee, R., *Inorg. Chim. Acta* **2006,** *359*, 1376-1382.

91. Custelcean, R.; Moyer, B. A., *Eur. J. Inorg. Chem.* **2007**, 1321-1340.

92. Dalrymple, S. A.; Shimizu, G. K. H., *Chem. Eur. J.* **2002,** *8*, 3010-3015.

93. Sudik, A. C.; Cote, A. P.; Yaghi, O. M., *Inorg. Chem.* **2005,** *44*, 2998-3000.

94. Mulfort, K. L.; Farha, O. K.; Stern, C. L.; Sarjeant, A. A.; Hupp, J. T., *J. Am. Chem. Soc.* **2009,** *131*, 3866-3868.

95. Yuan, G.; Zhu, C.; Liu, Y.; Xuan, W.; Cui, Y., *J. Am. Chem. Soc.* **2009,** *131*, 10452-10460.

96. Vilar, R., *Eur. J. Inorg. Chem.* **2008,** *3*, 357-367.

97. Tang, J.; Costa, J. S.; Pevec, A.; Kozlevcar, B.; Massera, C.; Roubeau, O.; Mutikainen, I.; Turpeinen, U.; Gamez, P.; Reedijk, J., *Cryst. Growth Des.* **2008,** *8*, 1005-1012.

98. Mondal, R.; Basu, T.; Sadhukhan, D.; Chattopadhyay, T.; Bhunia, M. K., *Cryst. Growth Des.* **2009,** *9*, 1095-1105.

99. Diaz, P.; Buchholz, J. B.; Vilar, R.; White, A. J. P., *Inorg. Chem.* **2006,** *45*, 1617-1626.

100. Reichert, W. M.; Holbrey, J. D.; Vigour, K. B.; Morgan, T. D.; Broker, G. A.; Rogers, R. D., *Chem. Commun.* **2006**, 4767-4779.

101. Jin, K.; Huang, X.; Pang, L.; Li, J.; Appel, A.; Wherland, S., *Chem. Commun.* **2002**, 2872-2873.

102. Dybtsev, D. N.; Chun, H.; Kim, K., *Chem. Commun.* **2004**, 1594-1595.

103. Blake, A. J.; Baum, G.; Champness, N. R.; Chung, S. S. M.; Cooke, P. A.; Fenske, D.; Khlobystov, A. N.; Lemenovskii, D. A.; Li, W. S.; Schroder, M., *J. Chem. Soc. Dalton Trans.* **2000**, 4285-4291.

104. Sharma, C. V. K.; Griffin, S. T.; Rogers, R. D., *Chem. Commun.* **1998**, 215-216.

105. Demessence, A.; D'Alessandro, D. M.; Foo, M. L.; Long, J. R., *J. Am. Chem. Soc.* **2009,** *131*, 8784-8786.

106. Hofmeister, F., *Arch. Exp. Pathol. Pharmakol.* **1888,** *24*, 247-250.

107. Khlobystov, A. N.; Champness, N. R.; Roberts, C.; Tendler, S. J. B.; Thompson, C.; Schroder, M., *CrystEngComm* **2002,** *4*, 426-431.

108. Marcus, Y., *J. Chem. Soc., Faraday Trans.* **1991,** *87*, 2995-2999.

109. Roobottom, H. K.; Jenkins, H. D. B.; Passmore, J.; Glasser, L., *J. Chem. Educ.* **1999,** *76*, 1570-1573.

110. Levitskaia, T. G.; Maya, L.; Van Berkel, G. J.; Moyer, B. A., *Inorg. Chem.* **2006,** *46*, 261-272.

111. Fei, H.; Paw, L. U.; Rogow, D. L.; Bresler, M. R.; Abdollahian, Y. A.; Oliver, S. R. J., *Chem. Mater.* **2010,** *22*, 2027-2032.

112. Fei, H.; Rogow, D. L.; Oliver, S. R. J., *J. Am. Chem. Soc.* **2010,** *132*, 7202-7209.

113. Fei, H.; Bresler, M. R.; Oliver, S. R. J., *J. Am. Chem. Soc.* **2011,** *133*, 11110-11113.

114. Hay, B. P.; Firman, T. K.; Moyer, B. A., *J. Am. Chem. Soc.* **2005,** *127*, 1810-1819.

115. Custelcean, R.; Haverlock, T. J.; Moyer, B. A., *Inorg. Chem.* **2006,** *45*, 6446-6452.

116. Feng, J.; Dong, Y.; Salamat-Miller, N.; Middaugh, C. R., *Nucleic Acids Res.* **2008,** *36*, D303-D306.

117. Chen, B.; Wang, L.; Zapata, F.; Qian, G.; Lobkovsky, E. B., *J. Am. Chem. Soc.* **2008,** *130*, 6718-6719.

118. Wong, K. L.; Law, G. L.; Yang, Y. Y.; Wong, W. T., *Adv. Mater.* **2006,** *18*, 1051-1054.

Chapter 2

Synthesis, Characterization and Catalytic Application of a Cationic Metal-Organic Framework: $Ag_2(4,4'\text{-bipy})_2(O_3S\text{-}C_2H_4\text{-}SO_3)$

Abstract

We report a silver-based cationic metal-organic framework with two mixed organic linkers directing the structure. The structure consists of 1-D Ag(4,4'-bipy) cationic chains arranged into close-packed layers. Weakly bound alkanedisulfonate anions charge-balance the layers, where only one oxygen of each sulfonate makes a long contact with the Ag. The unsaturated linear Ag centers likely allow the strong Lewis acidity displayed by the material for ketone protection as well as esterification. The material showed no reduction in yield after three catalytic runs with average 95% conversion yield for ketal formation and 57% for esterification without further water removal. In addition to hydrothermal conditions, the structure can be synthesized by reflux or room temperature, with almost identical catalytic ability. Other properties of this compound such as chemical and thermal stability are also described.

2.1 Introduction

Hybrid inorganic-organic solid-state compounds are an emerging class of materials with exponential growth in recent years, especially metal-organic frameworks (MOFs).[119] Considering some retain a robust and geometrically defined structure at elevated conditions, this group of extended coordination frameworks have a wide range of application, such as catalysis,[120-122] gas storage,[123,124] gas absorption,[125] ion exchange[126] and drug delivery[127]. Due to the great variety of metal units and organic linkers, these multifunctional materials have almost infinite possible combinations and more recent efforts have been made to establish their structure-property relationships.

Heterogeneous catalysis has attracted extensive effort due to increased environmental concerns, seeking stable and easily recoverable catalysts.[128] As yet, there are limited systematic reports concerning heterogeneous catalysis by porous coordination frameworks.[122,129] Microporous MOFs have been investigated in detail recently and proven that the active Lewis acid site is the open and coordinatively unsaturated metal.[121,122,130,131] Cationic metal-organic frameworks are a group of extended frameworks with positive charge of metals outnumbers than negative charge of organic linker, and charge-balancing extraframework anions functioned as structure directing agents (SDA) resided in the framework.[132-134] Considering cationic feature of MOFs might lead to coordination unsaturated metal sites owing to electrostatic interaction between metal and intercalated extraframework anions,

systematic studies need to be investigated on the heterogeneous catalytic properties of MOFs with cationic feature.[135]

Our group, among others, is taking initial steps of applying cationic hybrid inorganic-organic frameworks to catalysis. Nitrate, perchlorate and ethanedisulfonate anions have been shown to direct the growth of cationic oxides and fluorides based on lower p-block elements and encouraging results have been shown where hydrogen bonding or electrostatic interaction between cationic host and SDA anion give rise to coordinatively unsaturated metal sites, thus yielding efficient Lewis acidity.[135-139]

A recent goal of our group is to isolate cationic extended frameworks based on transition metals that are more predictable in terms of coordination and properties. Aside from the well-established layered double hydroxides (LDHs)/hydrotalcite minerals, there are very few reports detailing cationic extended coordination polymers constructed from transition metals templated by organic charge-balancing anions.[139,140] Silver(I), cadmium(II) and copper(I) are isoelectronic, with filled d^{10} shells that favor rigid, linear structures.[141] Several Ag(I) organosulfonate MOFs have been reported, but are condensed neutral or open anionic frameworks.[142-145] Catalysis application of open cationic structures based on d^{10} shell metal ions remains largely unexplored and may form low-coordinate open metal sites, thus possibly allowing strong Lewis acidity.

Herein, we report a silver-based 1-D cationic coordination polymer with 4,4'-bipyridine (4,4'-bipy) linker and templated by 1,2-ethanedisulfonate (EDS). The structure is a rare example employing mixed organic linkers to direct the cationic

extended frameworks. Two different organic linkers support Ag(I) with enough openness to allow access by incoming guests. The synthesis, thermal properties, catalytic reactivity and reusability are investigated in detail.

2.2 Experimental Section

2.2.1 Reagents

Silver nitrate ($AgNO_3$, Fisher ≥ 99.7%), 1,2-ethanedisulfonic acid ($HO_3SCH_2CH_2SO_3H$, TCI Inc. 95%) and 4,4'-bipyridine [$(C_5H_4N)_2$, Acros Organics, 98%] were used as-received for the synthesis. 2-butanone ($CH_3COCH_2CH_3$, Acros Organics, 99%), ethylene glycol ($HOCH_2CH_2OH$, Acros Organics, 99%), acetic acid (glacial, CH_3COOH, MP Biomedicals, 99%) and toluene ($C_6H_5CH_3$, Fisher, 99.7%) were used as-purchased for the catalytic studies.

2.2.2 Synthesis

Colorless crystals of $Ag_2(4,4'\text{-bipy})_2(O_3SCH_2CH_2SO_3)\cdot 4H_2O$ (which we denote SLUG-21: University of California, Santa Cruz No. 21) was synthesized under hydrothermal conditions. A reactant solution with a molar ratio of 1:1:1:400 for $AgNO_3$: EDSA : 4,4'-bpy : H_2O was stirred at room temperature for 10 min and then transferred to a 15 ml Teflon lined autoclave to 2/3 filling. The autoclaves were heated at 150°C for 5 days under autogeneous pressure, during which pH of the reactant solution increased from 1.8 to 2.2. Colorless large block crystals were

isolated after filtration and rinsed by acetone (yield: 0.54 g, 98.7% based on silver nitrate). IR (KBr pellets): 3467s, 3050m (O-H stretch); 1605s, 1535s, 1490s, 1418s (aromatic C-H stretch); 1328s (CH_2 stretch); 1200m, 1070m (SO_3^- stretch); 863s, 817s (aromatic C-H bending).

Crystals of $Ag_2(4,4'\text{-bipy})_2(O_3SCH_2CH_2SO_3)\cdot 4H_2O$ can also be synthesized with no need for autoclaves by refluxing or stirring at room temperature. Reactions were carried out with the same ratio of reactants and crystals were filtrated after ca. 60 hours (refluxing) and 5 days (stirring) reaction time. The yield is 74.1% (0.40 g) with refluxing and 83.3% (0.45 g) with stirring (both yields again based on silver nitrate).

2.2.3 Heterogeneous Catalysis

100 mg (0.13 mmol) of the as-synthesized crystal catalyst, 70 mmol of 2-butanone and 70 mmol of ethylene glycol were introduced into 80 mmol of toluene, the latter used as solvent for a ketal formation reaction. The reaction was refluxed at 110°C under Dean-Stark conditions for specified time intervals. The catalyst was isolated by filtration and reused on subsequent reactions without further treatment. 100 mg of SLUG-21 was also applied for an esterification between 70 mmol acetic acid and 70 mmol ethanol in 8 ml toluene. The reactants were refluxed for 8 hours without further methods for water removal. All product yields were determined by ^{1}H NMR (supporting information).

2.2.4 Instrumental Details

Samples for powder X-ray diffraction (PXRD) were measured on a Rigaku Americas Miniflex Plus diffractometer, and were scanned from 2 to 60°(2θ) at a rate of 2°(2θ) per minute and 0.04° step size, under Cu-Kα radiation (λ = 1.5418 Å). Single-crystal X-ray diffraction data was obtained a Bruker SMART APEX II CCD area detector X-ray diffractometer under graphite monochromated Mo-Kα radiation (λ = 0.71073 Å). An empirical absorption correction was applied using SADABS and the structure was solved by direct method and refined with SHELXTL.[146] All non-hydrogen atoms were refined with anisotropic thermal displacement parameters. Crystal structure views were obtained using Diamond v3.2 and rendered by POV-Ray v3.6.

Thermogravimetric analysis (TGA) was performed using a TA Instruments 2050 TGA by heating from 25 to 600°C under N_2 purge with a gradient of 15°C/min. *In-situ* mass spectra coupled to the TGA were collected on a Pfeiffer Vacuum ThermoStar GSD 301 T3 mass spectrometer with a 70 eV ionization potential. Scanning electron micrographs (SEM) were collected on a Hitachi S-2700 SEM. ^{1}H NMR spectra were collected with a Varian Oxford 600 MHz spectrometer by dissolving the sample in 700μL of deuterated choloroform with tetramethylsilane as internal standard.

2.3 Results and Discussion

2.3.1 Synthesis and Structural Characterization

Crystals of SLUG-22 can be synthesized hydrothermally between 125 °C and 150 °C temperatures with reproducible crystal size and morphology. Reflux without applied pressure as well as stirring under room temperature may also be used. Micrographs (Figures 2.1) show reflux also achieved high quality crystals with similar crystal morphology compared to the hydrothermal product. Room temperature stirring gave lower crystallinity but higher yield than reflux and larger specific surface area. PXRD of SLUG-21 prepared from the three methods confirms the products give the identical phase and match the theoretical pattern based on the single crystal solution (Figure 2.2). SLUG-21 crystallizes in a triclinic crystal system with P-1 space group. All of the products are chemically stable in deionized water and organic solvents, including chloroform, toluene and acetonitrile.

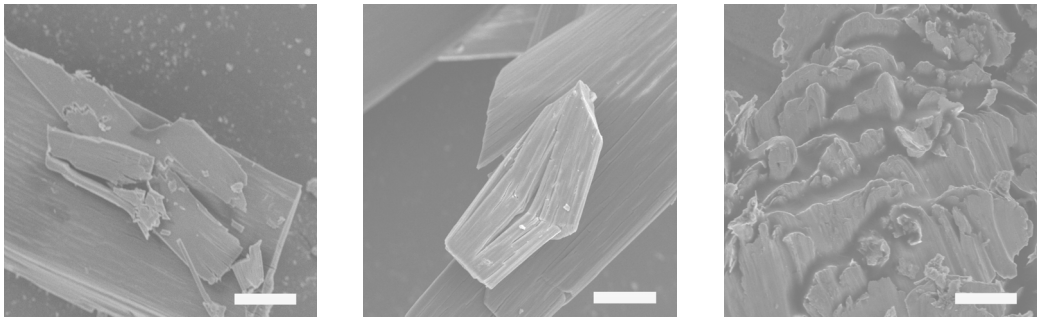

Figure 2.1 SEM images of SLUG-21 under hydrothermal conditions (left), refluxing (middle) and room temperature stirring (right). Scale bar is 40 μm on left image, and 20 μm on both middle and right images.

Table 2.1 Crystal Data and Structure Refinement of SLUG-21

empirical formula	$C_{22}H_{28}Ag_2N_4O_{10}S_2$
crystal system	Triclinic
space group	P-1
formula weight (g/mol)	788.36
a (Å)	8.1174(17)
b (Å)	9.2860(19)
c (Å)	10.297(2)
α (deg)	71.589(2)
β (deg)	75.392(2)
γ (deg)	71.286(2)
volume ($Å^3$)	687.6(2)
Z	1
crystal size (mm^3)	0.06×0.05×0.03
color of crystal	Colorless
goodness-of-fit on F^2	1.045
final R indices $I > 2\sigma(I)$	R_1=0.0262 wR_2=0.0559
R indices (all data)	R_1=0.0288 wR_2=0.0569

Single-crystal X-ray diffraction studies reveal that the structure of SLUG-21 is a cationic one-dimensional extended MOF of alternating Ag centers and 4,4'-bipy molecules bonded through Ag-N bonds (Figures 2.3 and 2.4). The chains are arranged into layers, with ethanedisulfonate (EDS) anions residing in the interlamellar space. The Ag-bipy layer is stabilized by 4,4'-bpy ligand π-π stacking between adjacent 1-D chains. Each end of the EDS molecule interacts electrostatically with adjacent cationic layers through one sulfonate oxygen, with Ag-O distance between 2.711(7) Å and 2.759(9) Å (Figure 2.4). The other two oxygens are involved in a hydrogen bonding network with interlamellar waters, which were resolved (Table 2.2). Silver(I) atoms with a full d shell form an almost linear geometry (two similar N-Ag-N angles of 171.5(3)° and 172.3(3)°), with Ag-N bond

lengths in the range of 2.156(6) Å to 2.170(7) Å. Two weak interactions occur between each Ag atom and the oxygen of the EDS anion, and the atom distances are between 2.711(7) Å and 2.759(9) Å. These distances are significantly longer than accepted Ag-O covalent bond lengths,[147] especially considering literature Ag(I) to sulfonate distances are in the range of 2.45 to 2.55 Å.[148-150] These values confirm that the EDS anions only interact electrostatically with the Ag(I)-bipy cationic extended framework.

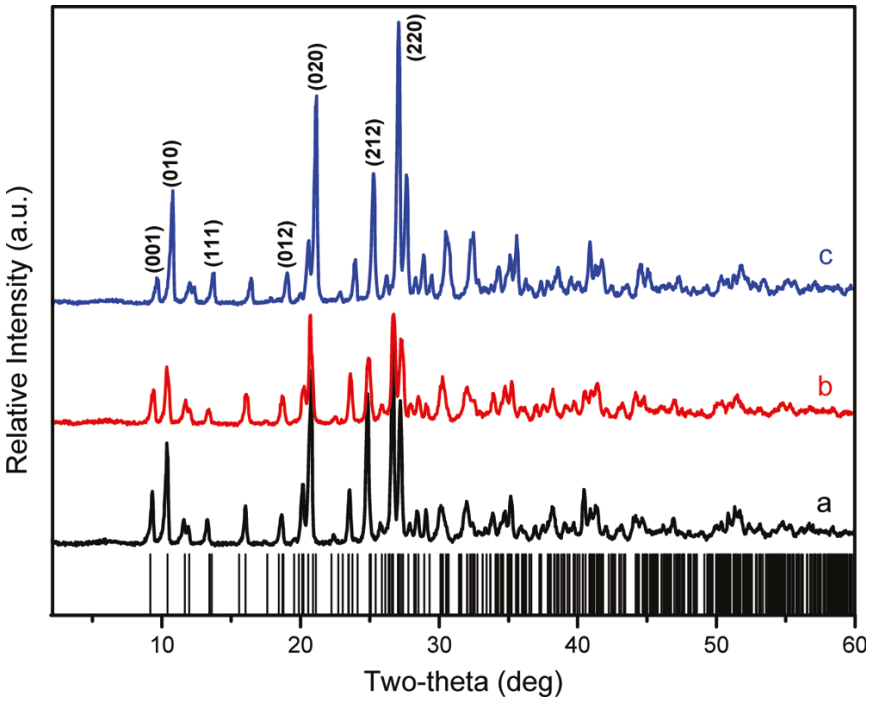

Figure 2.2 PXRD of as-synthesized SLUG-21 prepared from (a) hydrothermal methods, (b) refluxing, (c) stirring and their comparison with the theoretical

Four crystallographically identified water molecules verify that SLUG-21 cannot be obtained under non-aqueous medium, as attempts to use

Table 2.2 Selected Bond Lengths, Angles and Hydrogen Bonding in SLUG-21[a]

Ag(1)-N(1)	2.156(7)	Ag(1)-N(2)		2.171(7)
Ag(2)-N(3)	2.128(7)	Ag(2)-N(4)		2.156(7)
N(1)-Ag(1)-N(2)	171.5(3)	N(3)-Ag(2)-N(4)		172.3(3)
D-H...A	d(D-H)	d(H...A)	d(D...A)	<(DHA)
O(11)-H(12)...O(12)#1	0.81(4)	1.94(4)	2.711(15)	157(4)
O(14)-H(41)...O(13)#2	0.77(5)	2.27(5)	2.733(13)	119(4)
O(12)-H(21)...O(3)	0.61(7)	2.24(8)	2.784(13)	150(11)
O(13)-H(31)...O(7)	0.96(6)	1.89(7)	2.795(10)	158(5)
O(13)-H(32)...O(11)#3	0.76(6)	2.05(7)	2.724(13)	148(6)
O(11)-H(11)...O(6)	0.67(17)	2.31(16)	2.823(12)	135(17)
O(12)-H(22)...O(14)#4	0.74(9)	2.07(9)	2.751(12)	152(8)

[a] Symmetry transformations used to generate equivalent atoms:
#1 x,y,z-1 #2 x,y,z+1 #3 x+1,y,z #4 x-1,y,z

dimethylformamide, pyridine, 2-butanol as solvent were unsuccessful. The presence of hydrogen bonds between the EDS anion and intercalated water molecules (Figure 2.4 and Table 2.2) further stabilize the structure. Indeed, crystallinity was not lost after immersing SLUG-21 into unbuffered water or other common organic solvents for several weeks.

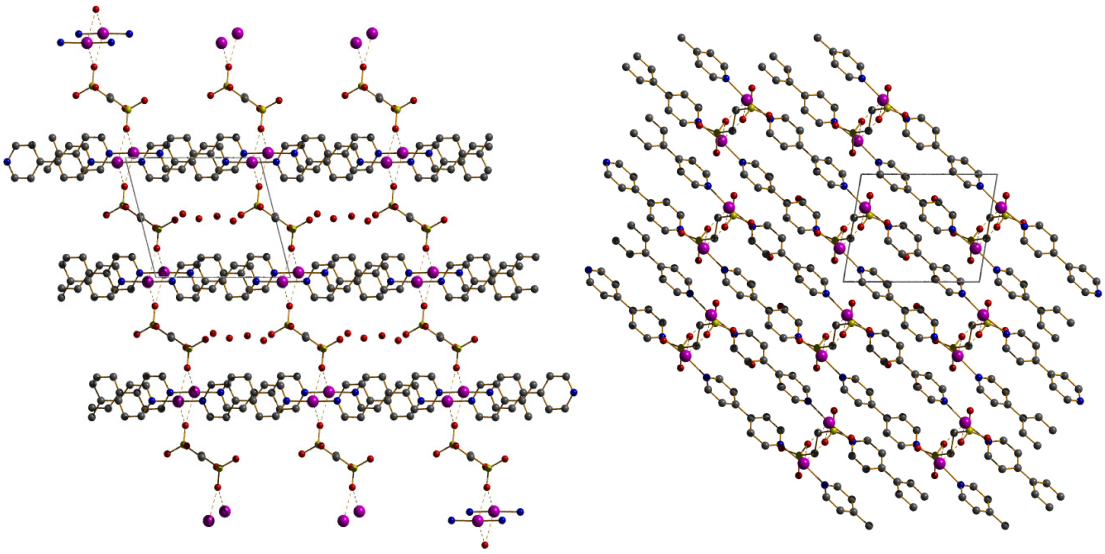

Figure 2.3 Crystallographic *a*-projection (left) and *b*-projection (right) of the structure with hydrogen atoms omitted for clarity (silver: purple; carbon: gray; sulfur: yellow; oxygen: red; nitrogen: blue).

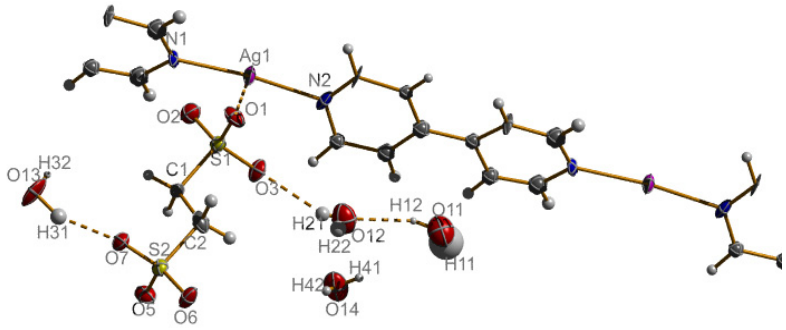

Figure 2.4 ORTEP diagram and atomic labeling of SLUG-21.

2.3.2 Thermal Characterization

The thermal stability of SLUG-21 was also investigated in detail by TGA-MS under nitrogen flow and *ex-situ* PXRD (Figure 2.5 and Figure 2.6, respectively). An 8.0 % weight loss occurs after heating to 120°C owing to the removal of most of interlamellar water molecules (calculated: 9.13 %). The increase in the m/e=18 signal also supports the loss of water. *ex-situ* PXRD shows reduction in crystallinity and slight phase transformation, but an open structure is retained. The higher temperature phase is stable up to ca. 300 °C, when the bipyridine decomposes by 350 °C (observed: 40.2 %, expected: 39.6%). No major signal for either m/e=18 or m/e =64

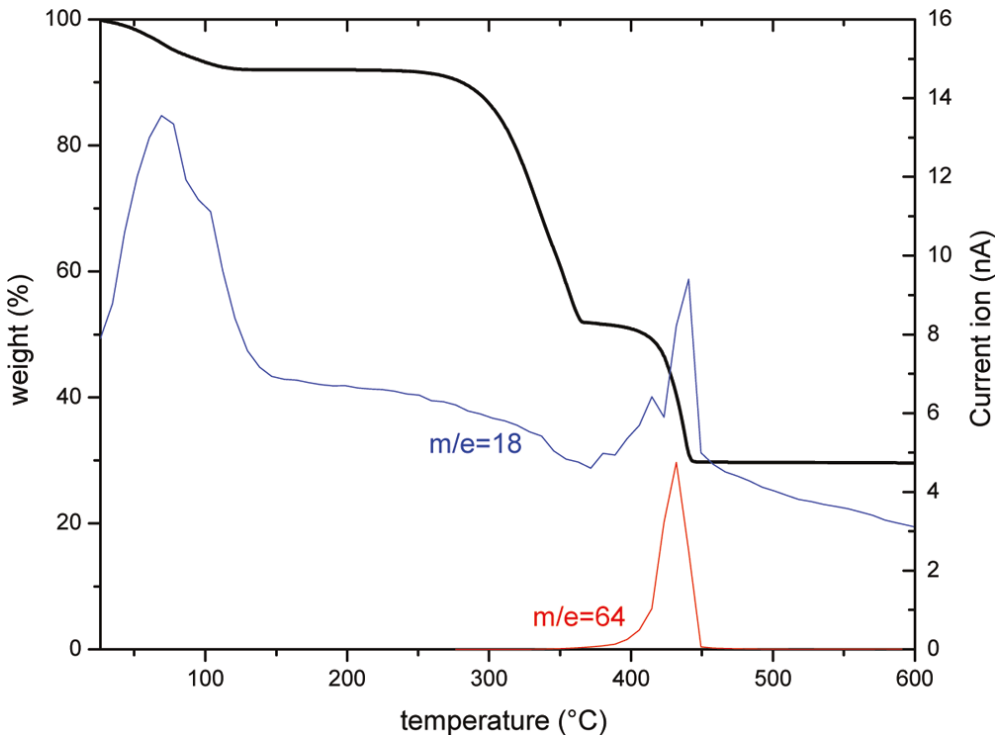

Figure 2.5 Thermogravimetric trace (black) and coupled mass spectra (red, blue) of SLUG-21.

also implies organic decomposition in this temperature range. The TGA trace is then stable state up to 400°C, when another weight loss occurs. This event corresponds to loss of EDS anion (observed: 27.6%, expected: 29.2 %), leaving a pure silver phase as confirmed by *ex-situ* PXRD after 450°C (Figure 2.6). The coupled mass spectra at m/e=64 appears to verify this decomposition step, with removal of SO_2 fragment.

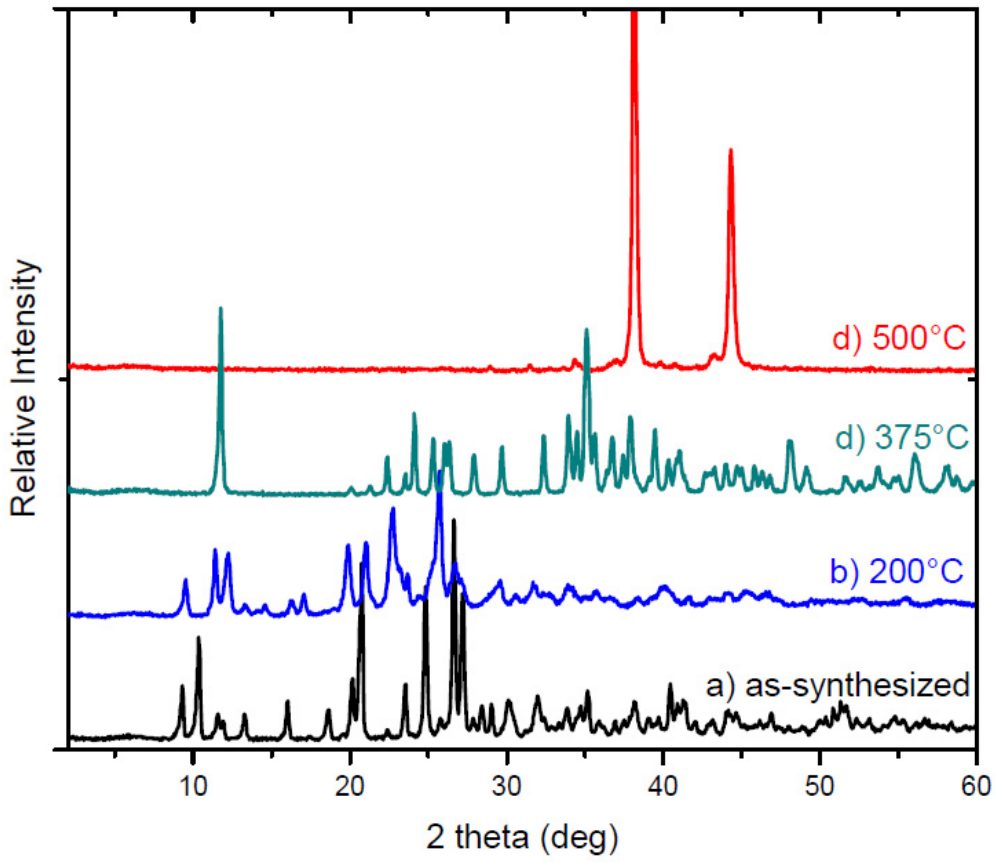

Figure 2.6 PXRD of (a) as-synthesized SLUG-21 and *ex-situ* measurements after heating in ambient atmosphere to (b) 200°C; (c) 375°C; (d) 500°C.

2.3.3 Catalytic Applications

Considering Ag(I) is typically three to six coordinate among coordination polymers,[142-145,151-153] the two-coordinate Ag(I) sites in SLUG-21 are coordinatively unsaturated owing to the weak bonding by the EDS anions. In addition, the linear geometry metal sites are accessible by one-dimensional pores running along both the *a*-axis (Figure 2.3). The lack of any metal hydroxyl groups and the observation of constant pH at 6.5 when SLUG-21 is placed in unbuffered deionized water indicates the material is Lewis rather than Bronsted catalytic. Considering these factors, we investigated the Lewis acid catalytic activity of the compound.

Scheme 2.1 Acid catalyzed ketal formation between 2-butanone and ethylene glycol.

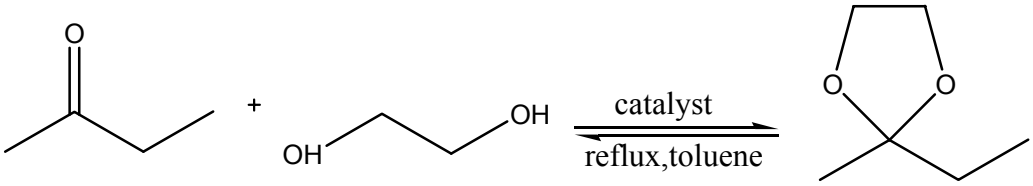

Ketalization of aldehydes and ketones is important for the protection of carbonyl groups in preparative organic synthesis, especially drug design.[154] While toluenesulfonate is a standard catalyst, it is homogeneous and must be separated from the product by concentrating the products under vacuum.[155] Recent heterogeneous catalysts such as tetrabutylammonium tribromide experience at least one of the following problems: (i) toxicity; (ii) high cost; (iii) difficulty in preparation; (iv) low

yield for catalytic reaction.[156-158] The mechanism of the reaction requires the Lewis acid catalyst to activate the oxygen of the carbonyl group, allowing glycol to substitute for the ketone group. Our cationic silver-based compound was tested for ketal formation between 2-butanone and ethylene glycol (Scheme 2.1). The results reveal that SLUG-21 is a strongly active and reusable catalyst.

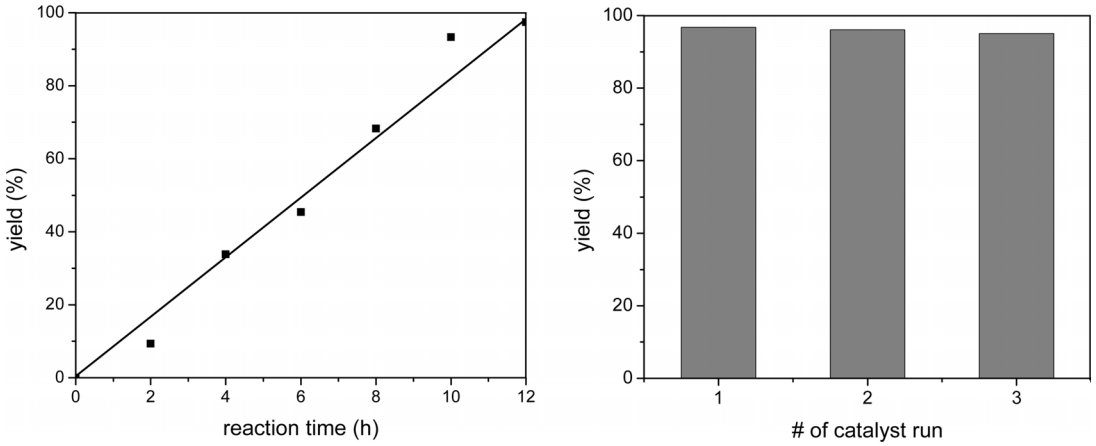

Figure 2.7 Yields for ketal formation by SLUG-21. left: yield vs. time plot; right: the high conversion yield is retained upon recycling the material.

We used 0.127 mmol of SLUG-21 to catalyze a reaction between 70 mmol 2-butanone and 70 mmol ethylene glycol, for a catalytic ratio of 1 to 552. With a Dean-Stark trap to constantly remove the water, ketal product increases linearly until almost complete conversion after 12 hours (Figure 2.7 left, Table 2.3). Compared with a blank experiment without catalyst under the same conditions and period of time, only negligible product has been formed (Table 2.3), confirming that SLUG-21 is an efficient Lewis acid catalyst. Controlled experiments for the catalysis have been

Scheme 2.2 Acid catalyzed esterification between acetic acid and ethanol.

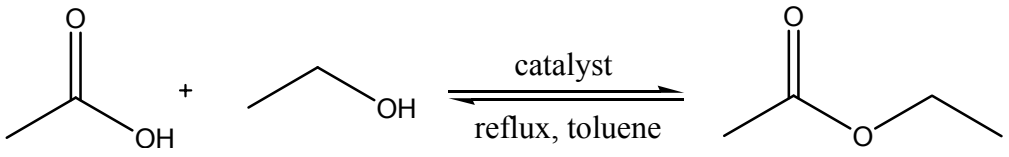

conducted by filtration off SLUG-21 after 6 hours' reaction to determine whether there is the Ag metal site or a certain species inside the SLUG-21 serves the catalytic function. Further 12 hours' reaction after catalysis achieving less than 2 % more ketal yields proves SLUG-21's open Ag metal site serving as Lewis acid catalytic function, and negligible mass loss of SLUG-21 further supports its stability during the reaction. Besides ketalization of 2-butanone, different ketone precursors, such as acetone and 2-pentanone, have also been carried out the same catalytic reactions. The ~ 90 %

Table 2.3 Conversion Yields for Catalytic Reactions

reaction	catalyst	time (h)	conv (%)[a]
ketalization	no catalyst	12	1
ketalization	hydrothermal SLUG-21	12	97
ketalization	reflux SLUG-21	12	96
ketalization	room-temp stirring SLUG-21	12	95
esterification	no catalyst	8	<10
esterification	hydrothermal SLUG-21	8	57

[a] The conversion efficiency is determined by ^{1}H NMR.

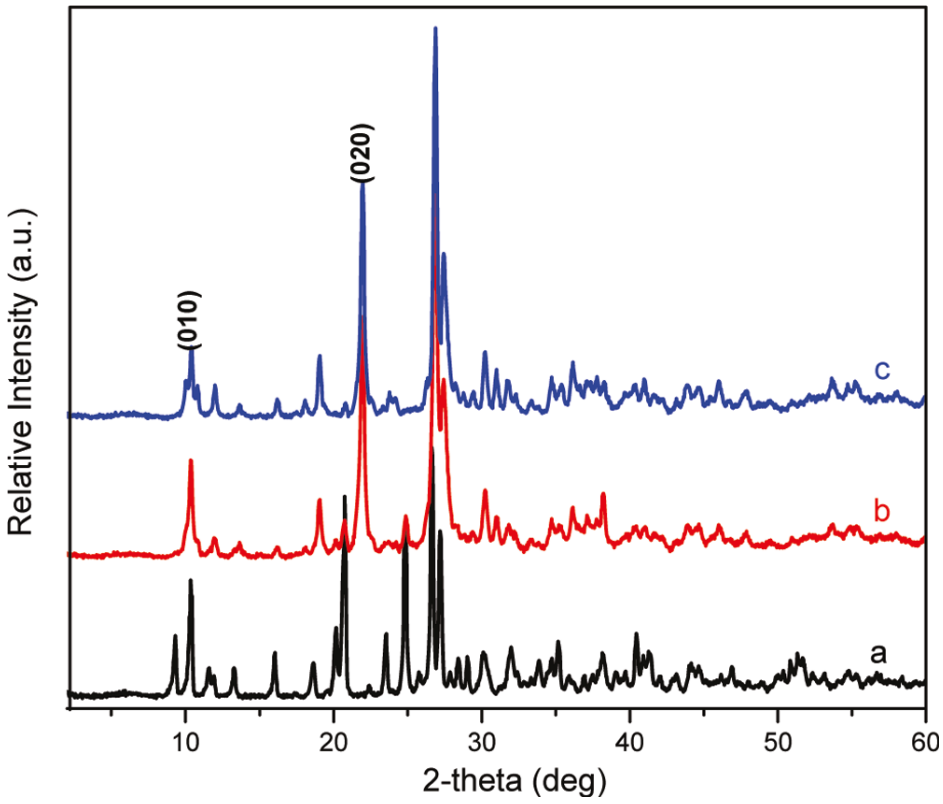

Figure 2.8 PXRD of (a) as-synthesized SLUG-21; post-catalysis after one (b) and three (c) catalytic cycles of ketal formation.

yield proves SLUG-21 is a highly efficient and general catalyst in catalyzing ketalization reactions, while the reactions lasts for the same period without SLUG-21 have negligible yield. The ketalization of 2-pentanone displayed relatively lower yield (87 %) is possibly due to slower diffusion into the MOF pores by the bulky precursor size .

As previously mentioned, the structure is slightly transformed upon partial removal of intercalated water (Figure 2.7). There is lattice shrinkage along b axis determined by the right shift of both (010) and (020) PXRD peaks, and b axis is along the EDS linker and intercalated water molecules. This activated form is likely the

responsible for the catalysis. There is a small amount of mass loss of catalyst after each cycle (ca. 10 % weight loss after the first cycle and negligible weight loss thereafter). The activated form of SLUG-21 is thus stable for this catalytic reaction and highly reusable, achieving similar yields through three cycles (Figure 2.7 right, and Figure 2.8). We also tested the catalytic ability of SLUG-21 prepared under ambient and reflux conditions and both showed similarly high yield (Table 2.3). All of the as-synthesized crystals thus have almost equivalent Lewis acid catalytic ability as well as reusability. Both ambient pressure routes also give the same activated form by TGA and *ex-situ* PXRD, achieving similar yields and reusability through at least three runs (Table 2.4).

To further test the Ag(I) Lewis acid catalytic site activity, we also carried out an esterification reaction. This reaction has attracted increasing interest for potential application in biofuels. A stronger acid catalyst, however, is required to activate the carbonyl group of carboxylic acid, the conventional homogeneous catalyst being condensed sulfuric acid.[159] We carried out the esterification between acetic acid and

Table 2.4 High yields are also achieved by different synthetic methods (hydrothermal, reflux and room temperature stirring) for ketal formation catalysis and show reusability after at least three cycles.

# of catalytic run	1	2	3
Hydrothermal made	97 %	96 %	95 %
Refluxing made	96 %	97 %	96 %
Room-temp stirring made	95 %	94 %	96 %

ethanol with SLUG-21 as catalyst, and 0.18 mol % of crystals (for a catalytic ratio of 556 to 1) gave a yield of 57 % after 8 hours reaction without taking further steps to remove the water byproduct (Table 2.3, Scheme 2.2). Longer reaction time gave no improvement to the yield. Nevertheless, the satisfactory yield proves that SLUG-21 functions as esterficiation catalyst. The additional esterification experiments between formic acid and ethanol with SLUG-21 as catalyst reached over 70 % yield further support the generality of its esterification catalyzing property. The higher yield in formic acid is possibly due to smaller precursor size, thus more swift diffusion into the pore of extended framework.

2.4 Conclusions

The cationic Ag(I)-based MOF was isolated using a mixture of organic linker and anionic template. This strategy may lead to the discovery of other cationic extended frameworks with open metal sites for catalytic applications. The compound exhibits chemical stability in various solvents, as well as excellent Lewis acid catalytic ability by viture of its open, coordinatively unsaturated metal sites. The catalyst can be continuously reused in the heterogeneous catalytic reaction without losing activity or significant mass of crystals. The material is synthesized in one step under ambient conditions, ideal for scale-up to industrial scale.

2.5 References

119. Cheetham, A. K.; Rao, C. N. R.; Feller, R. K. *Chem. Commun.* **2006**, 4780–4795.

120. Wu, C. D.; Hu, A.; Zhang, L.; Lin, W. B., *J. Am. Chem. Soc.* **2005,** *127*, 8940-8941.

121. Horike, S.; Dinca, M.; Tamaki, K.; Long, J. R., *J. Am. Chem. Soc.* **2008,** *130*, 5854-5855.

122. Lee, J.; Farha, O. K.; Roberts, J.; Scheidt, K. A.; Nguyen, S. T.; Hupp, J. T., *Chem. Soc. Rev.* **2009,** *38*, 1450-1459.

123. Service, R. F., *Science* **2004,** *305*, 958-961.

124. Murray, L. J.; Dinca, M.; Long, J. R., *Chem. Soc. Rev.* **2009,** *38*, 1294-1314.

125. Kondo, A.; Noguchi, H.; Ohnishi, S.; Kajiro, H.; Tohdoh, A.; Hattori, Y.; Xu, W. C.; Tanaka, H.; Kanoh, H.; Kaneko, K., *Nano Letters* **2006,** *6*, 2581-2584.

126. McIntyre, L. J.; Jackson, L. K.; Fogg, A. M., *Chem. Mater.* **2008,** *20*, 335-340.

127. Vallet-Regi, M.; Balas, F.; Arcos, D., *Angew. Chem. Int. Ed.* **2007,** *46*, 7548-7558.

128. Wight, A. P.; Davis, M. E., *Chem. Rev.* **2002,** *102* (10), 3589-3613.

129. Wang, Z.; Chen, G.; Ding, K. L., *Chem. Rev.* **2009,** *109* (2), 322-359.

130. Henschel, A.; Gedrich, K.; Kraehnert, R.; Kaskel, S., *Chem. Commun.* **2008,** 4192-4194.

131. Alaerts, L.; Seguin, E.; Poelman, H.; Thibault-Starzyk, F.; Jacobs, P. A.; De Vos, D. E., *Chem. Eur. J.* **2006,** *12*, 7353-7363.

132. Sudik, A. C.; Cote, A. P.; Yaghi, O. M., *Inorg. Chem.* **2005,** *44*, 2998-3000.

133. Chen, X. D.; Wan, C. Q.; Sung, H. H. Y.; Williams, I. D.; Mak, T. C. W., *Chem. Eur. J.* **2009,** *15*, 6518-6528.

134. Custelcean, R.; Gorbunova, M. G., *J. Am. Chem. Soc.* **2005,** *127*, 16362-16363.

135. Swanson, C. H.; Shaikh, H. A.; Rogow, D. L.; Oliver, A. G.; Campana, C. F.; Oliver, S. R. J., *J. Am. Chem. Soc.* **2008,** *130*, 11737-11741.

136. Rogow, D. L.; Zapeda, G.; Swanson, C. H.; Fan, X.; Campana, C. F.; Oliver, A. G.; Oliver, S. R. J., *Chem. Mater.* **2007,** *19*, 4658-4662.

137. Tran, D. T.; Zavalij, P. Y.; Oliver, S. R. J., *J. Am. Chem. Soc.* **2002,** *124*, 3966-3969.

138. Gandara, F.; Puebla, E. G.; Iglesias, M.; Proserpio, D. M.; Snejko, N.; Monge, M. A., *Chem. Mater.* **2009,** *21*, 655-661.

139. Oliver, S. R. J., *Chem. Soc. Rev.* **2009,** *38*, 1868-1881.

140. Forster, P. M.; Tafoya, M. M.; Cheetham, A. K., *J. Phys. Chem. Solids* **2004,** *65*, 11-16.

141. Hu, S.; He, K. H.; Zeng, M. H.; Zou, H. H.; Jiang, Y. M., *Inorg. Chem.* **2008,** *47*, 5218-5224.

142. Makinen, S. K.; Melcer, N. J.; Parvez, M.; Shimizu, G. K. H., *Chem. Eur. J.* **2001,** *7*, 5176-5182.

143. Hoffart, D. J.; Dalrymple, S. A.; Shimizu, G. K. H., *Inorg. Chem.* **2005,** *44*, 8868-8875.

144. Ma, J. F.; Yang, J.; Li, S. L.; Song, S. Y., *Cryst. Growth Des.* **2005,** *5*, 807-812.

145. Cote, A. P.; Ferguson, M. J.; Khan, K. A.; Enright, G. D.; Kulynych, A. D.; Dalrymple, S. A.; Shimizu, G. K. H., *Inorg. Chem.* **2002,** *41*, 287-292.

146. Fan, X. J.; Demaree, D. P.; John, J. M. S.; Tripathi, A.; Oliver, S. R. J., *Appl. Phy. Lett.* **2008,** *92*.

147. Nakade, S.; Saito, Y.; Kubo, W.; Kitamura, T.; Wada, Y.; Yanagida, S., *J. Phys. Chem. B* **2003,** *107*, 8607-8611.

148. Seward, C.; Chan, J. L.; Song, D. T.; Wang, S. N., *Inorg. Chem.* **2003,** *42*, 1112-1120.

149. Budka, J.; Lhotak, P.; Stibor, I.; Sykora, J.; Cisarova, I., *Supramolecular Chemistry* **2003,** *15*, 353-357.

150. Aguado, J. E.; Canales, S.; Gimeno, M. C.; Jones, P. G.; Laguna, A.; Villacampa, M. D., *Dalton Trans.* **2005,** 18, 3005-3015.

151. Gu, X. J.; Xue, D. F., *Crys Growth Des.* **2006,** *6*, 2551-2557.

152. Yaghi, O. M.; Li, H. L., *J. Am. Chem. Soc.* **1996,** *118*, 295-296.

153. Gu, X. J.; Xue, D. F., *Inorg. Chem.* **2006,** *45*, 9257-9261.

154. Tsuchiya, T.; Ohmuro, S., *Tetra. Lett.* **2002,** *43*, 611-615.

155. Patel, M. V.; Bell, R.; Majest, S.; Henry, R.; Kolasa, T., *J. Org. Chem.* **2004,** *69*, 7058-7065.

156. Gopinath, R.; Haque, S. J.; Patel, B. K., *J. Org. Chem.* **2002,** *67*, 5842-5845.

157. Wang, B.; Gu, Y. L.; Song, G. Y.; Yang, T.; Yang, L. M.; Suo, J. S., *J. Mol. Catal. A-Chemistry* **2005,** *233*, 121-126.

158. Ren, Y. M.; Cai, C., *Tetra. Lett.* **2008,** *49*, 7110-7112.

159. Wu, J. H.; Hao, S.; Lan, Z.; Lin, J. M.; Huang, M. L.; Huang, Y. F.; Li, P. J.; Yin, S.; Satot, T., *J. Am. Chem. Soc.* **2008,** *130*, 11568-11569.

Chapter 3

Anion Exchange and Catalytic Properties of Two Cationic Metal-Organic Frameworks Based on Cu(I) and Ag(I)

Abstract

We report the synthesis and characterization of two Ag(I)/Cu(I)-based cationic metal-organic frameworks and their application in both heterogeneous catalysis and anion exchange. The Cu(I)-based material was designed from our previously reported Ag(I) cationic topology. Both structures consist of cationic layers with π-π stacked chains of alternating metal and 4,4'-bipyridine. α,ω-alkanedisulfonate serves as anionic template, electrostatically bonding to the cationic layers. Due to weak interaction between the sulfonate template and cationic extended framework, both materials display reversible anion exchange for a variety of inorganic species. Indeed, the Ag(I)-based material exhibits highly efficient uptake of permanganate and perrhenate anion trapping, a model for pertechnetate trapping. The materials also display heterogeneous Lewis acidity, likely due to the coordinatively unsaturated metal sites which only bind to two bipy nitrogens and a

weak interaction with one sulfonate oxygen. A comparative study on the influence of structure versus size-selectivity and reusability for both exchange and catalysis is discussed.

3.1 Introduction

Anionic pollutants such as perchlorate (ClO_4^-), arsenate (AsO_4^{3-}) and chromate (CrO_4^-) are becoming increasingly problematic and are listed as EPA (U.S. Environmental Protection Agency) priority pollutants.[160] Perchlorate contamination of water by spent rocket fuel was reported in the lower Colorado River in 2002.[161] At the same time, organic anion pollution from pharmaceuticals—which are also intrinsically anionic—is now a worldwide problem, as most wastewater treatment ineffectively removes pharmacological anions.[162] Resins with cationic groups and exchangeable counter anions are still considered the standard ion exchanger.[163,164] These are of limited thermal and chemical stability, however, due to their organic polymer nature.[165] Layered double hydroxides (LDHs), an isostructural group of structures based on brucite with a general formula $[M^{2+}_{1-x}M^{3+}_{x}(OH)_2]A^{n-}_{x/n}\cdot mH_2O$, where M^{2+} and M^{3+} are a range of metals and A^{n-} are intercalated anions (e.g. CO_3^{2-}), are considered to be an ideal alternative to anion exchange materials.[166] A variety of both inorganic and organic species are able to reversibly exchange into LDHs.[167-169] In many cases, however, the anion either cannot be removed or will de-intercalate in the presence of common anions such as carbonate.[170-174] The need for materials

qualified to trap or exchange both inorganic and organic anions remains. A recent development is a nanoporous cationic metal borate that on initial studies reversibly traps anions including pertechnetate, though the material is based on slightly radioactive thorium and anion capacity was 72 %.[175]

New heterogeneous catalysts with greater reusability, efficiency and ease of synthesis are continuously sought for environmental concerns. Micro/mesoporous materials have been extensively studied for their high internal surface area where the pore/channel catalytic sites lead to improved efficiency.[176] Microporous inorganic-organic hybrid materials with coordinatively unsaturated metal sites continue to be discovered, with Lewis acid catalytic properties.[177-179] There have been few systematic investigations, however, on the rational design of extended frameworks with coordinatively unsaturated metal sites and controlled pore/channel size for size-selective Lewis acidity.

Metal-organic frameworks (MOFs) have received remarkable attention in recent years not only because of their intriguing structures but also their use in gas absorption/storage,[180,181] gas separation[182,183] and ion exchange.[184,185] As a small sub-group of MOFs, cationic MOFs occur when the positive charge on the metal ions outnumber the negative (or neutral) charge on the organic linkers. The net positive charge on the framework necessitates charge-balancing extra-framework anions.[186-192] Among this group of cationic MOFs, only a few have been investigated for reversible anion exchange.[187,189,191] There has been no investigation of anion pollutant trapping by exchange of organic species for inorganic molecules.

Herein, we report the first cationic MOFs that possess both chemical stability for recyclable heterogeneous catalysis and structural flexibility for reversible anion exchange. The first is a Cu(I)-based cationic MOF similar to our recently reported $Ag_2(4,4'\text{-bipy})_2(O_3SCH_2CH_2SO_3)\cdot 4H_2O$ (SLUG-21).[193] The materials were designed to have weak electrostatic interaction between the interlamellar anions and cationic MOF layers. As a result, both display reversible anion exchange between organosulfonate and various inorganic species. SLUG-21 has also been applied for anion trapping of MnO_4^- and ReO_4^- as a model for pertechnetate, a problematic pollutant.[194] We also report a detailed comparative study of the two materials towards size-selective heterogeneous Lewis acid catalysis.

3.2 Experimental Section

3.2.1 Reagents

Silver nitrate ($AgNO_3$, Fisher, 99 %), copper acetate monohydrate [$Cu(CH_3COO)_2\cdot H_2O$, Alfa-Aesar, 98 %], 1,2-ethanedisulfonic acid ($HO_3SCH_2CH_2SO_3H$, TCI Inc., 95 %) and 4,4'-bipyridine [$(C_5H_4N)_2$, Acros Organics, 98 %] were used as-received for the synthesis. Sodium nitrate ($NaNO_3$, Fisher, 99 %), sodium perchlorate monohydrate ($NaClO_4\cdot H_2O$, Fluka Analytical, 98 %), potassium permanganate ($KMnO_4$, Fisher, 99.8 %), potassium perrhenate ($KReO_4$, Acros Organics, 99 %) and 1,2-ethanedisulfonic acid disodium salt

($NaO_3SCH_2CH_2SO_3Na$, TCI Inc., 95 %) were used as-purchased for the reversible anion exchange reactions. 2-butanone ($CH_3COCH_2CH_3$, Acros Organics, 99 %), 2-pentanone ($CH_3COCH_2CH_2CH_3$, TCI America, 97 %), benzophenone ($C_6H_5COC_6H_5$, Alfa-Aesar, 99 %), ethylene glycol ($HOCH_2CH_2OH$, Acros Organics, 99 %) and toluene ($C_6H_5CH_3$, Fisher, 99.7 %) were used as-purchased for the catalytic studies.

3.2.2 Synthesis

Yellow-brown crystals of $Cu_2(4,4'\text{-bipy})_2(O_3SCH_2CH_2SO_3)\cdot 3H_2O$ (which we denote SLUG-22: University of California, Santa Cruz, structure no. 22) were synthesized under hydrothermal conditions. A mixture of $Cu(CH_3COO)_2\cdot H_2O$ (0.27 g, 1.35 mmol), $HO_3SCH_2CH_2SO_3H$ (0.29 g, 1.52 mmol), 4,4'-bipyridine (0.21 g, 1.34 mmol) and 10 ml water was stirred at room temperature for 10 min and then transferred to a 15 ml Teflon lined autoclave to 2/3 filling. The autoclaves were heated at 175 °C for 4 days under autogeneous pressure, followed by slow cooling at a rate of 6 °C/h to room temperature. During the reaction, the pH slightly decreased from 4.1 to 3.5. Yellow-brown block crystals were isolated after filtration and rinsed with water and acetone (yield: 0.46 g, 95 % based on copper acetate). IR (KBr pellets): 3467s (O-H stretch), 3050m (aromatic C-H stretch); 1605s, 1535s, 1490s, 1418s (aromatic C=C and C=N stretch); 1328s (CH_2 stretch); 1200m, 1070m (SO_3 stretch); 863s, 817s (aromatic C-H bending).

Colorless crystals of SLUG-21 were synthesized under hydrothermal conditions or at room temperature as previously reported.[193] A reactant solution with

a molar ratio of 1:1:1:400 for $AgNO_3$: EDSA : 4,4'-bpy : H_2O were placed into a 15 ml Teflon-lined autoclave to 2/3 filling and heated at 150 °C for 5 days under autogeneous pressure. For both compounds, the product was filtered, rinsed with acetone and allowed to air dry.

3.2.3 Anion Exchange

100 mg of either SLUG-21 (0.126 mmol) or SLUG-22 (0.147 mmol) solid was placed into 20 ml of 0.1 M $NaNO_3$ or $NaClO_4$ solution, and allowed to react either statically for 7 days or with mild stirring for 1 to 3 days. The exchange solution and solid were monitored at various time intervals to follow the exchange progress. The crystal products were isolated by filtration and rinsed with water/acetone. The crystals after $NaNO_3$ or $NaClO_4$ exchange were placed into excess 0.1 M EDS disodium salt solution. The mixture was gently stirred for 3 days, followed by filtration to isolate the solid product and exchange solution after the second exchange. The entire process was repeated several times.

3.2.4 Heterogeneous Catalysis

Ketal formation with various substrates was used to characterize the performance of both SLUG-21 and SLUG-22 as Lewis acid catalyst. 100 mg of the as-synthesized catalyst, 70 mmol of ketone (2-butanone, 2-pentanone or benzophenone) and 70 mmol of ethylene glycol were introduced into 80 mmol of

toluene, the latter used as solvent. The reaction was refluxed at 110 °C under Dean-Stark conditions for 12 hours and/or 24 hours. The catalyst was isolated by filtration and reused on subsequent runs without further treatment. All product yields were determined by ^{1}H NMR (supporting information).

3.2.5 Instrumental Details

Samples for powder X-ray diffraction (PXRD) were measured on a Rigaku Americas Miniflex Plus diffractometer, and were scanned from 2 to 60°(2θ) at a rate of 2° per minute and 0.04° step size under Cu-Kα radiation (λ = 1.5418 Å). Single-crystal X-ray diffraction data for SLUG-22 were collected at Beamline 11.3.1 at the Advanced Light Source (ALS), Lawrence Berkeley National Laboratory (λ = 0.77490 Å). The structure was solved by direct methods and refined with SHELXTL.[195] The models were refined by full-matrix least-squares analysis of F^2 against all reflections. All non-hydrogen atoms were refined with anisotropic thermal displacement parameters. Crystal structure views were obtained using Diamond v3.2 and rendered by POV-Ray v3.6. Thermogravimetric analysis (TGA) was performed using a TA Instruments 2050 TGA by heating from 30 to 700 °C under N_2 purge with a gradient of 15 °C/min. *In-situ* mass spectra coupled to the TGA were collected on a Pfeiffer Vacuum ThermoStar GSD 301 T3 mass spectrometer with a 70 eV ionization potential. UV-Vis spectroscopic studies were collected on a Hewlett-Packard Model 8452A spectrophotometer to monitor the exchange progress. Fourier transform infrared (FTIR) spectroscopy of the materials was collected on a Perkin-Elmer

Spectrum One spectrophotometer with KBr pellets. ^{1}H NMR spectra were collected with a Varian Oxford 600 MHz spectrometer by dissolving the sample in 700 μL of deuterated choloroform with tetramethylsilane as internal standard.

Table 3.1 Crystallographic information, data collection and refinement parameters for SLUG-22

empirical formula	$Cu_2C_{22}H_{26}O_9N_4S_2$
formula weight ($g \cdot mol^{-1}$)	681.71
temperature (K)	150(2)
wavelength (Å)	0.77490 (synchrotron)
crystal system	triclinic
space group	P-1
unit cell dimensions	*a*=8.9031(9) Å *b*=10.9120(11) Å *c*=14.4304(10) Å α=103.6150(10)° β=102.272(2)° γ=97.5290(10)°
volume ($Å^3$)	1307.0(2)
Z	2
crystal descriptions	yellow block
crystal size (mm^3)	0.05×0.04×0.04
index range	$-11 \leq h \leq 11$, $-13 \leq k \leq 13$, $-18 \leq l \leq 18$
density (calculated $g \cdot cm^{-3}$)	1.732
reflections collected	14355
unique reflections	5316
final *R* indices [$I > 2\sigma(I)$]	$R_1 = 0.0371$, $wR_2 = 0.0957$
R indices (all data)	$R_1 = 0.0500$, $wR_2 = 0.1021$
largest diff. peak and hole	-0.63 and $0.67\ e^- \cdot Å^{-3}$
goodness of fit on F^2	1.037

3.3 Results and Discussion

3.3.1 Synthesis

Yellow block crystals of SLUG-22 were obtained hydrothermally as pure phase and high yield at 175 °C and pH ~ 4.1. Lower temperature (125 °C or 150 °C) or slight change in the pH led to lower crystallinity and an unidentified impurity in the product that could be observed by optical microscopy. During the hydrothermal synthesis, the Cu(II) reagent was reduced to Cu(I), as observed by the color change between copper precursor and product. Unlike SLUG-21, the material cannot be

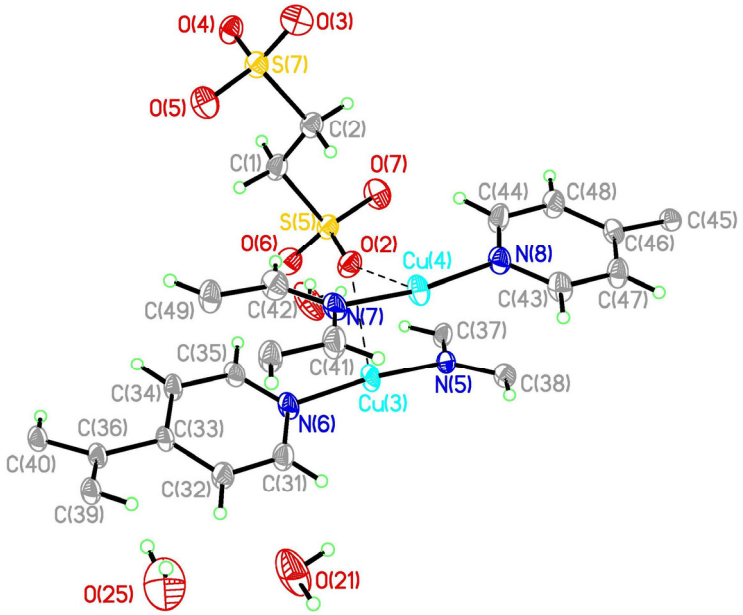

Figure 3.1 ORTEP diagram and atomic labeling of SLUG-22. Thermal ellipsoids are shown at 50% probability.

synthesized at room temperature or reflux conditions, and non-aqueous solvents were unsuccessful. The synthesized product was insoluble in water, acetone, ethanol and other common organic solvents.

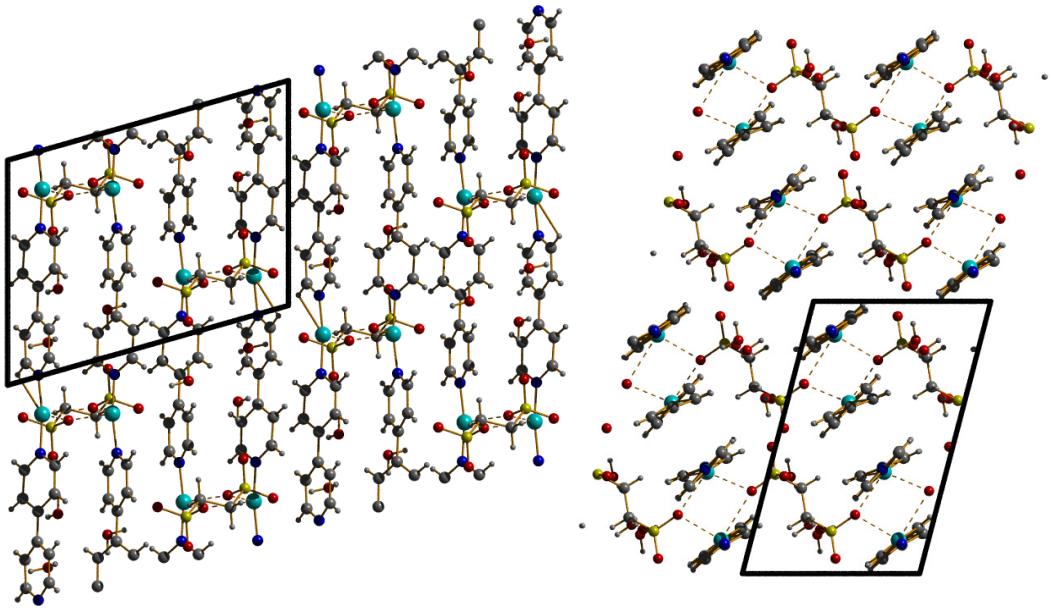

Figure 3.2 Crystallographic *a*-projection (left) and *b*-projection (right) of the SLUG-22 structure with hydrogen atoms omitted for clarity (copper: green; carbon: gray; sulfur: yellow; oxygen: red; nitrogen: blue).

3.3.2 Structural Characterization

SLUG-22 crystallizes in a triclinic system with P-1 space group (Table 3.1), which is the same as our previous reported SLUG-21 structure. Synchrotron single-crystal X-ray diffraction studies reveal that the structure of SLUG-22 is also a cationic one-dimensional MOF with infinite chains composed of alternating copper(I) centers and 4,4'-bipy organic linkers (Figures 3.1 and 3.2). The Cu(I)-bipy chains are arranged into close-packed layers by π-π stacking between adjacent 1D chains (Figure 3.2, right). The Cu(I) atoms and its full d shell form an almost linear two-coordinate environment, with N(5)-Cu(3)-N(6) and N(7)-Cu(4)-N(8) angles between 169.40(11)° and 169.48(11)°. The distance between the adjacent Cu(I)-bipy chains is *ca*. 3.466 Å, which is in the reasonable range of π-π stacking distance,[196] leading to a cationic layer. Only one oxygen of the interlamellar EDS anions has a weak interaction towards Cu(I), with distances in the range of 2.434(2) Å to 2.501(2) Å (Figure 3.1). The *Cambridge Crystal Structure Database* indicates the median bond length of Cu(I)-O is 1.978 Å.[197] The literature bond length values between Cu(I) and a sulfonate oxygen are 2.03 Å to 2.22 Å,[198-200] further supporting only weak electrostatic interaction between the cationic Cu(I)-bipy framework and the charge-balancing EDS anion. This feature is important for the anion exchange and catalytic properties of the material that will be discussed below.

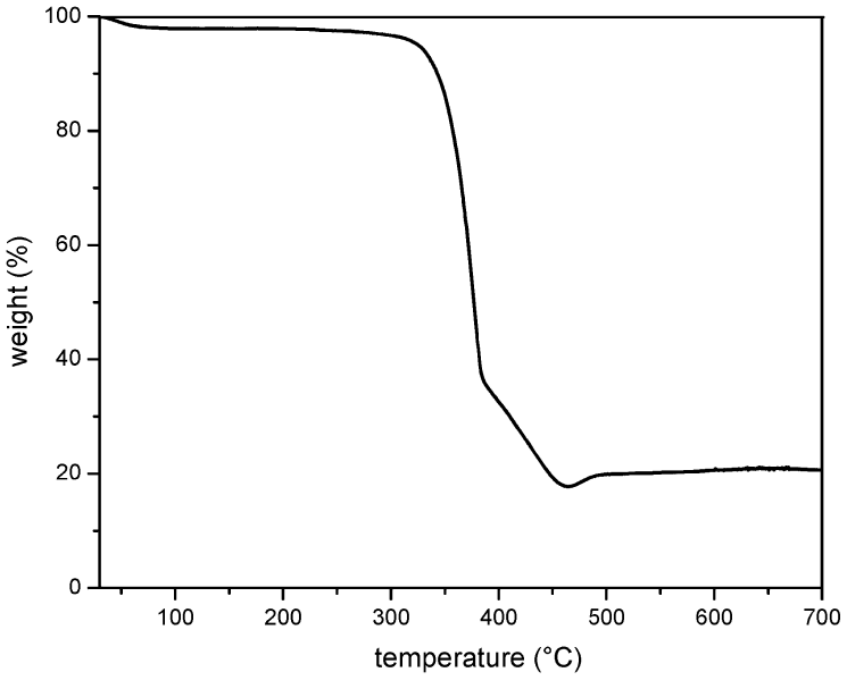

Figure 3.3 Thermogravimetric analysis of SLUG-22 in the range of 30 to 700 °C.

3.3.3 Thermal Characterization

The thermal stability of SLUG-22 was investigated by TGA under N_2 purge and *ex-situ* PXRD (Figures 3.3 and 3.4). The TGA trace of SLUG-22 indicates a slight mass loss of ~ 3 % at *ca.* 70 °C, likely due to partial loss of the interlamellar water (observed: 3.1 %; calculated: 7.9 %, Figure 3.3). In agreement with loss of the crystallographic water is a slight structural transformation observed by *ex-situ* PXRD. This structure is stable to *ca.* 325 °C, when both 4,4'-bipyridine and ethanedisulfonate ligands in the structure start to decompose. This gradual mass loss leads to metallic copper at *ca.* 450 °C (observed: 17.8 %; calculated: 18.8 %). *Ex-situ*

PXRD under N_2 flow also confirms the formation of pure phase Cu (PDF# 71-3761) above 450 °C. The slight mass increase from 450 °C to 490 °C is presumably due to nitrogen uptake.

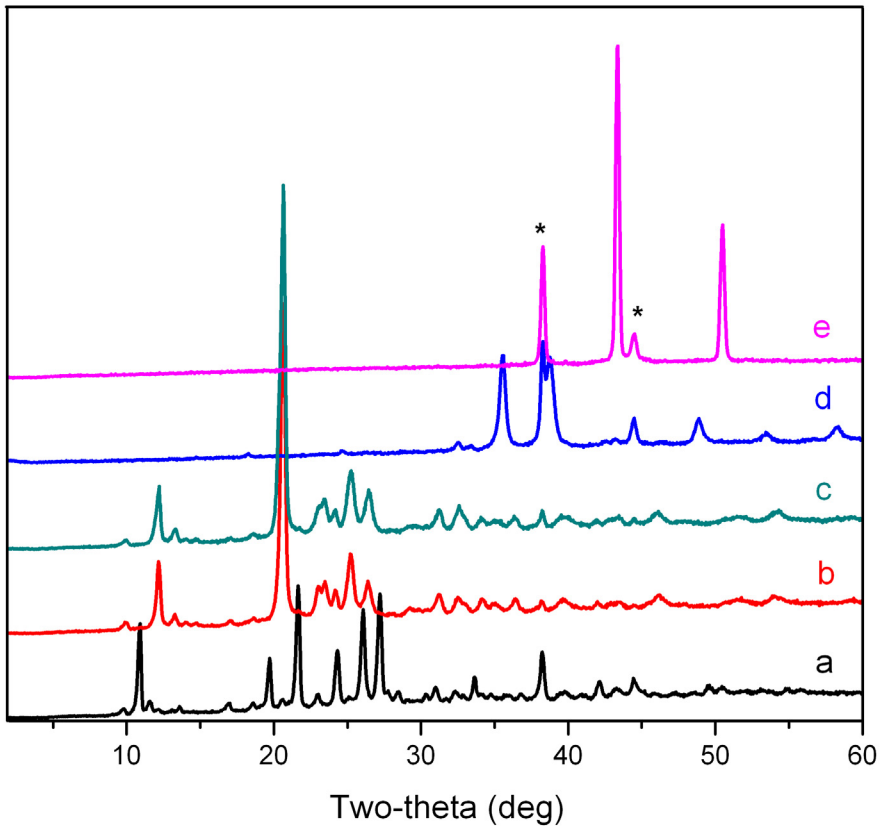

Figure 3.4 PXRD of (a) as-synthesized SLUG-22 and *ex-situ* measurements after heating in ambient atmosphere to: (b) 70°C; (c) 200°C; (d) 450°C; and (e) heating SLUG-22 under N_2 flow to 500°C indicating forming pure Cu phase. Asterisk indicates the peak of the aluminum sample holder.

3.3.4 Anion Exchange

Considering that both SLUG-22 and our previously reported SLUG-21 have only one oxygen of the EDS weakly interacting with the cationic metal-bipy layers, the materials were investigated systematically for reversible anion exchange. Many previously reported cationic inorganic materials can only exchange its extra-framework anions for smaller or similar sized inorganic anions. For example, Yu *et al.* reported Cl^- located in a microporous aluminoborate framework can be partially exchanged by Br^-.[201] A similar phenomenon is observed for the 2-D metal oxychloride francisite and its derivatives.[202] As mentioned earlier, coordination polymers have been investigated for reversible/irreversible anion exchange, including extra-framework NCS^-, N_3^-, NO_3^-, Cl^-, $CF_3SO_3^-$ and/or ClO_4^-.[187, 189, 191] Meanwhile, there have been no reports of exchange of bulky organic anions for inorganic species aside from the LDHs/hydrotalcites, which have limited reusability and anion uptake.

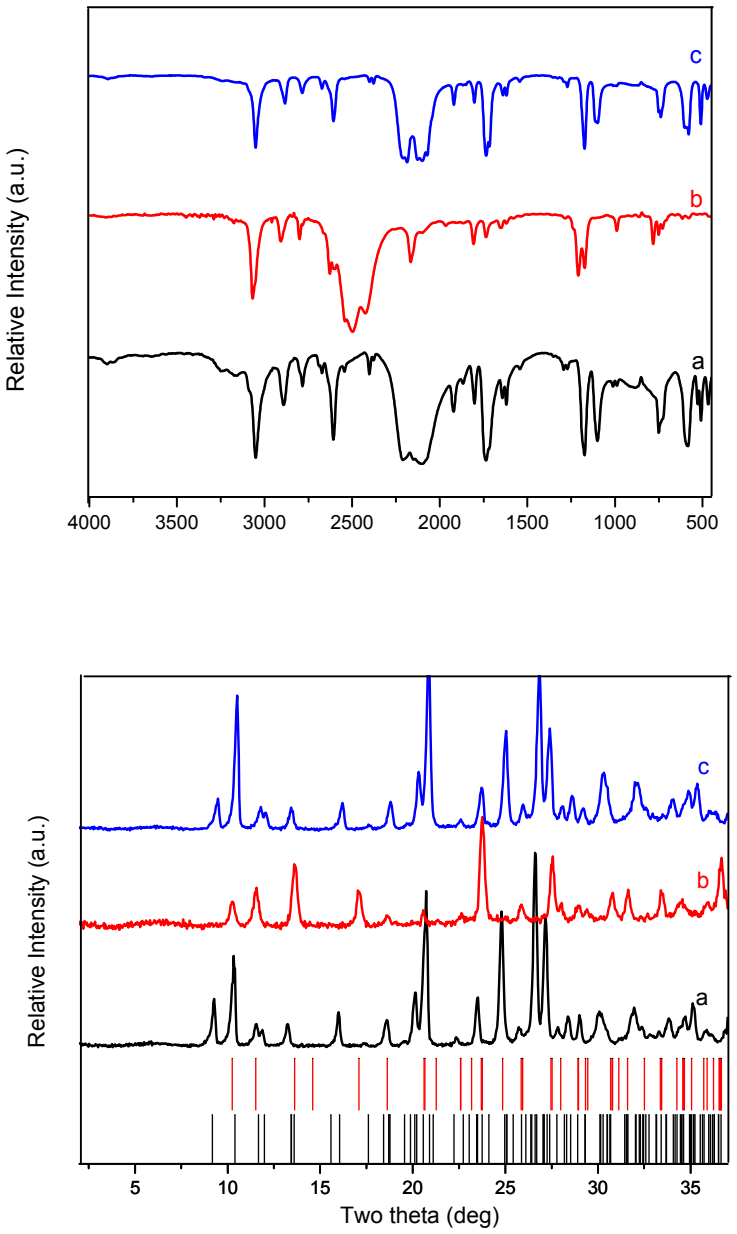

Figure 3.5 FTIR (top) and PXRD (bottom) of: (a) SLUG-21 (black); (b) the solid product after 3 days exchange reaction between SLUG-21 and 0.1 M $NaNO_3$ ("SLUG-21-NO_3", red); (c) the solid product after 3 days exchange reaction between "SLUG-21-NO_3" and 0.1 M EDS sodium salt solution (blue). Theoretical PXRD patterns of SLUG-21 (black) and SLUG-21-NO_3 (red) are shown as bars on the bottom figure.

As initial examples of exchange, we have focused on several inorganic anions for two reasons: (i) the oxo-anions of many metals are EPA priority pollutants; (ii) nitrate and perchlorate were successful templates for our previously reported cationic lead fluoride structures.[203,204] Figure 4 shows the FTIR and PXRD of the solid products after exchange of the EDS in SLUG-21 for nitrate. The four singlet bands at 1605 cm^{-1}, 1535 cm^{-1}, 1490 cm^{-1} and 1418 cm^{-1} are aromatic C=C and C=N bending, confirming the presence of 4,4'-bipy throughout the exchange, as expected. The strong, broad band at ~ 1200 cm^{-1} is characteristic of the SO_3^- group, confirming the presence of EDS anions in the initial SLUG-21 framework (Figure 3.5 top, black spectrum). By simply immersing as-synthesized SLUG-21 crystals in 0.1 M $NaNO_3$ solution at room temperature with mild stirring, both FTIR and PXRD indicate the EDS anions in SLUG-21 were completely exchanged for NO_3^- after three days

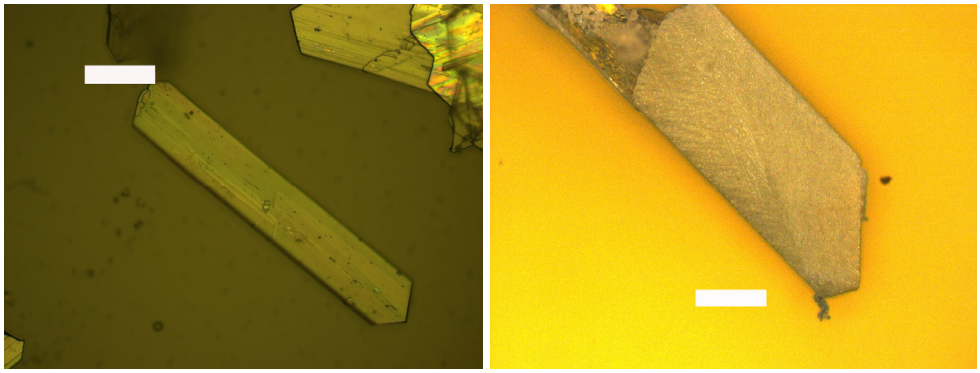

Figure 3.6 Optical micrographs of SLUG-21 before (left, 100 μm scale bar) and after (right, 200 μm scale bar) anion exchange with 0.1 M $NaNO_3$ solution.

(Figure 3.5 top, red spectra, 1330 cm^{-1}). The broad ~1200 cm^{-1} band has disappeared, with a new peak at ~ 1330 cm^{-1} characteristic of NO_3^- (N-O stretch).

PXRD further supports a complete, reversible exchange between EDS and nitrate. Although the exchanged product could not be solved by X-ray crystallography due to lower crystal quality (Figure 3.6), the resultant PXRD pattern after three days corresponds exactly to the theoretical pattern of the previously reported Ag(4,4'-bipy)NO_3.[205] The first peak is at higher angle, as expected for replacement of the larger EDS anions for the smaller nitrate molecules. The layer-to-layer distance decreased from *ca.* 4.6 Å to *ca.* 3.0 Å, with long Ag—Ag contact between the layers [*ca.* 2.976(2) Å] and the nitrates between adjacent Ag-bipy chains The bipyridine rings have thus "shuttered" upon nitrate intercalation, favoring interlayer π-π stacking. Simply immersing the nitrate exchanged product into an 0.1 M EDS disodium salt aqueous solution reforms the original SLUG-21, confirmed by both FTIR and PXRD (Figure 3.5, blue spectra) The reversibility implies that the bulky alkanesulfonate anions favors a more open framework with stronger intralayer π-π stacking. Indeed, SLUG-21 forms during the synthesis rather than Ag(4,4'-bipy)NO_3 despite the fact that silver nitrate was the synthetic reagent. In fact, SLUG-21-NO_3 reforms SLUG-21 when placed into a mixed aqueous solution of 0.1 M EDS disodium salt and 0.1 M $NaNO_3$, an analogous anionic mixture compared to the synthetic procedure. Based on these phenomenons, we conclude that SLUG-21

exchange reaction with nitrate is more induced by concentration rather than interactions between cationic framework and anion species.

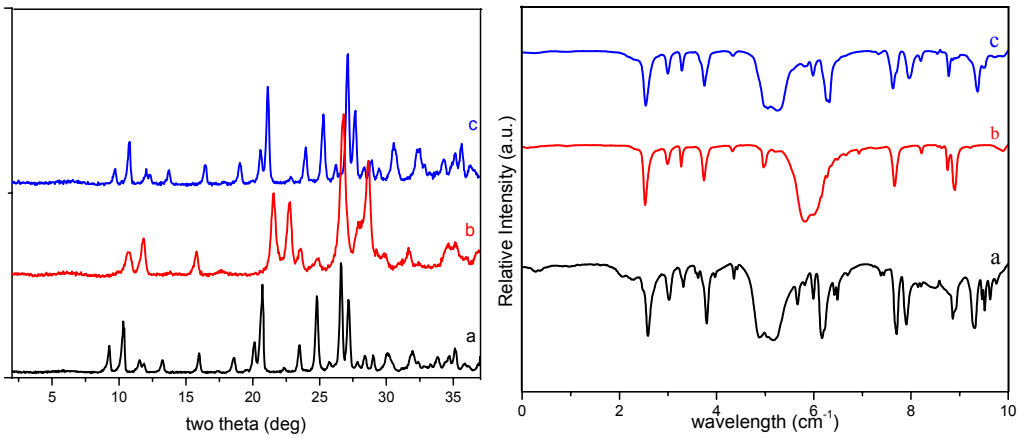

Figure 3.7 PXRD (top) and FTIR (bottom) of SLUG-21 (black traces) and SLUG-21-ClO_4 (red traces, the solid product after three days exchange reaction between SLUG-21 and 0.1 M $NaClO_4$). The solid product after three days exchange reaction between SLUG-21-ClO_4 and 0.1 M EDS sodium salt solution (blue traces) clearly indicates the reversibility.

In addition to reversible exchange with nitrate, SLUG-21 exhibits analogous chemistry with perchlorate. FTIR and PXRD (Figure 3.7) indicate that perchlorate anions intercalate into the cationic layered framework, releasing EDS and resulting in the previously reported phase Ag(4,4'-bipy)ClO_4.[206] The structure is again a cationic

layer where again the interlayer distance decreased due to smaller anion size, closer interaction to the anion [*ca.* 3.913(4) Å] and shuttering of the Ag-bipy chains to give interlayer π-π stacking.

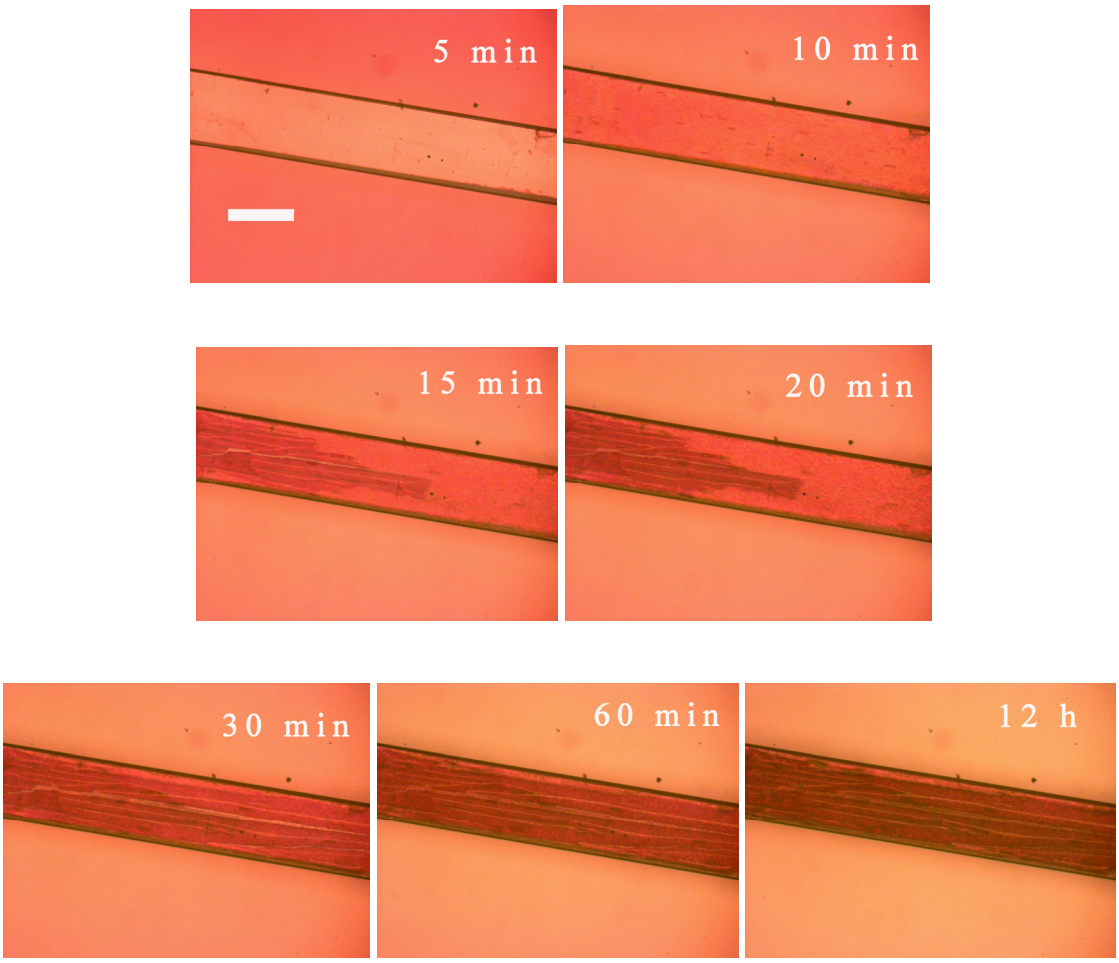

Figure 3.8 Optical micrographs of SLUG-21 crystals in permanganate solution versus time (scale bar: 500 μm).

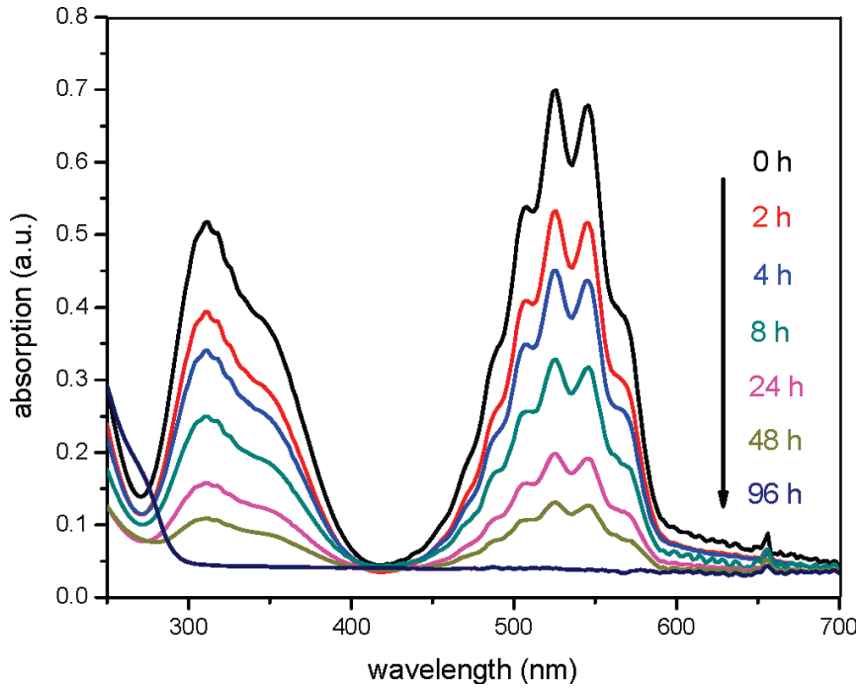

Figure 3.9 UV-Vis spectra of the permanganate solution during anion exchange with SLUG-21 at various time intervals, showing complete exchange for EDS.

As a final illustration of anion exchange capability, we investigated SLUG-21 for permanganate and perrhenate trapping. These anions were chosen as models for pertechnetate, a problematic radioactive pollutant. The trapping was monitored versus time by optical microscopy and UV-Vis spectroscopy. Figure 3.8 shows the *in-situ* optical microscopy of the anion exchange between an individual crystal of SLUG-21 and stoichiometric excess 1.26 mM aqueous permanganate solution. A visible color change of both crystals (more were present outside the image area) and

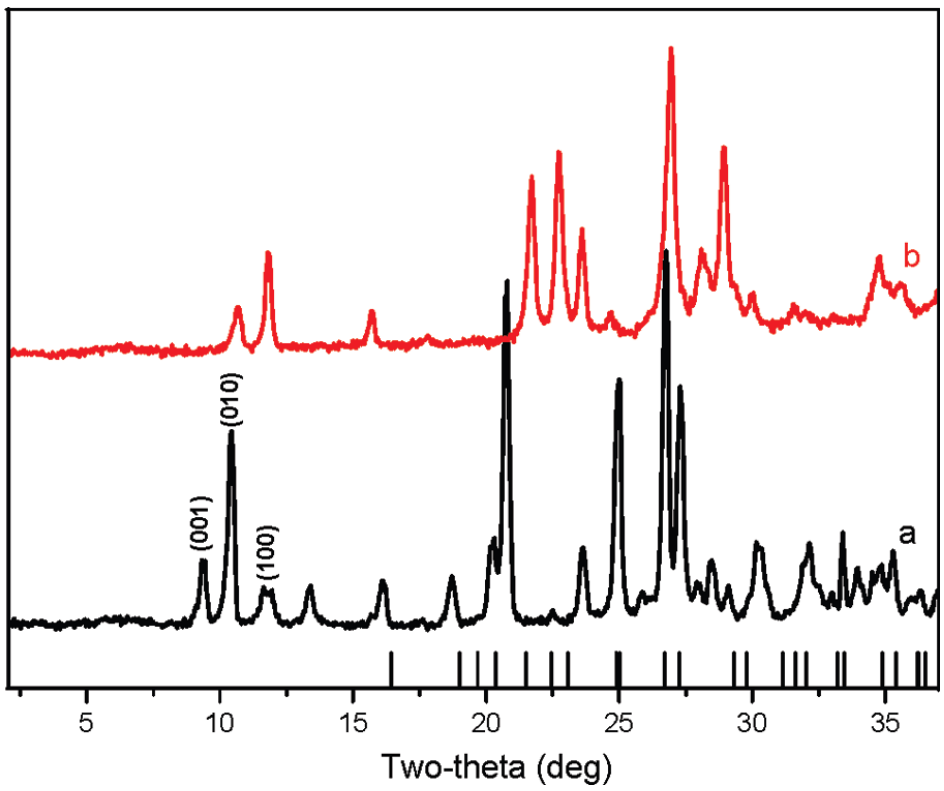

Figure 3.10 PXRD of (a) as-synthesized SLUG-21; (b) SLUG-21 after exchange with excess permanganate after 4 days. Theoretical pattern of $AgMnO_4$ is shown as bottom bars, indicating no structural decomposition occurred during the anion exchange.

surrounding solution occurred in 10 min. The permanganate anions can be seen diffusing into the structure from the left after 15 min immersion (Figure 3.8). No apparent morphology change occurred after immersion of the crystals in solution for 1 h. The crystals after exchange again could not be solved by single crystal X-ray diffraction due to reduction in crystallinity. Nevertheless, the crystals retain their morphology throughout, and the anion exchange reaction is therefore a solid-state process.

A series of UV-Vis patterns were collected on the permanganate solution during the anion exchange process (Figure 3.9). In this case, a stoichiometric excess of 150 mg as-synthesized SLUG-21 crystals were placed into 50 ml of 1.26 mM permanganate solution; the mixture was stirred mildly for 5 min before UV-Vis data collection to ensure homogeneity. To determine percent exchange, UV-Vis spectra were also collected of a saturated $KMnO_4$ solution, diluting from 1 ml to 5 ml with deionized water. Based on Beer's Law, 36.8 %, 68.3 %, and 100 % of the MnO_4^- from the solution were exchanged into SLUG-21 after 8 h, 24 h and 96 h, respectively. The absorption below 280 nm for the 96 h sample is due to EDS, which is now fully exchanged and present in sufficient concentration to absorb. Both crystal morphology and size are unchanged throughout the 4 day anion exchange. SLUG-21 remains heterogeneous at the bottom of the solution and can be readily recovered after exchange.

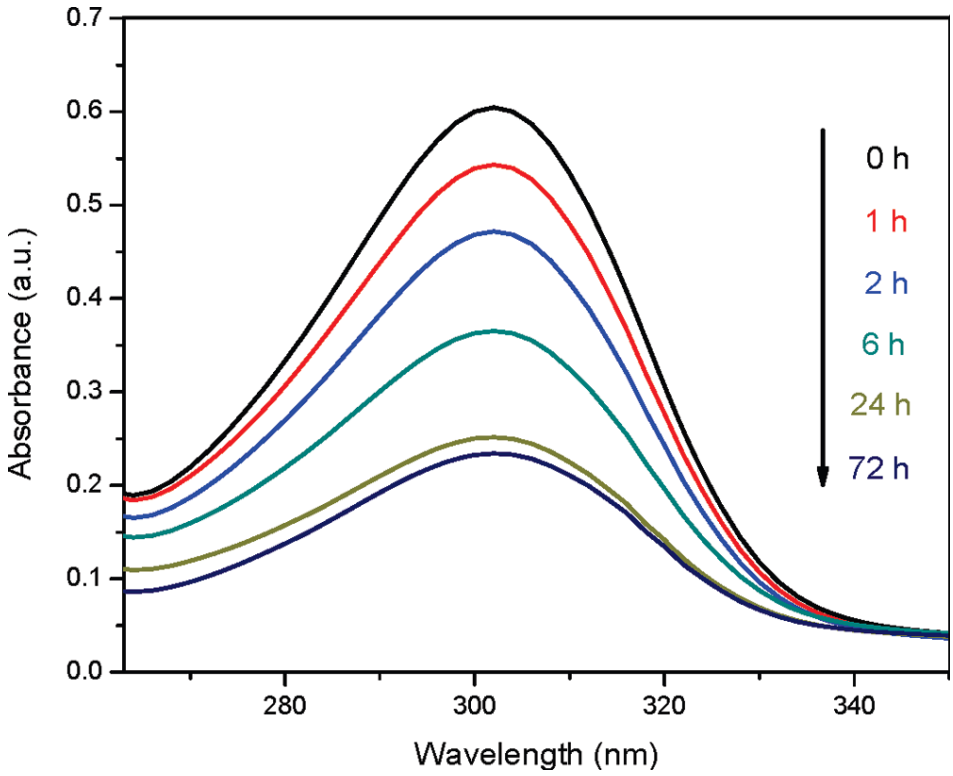

Figure 3.11 UV-Vis absorption spectra of the anion exchange solution for SLUG-22 and nitrate.

PXRD before and after the exchange reaction confirm that no $AgMnO_4$ phase formed (bottom bars in Figure 10). Instead, the new SLUG-21-MnO_4 phase is highly crystalline, with a shift of both (010) and (001) peaks to higher angle with d-spacing approximately decreasing from 9.63 Å and 8.50 Å to 7.49 Å and 8.25 Å, respectively. Considering ethanedisulfonate anions oriented along both *b* and *c* axis, this indicates lattice shrinkage along both axes probably due to the difference in anion size/shape

between permanganate and ethanedisulfonate. No known structure exists based on Ag-bipy and permanganate, nor was single crystal analysis possible. FTIR before and after anion exchange, however, confirm the presence of the Ag-bipy framework, while the sulfonate peaks were completely replaced by permanganate peaks. Although exchange of Ag-bipy-MnO_4 for EDS was unsuccessful, the permanganate anions can be trapped, with selectivity: SLUG-21 in a mixed solution of both permanganate and nitrate (0.1 M each) preferably reacts with permanganate, leading to the same phase as above using pure permanganate solution. All above phenomenon support that the permanganate pollutant trapping is based on stronger interaction between MnO_4^- and SLUG-21 cationic framework rather than concentration based anion exchange. This also explains the possible reason why reversible exchange attempts on permanganate were unsuccessful. In addition to solid-state anion pollutant trapping with permanganate, SLUG-21 display analogous chemistry with perrhenate. The material may therefore find application as a pertechnetate trapping material.

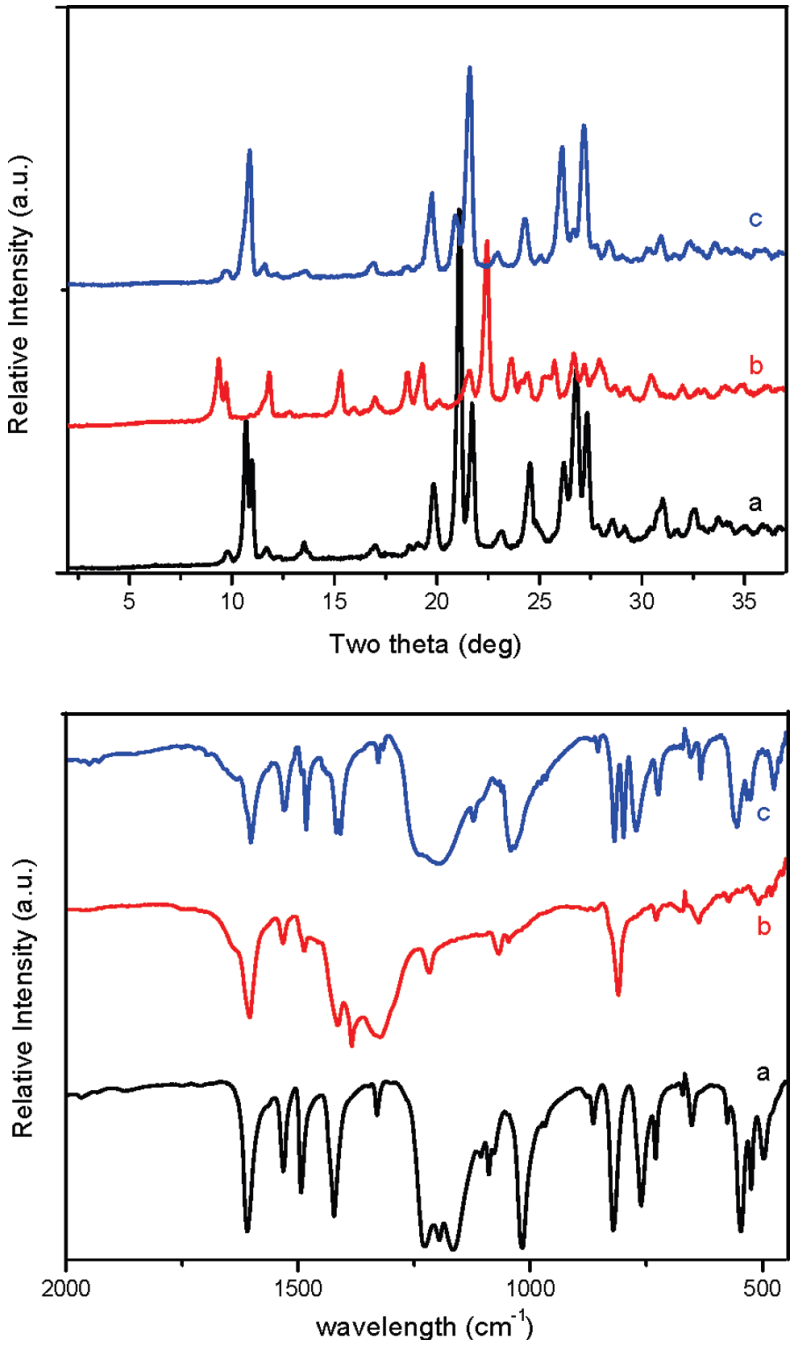

Figure 3.12 PXRD (top) and FTIR (bottom) of: (a) SLUG-22 (black); (b) the solid product after 3 days exchange reaction between SLUG-22 and 0.1 M $NaClO_4$ (SLUG-22-ClO_4, red); (c) the solid product after 3 days exchange reaction between SLUG-22-ClO_4 and 0.1 M EDS sodium salt solution (blue).

SLUG-22 was also employed in the same exchange reaction with nitrate and perchlorate in order to obtain structure-property insight. The structure is similar to SLUG-21, so we wished to understand if this anion exchange property is common for the bipy polymers of d^{10} group 11 metals. The characteristic absorption of nitrate in the UV region at 305 nm was followed since EDS has no absorption at wavelengths longer than 240 nm. Progression of UV-Vis absorption spectra for anion exchange of SLUG-22 in sodium nitrate solution was carried out for 3 days (Figure 3.11). Nitrate was added in 50 % molar excess (1.0 mmol SLUG-22 in 1.5 mmol nitrate solution), and SLUG-22 exhibits highly efficient anion exchange with over 90 % exchange (based on SLUG-22) after one day, forming the known structure.[207] EDS could be reintroduced, giving rise to the partially dehydrated material mentioned above, obtained after heating SLUG-22 to 70 °C. In addition to nitrate, SLUG-22 also displayed reversible anion exchange with perchlorate (Figure 3.12). Similar to the SLUG-21 exchange reaction above, FTIR shows the disappearance of the broad absorbance peak at ~ 1200 cm^{-1} and singlet band at 1020 cm^{-1} (sulfonate stretching) after three days exchange reaction. The appearance of a strong broad band at ~ 1100 cm^{-1} confirms that the perchlorate has exchanged with EDS with formation of previously reported structure,[208] and with complete reversibility after subsequent exchange in EDS solution.

3.3.5 Size-Selective Heterogeneous Catalysis

In addition to the excellent anion exchange properties of SLUG-21 and SLUG-22, both compounds are highly stable in common organic solvents. We then found these two materials are catalytically active in heterogeneous ketal formation. Ketalization is an important method to protect carbonyl groups in organic synthesis and drug design.[209] The reaction requires a Lewis acid catalyst to activate the oxygen of the carbonyl group, allowing glycol to substitute the ketone group. The reaction

Scheme 3.1 Acid catalyzed ketal formation between 2-butanone and ethylene glycol.

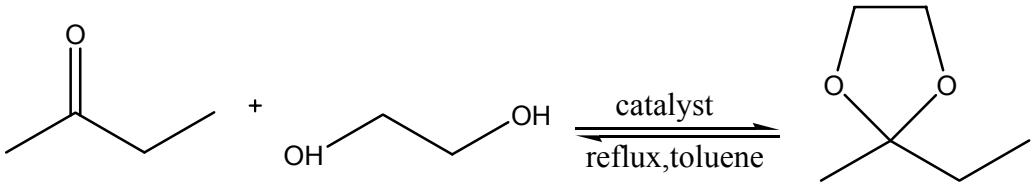

Table 3.2 Conversion Yields for the Ketalization of 2-Butanone

catalyst	number of run	time (h)	conv. (%)[a]
SLUG-21	run #1	12	97
	run #2	12	96
	run #3	12	95
SLUG-22	run #1	12	93
	run #2	12	72
	run #3	12	71

[a] Conversion yields were determined by ^{1}H NMR

typically uses homogeneous iodine or toluenesulfonate, with 56-94 % yield.[209]

Both structures as-prepared display heterogeneous Lewis acidity and reusability in activating 2-butanone to form 2-ethyl-2-methyl-[1,3]-dioxolane (Scheme 3.1 and Table 3.2). Unlike the conventional homogeneous catalyst, both SLUG-21 and SLUG-22 are heterogeneous and easily separated from the product. The catalyst can be reused without further treatment after catalytic runs. Removal of either catalyst by filtration after 6 hours reaction time gave only a 2 % increase in yield after an additional 6 hours of reflux. This observation confirms that the catalysis is heterogeneous, with no leaching of a homogeneously active species into the reaction solution. In addition, the sulfonate is retained by the material, as confirmed by post-catalysis FTIR of the solid. SLUG-21 shows almost no decrease in yield after additional runs, while SLUG-22 showed a decrease in yield from 93 % to 72 % for the second run and 71% for the third. Extending reaction time from 12 h to 24 h did not enhance the conversion efficiency. PXRD of the post-catalysis SLUG-22 material shows a transformation occurred, with a shift of the (10-1) and (20-2) peaks to lower angle (Figure 3.13). This expansion of the lattice is possibly due to reorientation of the EDS anions (Figure 3.2) and bonding to the Ag centers to reduce catalytic activity. Nevertheless, this activated form of SLUG-22 is stable under these conditions, retaining its crystallinity in spite of the lower ketal yield.

Table 3.3 Conversion Yields for the Ketalization of Larger Substrates

catalyst	ketone precursor	time (h)	conv. (%)[a]
no catalyst	2-butanone	12	1
	2-pentanone	12	0
	benzophenone	12	0
SLUG-21	2-butanone	12	97
	2-pentanone	12	87
	benzophenone	12	31
SLUG-22	2-butanone	12	89
	2-pentanone	12	91
	benzophenone	12	91

[a] Conversion yield is determined by ^{1}H NMR

We also investigated the size-selectivity of the catalyst for ketone precursor, to determine whether the reactions are occurring in the channels of the relatively open interlayer space (Figure 3.2) or on the crystal surface. Ketalization of 2-butanone, 2-pentanone and benzophenone by ethylene glycol were performed for both SLUG-21 and SLUG-22 (Table 3.3). A significant size-selectivity was observed for SLUG-21: the more bulky benzophenone led to a yield of only 31 %, less than one-third that of 2-butanone. This result demonstrates that ketal formation by SLUG-21 is likely occurring primarily in the 1D pore channels along the *b*-axis.[193] The approximate calculation of precursor and pore size shows cross-sectional pore channel area (*ca.* 4.1 Å × 3.7 Å) is large enough to reside both 2-butanone (*ca.* 3.5 Å × 1.6 Å × 5.1 Å) and 2-pentanone (*ca.* 3.8 Å × 1.8 Å × 6.8 Å) dimension, while three-dimensional molecule size of benzophenone (*ca.* 7.8 Å × 5.2 Å × 4.6 Å) is too bulky to easily diffuse into the 1D pore channel of SLUG-21. Meanwhile, no size-selectivity was

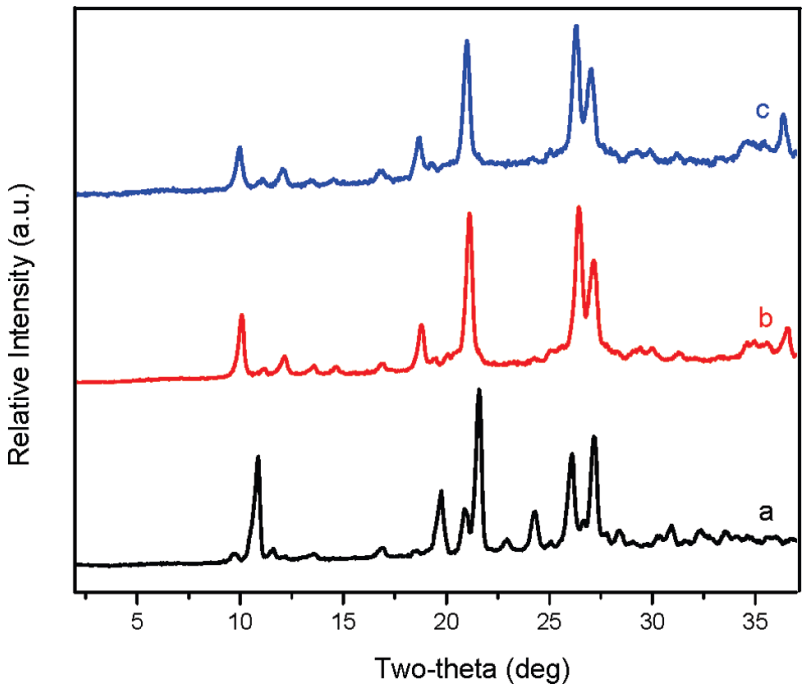

Figure 3.13 PXRD of SLUG-22: (a) as-synthesized; post-catalysis after one (b) and three (c) catalytic cycles of ketal formation.

observed for SLUG-22: all three ketone precursors formed similar yield, indicating that SLUG-22 catalysis likely occurs on the crystal surface. Even so, these yields are still higher than the conventional homogeneous iodine.[209, 210]

Based on these heterogeneous catalytic results, we investigated whether the structural differences between the two frameworks might be responsible for the varying ketalization mechanism and yields. Although both structures possess a similar cationic charge and topology, there are slight structural differences in the EDS anion orientation as well as the position of the crystallographic water. In addition, the silver atoms are larger. The percent solvent/guest accessible void volume was

estimated by PLATON.[211] SLUG-21 possesses 16 % void space, compared with only 12 % for SLUG-22. Moreover, SLUG-21 contains open 1D channels[193] whereas the intercalated water molecules of SLUG-22 are distributed throughout the interlamellar region and should restrict access. Without accessible channels for diffusion of the organic precursor into the structure, surface catalysis would be expected. It is possible that surface Lewis acid sites more easily lose their catalytic activity compared to interior sites due to long-term exposure to the chemical solvent, which would account for the drop in yield versus runs for SLUG-22.

3.4 Conclusions

Two cationic Ag(I)/Cu(I)-based cationic metal-organic frameworks have been rationally synthesized using both an organic metal linker and organic structure directing agent. Both materials display efficient anion exchange as well as heterogeneous Lewis acidity. SLUG-21 exhibits reversible anion exchange of its charge-balancing organosulfonate anions for nitrate/perchlorate, as well as a potentially applicable selective solid-state trapping of group(VII) oxometal anions. Although SLUG-22 is not useful for permanganate trapping, likely due to the lower redox stability of Cu(I) versus Ag(I), nitrate and perchlorate can be reversibly exchanged in high percentage. Cationic MOFs are potentially useful for heterogeneous catalysis due to their positive charge compared to the majority of reported MOFs. Our comparative study into the structure-property behavior of two similar extended frameworks on varying substrate size shows that 1-D channels are important in obtaining size-selective, high yield, recyclable heterogeneous catalysts. We are further exploring this two-pronged approach of organic MOF linker and organosulfonate anionic template with other d-block metals to tune the charge density as well as openness, which should further enhance the anion exchange and catalytic properties of cationic MOFs.

3.5 References

160. *Perchlorate environmental contamination: toxicological review and risk characterization*. Second external review draft, NCEA-1-0503; U.S. EPA, Office of Research and Development, National Center for Environmental Assessment, U.S. Government Printing Office: Washington, DC, 2002.

161. Urbansky, E. T., *Environ. Sci. Pollut. Res. Int.* **2002,** *9*, 187-192.

162. Castiglioni, S.; Bagnati, R.; Fanelli, R.; Pomati, F.; Calamari, D.; Zuccato, E., *Environ. Sci. Technology* **2006,** *40*, 357-363.

163. Praharaj, S.; Nath, S.; Panigrahi, S.; Ghosh, S. K.; Basu, S.; Pande, S.; Jana, S.; Pal, T., *Inorg. Chem.* **2006,** *45*, 1439-1441.

164. Jana, S.; Praharaj, S.; Panigrahi, S.; Basu, S.; Pande, S.; Chang, C. H.; Pal, T., *Org. Lett.* **2007,** *9*, 2191-2193.

165. Mark, R.; Findley, W. N., *Polymer Eng. Sci.* **1978,** *18*, 6-15.

166. Slade, D. G. E. a. R. C. T., *Layered Double Hydroxides*. X. Duan and D. G. Evans ed.; Springer-Verlag, New York, NY, USA: **2006**; pp. 1-87.

167. Prasanna, S. V.; Kamath, P. V., *Solid State Sci* **2008,** *10*, 260-266.

168. Ma, R. Z.; Liu, Z. P.; Li, L.; Iyi, N.; Sasaki, T., *J. Mater. Chem.* **2006,** *16*, 3809-3813.

169. Goh, K. H.; Lim, T. T.; Dong, Z. L., *Environ. Sci. Technology* **2009,** *43*, 2537-2543.

170. Chibwe, K.; Jones, W., *J. Chem. Soc. Chem. Commun.* **1989,** 14, 926-927.

171. Mackenzie, K. J. D.; Meinhold, R. H.; Sherriff, B. L.; Xu, Z., *Journal of Materials Chemistry* **1993,** *3*, 1263-1269.

172. Hibino, T.; Tsunashima, A., *Chemistry of Materials* **1998,** *10*, 4055-4061.

173. Stanimirova, T. S.; Kirov, G.; Dinolova, E., *Journal of Materials Science Letters* **2001,** *20*, 453-455.

174. Lima, E.; Lasperas, M.; de Menorval, L. C.; Tichit, D.; Fajula, F., *Journal of Catalysis* **2004,** *223*, 28-35.

175. Wang, S.; Alekseev, E. V.; Diwu, J. C.; W. H.; Phillips; B. L.; Depmeier, W.; Albrecht-Schmitt, T. E., *Angew. Chem. Int. Ed.* **2010,** *49*, 1057-1060.

176. Joo, S. H. C., S. J.; Oh, I.; Kwak, J.; Liu, Z.; Terasaki, O.; Ryoo, R., *Nature* **2001,** *412*, 169-172.

177. Lee, J. F., O. K.; Roberts, J.; Scheidt, K. A.; Nguyen, S. T.; Hupp, J. T. , *Chem. Soc. Rev.* **2009,** *38*, 1450-1464.

178. Swanson, C. H.; Shaikh, H. A.; Rogow, D. L.; Oliver, A. G.; Campana, C. F.; Oliver, S. R. J., *J. Am. Chem. Soc.* **2008,** *130*, 11737-11741.

179. Horike, S.; Dinca, M.; Tamaki, K.; Long, J. R., *J. Am. Chem. Soc.* **2008,** *130*, 5854-5855.

180. Chae, H. K.; Siberio-Perez, D. Y.; Kim, J.; Go, Y.; Eddaoudi, M.; Matzger, A. J.; O'Keeffe, M.; Yaghi, O. M., *Nature* **2004,** *427*, 523-527.

181. Murray, L. J.; Dinca, M. L., J. R., *Chem. Soc. Rev.* **2009,** *38*, 1294-1314.

182. Wang, B. C., A. P.; Furukawa, H.; O'Keeffe, M.; Yaghi, O. M., *Nature* **2008,** *453*, 207-211.

183. Banerjee, R. P., A.; Wang, B.; Knobler, C.; Furukawa, H.; O'Keeffe, M.; Yaghi, O. M., *Science* **2008,** *319*, 939-943.

184. Oliver, S. R. J., *Chem. Soc. Rev.* **2009,** *38*, 1868-1881.

185. Custelcean, R.; Moyer, B. A., *Eur. J. Inorg. Chem.* **2007,** 10, 1321-1340.

186. Yaghi, O. M.; Li, H. L.; Groy, T. L., *Inorg. Chem.* **1997,** *36*, 4292-4293.

187. Min, K. S.; Suh, M. P., *J. Am. Chem. Soc.* **2000,** *122*, 6834-6840.

188. Sudik, A. C.; Cote, A. P.; Yaghi, O. M., *Inorg. Chem.* **2005,** *44*, 2998-3000.

189. Du, M.; Zhao, X. J.; Guo, J. H.; Batten, S. R., *Chem. Commun.* **2005,** 4836-4838.

190. Bao, S. S.; Ma, L. F.; Wang, Y.; Fang, L.; Zhu, C. J.; Li, Y. Z.; Zheng, L. M., *Chem. Eur. J.* **2007,** *13*, 2333-2343.

191. Michaelides, A.; Skoulika, S., *Cryst. Growth Des.* **2009,** *9*, 2039-2042.

192. Chen, X. D.; Wan, C. Q.; Sung, H. H. Y.; Williams, I. D.; Mak, T. C. W., *Chem. Eur. J.* **2009,** *15*, 6518-6528.

193. Fei, H.; Paw, L. U.; Rogow, D. L.; Bresler, M. R.; Abdollahian, Y. A.; Oliver, S. R. J., *Chem. Mater.* **2010,** *22*, 2027-2032.

194. Wang, Y. F. G., H. Z., *J. Colloid. Interface Sci.* **2006,** *301*, 19-26.

195. *SHELXTL Crystal Structure Determination Package*. Bruker Analytical X-ray Systems Inc.: Madison, WI, 1995-99.

196. Lucassen, A. C. B. K., A.; Leitus, G.; Shimon, L. J. W.; Martin, J. M. L.; van der Boon, M. E., *Crys. Growth Des.* **2007,** *7*, 386-392.

197. *Cambridge Structural Database*. A covalent Sb-O bond length is generally between 1.9 Å and 2.1 Å, while 90.8% Sb-O bonds with a bond length less than 2.27 Å.

198. Wu, M. Y.; Yuan, D. Q.; Han, L.; Wu, B. L.; Xu, Y. Q.; Hong, M. C., *Eur. J. Inorg. Chem.* **2006,** 526-530.

199. Ju, J.; Lin, J. H.; Li, G. B.; Yang, T.; Li, H. M.; Liao, F. H.; Loong, C. K.; You, L. P., *Angew. Chem. Int. Ed.* **2003,** *42*, 5607-5610.

200. Liu, S. X.; Xie, L. H.; Gao, B.; Zhang, C. D.; Sun, C. Y.; Li, D. H.; Su, Z. M., *Chem. Commun.* **2005,** *40*, 5023-5025.

201. Yu, J. H.; Xu, R. R.; Chen, J. S.; Yue, Y., *J. Mater. Chem.* **1996,** *6*, 465-468.

202. Ok, K. M. H., P. S., *Inorg. Chem.* **2002,** *41*, 3805-3807.

203. Tran, D. T.; Zavalij, P. Y.; Oliver, S. R. J., *J. Am. Chem. Soc.* **2002,** *124*, 3966-3969.

204. Rogow, D. L.; Russell, M. P.; Wayman, L. M.; Swanson, C. H.; Oliver, A. G.; J., O. S. R., *Cryst. Growth Des.* **2010,** *10*, 823-829.

205. Yaghi, O. M.; Li, H. L., *J. Am. Chem. Soc.* **1996,** *118*, 295-296.

206. Wang, L. S.; Zhang, J. F.; Yang, S. P., *Acta Cryst. Sect. E* **2004,** *E60*, m1484-m1486.

207. Yaghi, O. M.; Li, H., *J. Am. Chem. Soc.* **1995,** *117*, 10401-10402.

208. Zhang, J. K., Y.; Wen, Y.; Li, Z.; Qin, Y.; Cheng, J.; Yao, Y.;, *Acta Cryst. Sect. E* **2004,** *E60*, m504-m505.

209. Banik, B. K. C., M.; Marquez, J.; Cardona, M., *Tetra. Lett.* **2005,** *46*, 2341-2343.

210. Ren, Y. M. C., C., *Tetra. Lett.* **2008,** *49*, 7110-7112.

211. Spek, A. L., *PLATON, A Multipurpose Crystallographic Tool*. Utrecht, The Netherland, 2007.

Chapter 4

A New Paradigm for Anion Trapping in High Capacity and Selectivity: Crystal-to-Crystal Transformation of Cationic Materials

Abstract

We describe a new methodology to the selective trapping of priority pollutants that occur inherently as oxo-anions (e.g. perchlorate, chromate, arsenate, pertechnetate, etc.) or organic anions (e.g. salicylate, pharmaceuticals and their metabolites, which are often chlorinated into potentially more harmful compounds). The typical approach to trapping anions is exchange into cationic hosts such as resins or layered double hydroxides. Both capacity and selectivity are limited by the equilibrium of the process and moreover are often subject to interference, e.g. by carbonate that is always present in water from atmospheric CO_2. Our approach takes advantage of the metastability of our cationically charged materials to instead trap by recrystallization to a new structure. Exceptionally high adsorption capacities for

permanganate and perrhenate—studied as models for pertechnetate—were found for an Ag(I)-based cationic extended framework. The exchange capacity reached 292 mg/g and 602 mg/g, respectively, over five times the exchange capacity compared to conventional layered double hydroxides. Our cationic material can also selectively trap these and other toxic oxo-anions when non-toxic anions (e.g. nitrate, carbonate) were present in over 100-fold excess concentration.

4.1 Introduction

Many of the metal pollutants listed as priorities by the EPA (U.S. Environmental Protection Agency) occur in water as their oxo-hydroxo anionic forms (e.g. perchlorate, chromate, selenite, etc.).[212] Radioactive technetium (Tc-99) in the form of soluble pertechnetate (TcO_4^-) is highly problematic in low-activity waste (LAW) to separate the nuclear waste into primary solids. Its easy leakage from glass after vitrification does not meet long-term storage performance assessment requirements.[213] LAW also contains other non-radioactive inorganic and organic species [e.g. carbonate (CO_3^{2-}), nitrate (NO_3^-), etc.] that may interfere with immobilizing radioactive species in solid-state ion-exchange materials. Chromate is another problematic anion for vitrification because it weakens the integrity of the waste glass by forming spinels; such particles can also obstruct the glass flow within the melter during vitrification.[214]

Conventional ion-exchange resins with cationic groups and exchangeable counter anions are of limited thermal and chemical stability due to their organic nature, yet are still the standard ion exchanger.[215] Layered double hydroxides (LDHs) is an isostructural set of materials consisting of cationic brucite-type layers charge balanced by interlayer anions, with general formula $[M^{2+}_{1-x}M^{3+}_{x}(OH)_2]A^{n-}_{x/n}\cdot mH_2O$. They have been extensively studied and are considered to be an ideal alternative to anion exchange resins.[216] This group of materials, however, has limited capacity as evidenced by adsorption titration and isotherms. They also display low selectivity towards anion pollutants, especially in the presence of carbonate.[217]

Metal-organic frameworks (MOFs) are an emerging class of materials with a vast array of topologies and potential applications in gas adsorption/storage, catalysis and drug delivery.[218] As a sub-group of these known compounds, cationic extended frameworks have received limited investigation. Two of our previously reported cationic inorganic frameworks, $[Pb_3F_5^+][NO_3^-]$ and $[Pb_{4.5}F_8^+][ClO_4^-]$, exhibited anion exchange with dichromate, but with some decomposition to PbF_2 or $PbCrO_4$.[219,220] Meanwhile, one recent development is the synthesis of cationic 3D metal borates with initial studies of TcO_4^- trapping. The overall adsorption capacity was not given, though the removal rate was 72% with dilute TcO_4^- solution, and the framework is based on slightly radioactive thorium.[221] Though some exchange for anions of comparable size has been shown among other extended frameworks, the process is again guided by weak, non-specific interaction between cationic host and anionic

guest.[222-224] Fogg and co-workers recently reported an ytterbium oxyhydroxide 3D cationic framework with initial anion exchange but not for anionic pollutants.[225]

Herein, we report unprecedented capacity and selectivity for trapping permanganate (MnO_4^-), perrhenate (ReO_4^-) and chromate (CrO_4^{2-}) by our cationic MOF (SLUG-21, $[Ag_2(4,4'\text{-bipy})_2(O_3SCH_2CH_2SO_3)\cdot 4H_2O]$[226,227] Unlike the strong affinity of LDHs for carbonate, SLUG-21 selectively traps these problematic oxo-anion pollutants *in record levels over all previous materials*. The mechanism of the high selectivity and adsorption capacity occurs *via* a crystal transition upon oxo-metal uptake. While crystal transformation for selective guest adsorption/desorption has been investigated for neutral materials,[228-230] this report is the first to extend this approach to cationic materials for the trapping of anionic pollutants.

4.2 Experimental Section

4.2.1 Reagents

Silver nitrate ($AgNO_3$, Fisher, ≥ 99.7%), 1,2-ethanedisulfonic acid (EDSA, $HO_3SCH_2CH_2SO_3H$, TCI Inc., 95%), 4,4'-bipyridine [$(C_5H_4N)_2$, Acros Organics, 98%] were used as-received for the synthesis of SLUG-21. Sodium nitrate ($NaNO_3$, Fisher, 99%), sodium perchlorate monohydrate ($NaClO_4\cdot H_2O$, Fluka Analytical, 98%), potassium permanganate ($KMnO_4$, Fisher, 99.8%) and 1,2-ethanedisulfonic acid disodium salt ($KReO_4$, Acros Organics, 99%) were used as-purchased for the anion exchange reactions. Hydrotalcite (synthetic, Aldrich, CAS# 11097-59-9,

$CH_{16}Al_2Mg_6O_{19}\cdot 4H_2O$) was used as-received for comparison of anion exchange to $Ag_2(C_5H_4N)_4(O_3SCH_2CH_2SO_3)\cdot 4H_2O$ (which we denote SLUG-21).

4.2.2 Synthesis

The synthesis of SLUG-21 is a slight modification over our previously reported procedure.[226] Colorless crystals were synthesized under hydrothermal conditions. A reactant solution with a molar ratio of 1:1:1:400 for $AgNO_3$:EDSA:4,4'-bpy:H_2O was stirred at room temperature for 10 min and then transferred to a 15 ml Teflon lined autoclave to 2/3 filling. The autoclaves were heated at 150 °C for 72 hours under autogenous pressure, during which pH of the reactant solution increased from 1.8 to 2.2. Large block crystals were isolated after filtration and rinsed by acetone (yield: 0.54 g, 98.7% based on silver nitrate).

Crystals of SLUG-21 can also be synthesized by reflux or stirring at room temperature using the same ratio of reactants. The crystals were filtered after 72 hours reaction time. The yield was 74.1% (0.40 g) from reflux and 83.3% (0.45 g) from room temperature stirring (both yields again based on silver nitrate).

4.2.3 Anion Exchange

(i) Anion adsorption capacity measurements. 25 mg (3.17×10^{-5} mol) as-synthesized SLUG-21 were introduced into 50 ml aqueous solution containing 10 mg (6.33×10^{-5} mol) $KMnO_4$. The solution was stirred gently up to 48 hours to allow complete exchange, and both the solid and solution were monitored at various time

intervals to follow the exchange progress. Both uncalcined and calcined hydrotalcite were also studied for comparison of adsorption capacity. The calcined form of hydrotalcite was prepared by annealing the as-purchased hydrotalcite at 450 °C for 2 hours and used for anion exchange within 12 hours. 38 mg (6.33×10^{-5} mol) uncalcined or calcined hydrotalcite was introduced into the same solution as above, with the same reaction and monitoring process. The separation of hydrotalcite (both uncalcined and calcined) and solution required 30 min centrifuging.

(ii). Anion exchange selectivity studies. *Permanganate*: 78.8 mg (0.1 mmol) SLUG-21 was introduced into 50 ml aqueous solution consisting of 47.4 mg (0.3 mmol) $KMnO_4$ and 2.55 g (30 mmol) $NaNO_3$ under mild stirring for 48 hours. The solid products were isolated by filtration and rinsed by water/acetone, followed by Fourier transform infrared (FTIR) spectroscopy and powder X-ray diffraction (PXRD) measurements to support that SLUG-21 selectively trapped the permanganate over nitrate. In a separate experiment, sodium carbonate (Na_2CO_3) was also added in equimolar ratio to $NaNO_3$ to further study selectivity. *Perrhenate*: 78.8 mg (0.1 mmol) SLUG-21 was introduced into 50 ml aqueous solution consisting of 91.6 mg (0.3 mmol) $KReO_4$ and 2.55 g (30 mmol) $NaNO_3$ (or 2.97g 30 mmol Na_2CO_3) with conditions same as for permanganate trapping. *Perchlorate*: 78.8 mg (0.1 mmol) SLUG-21 was introduced into 50 ml aqueous solution consisting of 42.14 mg (0.3 mmol) $NaClO_4$ and 25.5 mg (0.3 mmol) $NaNO_3$ under the same conditions as for permanganate trapping.

4.2.4 Instrumental Details

Samples for PXRD were measured on a Rigaku Americas Miniflex Plus diffractometer and were scanned from 2 to 60 ° (2θ) at a rate of 2 °·min^{-1} and 0.04 ° step size, under Cu-Kα radiation (λ = 1.5418 Å). Crystal structure views were obtained using Diamond v3.2 and rendered by POV-Ray v3.6. UV-Vis spectroscopic studies were performed with a Hewlett-Packard Model 8452A UV-Vis spectrophotometer to monitor the exchange progress. FTIR spectroscopy of the materials was accomplished using a Perkin-Elmer Spectrum One spectrophotometer with KBr pellets. Inductively Coupled Plasma (ICP) was collected on a Perkin-Elmer Optima 7000 DV Inductively Coupled Plasma-Optical Emission Spectroscopy instrument.

4.3 Results and Discussion

4.3.1 Synthesis and Structure

SLUG-21 crystals can be synthesized hydrothermally, under reflux or at room temperature with stirring. The crystal structure of SLUG-21 (Figure 4.1 left) consists of a cationic layer of π–π stacked Ag-bipy chains, charge balanced by interlamellar 1,2-ethanedisulfonate (EDS) anions. Only one oxygen of each sulfonate end weakly interacts with the Ag metal center. The distance is in the range of 2.711(7) to 2.759(9) Å, significantly longer than accepted covalent Ag-O length (median: 2.44 Å, CSD). These distances indicate the EDS anions only electrostatically interact with

the cationic layers, supporting the cationic feature and anion exchangeability of SLUG-21.

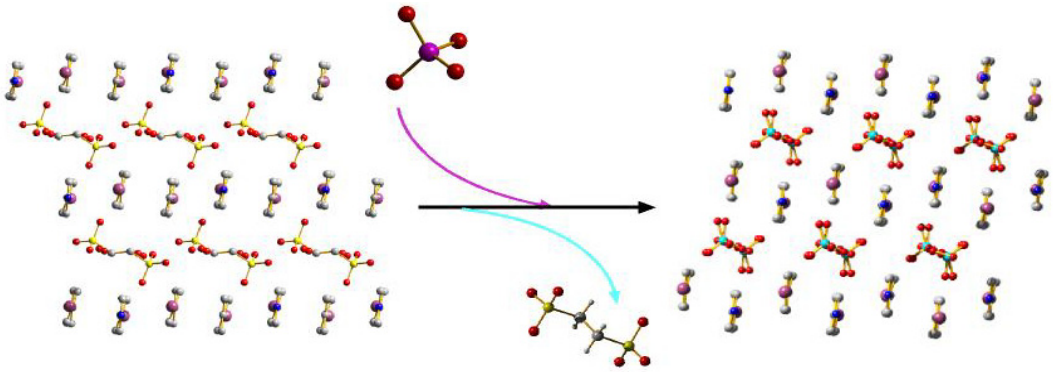

Figure 4.1 Left: Crystallographic view along the [10-1] direction of the SLUG-21 structure with hydrogen atoms omitted for clarity. Right: Crystallographic view along the [01-1] direction of the crystal structure after perchlorate anion exchange (hydrogen atoms omitted for clarity; silver-purple; carbon-gray; sulfur-yellow; oxygen-red; nitrogen-blue; chlorine: green). The scheme is shown for the anion exchange process of trapping oxo-anions and loss of EDS anions.

4.3.2 Anion Exchange: Absorption Capacity

(i) Permanganate (MnO_4^-)

For a detailed investigation of SLUG-21 anion uptake capacity, permanganate and perrhenate were chosen as models for pertechnetate since all are group 7 oxo-anions. 25 mg (3.17×10^{-5} mol) of as-synthesized SLUG-21 were introduced into 50 ml solution containing 10 mg (6.33×10^{-5} mol) $KMnO_4$. The molar amount of permanganate was doubled compared to the trapping material since EDS is divalent and bifunctional. The entire reaction was performed under ambient conditions with mild stirring (see Experimental Section details). As monitored by UV-Vis spectroscopy, the permanganate concentration in the solution decreased by 64 % and 94 % with reaction intervals of 24 hours and 48 hours, respectively, for adsorption

Table 4.1 Absorption capacity of 6.33×10^{-5} mol permanganate or perrhenate in 50 ml aqueous solution with half molar ratio of SLUG-21 and equimolar uncalcined/calcined LDHs during 24 or 48 hour intervals, as monitored by ICP and UV-Vis.

Anion	Anion Exchanger	Time (h)	ICP		UV-Vis	
			Oxoanion Removal	Abs. Cap. (mg/g)	Oxoanion Removal	Abs. Cap. (mg/g)
MnO_4^-	SLUG-21	24	65 %	195.73	64 %	192.72
	SLUG-21	48	97 %	292.09	94 %	283.06
	uncalcined LDH	48	4 %	7.92	3 %	5.94
	calcined LDH	48	21 %	41.60	18 %	35.66
ReO_4^-	SLUG-21	24	91 %	576.49	N/A	N/A
	SLUG-21	48	95 %	601.83	N/A	N/A
	uncalcined LDH	48	9 %	37.51	N/A	N/A
	calcined LDH	48	30 %	125.03	N/A	N/A

capacity (mol/mol) of 1.28 and 1.88 (Figure 4.2, Table 4.1). Inductively coupled plasma (ICP) gave similar percent loss, indicating an adsorption capacity (mol/mol) of 1.30 and 1.94 (Table 4.1). The slight difference is likely due to experimental error and the greater uncertainty for UV-Vis at low concentration. The overall adsorption capacity of permanganate trapping by SLUG- SLUG-21 after 48 hours is therefore 292 mg/g (by UV-Vis) and 283 mg/g (by ICP, Table 4.1). No further decrease in anion concentration was detected after 48 hours, demonstrating completion of the recrystallization process. The widely accepted adsorption capacity for oxo-anions *via* LDHs is in the range of between 10 mg/g to 150 mg/g based on a recent review.[217] To verify, we also carried out the anion exchange reaction with commercially available synthetic hydrotalcite (magnesium aluminum hydroxycarbonate, Aldrich) in both the uncalcined and calcined form. After 48 hours exchange under the same conditions as SLUG-21, only 3 % and 18 % of the anions were adsorbed by LDHs, respectively. The adsorption capacity for calcined hydroxycarbonate-based LDHs is thus 36 mg/g and 42 mg/g *via* UV-Vis and ICP respectively. These values are less than 14% compared to our SLUG-21 material (Table 4.1).

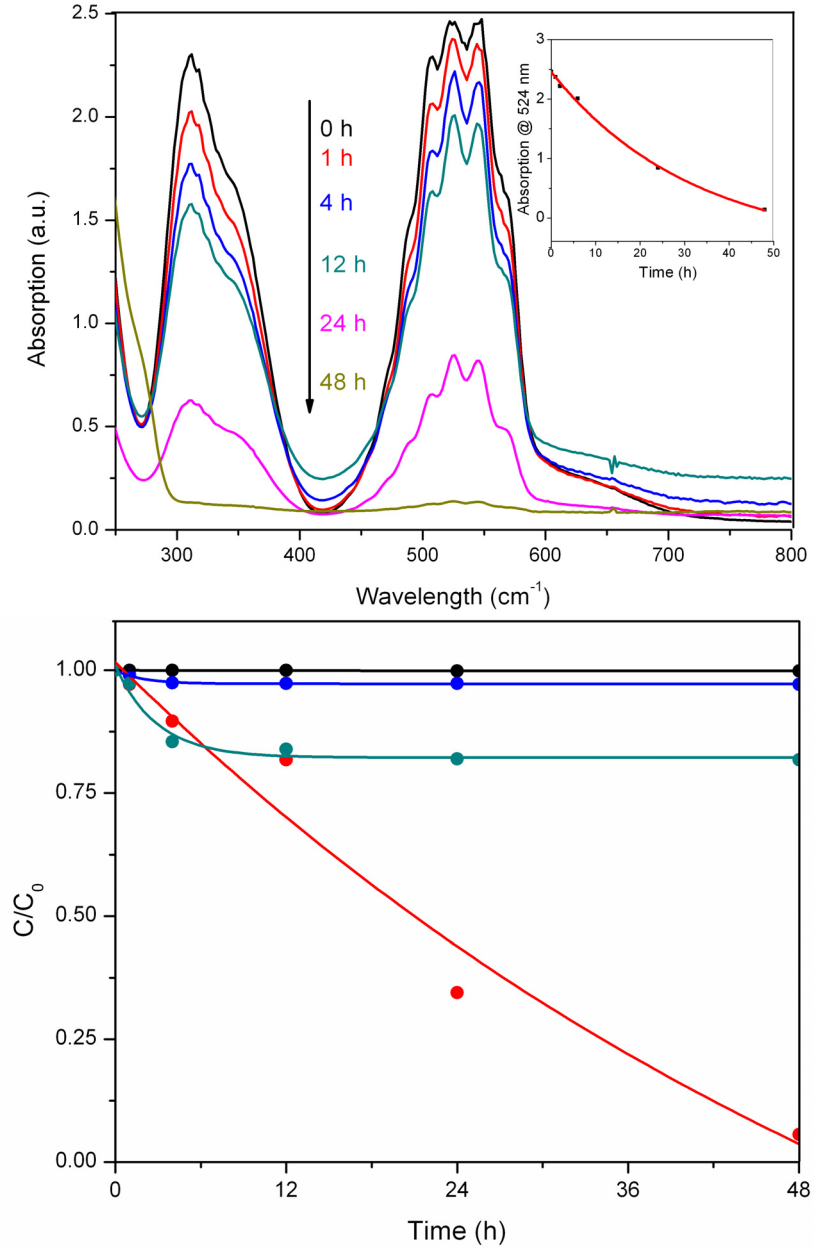

Figure 4.2 Top: UV-Vis absorption spectra of the permanganate solution with initial concentration of 6.33×10^{-5} mol in 50 ml solution and 3.17×10^{-5} mol SLUG-21 at various intervals. Inset: relative intensity of the 524 nm MnO_4^- maximum versus time. Bottom: concentration of permanganate (based on UV-Vis) *vs*. time for anion exchange by blank (no solid, black), uncalcined LDH (blue), calcined LDH (cyan) and SLUG-21 (red).

The reason for the much greater uptake by our material we believe is due to crystal transformation by the host and the stability of the oxo-anion in the resultant structure, rather than undergoing a typical equilibrium-driven anion exchange. The limited adsorption capacity of LDHs also necessitates pre-removal of intercalated carbonate by calcination.[216, 217] As-synthesized SLUG-21 may be used for the anion exchange, with much higher adsorption capacity based on a stronger interaction towards the oxo-anion pollutant by the resultant crystal structure, which can be seen to take the place of each end of the EDS molecules (Figure 4.1). The replacing permanganate anion plays important role in high capacity trapping to reach a thermodynamically favorable anion exchanged product, which is further supported by its resulting in the same structure using nitrate and perchlorate intercalated Ag-bipy chain materials as starting materials to trap MnO_4^-. This important distinction between SLUG-21 and LDHs is further supported by selectivity studies (*vide infra*).

(ii) Perrhenate (ReO_4^-)

In order to further demonstrate the potential application of SLUG-21 towards pertechnetate abatement, perrhenate was also investigated. The resultant exchange solution was monitored only by ICP due to the overlap between EDS and perrhenate in the UV region. ReO_4^- trapping by SLUG-21 is even more rapid than MnO_4^-, reaching over 90% removal from solution in only 24 hours, saturating in 48 hours with 95% removal. Although the crystals were not suitable for single crystal analysis, the overall adsorption capacity of 1.90 (mol/mol) is comparable with the previous

permanganate study, as expected. The adsorption capacity based on weight, however, reaches an exceptionally high 602 mg/g based on the molecular weight of ReO_4^- as compared to that of MnO_4^-. Meanwhile, adsorption capacity of the uncalcined and calcined LDHs is only 37 mg/g and 125 mg/g, respectively, a mere 6 % and 20 % with respect to SLUG-21. FTIR of the solid products after exchange support that perrhenate exchanged into the structure, with a prominent Re-O stretch band and significant reduced intensity of the sulfonate absorption band, and PXRD indicate that the structure after exchange is not decomposed to $AgReO_4$ (Figure 4.3).

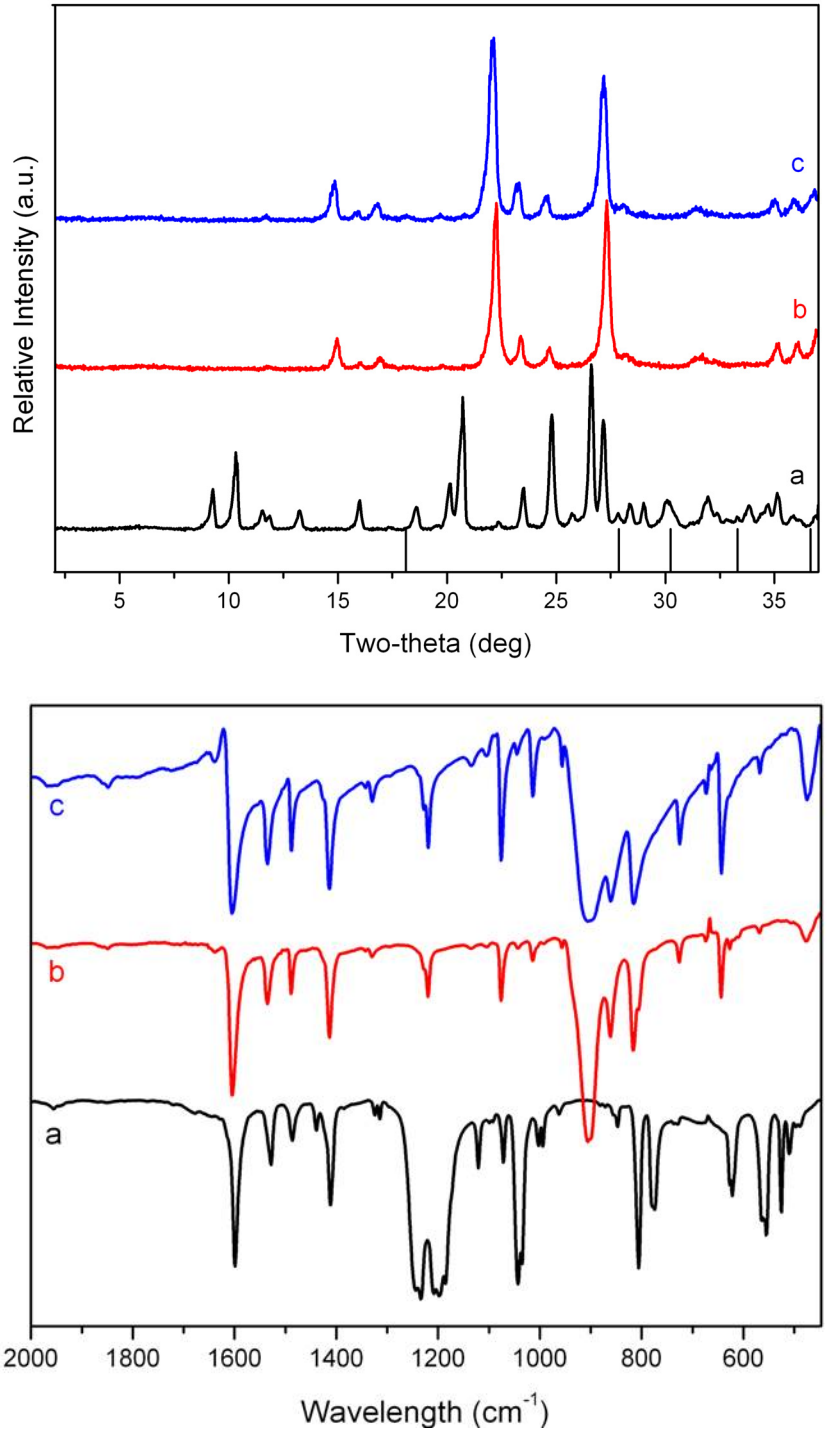

Figure 4.3 PXRD (top) and FTIR (bottom) of: (a) as-synthesized SLUG-21; (b) solid after exchange with perrhenate and 100-fold molar excess nitrate; (c) solid after exchange with perrhenate and 100-fold molar excess carbonate. The theoretical pattern of $AgReO_4$ is shown as bottom bars in the PXRD.

(iii) Chromate (CrO_4^{2-})

Chromate exchange and adsorption capacity was also studied for SLUG-21. UV-Vis shows that 25 %, 33 % and 41 % of the chromate were exchanged after 8 h, 24 h and 48 h, respectively (Table 4.2). The adsorption capacity for chromate was thus 0.41 mol/mol and 60 mg/g, while the capacity for uncalcined LDHs and calcined LDHs was 6 mg/g and 17 mg/g. FTIR of the solid products after exchange support that chromate exchanged into the structure, with a prominent Cr-O stretch band and concomitant reduced intensity of the sulfonate absorption band (Figure 4.4). The broad absorption located at ~1200 cm^{-1} and singlet at ~1050 cm^{-1} before anion exchange is characteristic of the sulfonate (RSO_3^{2-}) groups in the original SLUG-21. Disappearance of these two bands after anion exchange, along with survival of the 4,4'-bipyridine stretches (1605s, 1535s, 1490s, 1418s, aromatic C=C and C=N), further support the anion exchange process. No nitrate or carbonate absorption bands

Table 4.2 UV-Vis data of chromate solution during anion exchange and adsorption capacity of different anion sorbents after anion exchange.

Anion exchanger	Absorption[i]	Conc.vs initial[ii]	Capacity (mol/mol)	Capacity (mg/g)
None	1.34146	100 %	N/A	N/A
Uncalcined LDHs	1.26100	94 %	0.03	5.80
Calcined LDHs	1.09348	82 %	0.09	17.39
SLUG-21	0.78928	59 %	0.41	60.10

[i]Absorption intensity at 372 nm was employed.
[ii]Beer's law was used to calculate the concentration.

(~1300 cm^{-1} or ~1420 cm^{-1}) are observed in the solid after anion exchange. Powder X-ray diffraction (PXRD) demonstrates the structure after exchange retained its layered feature with prominent (010) and (020) peaks and no structural decomposition to Ag_2CrO_4 (Figure 4.4, top).

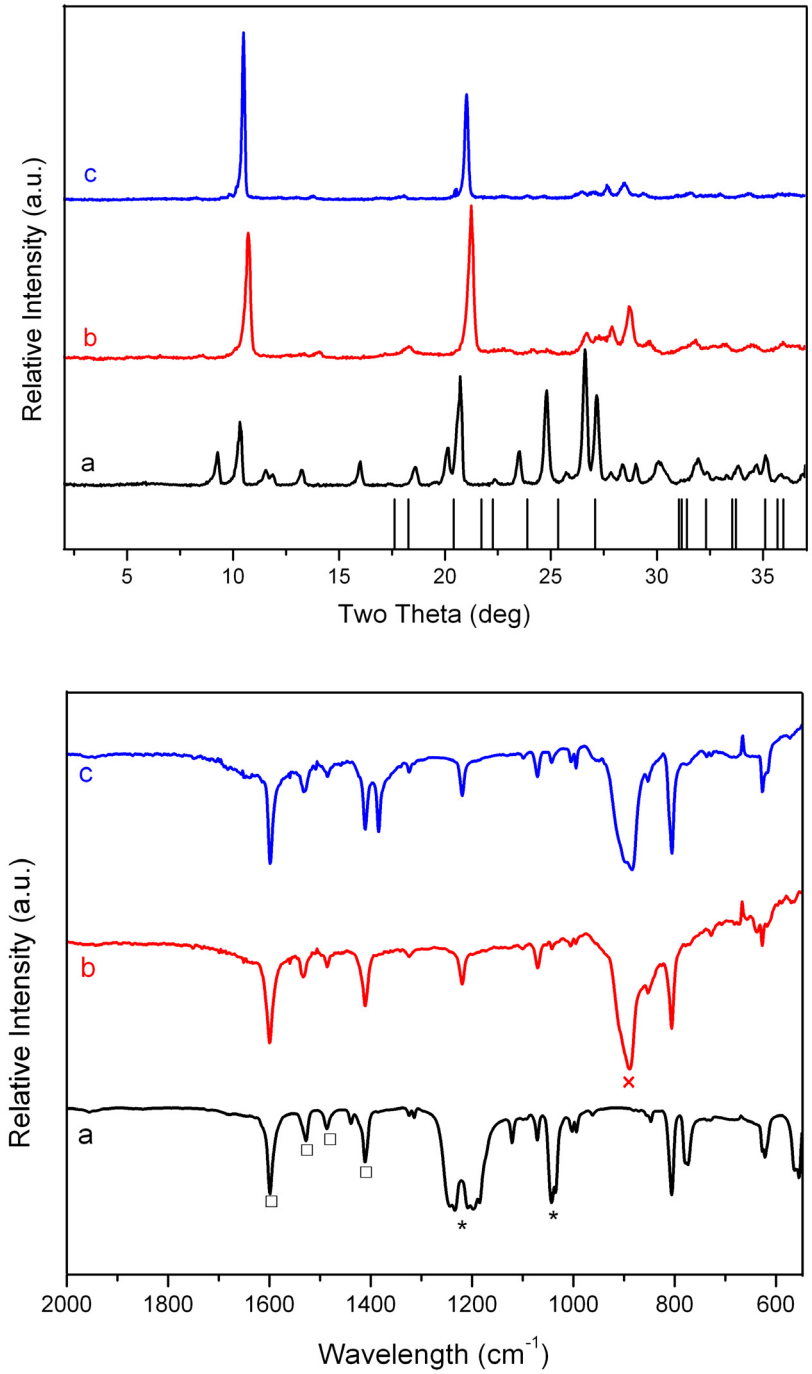

Figure 4.4 PXRD (top) and FTIR (bottom) of: (a) as-synthesized SLUG-21; (b) solid after exchange with chromate and 100-fold molar excess carbonate; (c) solid after exchange with chromate and 100-fold molar excess nitrate. The theoretical pattern of Ag_2CrO_4 is shown as bottom bars in the PXRD. □: aromatic C=C and C=N stretch of 4,4'-bipyridine; ×: Cr-O stretch; *: sulfonate stretches.

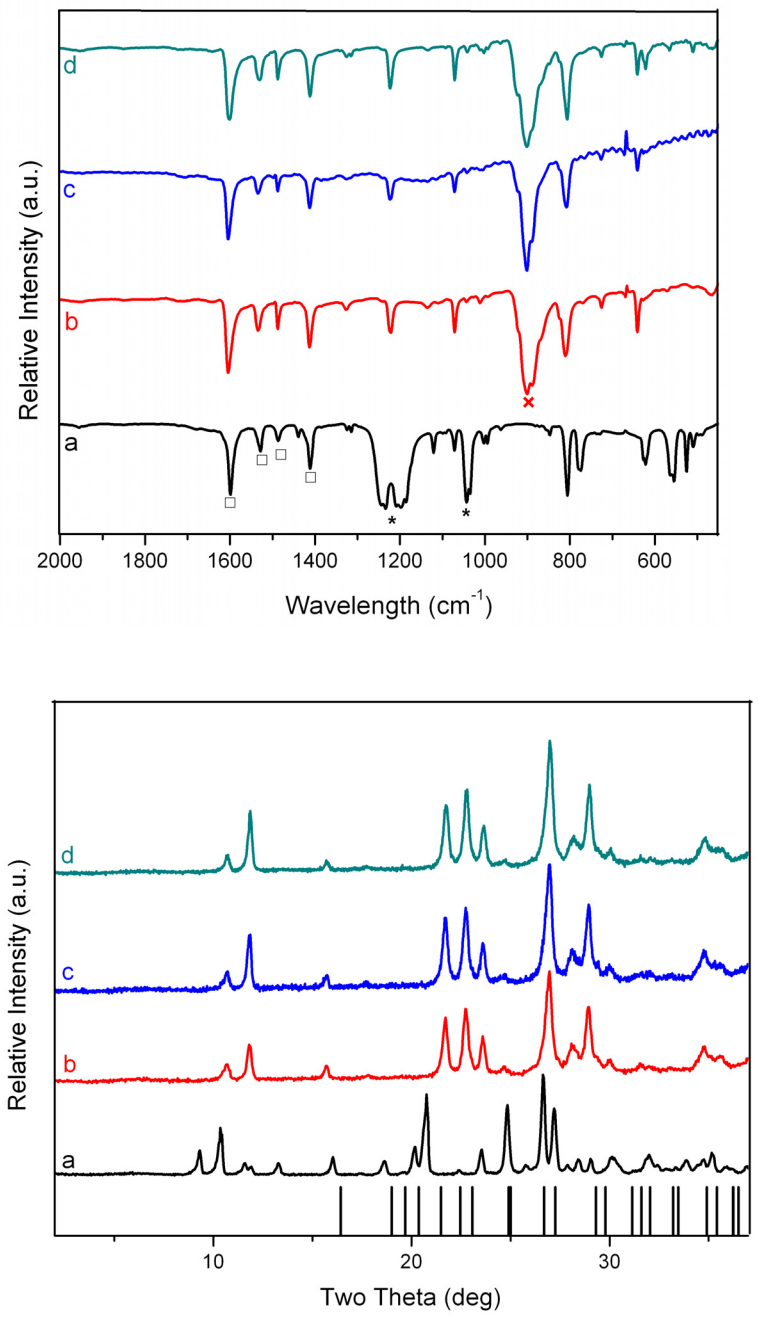

Figure 4.5 FTIR (top) and PXRD (bottom) of (a) as-synthesized SLUG-21; (b) SLUG-21 after exchange with permanganate; (c) SLUG-21 after exchange with permanganate and 100-fold molar excess of nitrate; (d) SLUG-21 after exchange with permanganate and 100-fold molar excess of carbonate. Theoretical pattern of $AgMnO_4^-$ is shown as bars. □ indicates the aromatic C=C and C=N stretches of 4,4'-bipyridine; × indicates the Mn-O stretch; * indicates sulfonate stretches.

4.3.3 Anion Exchange: Selectivity

Equally important to capacity is anion selectivity for controlling the anion that is captured. Selectivity has been a long-term problem for LDHs, mainly owing to high affinity of the cationic layers to carbonate as well as a variety of other anions that may be present in solution. The affinity obeys the following order:[231]

$$CO_3^{2-} > SO_4^{2-} > OH^- > F^- > Cl^- > Br^- > NO_3^- > I^-$$

Calcination is usually necessary to partially remove the carbonate anions in LDHs before anion exchange. It is therefore never possible to remove all anions and/or introduce complete selectivity. Meanwhile, the selectivity of anion trapping in SLUG-21 was studied with multiple competing anions of varying excess concentration in the presence of a low concentration of the target anion pollutant. A selective reaction with 78.8 mg (0.1 mmol) SLUG-21 was introduced into 50 ml aqueous solution consisting of 47.4 mg (0.3 mmol) $KMnO_4$ and 2.55 g (30 mmol) $NaNO_3$. FTIR and PXRD measurements of crystals after anion exchange indicate only MnO_4^- entered the cationic material to replace the EDS anions. No NO_3^- is present inside the solid (Figure 4.5, top). Indeed, the PXRD pattern is identical to the material after exchange in permanganate-only solution (Figure 4.5, bottom). Furthermore, the theoretical PXRD pattern of $AgMnO_4$ (shown as bars at the bottom of Figure 4.5) indicates no structural decomposition occurred during the anion exchange. Similarly, carbonate in 100-fold excess did not interfere with permanganate, which was again selectively trapped by SLUG-21 (Figure 4.5d). This high selectivity is based on its unconventional recrystallization upon anion trapping,

unlike the host-guest equilibrium driven process of LDHs and resins. PXRD indicates a crystal transition from SLUG-21 to the post-anion exchange products with a specific new pattern. Selectivity towards perrhenate was also carried out with both of the competing nitrate and carbonate anions, with the same trapping behavior as

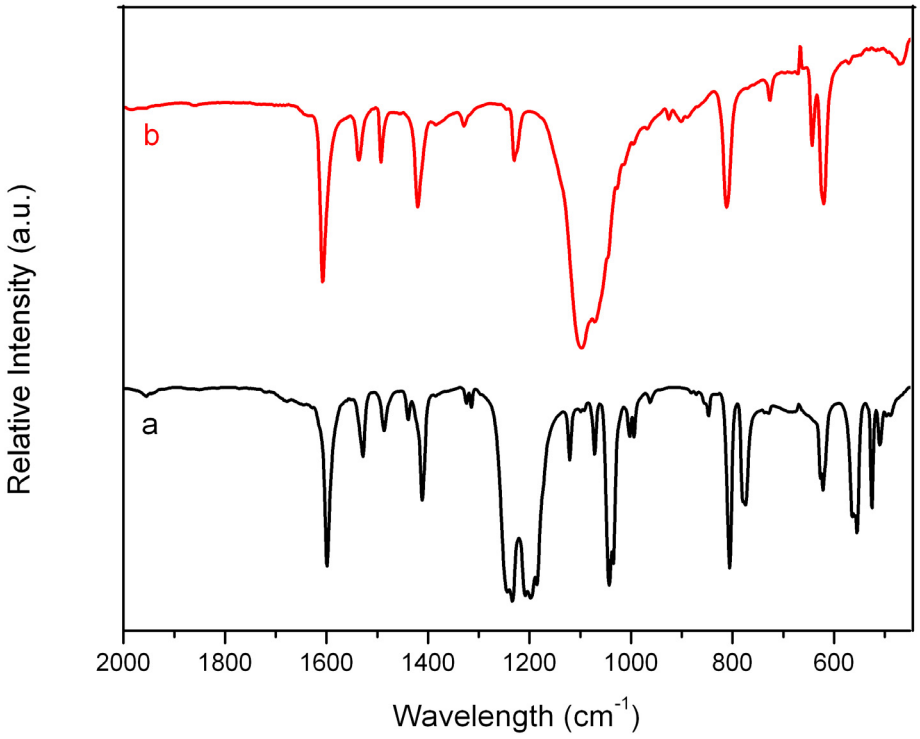

Figure 4.6 FTIR of: (a) as-synthesized SLUG-21; (b) solid after exchange in a solution containing perchlorate and nitrate. The change from broad band at ~1200 cm^{-1} (characteristic of sulfonate) to ~1100 cm^{-1} (characteristic of perchlorate) and survival of the 4,4'-bipyridine stretch (1605s, 1535s, 1490s, 1418s aromatic C=C and C=N) confirm the anion exchange process.

permanganate.

Perchlorate is another problematic anion that diffuses rapidly and widely, emitted from rocket fuel waste along with other sources including pyrotechnics.[232, 233] A mixed anion solution indicates perchlorate is preferred over nitrate by SLUG-21 (Figure 4.6). The anion affinity for SLUG-21 thus displays the following order, with the problematic metalates pollutants topping the list:

$$MnO_4^- > ReO_4^- > ClO_4^- > CrO_4^{2-} > NO_3^- > CO_3^{2-}$$

In addition to the exceptionally high adsorption capacity and selectivity towards problematic anions, there are two other properties that make SLUG-21 advantageous over LDHs: (i) SLUG-21 remains heterogeneous throughout the anion exchange at the bottom of the aqueous solution and can be recovered without centrifuging. LDHs often form a paste, and *ca*. 30 min centrifuging are required for total separation from the solution; (ii) as-synthesized SLUG-21 can be directly employed in anion exchange without pre-treatment. LDHs require calcination up to 450 °C to partially remove the carbonate and render the layers more basic in order to facilitate the anion exchange. Moreover, this state is metastable: calcined LDH retins its optimized adsorption capacity only within 24 hours after calcination due to the memory effect, where the layers rehydrate and reintercalate anions into the interlayer.[217]

4.4 Conclusion

Our cationic material shows superior performance over the extensively studied LDHs and anion exchange resins. SLUG-21 has the potential to selectively trap pertechnetate in high capacity for the treatment of radioactive waste (*cf*. 292 mg/g and 602 mg/g for permanganate and perrhenate, respectively). With the formation of a new crystal structure driving the reaction, the anions would be permanently trapped. Re-use of the material would in fact be undesirable for a highly problematic radionuclide. Under the same experimental conditions, the calcined form of hydrotalcites only reaches 41 mg/g for permangnate and 134 mg/g for perrhenate. Our cationic material therefore overcomes both the low capacity and retention problems of hydrotalcites. It also displays high selectivity towards group 7 oxo-anions over other non-radioactive and non-toxic anions such as nitrate and carbonate, even in 100-fold excess. Other advantageous properties include complete heterogeneity and no need for pre-treatment. Further investigation of this and related cationic extended frameworks are underway to evaluate and exploit their anion trapping properties.

4.5 References

212. Keith, L. H.; Teillard, W. A., *Environ. Sci. Technol.* **1979,** *13*, 416.

213. Wang, Y.; Bryan, C.; Gao, H.; Phol, P. I.; Brinker, C. J.; Yu, K.; Xu, H.; Yang, Y.; Braterman, P. S.; Xu, Z., *Sandia Report (Potential Applications of Nanostructured Materials in Nuclear Waste Management* **2003,** *SAND2003-3313*, 1-95.

214. Izak, P.; Hrma, P.; Arey, B. W.; Plaisted, T. J., *J. Non-Cryst. Solids* **2001,** *289*, 17-29.

215. Mark, R.; Findley, W. N., *Polym. Eng. Sci.* **1978,** *18*, 6-15.

216. Rives, V., *LDHs: Layered Double Hydroxides: Present and Future*. Nova Science Publishers Inc., Hauppauge, New York, USA: **2001**.

217. Goh, K. H.; Lim, T. T.; Dong, Z., *Water Res.* **2008,** *42*, 1343-1368.

218. Long, J. R.; Yaghi, O. M., *Chem. Soc. Rev.* **2009,** *38*, 1213-1214.

219. Tran, D. T.; Zavalij, P. Y.; Oliver, S. R. J., *J. Am. Chem. Soc.* **2002,** *124*, 3966-3969.

220. Rogow, D. L.; Russell, M. P.; Wayman, L. M.; Swanson, C. H.; Oliver, A. G.; J., O. S. R., *Crystal Growth & Design* **2010,** *10*, 823-829.

221. Wang, S.; Alekseev, E. V.; Diwu, J. C.; W. H.; Phillips; B. L.; Depmeier, W.; Albrecht-Schmitt, T. E., *Angew. Chem. Int. Ed.* **2010,** *49*, 1057-1060.

222. Min, K. S.; Suh, M. P., *J. Am. Chem. Soc.* **2000,** *122*, 6834-6840.

223. Du, M.; Zhao, X. J.; Guo, J. H.; Batten, S. R., *Chem. Commun.* **2005**, 4836-4838.

224. Michaelides, A.; Skoulika, S., *Cryst. Growth Des.* **2009,** *9*, 2039-2042.

225. Goulding, H. V.; Hulse, S. E.; Clegg, W.; Harrington, R. W.; Playford, H. Y.; Walton, R. I.; Fogg, A. M., *J. Am. Chem. Soc.* **2010,** *132*, 13618-13620.

226. Fei, H.; Paw, L. U.; Rogow, D. L.; Bresler, M. R.; Abdollahian, Y. A.; Oliver, S. R. J., *Chem. Mater.* **2010,** *22*, 2027-2032.

227. Fei, H.; Rogow, D. L.; Oliver, S. R. J., *J. Am. Chem. Soc.* **2010,** *132*, 7202-7209.

228. Nihei, M.; Han, L.; Oshio, H., *J. Am. Chem. Soc.* **2007,** *129*, 5312-5313.

229. Xue, D.; Zhang, W. X.; Chen, X. M.; Wang, H. Z., *Chem. Commun.* **2008**, 1551-1553.

230. Choi, H. J.; Suh, M. P., *J. Am. Chem. Soc.* **2004,** *126*, 15844-15851.

231. Miyata, S., *Clays Clay Miner.* **1983,** *31*, 305-311.

232. Urbansky, E. T., *Environ. Sci. Pollut. Res. Int.* **2002,** *9*, 187-192.

233. Motzer, W. E., *Environ. Forensics* **2001,** *2*, 301-311.

Chapter 5

Synthesis and Characterization of Two Three-Dimensional Cationic Metal-Organic Frameworks Based on Cadmium and α,ω-Alkanedisulfonate Anions

Abstract

We have successfully synthesized three cadmium-based metal-organic frameworks by utilizing two separate organic linkers to direct the structure. The first material is a three-dimensional neutral framework based on 2D cadmium ethanedisulfonate layers pillared by a 4,4'-bipyridine linker. The other two materials are 3-D cationic frameworks and are the first with propanedisulfonate and butanedisulfonate as extraframework charge balancing anions. Both structures occupy a high symmetry hexagonal crystal system where Cd-bipy chains are arranged into three crystallographically distinct layers that stack spirally along [001]. The framework is stabilized by alkanesulfonate anions that are electrostatically and hydrogen bonded to the framework. Each material was characterized by single-crystal and powder X-ray diffraction. The thermal and luminescent properties were also investigated by thermogravimetric analysis and photoluminescence spectroscopy, respectively. All three materials exhibit high thermal stability to above 300 °C and

efficient blue emissive photoluminescence centered at 425 nm to 450 nm upon 350 nm excitation.

5.1 Introduction

Metal-organic frameworks (MOFs) are an emerging class of inorganic-organic hybrid materials attracting much attention due to not only the vast array of possible topologies[234-238] but potential applications in gas storage/separation,[239-244] size-selective catalysis[245-249] and chemical sensors.[250-252] A continuing challenge in the field of MOFs is the ability to relate structural features and/or functionalities to their properties[253-257] for enhanced efficiency in the desired application, such as gas uptake capacity, degree of separation, catalytic yield, etc. Sulfonate based MOFs are significantly less studied than those of carboxylates and phosphonates mostly due to their weaker coordination strength. Almost all sulfonate networks are based on arylsulfonate due to their considerable linker strength, whereas alkanesulfonates especially with extended carbon chain length have been less studied based on recent reviews.[253-257]

Our research is focused on the solvothermal synthesis of cationic framework materials, including zeotypes, inorganic extended materials and cationic MOFs. The structures are templated by anionic extraframework structure directing agents (SDAs) and are useful for both heterogeneous catalysis and anion-exchange.[258-263] Our previously reported 2D cationic layered structures $[Sb_4O_4(OH)_2][O_3SC_2H_4SO_3]\cdot H_2O$

and $[Ag(4,4'\text{-bipy})]_2[O_3SC_2H_4SO_3]\cdot 4H_2O$ with 1,2-ethanedisulfonate (EDS) as anionic SDA exhibit highly efficient and reusable Lewis acidity in ketalization and esterification, likely due to coordinatively unsaturated Sb^{3+}/Ag^{+} metal sites.[260,261] Our two cationic lead fluoride layers [$Pb_3F_5NO_3$ and $Pb_9F_{16}(ClO_4)_2$] have nitrate (NO_3^-) and perchlorate (ClO_4^-) as anionic SDAs. The former displays dichromate ($Cr_2O_7^{2-}$) anion pollutant trapping, although partial decomposition to α-PbF_2 occurs.[262,263]

Recently, we have extended our approach to the utilization of two mixed organic SDAs, one as anionic extraframework SDA and the other as a neutral intraframework ligand for the formation of cationic MOFs. Transition metals were successful as the metal building block, with the Ag(I) and Cu(I) based materials exhibiting both size-selective heterogeneous catalysis and reversible, selective anion-exchange.[259,260] Attempts to extend the alkylene chain of the anionic SDAs from EDS to 1,3-propanedisulfonate or 1,4-butanedisulfonate have thus far been unsuccessful. This design approach, however, did succeed for $[Pb_2F_2]^{2+}$, where the sulfonate head groups covalently bond to the cationic layers and form neutral, 3D organosulfonate based MOFs.[263] In addition, we obtained a copper hydroxide structure where $[Cu_3(OH)_4]^{2+}$ cationic layers are bridged covalently by 2,6-naphthalenedisulfonate.[264] Anionic templating by larger organopolysulfonates might lead to 3-D cationic nanoporous structures for enhanced efficiency in size-selective catalysis and anion exchange.

MOFs based on transition metal ions with d^{10} electronic configuration [especially Zn(II) and Cd(II)] has been an area of intense research, primarily due to

photoluminescence.[265-269] Transition metal ions with filled d-shell orbitals have no unpaired electrons and facilitate linker-based photoemission. In addition, luminescent MOFs are also more chemically and thermally stable compared to free organic ligands. As a result, MOFs based on transition metals coupled with photoemissive organic linkers have potential applications in white light-emitting diodes,[270-272] chemical sensors,[252,273-275] electroluminescent displays[276] and related applications.

Herein, we report the synthesis and characterization of three Cd(II) based MOFs using two mixed linkers, 4,4'-bipyridine and varying chain length α,ω-alkanedisulfonates. The first material, $[Cd(4,4'\text{-bipy})]_3[O_3S(CH_2)_2SO_3]_3\cdot(4,4'\text{-bipy})_2$, is a neutral three-dimensional framework, while the other two, $[Cd(H_2O)4(4,4'\text{-bipy})][O_3S(CH_2)_3SO_3]$ and $[Cd(H_2O)_4(4,4'\text{-bipy})][O_3S(CH_2)_4SO_3]$, are isoreticular cationic 3-D extended frameworks with extraframework anions. All three solid-state materials are blue luminescent frameworks with λ_{em} ranging from 425 to 450 nm as evidenced by photoluminescence spectroscopy. They are also thermally stable to ca. 300 °C, as determined by thermogravimetric analysis and *ex-situ* thermodiffraction.

5.2 Experimental Section

5.2.1 Reagents

Cadmium nitrate [$Cd(NO_3)_2 \cdot 4H_2O$, Fisher, 99%], 1,2-ethanedisulfonate disodium salt [$NaO_3S(CH_2)_2SO_3Na$ ($EDSNa_2$), TCI America, 98%], 1,3-propanedisulfonate disodium salt [$NaO_3S(CH_2)_3SO_3Na$ ($PDSNa_2$), Acros, 99%], 1,4-butanedisulfonate disodium salt [$NaSO_3(CH_2)_4SO_3Na$ ($BDSNa_2$), TCI America, 98%] and 4,4'-bipyridine [$(C_5H_4N)_2$, TCI America, 98%] were used as purchased for the synthesis.

5.2.2 Synthesis

(i) $[Cd(4,4'\text{-bipy})]_3[O_3S(CH_2)_2SO_3]_3 \cdot (4,4'\text{-bipy})_2$ (which we denote SLUG-23: University of California, Santa Cruz No. 23) was synthesized under hydrothermal conditions. A reactant mixture of $Cd(NO_3)_2 \cdot 4H_2O$ (0.43 g, 1.39 mmol), $EDSNa_2$ (0.65 g, 2.80 mmol), 4,4'-bipy (0.43 g, 2.75 mmol) and H_2O (10.00 g, 556 mmol) was stirred at room temperature for 10 min and then transferred to a 15 mL Teflon lined autoclave to 2/3 filling. The autoclave was heated statically at 180 °C for 3 days under autogenous pressure, followed by slow cooling to room temperature at a rate of 6 °C/h. The pH of the reactant solution decreased slightly from 6.1 to 5.4 during the reaction. Single-crystal colorless blocks were isolated after vacuum filtration and rinsed by water/acetone (yield: 0.70 g, 89.5% based on Cd).

(ii) $[Cd(H_2O)_4(4,4'\text{-bipy})][O_3S(CH_2)_3SO_3]$ (denoted SLUG-24) was synthesized under hydrothermal conditions. A reactant mixture of $Cd(NO_3)_2 \cdot 4H_2O$ (0.43 g, 1.39 mmol), $PDSNa_2$ (0.35 g, 1.40 mmol) 4,4'-bipy (0.43 g, 2.75 mmol) and H_2O (10.00 g,

556 mmol) was stirred at room temperature for 10 min and then transferred to a 15 mL Teflon lined autoclave to 2/3 filling. The autoclave was heated and cooled using the same parameters as above. The pH of the reactant solution slightly decreased from 5.3 to 4.8 during the reaction. Colorless needle-like crystals were isolated after vacuum filtration and rinsed by water/acetone (yield: 0.53 g, 70.5% based on Cd).

(iii) $[Cd(H_2O)_4(4,4'\text{-bipy})][O_3S(CH_2)_4SO_3]$ (denoted SLUG-25) was synthesized with the same ratios and conditions as SLUG-24, using $BDSNa_2$ in place of $PDSNa_2$. The pH of the reactant solution slightly increased from 5.1 to 5.8 during the reaction. Colorless large block crystals were isolated after vacuum filtration and rinsed by water/acetone (yield: 0.72 g, 93.3% based on Cd).

5.2.3 X-ray Crystallography

Single crystal data were collected on a Bruker APEX-II CCD area detector diffractometer under graphite monochromated Mo-Kα radiation (λ=0.71073 Å) using a combination of ω- and φ-scans of 0.3°. An empirical absorption correction was applied using SADABS and the structure was solved by direct methods and expanded routinely. The model was refined by full-matrix least-squares analysis of F^2 against all reflections. All non-hydrogen atoms were refined with anisotropic thermal displacement parameters. Programs used: APEX-II v2.1.4;[277] SHELXTL v6.14;[278] Diamond v3.2e.[279]

5.2.4 Instrumental Details

Samples for powder X-ray diffraction (PXRD) were measured on a Rigaku Americas Miniflex Plus diffractometer, and were scanned from 2 to 60° (2θ) at a rate of 2° per minute and 0.04° step size under Cu-Kα radiation (λ = 1.5418 Å). Thermogravimetric analysis (TGA) was performed using a TA Instruments 2050 TGA by heating from 30 to 600 °C under N_2 purge with a gradient of 15°C/min. Fourier transform infrared (FTIR) spectra were collected on a Perkin-Elmer Spectrum One spectrophotometer using KBr pellets. Photoluminescence spectra were obtained on a Perkin-Elmer LS 50B luminescence spectrometer, tightly packing the finely ground microcrystals on the solid-state aluminum sample holder.

5.3 Results and Discussion

5.3.1 Synthesis and Structure of SLUG-23

SLUG-23 is synthesized hydrothermally in one step and can be prepared in the temperature range of 150 to 180 °C, though with reduced crystallinity for the lower region. Colorless crystals of block shape and suitable size for single-crystal crystallography were found at the bottom of the Teflon liner for the 180 °C reaction. Greater temperature led to lower purity and an unknown phase, while lowering the molar ratios of both organic ligand reactants (EDS and 4,4'-bipy) by 50% to be equal to that of the metal precursor greatly reduced the yield (~ 40% based on Cd).

Table 5.1 Crystallographic data collection and refinement statistics for SLUG-23, SLUG-24 and SLUG-25.

Identification code	SLUG-23	SLUG-24	SLUG-25
Empirical formula	$Cd_3C_{56}H_{52}N_{10}O_{18}S_6$	$Cd_{1.5}C_{19.5}H_{27}N_3O_{15}S_3$	$Cd_{1.5}C_{21}H_{30}N_3O_{15}S_3$
Formula weight	1682.73	808.22	829.26
Temperature	150(2) K	150(2) K	150(2) K
Wavelength	0.71073 Å	0.71073 Å	0.71073 Å
Crystal system	Triclinic	Hexagonal	Hexagonal
Space group	P-1	P3(2)21	P3(2)21
Unit cell dimensions	a = 8.4243(9) Å b = 11.6368(12) Å c = 15.7095(16) Å α = 95.4940(10)° β = 104.7250(10)° γ = 99.1220(10)°	a = 11.7810(10) Å b = 11.7810(10) Å c = 12.6868(15) Å α = 90° β = 90° γ = 120°	a = 11.8001(8) Å b = 11.8001(8) Å c = 12.7024(10) Å α = 90° β = 90° γ = 120°
Volume	1455.6(3) $Å^3$	1524.9(3) $Å^3$	1531.75(19) $Å^3$
Z	1	2	2
Density (calculated)	1.920 $g.cm^{-3}$	1.760 $g.cm^{-3}$	1.798 $g.cm^{-3}$
Absorption coefficient	1.387 mm^{-1}	1.332 mm^{-1}	1.328 mm^{-1}
F(000)	842	810	834
Crystal size (mm^3)	0.075 × 0.05 × 0.025	0.15 × 0.04 × 0.03	0.17 × 0.10 × 0.09
ω range for data collection	2.09 to 26.73°	2.00 to 28.24°	1.99 to 28.28°
Index ranges	$-10 \le h \le 10$, $-14 \le k \le 14$, $-19 \le l \le 19$	$-13 \le h \le 13$, $-15 \le k \le 15$, $-16 \le l \le 16$	$-15 \le h \le 15$, $-15 \le k \le 15$, $-16 \le l \le 16$
Reflections collected	14904	8162	17382
Independent reflections	6107 [R_{int} = 0.0206]	1432 [R_{int} = 0.0211]	2546 [R_{int} = 0.0223]
Completeness to θ	θ=26.73° / 98.8 %	θ=28.24° / 100.0 %	θ=28.28° / 100.0 %
Absorption correction	Empirical	Empirical	Empirical
Max. and min. transmission	0.7459 and 0.6724	0.7459 and 0.6571	0.7459 and 0.6542
Data / restraints / parameters	6107 / 0 / 425	1432 / 0 / 142	2546 / 0 / 150
Goodness-of-fit on F^2	1.021	1.081	1.063
Final R indices [I>2σ(I)]	R_1 = 0.0230, wR_2 = 0.0578	R_1 = 0.0169, wR_2 = 0.0409	R_1 = 0.0179, wR_2 = 0.0471
R indices (all data)	R_1 = 0.0275, wR_2 = 0.0603	R_1 = 0.0176, wR_2 = 0.0412	R_1 = 0.0180, wR_2 = 0.0472
Largest diff. peak and hole ($e^-.Å^{-3}$)	0.642 and -0.575	0.274 and -0.373	0.538 and -0.381

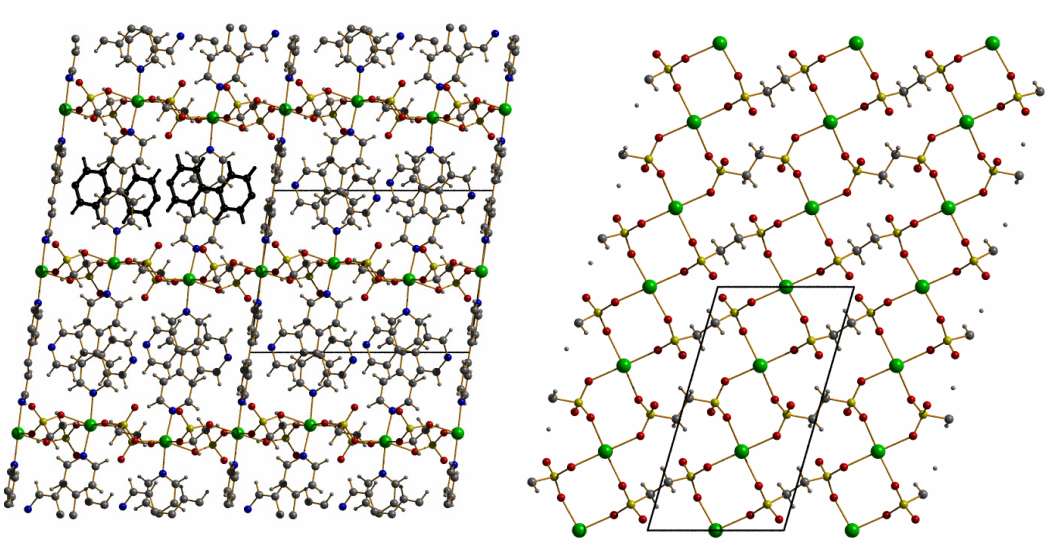

Figure 5.1 Crystallographic views of the SLUG-23 structure: (a) along the *a*-axis, with one of the extraframework 4,4'-bipy molecules highlighted in black; (b) one single layer of Cd-EDS (cadmium: bright green; carbon: gray; sulfur: yellow; oxygen: red; nitrogen: blue; hydrogen: white).

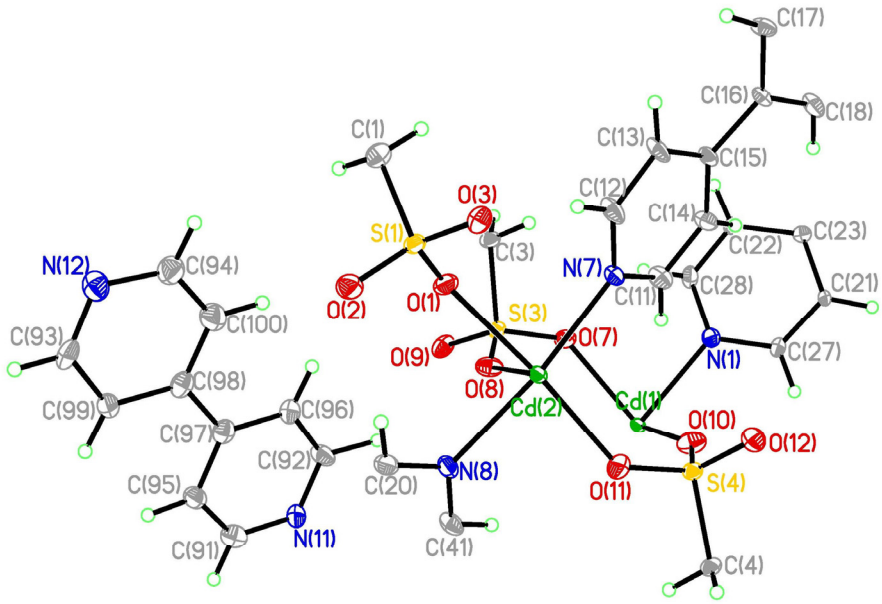

Figure 5.2 ORTEP diagram of the SLUG-23 structure. Thermal ellipsoids are shown at 50% probability.

SLUG-23 crystallizes in a triclinic crystal system with P-1 space group (Table 5.1). The structure consists of Cd(EDS) extended neutral layers with alternating Cd centers and alkanesulfonates (Figures 5.1 and 5.2). Each Cd atom is covalently bonded to four oxygen atoms of four different ethanedisulfonate (EDS) linkers in a square planar manner (Figure 5.1b). Each EDS connects to four Cd atoms through the two oxygens of each sulfonate end. Our previously reported EDS structures based on Sb,[261] Ag,[259,260] and Cu[259] possessed only long metal-oxygen contacts between sulfonate and the metal centers. For SLUG-23, all of the Cd-O distances range from 2.277(2) to 2.380(2) Å (Table 5.2), within the reasonable covalent bond range as evidenced by a search of the CSD.[280] This structure is thus our first example of alkanesulfonate-metal covalent bonding beyond the $[Pb_2F_2]^{2+}$ layered structures. Both series have an analogous bonding feature in that two of the three sulfonate oxygens connect to metal centers.[263, 281]

In addition to four oxygens, each Cd center connects to two 4,4'-bipy nitrogens in a trans configuration, giving a slightly distorted octahedral geometry (Table 5.2 and Figure 5.1a). This latter connectivity forms infinite 1D chains of alternating metal sites and 4,4'-bipy linkers along [010] and connect the Cd(EDS) layers to render SLUG-23 a 3-D neutral MOF. The two aromatic ring planes define a torsion angle of 62.6° and 66.2° for the two crystallographically independent Cd-bipy moieties. Interestingly, free neutral 4,4'-bipy ligands were solved

Table 5.2 Bond Lengths and Angles of SLUG-23 around Cadmium Atom[a]

Cd(1)-N(1)^{i}	2.2659(19)	Cd(1)-N(1)	2.2660(19)
Cd(1)-O(10)	2.3183(16)	Cd(1)-O(10)^{i}	2.3183(16)
Cd(1)-O(7)^{i}	2.3240(15)	Cd(1)-O(7)	2.3240(15)
Cd(2)-N(7)	2.2773(18)	Cd(2)-N(8)	2.2837(19)
Cd(2)-O(11)	2.3077(16)	Cd(2)-O(3)^{ii}	2.3242(15)
Cd(2)-O(1)	2.3495(15)	Cd(2)-O(8)	2.3797(16)
N(1)^{i}-Cd(1)-N(1)	180.00(9)	N(1)i-Cd(1)-O(10)	95.01(6)
N(1)-Cd(1)-O(10)	84.99(6)	N(1)i-Cd(1)-O(10)^{i}	84.99(6)
N(1)-Cd(1)-O(10)^{i}	95.01(6)	O(10)-Cd(1)-O(10)^{i}	180.0
N(1)^{i}-Cd(1)-O(7)^{i}	82.90(6)	N(1)-Cd(1)-O(7)^{i}	97.10(6)
O(10)-Cd(1)-O(7)^{i}	85.76(6)	O(10)^{i}-Cd(1)-O(7)^{i}	94.23(6)
N(1)^{i}-Cd(1)-O(7)	97.10(6)	N(1)-Cd(1)-O(7)	82.90(6)
O(10)-Cd(1)-O(7)	94.24(6)	O(10)^{i}-Cd(1)-O(7)	85.77(6)
O(7)^{i}-Cd(1)-O(7)	180.0	N(7)-Cd(2)-N(8)	168.84(6)
N(7)-Cd(2)-O(11)	97.37(6)	N(8)-Cd(2)-O(11)	86.38(6)
N(7)-Cd(2)-O(3)^{ii}	105.96(6)	N(8)-Cd(2)-O(3)^{ii}	84.42(6)
O(11)-Cd(2)-O(3)^{ii}	90.73(6)	N(7)-Cd(2)-O(1)	86.72(6)
N(8)-Cd(2)-O(1)	89.40(6)	O(11)-Cd(2)-O(1)	175.76(6)
O(3)^{ii}-Cd(2)-O(1)	89.20(5)	N(7)-Cd(2)-O(8)	90.45(6)
N(8)-Cd(2)-O(8)	78.98(6)	O(11)-Cd(2)-O(8)	90.56(6)
O(3)^{ii}-Cd(2)-O(8)	163.23(6)	O(1)-Cd(2)-O(8)	88.29(5)

[a]Symmetry transformations used to generate equivalent atoms:
^{i}-x+1,-y+1,-z ^{ii}-x+1,-y+1,-z+1

crystallographically and reside in the open areas defined by the framework. These molecules stabilize the structure and are perpendicular to the intraframework 4,4'-bipy linker (Figure 5.1a).

5.3.2 Synthesis and Structures of SLUG-24 and SLUG-25

Both SLUG-24 and SLUG-25 crystallize in the same high symmetry hexagonal crystal system with a chiral P3(2)21 space group (Table 5.1). The two isoreticular cationic extended frameworks have slight variation in unit cell dimension owing to the different size of anionic alkanesulfonate. SLUG-24 consists of three crystallographically distinct layers containing infinite Cd-bipy chains of alternating metal and 4,4'-bipy. The chains are oriented along [100] within the first layer, followed by [110] in the second layer and [010] in the third (Figure 5.3a). The chains thus define a 60° angle to the next layer, forming a spiral along [001] and consequently the hexagonal symmetry and chirality of the framework. The distance between interlayer bipy rings (*ca.* 4.2 Å), however, is beyond the accepted distance for any π-π interaction. Instead, the extraframework 1,3-propanedisulfonate anions stabilize the structure through electrostatic charge balancing of the cationic 3-D framework.

Similar to SLUG-23, the Cd atoms in SLUG-24 possess an octahedral geometry (Table 5.3, Figures 5.3 and 5.4), but the square plane instead is occupied by four terminal water molecules; the nitrogen atoms of two different 4,4'-bipy linkers trans to each other again completes the coordination. All three oxygens of each

sulfonate end are hydrogen bonded to the terminal water molecules of three different Cd centers, with donor-acceptor distances between 2.691(3) and 2.780(3) Å (Table 5.4). This large degree of interaction further accounts for the structural and chemical stability of the structure, as well as the inability of the propanedisulfonate anions to be exchanged with other anions in solution such as nitrate, perchlorate, permanganate and ethanedisulfonate.

SLUG-25 displays the analogous cationic structural framework as SLUG-24, with three crystallographically independent Cd(II)-bipy chains packed in an ABCABC manner and connected into a three-dimensional cationic framework *via* the butanedisulfonates (Figure 5.3c). Each of the three distinct Cd centers again have an octahedral coordination environment with a square plane of four water molecules and two trans nitrogen atoms of separate 4,4'-bipy molecules (Table 5.3, Figure 5.4). The six sulfonate oxygens of the anionic 1,4-butanedisulfonates hydrogen bond to six terminal water molecules of five different Cd atoms, with acceptor and donor distance ranging between 2.664(2) and 2.820(2) Å (Table 5.4). Interestingly, the two central carbons of the 1,4-butanedisulfonate anions define a *cis* linkage within the 3D cationic framework (Figure 5.4). This conformation is likely due to the high hexagonal symmetry which forces the long alkyl chain to bend in order to stabilize the structure. In this geometry, the hexagonal center of SLUG-25 is surrounded by three butanedisulfonate anions (Figure 5. 3d).

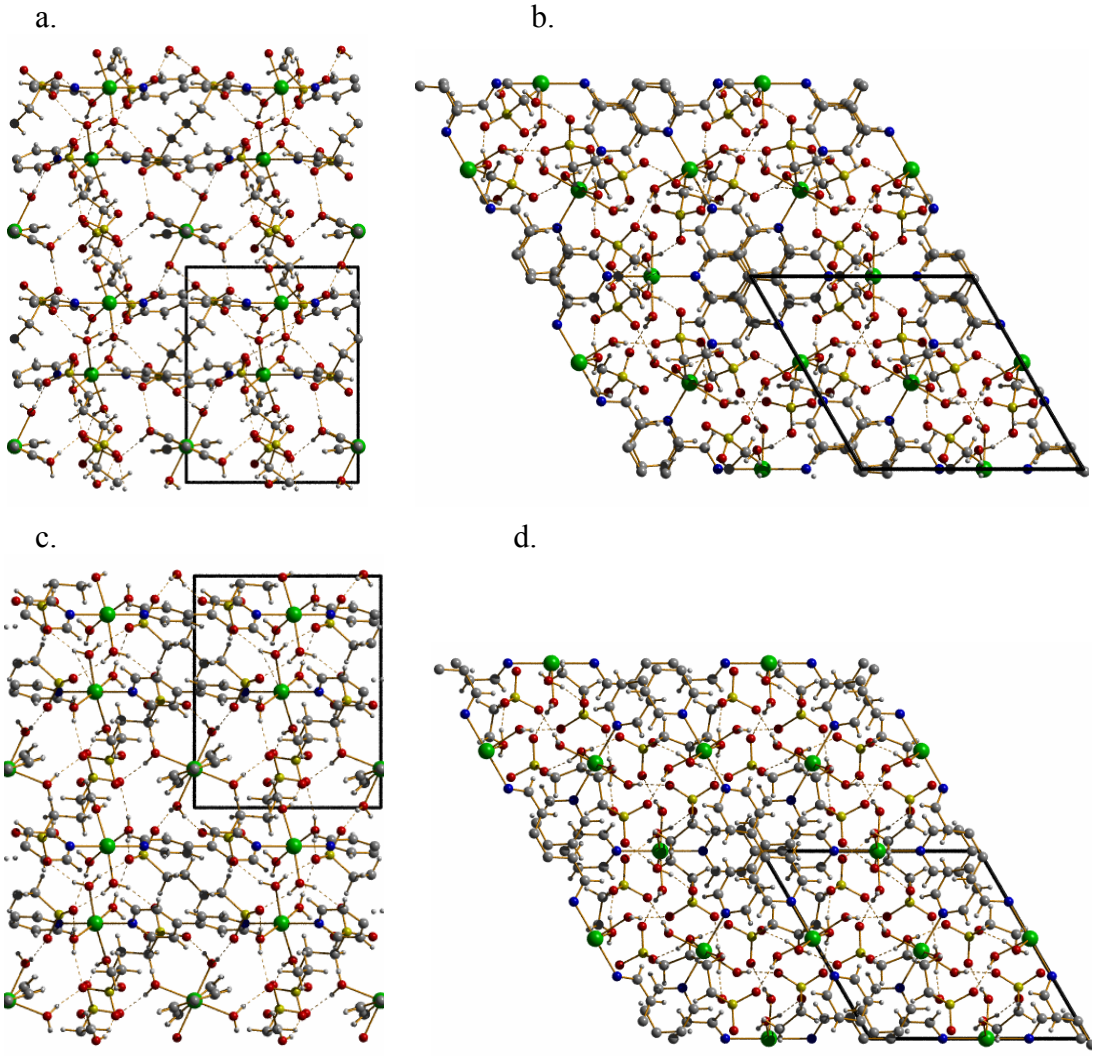

Figure 5.3 Crystallographic *a*-projection (a) and *c*-projection (b) of the SLUG-24 structure, and *a*-projection (c) and *c*-projection (d) of the SLUG-25 structure (cadmium: bright green; carbon: gray; sulfur: yellow; oxygen: red; nitrogen: blue, hydrogen: white).

These two materials are the first examples employing an alkanesulfonate other than the ethylene derivative as extraframework anionic SDA. They are also the first cationic MOFs with strong hydrogen bonding to stabilize the framework instead of

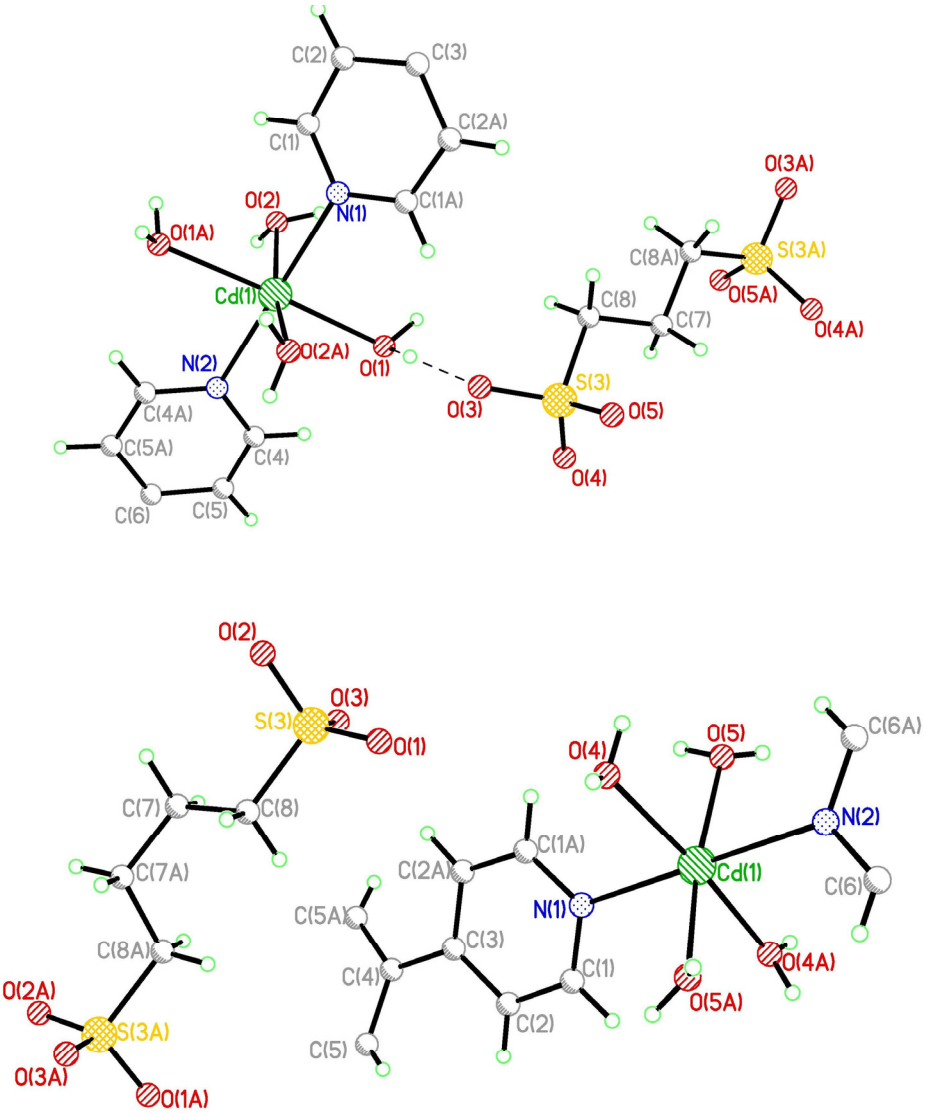

Figure 5.4 ORTEP diagrams of the asymmetric units of SLUG-24 (top) and SLUG-25 (bottom). Thermal ellipsoids are shown at 50% probability.

only conventional electrostatic interactions.[258-261, 263] In general, a large degree of covalent and hydrogen bonding from the anionic SDA imparts high chemical and thermal stability. Employing sulfonates with an extended alkylene chain might give rise to structures with sufficient pore volume to be solvent accessible for possible application in heterogeneous catalysis. On the other hand, more weakly bonded SDAs give the framework greater structural flexibility for solid-state anion-based applications (e.g. anion pollutant trapping, anion exchange, and anion chemical

Table 5.3 Selected Bond Lengths and Angles of SLUG-24[b] and SLUG-25[c]

SLUG-24		SLUG-25	
Cd(1)-O(2)^{i}	2.2618(19)	Cd(1)-O(5)^{i}	2.2536(15)
Cd(1)-O(2)	2.2618(19)	Cd(1)-O(5)	2.2536(15)
Cd(1)-O(1)^{i}	2.3125(18)	Cd(1)-O(4)^{i}	2.3098(15)
Cd(1)-O(1)	2.3125(18)	Cd(1)-O(4)	2.3098(15)
Cd(1)-N(2)	2.323(3)	Cd(1)-N(1)	2.323(3)
Cd(1)-N(1)	2.369(3)	Cd(1)-N(2)	2.370(2)
O(2)^{i}-Cd(1)-O(2)	166.03(10)	O(5)^{i}-Cd(1)-O(5)	171.58(8)
O(2)^{i}-Cd(1)-O(1)^{i}	93.57(7)	O(5)^{i}-Cd(1)-O(4)^{i}	87.01(6)
O(2)-Cd(1)-O(1)^{i}	86.73(7)	O(5)-Cd(1)-O(4)^{i}	93.41(6)
O(2)^{i}-Cd(1)-O(1)	86.73(7)	O(5)^{i}-Cd(1)-O(4)	93.41(6)
O(2)-Cd(1)-O(1)	93.57(7)	O(5)-Cd(1)-O(4)	87.01(6)
O(1)^{i}-Cd(1)-O(1)	177.52(9)	O(4)^{i}-Cd(1)-O(4)	174.29(9)
O(2)^{i}-Cd(1)-N(2)	96.98(5)	O(5)^{i}-Cd(1)-N(1)	94.21(4)
O(2)-Cd(1)-N(2)	96.98(5)	O(5)-Cd(1)-N(1)	94.21(4)
O(1)^{i}-Cd(1)-N(2)	88.76(5)	O(4)^{i}-Cd(1)-N(1)	87.14(4)
O(1)-Cd(1)-N(2)	88.76(5)	O(4)-Cd(1)-N(1)	87.14(4)
O(2)^{i}-Cd(1)-N(1)	83.02(5)	O(5)^{i}-Cd(1)-N(2)	85.79(4)
O(2)-Cd(1)-N(1)	83.02(5)	O(5)-Cd(1)-N(2)	85.79(4)
O(1)^{i}-Cd(1)-N(1)	91.24(5)	O(4)^{i}-Cd(1)-N(2)	92.86(4)
O(1)-Cd(1)-N(1)	91.24(5)	O(4)-Cd(1)-N(2)	92.86(4)
N(2)-Cd(1)-N(1)	180.0	N(1)-Cd(1)-N(2)	180.0

[b]SLUG-24: Symmetry transformations used to generate equivalent atoms: ^{i}x-y,-y,-z+1/3

[c]SLUG-25: Symmetry transformations used to generate equivalent atoms: ^{i}x-y,-y,-z+1/3

sensors).[252, 258, 260, 262, 263, 273, 282] There is a delicate balance between these two factors for the application of interest. Heterogeneous Lewis acidity was not probed based on the non-porous character for all three materials, though surface activity is possible. Both SLUG-24 and SLUG-25 were investigated for anion exchange due to their cationic nature. Initial attempts to exchange the organosulfonates groups for various organic/inorganic anions including EDS, nitrate, perchlorate, permanganate, and perrhenate, however, were unsuccessful. In all cases, the PXRD patterns and FTIR spectra remain the same as the as-synthesized phase. The lack of exchange is likely due to the strong electrostatic interaction and hydrogen bonding between the sulfonate and cationic framework.

Table 5.4 Hydrogen Bonding in SLUG-24[d] and SLUG-25[e]

D-H···A	d(D-H)	d(H···A)	d(D···A)	< (DHA)
SLUG-24				
O(1)-H(1B)···O(3)	0.84	1.94	2.780(3)	174.6
O(2)-H(2B)···O(4)^{i}	0.84	1.93	2.691(3)	150.4
SLUG-25				
O(4)-H(4A)···O(2)^{i}	0.84	1.90	2.738(2)	171.1
O(5)-H(5B)···O(3)^{ii}	0.84	1.88	2.664(2)	154.8
O(4)-H(4B)···O(2)^{iii}	0.75(3)	2.08(3)	2.820(2)	168(3)
O(5)-H(5A)···O(1)^{iv}	0.79(4)	1.89(4)	2.664(2)	165(3)

[d]SLUG-24: Symmetry transformations used to generate equivalent atoms: ^{i}y,x-1,-z

[e]SLUG-25: Symmetry transformations used to generate equivalent atoms: ^{i}x-y,-y+1,-z+1/3; ^{ii} -x+2,-x+y+1,-z+2/3; ^{iii} y,x-1,-z; ^{iv} -x+y+1,-x+1,z+1/3

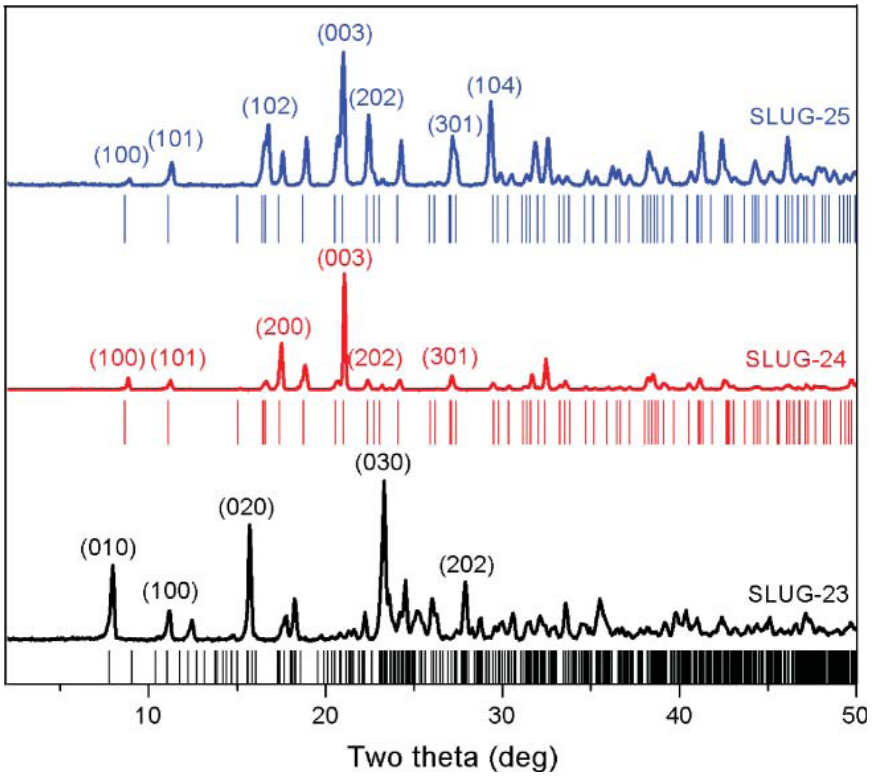

Figure 5.5 PXRD of SLUG-23 (black), SLUG-24 (red), and SLUG-25 (blue) with indication of Miller indices of major reflections. Theoretical peaks are shown as bars below each pattern.

For all three extended frameworks, the PXRD patterns verify high yield (experimental section) and phase purity by matching to the theoretical PXRD pattern from single crystal data (Figure 5.5). Due to the isoreticular nature and close unit cell dimensions of SLUG-24 and SLUG-25, PXRD of both materials display similar peak positions for both theoretical and experimental patterns. FTIR spectra for all three compounds confirm the presence of aromatic linkers [1605s, 1535s, 1490s, 1418s

(cm^{-1}): C=C and C=N aromatic stretch] and sulfonate ligands [1200m, 1070m (cm^{-1}): SO_3^- stretch].

5.3.3 Thermal Characterization

The TGA trace of SLUG-23 (Figure 5.6) shows thermal stability to *ca*. 300 °C, indicating that the intercalated extraframework 4,4'-bipy could not be removed before structure collapse. *Ex-situ* PXRD shows that no structure transformation or loss of crystallinity occurs before 250 °C. The major weight loss at *ca.* 350 °C is due to decomposition of both (i.e. intraframework and extraframework) organic 4,4-bipy ligands and EDS molecules (weight loss: 76.9 % observed; 77.1 % calculated). Accordingly, CdO (ICDD PDF No: 05-0640) was observed by *ex-situ* PXRD after heating to 500 ºC.

The TGA traces of SLUG-24 and SLUG-25 (Figure 5.6) exhibit very similar thermal transitions, although the latter displays slightly lower stability. SLUG-24 exhibits a first gradual weight loss until *ca.* 170 °C, presumably due to removal of the four water molecules bonded to each Cd metal site (observed: 13.1 %; calculated: 13.3 %). *Ex-situ* PXRD after heating the crystals to 180 °C under vacuum indicated no apparent structure rearrangement of the framework. This activated form of SLUG-24 was thermally stable to *ca*. 375 °C, followed by the major decomposition step which occurs in two convoluted stages. The first is likely removal of 4,4'-bipy (observed: 27.0 %; calculated: 27.5 %) and the second removal of propanedisulfonate (observed: 37.4 %; calculated: 38.3 %).

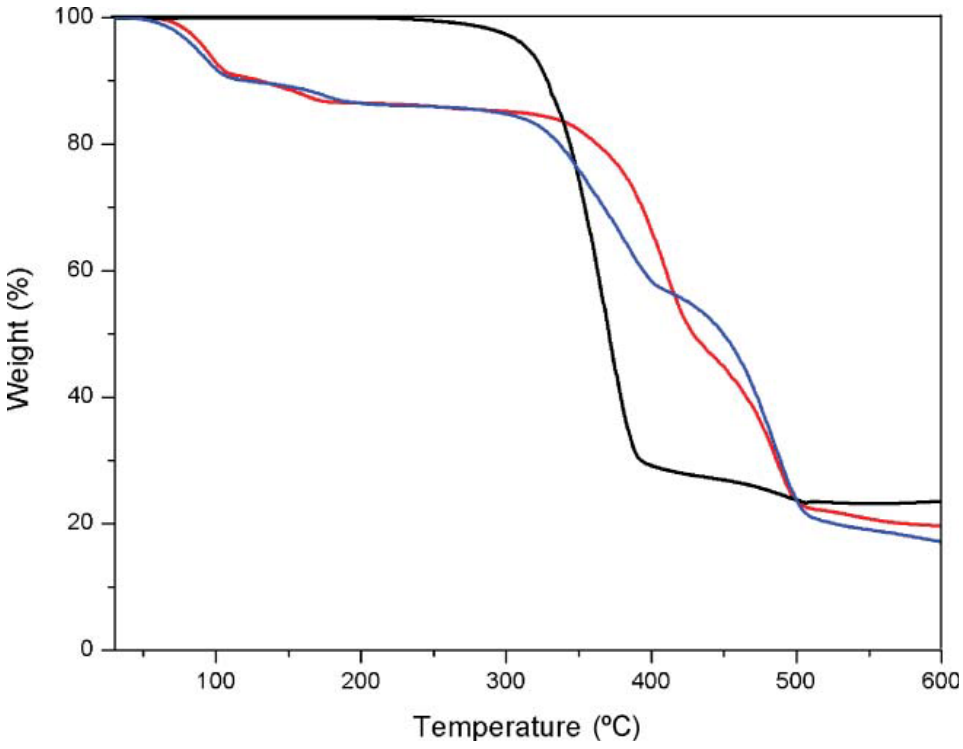

Figure 5.6 TGA traces of SLUG-23 (black), SLUG-24 (red) and SLUG-25(blue) under N_2 purge in the range of 30 to 600 °C.

The major decomposition step of SLUG-25 occurs at slightly lower temperature than SLUG-24 (Figure 5.6). As for SLUG-24, the terminal water molecules are removed between 50 and 170 °C, but the activated form of material is only stable to *ca*. 300 °C. Gradual removal of 4,4'-bipy and butanedisulfonate ligands leaves pure Cd metal (ICDD PDF No. 05-0674) by *ca*. 500 °C. The ultimate phase (Cd) is different from that of SLUG-23 (CdO) likely due to the lack of covalent bonding between Cd and sulfonate oxygens for SLUG-24 and SLUG-25. Indeed, the four terminal water molecules of Cd in SLUG-24 and SLUG-25 do not remain on the

structure after the first decomposition step, leaving no electronegative atoms bonded to Cd after 4,4'-bipy decomposition.

5.3.4 Photoluminescence Spectroscopy

The photoluminescent properties of 2D and 3D MOFs have attracted attention owing to their impressive photostability compared to free organic ligands.[283] All three materials have a strong photoexcitation peak slightly above 350 nm (left, Figure

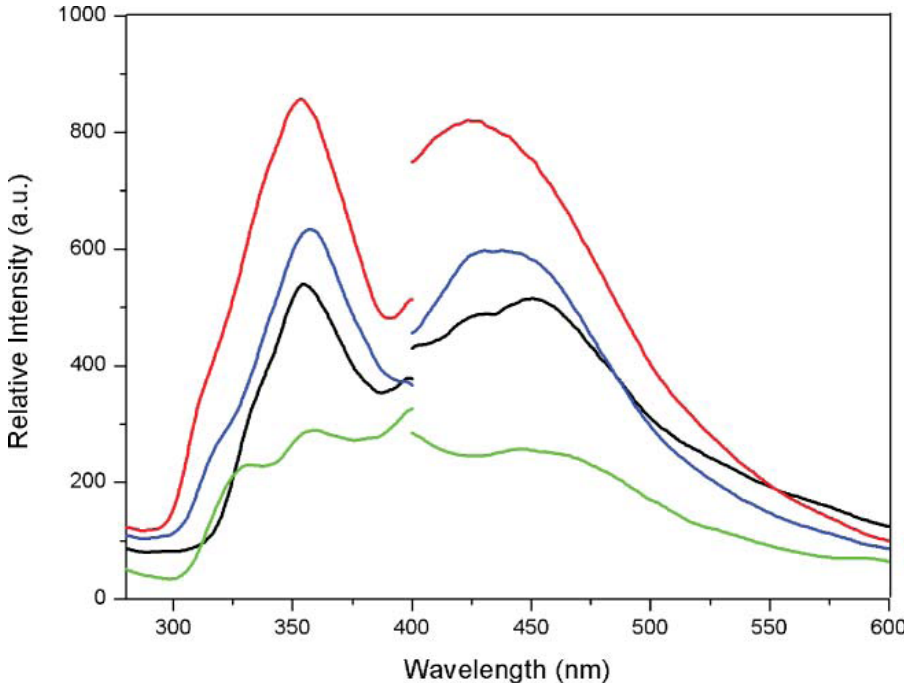

Figure 5.7 Photoluminescence excitation spectra (240 nm to 400 nm; 450 nm monitoring wavelength) and emission spectra (400 nm to 600 nm; 350 nm excitation wavelength) of SLUG-23 (black), SLUG-24 (red), SLUG-25 (blue) and free 4,4'-bipy ligands (green).

5.7). SLUG-23 displayed a broad emission band centered at 450 nm and a weak shoulder at ~ 428 nm with λ_{ex} = 350 nm (right, Figure 5.7). Considering that free 4,4'-bipy has weak emission at 450 nm (green, Figure 5.7), the main emission of SLUG-23 is assigned to a π-π^* intraligand transition due to the 4,4'-bipy pillars as well as the free molecules of crystallization residing in the framework.[284] The weak emissive broad shoulder at 425 nm is likely due to a ligand-to-metal charge transfer (LMCT) emission.[285]

Meanwhile, SLUG-24 (red, Figure 5.7) and SLUG-25 (blue, Figure 5.7) exhibited a similar strong blue emission peak at 424 nm and 428 nm, respectively, under λ_{ex} = 350 nm. Both bands are possibly due to LMCT since all 4,4'-bipy molecules in this case are anchored and part of the MOF framework, leading to the emission at 450 nm. The efficient luminescence for all three materials is possibly due to the high degree of crystallographic orientation of the intraframework 4,4'-bipy linkers.[265] The 4,4'-bipy photoluminescence intensity increases in the order of SLUG-23, SLUG-25 and SLUG-24. The higher PL intensity of SLUG-24 is likely due to the greater 4,4'-bipy alignment between adjacent 1-D chains (torsion angle in the range of 14.9° and 44.0°, Figure 3). SLUG-23 forms the largest dihedral angel between the pillared bipy planes (64.6°, Figure 1) among all three materials.

5.4 Conclusions

These compounds are further examples of using two organic linking agents simultaneously to construct cationically charged MOF structure types. The Cd-EDS layers of SLUG-23 are bridged by 4,4'-bipy at the Cd atoms to construct a neutral 3-D extended framework with thermal stability up to 300 °C. SLUG-24 and SLUG-25 are cationic 3-D MOFs with longer chain alkanedisulfonates. The anions are extraframework and interact through electrostatic and hydrogen bonds to the framework, imparting high thermal and chemical stability. All three compounds were synthesized by a one-step hydrothermal method, with high yield and phase purity. Each exhibits efficient blue-emissive photoluminescence under 350 nm excitation. While the strong bonding of the three materials prevents anion intercalation/exchange, these structures are an important step in the discovery of cationic extended frameworks based on transition metals for anion-based applications.

5.5 References

234. Cheetham, A. K.; Rao, C. N. R.; Feller, R. K., *Chem. Commun.* **2006**, 4780-4795.

235. Ni, Z.; O'Keeffe; M.; Yaghi, O. M., *Angew. Chem. Int. Ed.* **2008,** *47*, 5136-5147.

236. Ferey, G., *Chem. Soc. Rev.* **2008,** *37*, 191-214.

237. Eddaoudi, M.; Moler, D. B.; Li, H.; Chen, B.; Reineke, T. M.; O'Keeffe, M.; Yaghi, O. M., *Acc. Chem. Res.* **2001,** *34*, 319-330.

238. Kitagawa, S.; Kitaura, R.; Noro, S., *Angew. Chem. Int. Ed.* **2004,** *43*, 2334-2375.

239. Morris, R. E.; Wheatley, P. S., *Angew. Chem. Int. Ed.* **2008,** *47*, 4966.

240. Murray, L. J.; Dinca, M.; Long, J. R., *Chem. Soc. Rev.* **2009,** *38*, 1294-1314.

241. Banerjee, R. P., A.; Wang, B.; Knobler, C.; Furukawa, H.; O'Keeffe, M.; Yaghi, O. M., *Science* **2008,** *319*, 939-943.

242. Matsuda, R.; Kitaura, R.; Kitagawa, S.; Kawazoe, Y.; Mita, Y., *Nature* **2005,** *436*, 238-241.

243. Dybtsev, D. N.; Chun, H.; Yoon, S. H.; Kim, D.; Kim, K., *J. Am. Chem. Soc.* **2004,** *126*, 32-33.

244. Li, J.-R.; Kuppler, R. J.; Zhou, H.-C., *Chem. Soc. Rev.* **2009,** *38*, 1477-1504.

245. Hwang, Y. K.; Hong, D. Y.; Chang, J. S.; H.;, J. S.; Seo, Y. K.; Kim, J.; Vimont, A.; Daturi, M.; Serre, C.; Ferey, G., *Angew. Chem. Int. Ed.* **2008,** *47*, 4144-4148.

246. Lee, J. F., O. K.; Roberts, J.; Scheidt, K. A.; Nguyen, S. T.; Hupp, J. T. , *Chem. Soc. Rev.* **2009,** *38*, 1450.

247. Horike, S.; Dinca, M.; Tamaki, K.; Long, J. R., *J. Am. Chem. Soc.* **2008,** *130*, 5854-5855.

248. Seo, J. S.; Whang, D.; Lee, H.; Jun, S. I.; Oh, J.; Jeon, Y. J.; Kim, K., *Nature* **2000,** *404*, 982-986.

249. Cho, S. H.; Ma, B.; Nguyen, S. T.; Hupp, J. T.; Albrecht-Schmitt, T. E., *Chem. Commun.* **2006**, 2563-2565.

250. Allendorf, M. D. H., R. J. T.; Andruszkiewicz, L.; Talin, A. A.; Pikarsky, J.; Choudhury, A.; Gall, K. A.; Hesketh, P. J., *J. Am. Chem. Soc.* **2008,** *130*, 14404-14405.

251. Albrecht, M.; Lutz, M.; Spek, A. L.; van Koten, G., *Nature* **2000,** *406*, 970.

252. Chen, B.; Yang, Y.; Zapata, F.; Lin, G.; Qian, G.; Lobkovsky, E. B., *Adv. Mater.* **2007,** *19*, 1693-1696.

253. Wang, Z.; Cohen, S. M., *Chem. Soc. Rev.* **2009,** *38*, 1315-1329.

254. Chui, S. S.; Lo, S. M.; Charmant, J. P.; Orpen, A. G.; Williams, I. D., *Science* **1999,** *283*, 1148-1150.

255. Song, Y. F.; Cronin, L., *Angew. Chem. Int. Ed.* **2008,** *47*, 4635-4637.

256. Ingleson, M. J.; Barrio, J. P.; Bacsa, J.; Dickinson, C.; Park, H.; Rosseinsky, M. J., *Chem. Commun.* **2008**, 1287-1289.

257. Vimont, A.; Goupil, J.-M.; Lavalley, J.-C.; Daturi, M.; Surble, S.; Serre, C.; Millange, F.; Ferey, G.; Audebrand, N., *J. Am. Chem. Soc.* **2006,** *128*, 3218-3227.

258. Oliver, S. R. J., *Chem. Soc. Rev.* **2009,** *38*, 1868-1881.

259. Fei, H.; Rogow, D. L.; Oliver, S. R. J., *J. Am. Chem. Soc.* **2010,** *132*, 7202-7209.

260. Fei, H.; Paw, L. U.; Rogow, D. L.; Bresler, M. R.; Abdollahian, Y. A.; Oliver, S. R. J., *Chem. Mater.* **2010,** *22*, 2027-2032.

261. Swanson, C. H.; Shaikh, H. A.; Rogow, D. L.; Oliver, A. G.; Campana, C. F.; Oliver, S. R. J., *J. Am. Chem. Soc.* **2008,** *130*, 11737-11741.

262. Tran, D. T.; Zavalij, P. Y.; Oliver, S. R. J., *J. Am. Chem. Soc.* **2002,** *124*, 3966-3969.

263. Rogow, D. L.; Russell, M. P.; Wayman, L. M.; Swanson, C. H.; Oliver, A. G.; J., O. S. R., *Crystal Growth & Design* **2010,** *10*, 823-829.

264. Tran, D. T.; Chernova, N. A.; Chu, D.; Oliver, A. G.; Oliver, S. R. J., *Crystal Growth & Design* **2010,** *10*, 874-879.

265. Allendorf, M. D.; Bauer, C. A.; Bhakta, R. K.; Houk, R. J. T., *Chem. Soc. Rev.* **2008,** *38*, 1330-1352.

266. Bauer, C. A.; Timofeeva, T. V. S., T. B.; Patterson, B. D.; Liu, V. H.; Simmons, B. A.; Allendorf, M. D., *J. Am. Chem. Soc.* **2007,** *129*, 7136-7144.

267. Xue, M.; Zhu, G. Z., Y.; Fang, Q.; Hewitt, I. J.; Qiu, S.;, *Crystal Growth & Design* **2008,** *8*, 427-434.

268. Bordiga, S.; Lamberti, C.; Ricchiardi, G.; Regli, L.; Bonino, F.; Damin, A.; Lillerud, K. P.; Bjorgen, M.; Zecchina, A., *Chem. Commun.* **2004**, 2300-2301.

269. Fang, Q.; Zhu, G. Z., Y.; Fang, Q.; Hewitt, I. J.; Qiu, S.;; Xue, M.; Sun, J.; Sun, F.; Qiu, S., *Inorg. Chem.* **2006,** *45*, 3582-3587.

270. Wang, M.; Guo, S. L., Y.; Cai, L.; Zou, J.; Xu, G.; Zhou, W.; Zheng, F.; Guo, G.;, *J. Am. Chem. Soc.* **2009,** *131*, 13572-23573.

271. Liao, Y.-C.; Lin, C.-H.; Wang, S.-L., *J. Am. Chem. Soc.* **2005,** *127*, 9986-9987.

272. Wang, M.-S.; Guo, G.-C.; Chen, W.; Xu, G.; Zhou, W. W.; Wu, K.; Huang, J.-S., *Angew. Chem. Int. Ed.* **2007,** *46*, 3909-3911.

273. Chen, B.; Wang, L.; Zapata, F.; Qian, G.; Lobkovsky, E. B., *J. Am. Chem. Soc.* **2008,** *130*, 6718-6719.

274. McGarrah, J. E.; Kim, Y. J. H., M.; Eisenberg, R., *Inorg. Chem.* **2001,** *40*, 4510-4511.

275. Bai, Y.; He, G. Z., Y.; Duan, C.; Dang, D.; Meng, Q.;, *Chem. Commun.* **2006**, 1530-1533.

276. Wu, Q.; Esteghamatian, M. H., N.; Popovic, Z.; Enright, G.; Tao, Y.; D'lorio, M.; Wang, S.;, *Chem. Mater.* **2000,** *12*, 79-83.

277. *APEX-II, 2.1.4;*. Bruker-AXS: Madison, WI, 2007.

278. *SHELXTL Crystal Structure Determination Package*. Bruker Analytical X-ray Systems Inc.: Madison, WI, 1995-99.

279. Klaus Brandenburg; H. P. Diamond; Crystal-Impact: Germany, **2007**.

280. *Cambridge Crystal Structure Database*. Bond length of Cu-O: mean=2.062 Å, median=1.958 Å, standard deviation=0.204 Å. 93.4 % of the bond length is shorter than 2.4 Å.

281. Rogow, D. L.; Zapata, G.; Swanson, C. H.; Fan, X.; Campana, C. F.; Oliver, A. G.; Oliver, S. R. J., *Chem. Mater.* **2007,** *19*, 4658-4662.

282. Wang, S.; Alekseev, E. V.; Diwu, J. C.; W. H.; Phillips; B. L.; Depmeier, W.; Albrecht-Schmitt, T. E., *Angew. Chem. Int. Ed.* **2010,** *49* (6), 1057-1060.

283. Doty, F. P.; Bauer, C. A. S., A. J.; Grant, P. G.; Allendorf, M. D.;, *Adv. Mater.* **2008,** *20*, 1-7.

284. de Lill, D. T.; de Bettencourt-Dias, A.; Cahill, C. L., *Inorg. Chem.* **2007,** *46*, 3960-3965.

285. Lu, W.-G.; Jiang, L.; Feng, X.-L.; Lu, T.-B., *Crystal Growth & Design* **2006,** *6*, 564-571.

Chapter 6

Copper Hydroxide Ethanedisulfonate: A Cationic Layered Material for High-Capacity Anion Exchange

Abstract

We have discovered the first Cu(II)-based cationic layered inorganic framework $[Cu_4(OH)_6][O_3SCH_2CH_2SO_3]$ (SLUG-26) beyond layered double hydroxides. This is one rare example that depends on M-O-M inorganic connectivity to construct 2D positively charged infinite sheets, and 1,2-ethanedisulfonate in the interlamellar regions are electrostatically intercalated into the layered structure to charge-balance the framework. SLUG-26 represents an entirely new transition metal based cationic metalates. Moreover, this cationic inorganic material displays excellent anion exchange properties in both inorganic and organic anionic pollutants, which are characteristic of metal oxo-hydroxo anions and pharmaceuticals, respectively. Despite its structural similarities to hydrotalcites, it overcomes the low capacity problem residing in LDHs due to latter strong affinity towards carbonate. SLUG-26 demonstrates five time higher adsorption capacity for permanganate with a value over 200 mg/g, thus potentially applicable in trapping the other group 7 oxo-anion pertechnetate. In addition to metal oxo-anion pollutant, the material displayed flexibility in anion exchange for variable-length α,ω-alkanedicarboxylate, which may

be a pathway to adsorbing other problematic anions and/or increasing capacity. Besides anion exchange applications, the inorganic nature of this material also help SLUG-26 to possess a high thermal stability up to ~ 300 °C and chemical stability in water and common organic solvents.

6.1 Introduction

Many inorganic pollutants in the form of metal oxo-hydroxo anions are listed as EPA (U.S. Environmental Protection Agency) priority pollutants.[286] Recently, EPA set a national limit for perchlorate (ClO_4^-, a widespread anion occurring from rocket fuel, fireworks and other sources) in drinking water.[287] Chromate (CrO_4^{2-}) and pertechnetate (TcO_4^-) are also problematic monomeric oxo-anions, in this case upon the vitrification of radioactive waste.[288,289] Meanwhile, pharmaceuticals and their metabolites have gained increasing attention as pollutants, many existing as organic anions at neutral pH. Current treatment processes are insufficient to adsorb them in high capacity and at reasonable cost.[290] Chlorination can lead to even more toxic compounds, such as monohalogenated or oxidized by-products.[291] The typical approach to trap these intrinsically anionic pollutants remains ion exchange resins, though these organic polymers possess limited thermal and chemical stability and thus longevity.[291]

Cationic inorganic layered materials are 2-D extended architectures where the positively charged layers are held together electrostatically by charge-balancing

anions. One typical and widely studied example is the layered double hydroxides with general formula $[M^{2+}_{1-x}M^{3+}_{x}(OH)_2][A^{n-}_{x/n} \cdot mH_2O]$, where M^{2+} and M^{3+} are a range of metals (e.g. Mg^{2+} and Al^{3+}), x is the ratio of $M^{3+}/(M^{2+}+M^{3+})$ and A^{n-} are n-valent interlamellar anions (e.g. CO_3^{2-}).[292,293] Copper-containing LDHs with a second transition or main-group metal has been shown to catalyze benzene oxidation. Also known as hydrotalcites, LDHs are considered plausible alternatives to resins and can exchange many inorganic and organic anions reversibly. Their selectivity towards toxic anions over carbonate and other interfering anions, however, limits adsorption capacities and thus potential application in water purification. Indeed, this class of materials often requires calcination pre-treatment before ion exchange and displays difficulty in recovery and reuse.[294]

Our group has reported a series of cationic layered inorganic materials consisting of lower p-block metal fluoride and oxide-hydroxide layers charge-balanced by nitrate, perchlorate or alkanedisulfonate.[295-298] Attempts to anion exchange the interlamellar anions for toxic pollutants, however, were either unsuccessful or led to decomposition of the host layers. Meanwhile, layered rare earth hydroxides are an emerging class of inorganic materials with halide, nitrate or other anions in the interlayer region.[299-302] In addition, two three-dimensional cationic inorganic extended frameworks were also reported last year. The structures are based on thorium and ytterbium, charge-balanced by borate and chloride, respectively.[303,304] The structures exchange for several smaller anions to 72%, though excess solid was required. Unlike metal-organic frameworks, no investigation has

been made on synthesis of cationic inorganic extended materials based on the less toxic, lower cost and more chemically understood first row transition metals.

Herein, we report the successful synthesis and crystallographic characterization of the first example beyond LDHs of a copper based cationic inorganic material. $[Cu_4(OH)_6][O_3SCH_2CH_2SO_3]\cdot 2H_2O$ (which we denote SLUG-26, University of California, Santa Cruz, Structure No. 26) possesses high thermal and chemical stability. Infinite M-O-M 2-D inorganic connectivity results in a rare cationic copper hydroxide layer. This first non-LDH copper hydroxide cationic inorganic extended structure displays rich anion intercalation chemistry, with exchange for variable-length α,ω-alkanedicarboxylates and anion pollutant trapping properties.

6.2 Experimental Section

6.2.1 Synthesis

Copper(II) nitrate pentohemi-hydroxide [0.65 g, $Cu(NO_3)_2\cdot 2.5H_2O$, Riedel-de Haen, 98 %], 1,2-ethanedisulfonate, disodium salt (2.11 g, $NaO_3SCH_2CH_2SO_3Na$, Acros Organic, 99 %), Hexadecyltrimethylammonium bromide [0.025g, $(C_{16}H_{33})N(CH_3)_3Br$, Sigma, 99 %], and deionized water (8 ml) were introduced into a 15 ml autoclave. The autoclave was sealed and heated statically at 150 °C for 5 days under autogeneous pressure, followed by cooling to room temperature at a rate of 6 °C/h. Colorless large block crystals were isolated after filtration and rinsed by acetone and deionized water (yield: 0.30 g, 74 % based on copper).

6.2.2 Anion exchange

Absorption capacity experiment was carried out by 0.0290 g (1×10^{-3} mol) as-synthesized SLUG-26 introduced into 0.0158 g (1×10^{-3} mol) $KMnO_4$ (Fisher, 99.8%) aqueous solution. Both calcined and uncalcined LDHs were also studied for comparison. The calcined form of hydrotalcite was prepared by annealing at 450 °C for 2 hours and used for anion exchange within 6 hours. 0.0603 g (1×10^{-3} mol) of both forms of LDHs was introduced into the same solution as above, followed by the same reaction. Intercalation chemistry was carried out between 0.0580 g (2×10^{-3} mol) SLUG-26 into aqueous solution containing 3 molar fold excess (6×10^{-3} mol) disodium malonate (Sigma, 99%), disodium succinate (TCI America, 99%), or disodium glutarate (TCI America, 99%). The solution was stirred for 24 hours, followed by filtration to separate the solids for characterization.

6.2.3 Synchrotron X-ray Crystallography

Crystallography intensity data were collected at 150K on a D8 goniostat equipped with a Bruker APEXII CCD detector at Beamline 11.3.1 at the Advanced Light Source (Lawrence Berkeley National Laboratory) using synchrotron radiation tuned to λ=0.7749Å. $[Cu_4(OH)_6][O_3SCH_2CH_2SO_3]\cdot 2H_2O$ (SLUG-26): blue needle-like, crystal dimensions 0.700×0.005×0.005 mm; Monoclinic; space group P2(1)/c; *a* = 5.5798(5) Å; *b* = 6.1164(6) Å; *c*= 19.2058(18) Å; α = 90°; β = 97.672(5)°; γ = 90°; V = 649.59(11) $Å^3$; Z = 4; T = 150(2) K; λ(synchrotron) = 0.77490 Å; μ(synchrotron) = 6.857 mm^{-1}; d_{calc} = 2.967g.cm^{-3}; 7481 reflections collected; 1274

unique (R_{int} = 0.0739); giving R_1 = 0.0394, wR_2 = 0.1088 for 1022 data with [I>2σ(I)] and R_1 = 0.0483, wR_2 = 0.1145 for all 1274 data. The data were corrected for absorption and beam corrections based on the multi-scan technique as implemented in SADABS. The structure was solved by direct methods with anisotropic refinement of F^2 by full-matrix least-squares.

6.2.4 Instrumental Details

Samples for PXRD were measured on a Rigaku Americas Miniflex Plus diffractometer, and were scanned from 2 to 60 ° (2θ) at a rate of 2 °·min^{-1} and 0.04 ° step size, under Cu-Kα radiation (λ = 1.5418 Å). UV-Vis spectroscopic studies were performed with a Hewlett-Packard Model 8452A UV-Vis spectrophotometer to monitor the exchange progress. FTIR spectroscopy of the materials was accomplished using a Perkin-Elmer Spectrum One spectrophotometer with KBr pellets. Thermogravimetric analysis (TGA) was performed using a TA Instruments 2050 TGA by heating from 25 to 600 °C under N_2 purge with a gradient of 15 °C/min. *In-situ* mass spectra coupled to the TGA were collected on a Pfeiffer Vacuum ThermoStar GSD 301 T3 mass spectrometer with a 70 eV ionization potential.

Table 6.1 Crystallographic Information, Data Collection, and Refinement Parameters for SLUG-26

Empirical formula	$Cu_2CH_7SO_7$	
Formula weight	290.21	
Temperature	150(2) K	
Wavelength	0.77490 Å (synchrotron)	
Crystal system	Monoclinic	
Space group	P2(1)/c	
Unit cell dimensions	a = 5.5798(5) Å	α = 90°
	b = 6.1164(6) Å	β = 97.672(5)°
	c = 19.2058(18) Å	γ = 90°
Volume ($Å^3$)	649.59(11)	
Z	4	
Density (calculated, $g \cdot cm^{-3}$)	2.967	
Absorption coefficient (μ, mm^{-1})	6.857	
F(000)	572	
Crystal size (mm^3)	0.700 × 0.005 × 0.005	
ω range for data collection (°)	3.50 to 26.02	
Index ranges	$-6 \le h \le 6$, $-7 \le k \le 7$, $-23 \le l \le 23$	
Reflections collected	7481	
Independent reflections	1274 [R_{int} = 0.0739]	
Completeness to θ = 26.02°	99.7 %	
Absorption correction	Empirical	
Refinement method	Full-matrix least-squares on F^2	
Max. and min. transmission	0.7471 and 0.4442	
Data / restraints / parameters	1274 / 0 / 114	
Goodness-of-fit on F^2	1.058	
Final R indices [I>2σ(I)]	R_1 = 0.0394, wR_2 = 0.1088	
R indices (all data)	R_1 = 0.0483, wR_2 = 0.1145	

6.3 Results and Discussion

6.3.1 Synthesis

Blue crystals of SLUG-26 were synthesized under hydrothermal conditions with pure phase at optimized conditions (experimental section). Synthesis temperature higher than the ideal 150 °C (160 °C to 180 °C) resulted in CuO (PDF-ICDD #98-000-0429) as the majority phase. Lower temperature (< 125 °C) produced

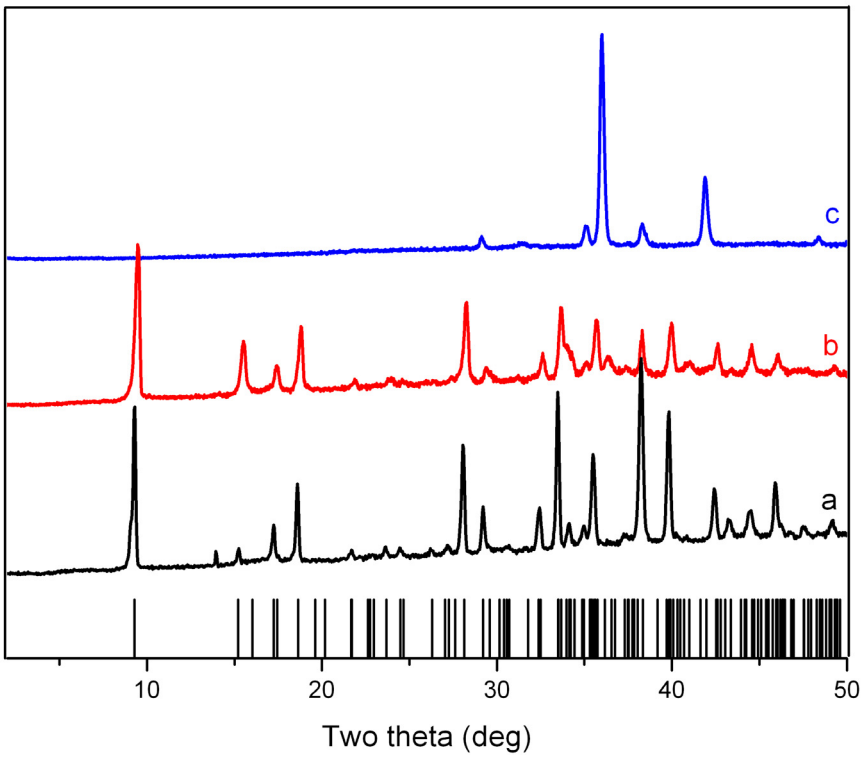

Figure 6.1 PXRD of the as-prepared material (theoretical data from single-crystal X-ray data shown at bottom) and ex-situ measurements after heating to 275 °C (b), 500 °C (c) under N_2 flow.

either clear solution or lower yield of the product. Excess 1,2-ethanedisulfonate (EDS) with a molar ratio of 1:4 for copper nitrate to disodium ethanedisulfonate was necessary, since lower molar ratios (1:1 to 1:2) gave no solid product. Presence of the cationic surfactant hexadecyltrimethyl-ammonium (CTAB) was also necessary for crystal formation, which is known to facilitate rod-like crystal growth.[305] The high yield and phase purity was supported by experimental powder X-ray diffraction (PXRD) matching well with the theoretical pattern simulated from single-crystal data (Figure 6.1).

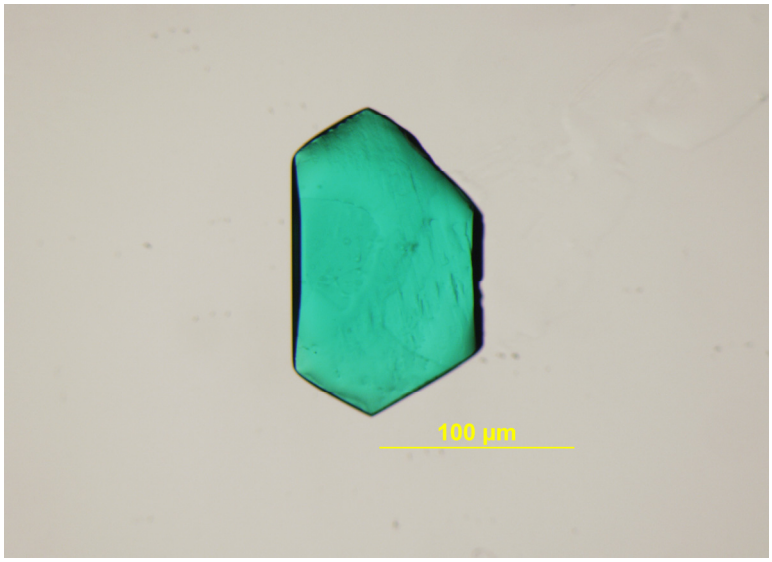

Figure 6.2 Optical microscopy of SLUG-26 crystals.

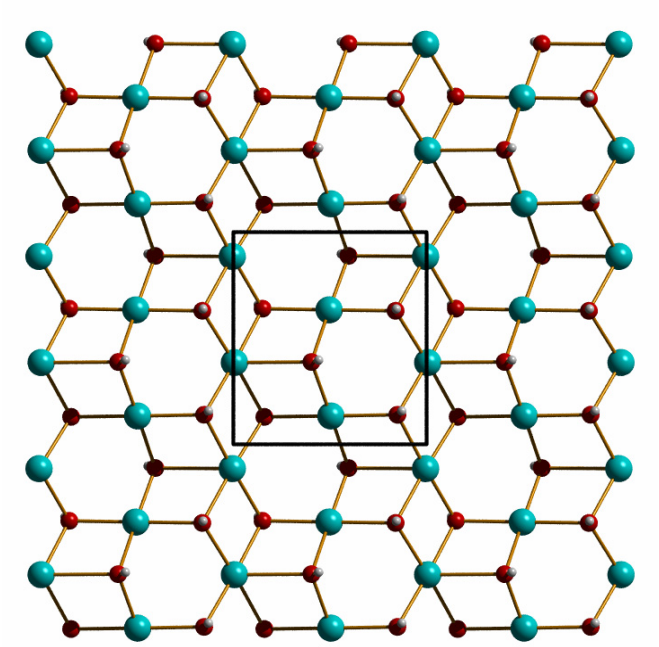

Figure 6.3 Crystallographic view of SLUG-26 along c-axis of one layer of $[Cu_4(OH)_6]^{2+}$.(Cu-blue, O-red, S-yellow, C-gray, H-light gray)

6.3.2 Structural Characterization

SLUG-26 crystallizes with a blue needle-like morphology (Figure 6.2). Synchrotron single-crystal X-ray diffraction reveals that the structure consists of a cationic copper hydroxide layer with EDS as interlamellar charge-balancing anion (Figures 6.3 and 6.4). The $[Cu_4(OH)_6]^{2+}$ layer has two crystallographically independent Cu centers with similar octahedral coordination environments (Figures 6.3 and 6.5). Four oxygens in the positively charged layer define a square-plane

around Cu1, while one oxygen (O1) of two separate EDS molecules (one above the given layer, one below) weakly bond to complete the octahedral geometry. The other copper atom (Cu2) has the same square-planar connectivity to four intralayer oxygens, with an axial connection to an intralayer hydroxyl group and another weak bond to O1 of EDS. All oxygens in the $[Cu_4(OH)_6]^{2+}$ layer are protonated and triply bridge to metal centers as for LDHs, with the proton of each pyramidal OCu_3 center pointing towards the interlamellar region.

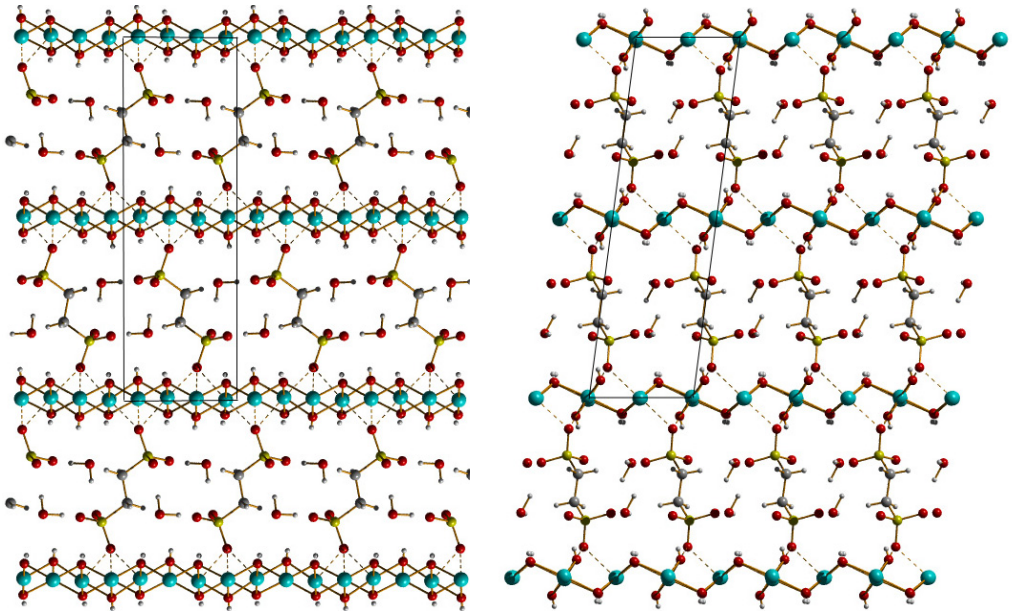

Figure 6.4 Crystallographic view of SLUG-26 along a-axis (left) and along b-axis (right). (Cu-blue, O-red, S-yellow, C-gray, H-light gray)

The cationic feature of this new inorganic topology is defined by electrostatic interaction between EDS and positively charged cuprate layers. Only one oxygen (O1) of each sulfonate coordinates to the Cu centers (O_2SO--Cu) by weak interaction [2.409(3) Å to 2.488(4) Å]. These contact distances are not only significantly longer than the intralayer square planar Cu-O bond lengths [1.914(3) Å to 2.001(3) Å] but also longer than the intralayer axial Cu-O bond length [2.304(3) Å] which is elongated by a d^9 Jahn-Teller distortion. The Cambridge Crystal Structure Database (CSD) indicates that 2.4 Å is well outside the accepted distance for a covalent Cu-O

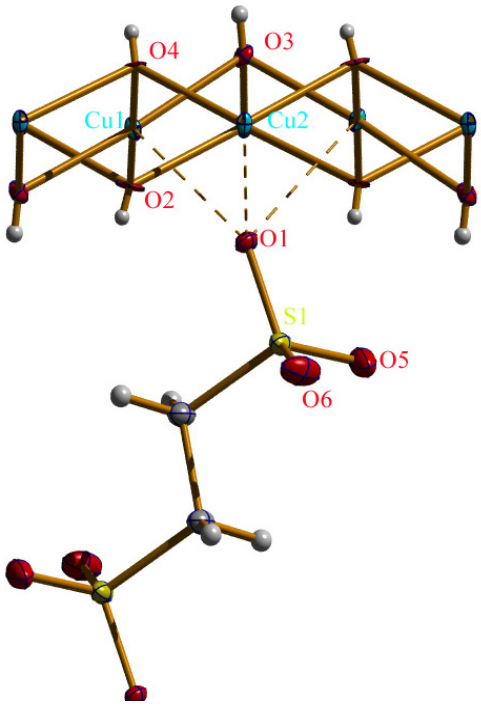

Figure 6.5 Oak Ridge thermal ellipsoid plot diagrams and atom labeling schemes of the coordination spheres of SLUG-26.

bond [2.062 ± 0.204 Å].[306] Indeed, CSD indicates that 92 % of Cu-O bonds are shorter than 2.4 Å, even with the Jahn-Teller effect. Most of the longer bond distances are weakly coordinating monodentate water ligands, which are easily dissociated and thus not ascribed to covalent bonding.[307-310] The cuprate layers are thus not covalently bonded to the EDS anions, indicating this material is indeed a cationic 2-D layered inorganic structure. Two water molecules are intercalated in the

Table 6.2 Bond Lengths (Å) and Angles (°) around the Copper Atoms in SLUG-26

Cu(1)-O(3)	1.914(3)	Cu(1)-O(3)^{i}	1.926(3)
Cu(1)-O(2)	1.975(4)	Cu(1)-O(4)	2.001(3)
Cu(1)-O(1)	2.446(3)	Cu(1)-O(1)^{i}	2.488(4)
Cu(2)-O(4)^{ii}	1.987(4)	Cu(2)-O(2)^{iii}	1.994(4)
Cu(2)-O(2)^{iv}	1.995(4)	Cu(2)-O(4)	2.005(3)
Cu(2)-O(3)	2.304(3)	Cu(2)-O(1)^{ii}	2.409(3)
O(3)-Cu(1)-O(3)^{i}	175.54(8)	O(3)-Cu(1)-O(2)	97.46(16)
O(3)^{i}-Cu(1)-O(2)	85.10(16)	O(3)-Cu(1)-O(4)	83.66(14)
O(3)^{i}-Cu(1)-O(4)	93.65(14)	O(2)-Cu(1)-O(4)	177.61(14)
O(3)-Cu(1)-O(1)^{i}	88.28(14)	O(3)-Cu(1)-O(1)	93.93(16)
O(4)-Cu(1)-O(1)^{i}	94.79(13)	O(2)-Cu(1)-O(1)^{i}	83.18(15)
O(4)-Cu(1)-O(1)	83.00(14)	O(2)-Cu(1)-O(1)	89.26(15)
O(1)-Cu(1)-O(1)^{i}	170.67(11)	O(3)^{i}-Cu(1)-O(1)^{i}	88.39(16)
O(3)^{i}-Cu(1)-O(1)^{i}	93.93(13)	O(4)^{ii}-Cu(2)-O(2)^{iii}	80.12(17)
O(4)^{ii}-Cu(2)-O(2)^{iv}	97.68(16)	O(2)^{iii}-Cu(2)-O(2)^{iv}	177.67(13)
O(4)^{ii}-Cu(2)-O(4)	177.21(11)	O(2)^{iii}-Cu(2)-O(4)	102.53(16)
O(2)^{iv}-Cu(2)-O(4)	79.66(17)	O(4)^{ii}-Cu(2)-O(3)	107.44(13)
O(2)^{iii}-Cu(2)-O(3)	75.36(14)	O(2)^{iv}-Cu(2)-O(3)	106.13(14)
O(4)-Cu(2)-O(3)	74.25(12)	O(4)^{ii}-Cu(2)-O(1)^{ii}	84.25(12)
O(2)^{iii}-Cu(2)-O(1)^{ii}	94.13(14)	O(2)^{iv}-Cu(2)-O(1)^{ii}	84.86(14)
O(4)-Cu(2)-O(1)^{ii}	94.64(12)	O(3)-Cu(2)-O(1)^{ii}	162.26(13)

Symmetry transformations used to generate equivalent atoms:
^{i}-x+1,y-1/2,-z+1/2 ^{ii}-x,y+1/2,-z+1/2 ^{iii}-x+1,y+1/2,-z+1/2 ^{iv}x-1,y,z

interlamellar regions as for LDHs, and calculations of solvent accessible void space per unit cell is 36.3 $Å^3$.[311] The resultant 1-D hydrophilic channels along the c-axis define 5.6 % of the entire structure and are stabilized by hydrogen bonding to the cuprate-EDS network. This interaction contributes to the chemical stability observed in water, ethanol and other common organic solvents.

This topology is the first example of a 2-D cationic pure cuprate and one rare non-LDH example based on only a first row transition metal. There are three similarities between SLUG-26 and LDHs: (i) octahedral coordination around metal centers, which have not been seen with non-LDH type cationic inorganic materials; (ii) triply bridging oxygens that are protonated; (iii) hydrogen bonding network with the intercalated anion and water molecules. These structural characteristics likely allow the formation of a cationic structure, for a range of potential applications similar to LDHs such as anion exchange, catalysis and drug delivery.[292] In addition to PXRD, Fourier-transform infrared spectroscopy (FTIR) also confirms the presence of sulfonate ligands [1200 m, 1070 m (cm^{-1}): RSO_3^- stretch].

6.3.3 Thermal Characterization

Thermalgravimetric analysis-mass spectroscopy (TGA-MS) indicates SLUG-26 is thermally stable to *ca*. 300 °C, which is also observed *ex-situ* thermodiffraction by heating the crystals to 275 °C with no structure rearrangement (Figure S1). The major decomposition step occurred in the temperature range from 300 °C to 400 °C with mass spectrum fragments indicating the removal of organosulfonate. The theoretical mass loss from SLUG-26 to CuO is consistent with the major

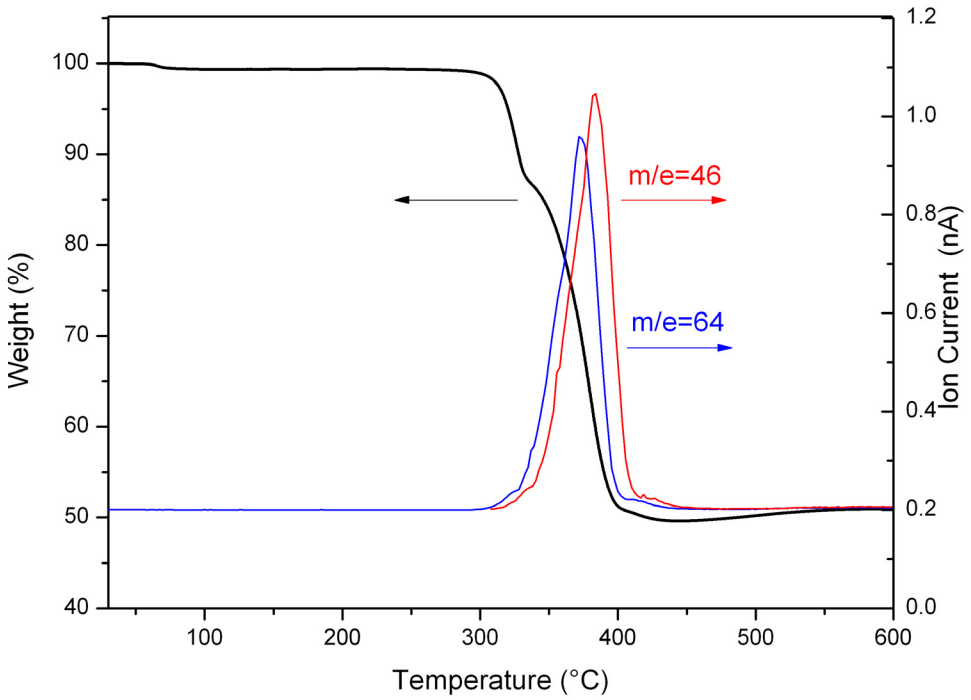

Figure 6.6. Thermogravimetric trace (black) and coupled mass spectra (blue and red for m/e = 46 and 64, respectively) of SLUG-26.

decomposition in TGA (experimental: 49.0 %, theoretical: 45.6 %). The 64 m/z fragment corresponds to the decomposition of sulfonate end to SO_2, and the 46 m/z fragment observed is likely to be $-SCH_2-$ in EDS. TGA traces indicate the collapse of the structure from layered framework to metal oxides, which is also supported by thermodiffraction after 500 °C under N_2 flow decomposing to CuO (ICDD PDF# 98-000-429) phase.

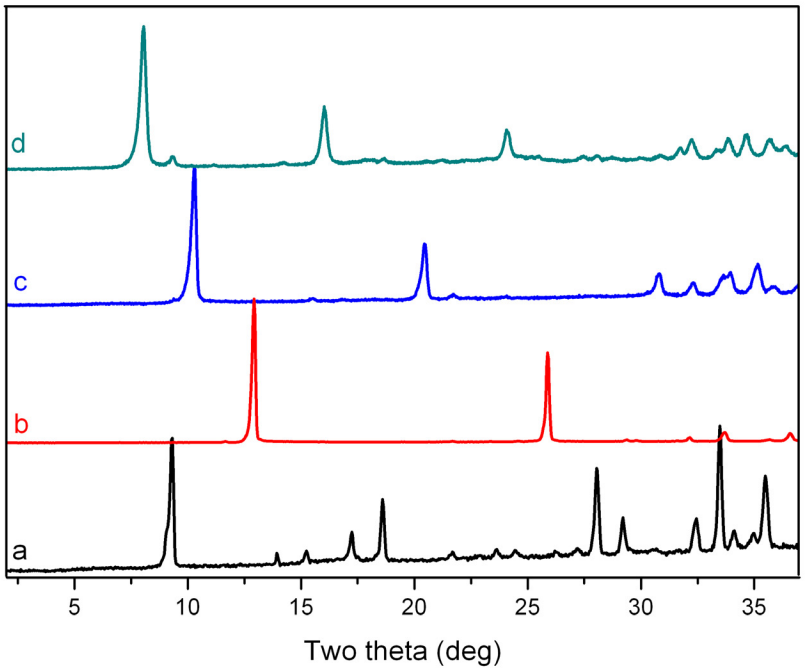

Figure 6.7 PXRD of (a) as-synthesized SLUG-26; (b) SLUG-26 after exchange with malonate; (c) SLUG-26 after exchange with succinate; (d) SLUG-26 after exchange with glutarate.

6.3.4 Intercalation Chemistry

Since SLUG-26 represents an entirely new transition metal based cationic metalate, the intercalation chemistry was investigated by anion exchange, first with various α,ω-alkanedicarboxylate salts. A 3-fold molar excess of malonate, succinate and glutarate in aqueous solution was studied (see details in experimental section). Low-angle (001) diffraction peaks characteristic of the layer–to-layer distance shifted as expected for anion uptake of malonate [$^{-}O_2CCH_2CO_2^{-}$], succinate [$^{-}O_2C(CH_2)_2CO_2^{-}$], and glutarate [$^{-}O_2C(CH_2)_3CO_2^{-}$] (Figure 6.7). The exchange gave a decrease of d-spacing from 9.6 Å to 7.2 Å for malonate and to 8.6 Å for succinate. The intercalation of glutarate between the $[Cu_4(OH)_6]^{2+}$ layers was also successful and resulted an increase of d-spacing from 9.6 Å to 11.1 Å. The completeness of each anion exchange is 100 % for malonate, 98.7 % for succinate, and 92.4 % for glutarate based on the intensity of (001) peak, indicating that shorter dicarboxylate chains more readily intercalate into the positively charged framework. The overall adsorption capacity is 175 mg/g (1.00 mol/mol) for malonate, 197 mg/g (0.99 mol/mol) for succinate, and 207 mg/g (0.92 mol/mol) for glutarate. FTIR before and after anion exchange confirms the exchange process, with sulfonate peaks [1200 m, 1070 m (cm^{-1}): RSO_3^{-}] completely replaced by carboxylate stretch bands [1570 m (cm^{-1}): C=O; 1300 s (cm^{-1}): C-O, Figure 6.8]. The intact crystals, colorless solution and solid and low-angle PXRD diffraction peaks confirm the stability of the cuprate layers. Attempts to exchange EDS for 1,3-propanedisulfonate (PDS) were also successful. The d-spacing expanded to 10.2 Å but with only ~ 60 %

completeness of exchange and partial loss of crystallinity. Hydrothermal syntheses between various Cu precursors and PDS were unsuccessful in obtaining a stable structure with no solids formed.

In addition to α,ω-alkanedicarboxylates, SLUG-26 displayed anion exchange for metal oxo-anion pollutants in far greater capacity than LDHs. Permanganate was employed as a group 7 oxo-anion model for pertechnetate, which is a highly problematic radioactive pollutant during the vitrification of nuclear waste.[288, 312, 313] An equimolar amount of permanganate and as-synthesized SLUG-26 were introduced into aqueous solution under mild stirring (experimental section). As monitored by UV-Vis spectroscopy, the permanganate concentration decreased by 36 % and 49 % with reaction intervals of 8 hours and 48 hours, respectively (Figure 6.9). No further decrease in permanganate solution was detected after 48 hours, indicating the completion of the process. The overall adsorption capacity of permanganate trapping is therefore 0.51 mol/mol and 201 mg/g. These values exceed the majority of LDHs for oxo-anions based on a recent review, commonly in the range of 10 mg/g to 150 mg/g.[294] To verify, we employed both the uncalcined and calcined forms of synthetic hydrotalcite (magnesium aluminum hydroxycarbonate, Aldrich) to perform the anion exchange reactions under the same conditions as SLUG-26. Only 3 % and 18 % of the permanganate were adsorbed, for adsorption capacity of 6 mg/g and 36 mg/g, respectively. These values are less than one-fifth compared to our SLUG-26 material. The lower adsorption capacity of LDHs is likely due to their lower selectivity, which favors carbonate or hydrocarbonate over all other anions. PXRD

before and after anion exchange confirmed that SLUG-26 retains its crystalline layered character after permanganate intercalation, with d-spacing decreasing from 9.6 Å to 7.4 Å. The permanganate is permanently trapped, and reusability is in fact undesirable for a highly problematic pollutant such as the radionuclide pertechnetate.

In addition to exceptionally high adsorption capacity, SLUG-26 displays twother advantageous properties over LDHs: (i) SLUG-26 remains heterogeneous

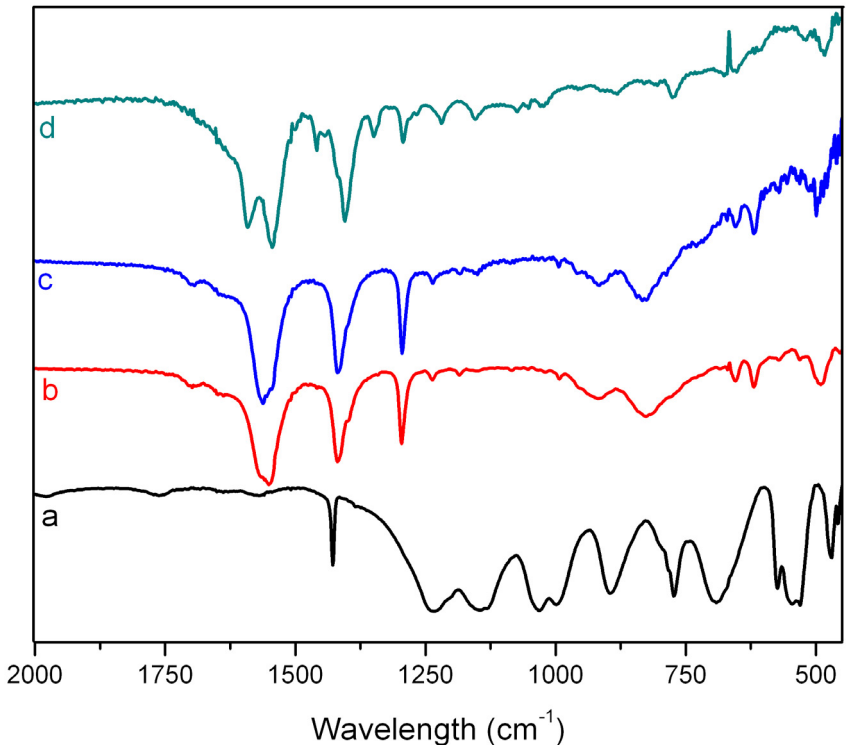

Figure 6.8 FTIR of (a) as-synthesized SLUG-26; (b) SLUG-26 after exchange with malonate; (c) SLUG-26 after exchange with succinate; (d) SLUG-26 after exchange with glutarate.

throughout anion exchange and can be recovered simply by filtration from the anion solution. LDHs require ca. 30 min centrifugation for total separation; (ii) SLUG-26 materials can be used as-synthesized for anion pollutant trapping without pretreatment. LDHs require calcination to partially remove the intercalated water and carbonate in order to achieve its lower capacity anion exchange. Indeed, the memory effect of LDHs necessitates use within 24 hours of calcination due to rehydration and reconstruction of the layers.[314-316]

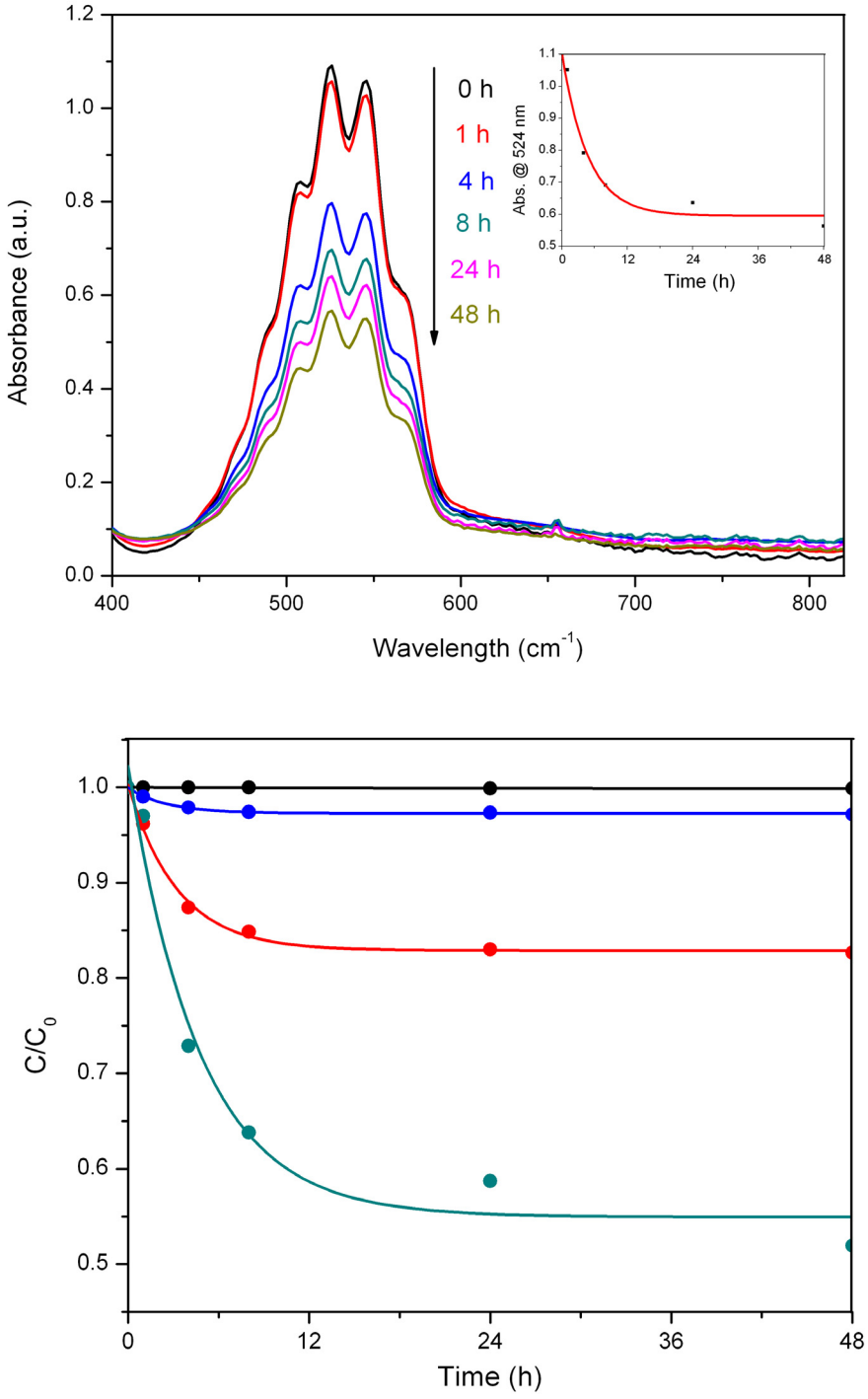

Figure 6.9 Top: UV-Vis absorption spectra of the permanganate solution in 50 ml anion exchange with the presence of 1×10^{-5} mol SLUG-26 at various invervals. Inset: relative intensity of the 524 nm maximum versus time. Bottom: Concentration of permanganate (based on UV-Vis) vs. time for anion exchange by uncalcined LDH (blue), calcined LDH (red), SLUG-26 (dark cyan), and blank (no solid, black).

6.4 Conclusions

We have synthesized a rare example of a cationic layered inorganic metalate based on a 3d metal, with high thermal stability and excellent anion exchange properties. Despite the structural similarities with LDHs, SLUG-26 demonstrated five time higher adsorption capacity for permanganate with a value over 200 mg/g. In addition to metal oxo-anion exchange, the material displays flexibility for variable-length α,ω-alkanedicarboxylates, which may be a pathway to adsorbing other problematic anions and/or increasing capacity. Considering the openness of the structure with ordered hydroxyl groups pointing towards the 1D channels, catalysis and exfoliation studies are under investigation.

6.5 References

286. Keith, L. H.; Teillard, W. A., *Environ. Sci. Technol.* **1979,** *13*, 416.

287. Hogue, C., *Chemical & Engineering News* **2011,** *89*, 6.

288. Wang, Y.; Bryan, C.; Gao, H.; Phol, P. I.; Brinker, C. J.; Yu, K.; Xu, H.; Yang, Y.; Braterman, P. S.; Xu, Z., *Sandia Report (Potential Applications of Nanostructured Materials in Nuclear Waste Management* **2003,** *SAND2003-3313*, 1-95.

289. Izak, P.; Hrma, P.; Arey, B. W.; Plaisted, T. J., *J. Non-Cryst. Solids* **2001,** *289*, 17-29.

290. Wu, M.; Janssen, S., *Environ. Sci. Technol.* **2011,** *45*, 366-367.

291. Mark, R.; Findley, W. N., *Polym. Eng. Sci.* **1978,** *18*, 6-15.

292. Rives, V., *LDHs: Layered Double Hydroxides: Present and Future*. Nova Science Publishers Inc., Hauppauge, New York, USA: **2001**.

293. Slade, D. G. E. a. R. C. T., *Layered Double Hydroxides*. X. Duan and D. G. Evans ed.; Springer-Verlag, New York, NY, USA: **2006**; pp 1-87.

294. Goh, K. H.; Lim, T. T.; Dong, Z., *Water Res.* **2008,** *42*, 1343-1368.

295. Tran, D. T.; Zavalij, P. Y.; Oliver, S. R. J., *J. Am. Chem. Soc.* **2002,** *124*, 3966-3969.

296. Swanson, C. H.; Shaikh, H. A.; Rogow, D. L.; Oliver, A. G.; Campana, C. F.; Oliver, S. R. J., *J. Am. Chem. Soc.* **2008,** *130*, 11737-11741.

297. Rogow, D. L.; Russell, M. P.; Wayman, L. M.; Swanson, C. H.; Oliver, A. G.; J., O. S. R., *Crystal Growth & Design* **2010,** *10*, 823-829.

298. Oliver, S. R. J., *Chem. Soc. Rev.* **2009,** *38*, 1868-1881.

299. Gandara, F.; Perles, J.; Snejko, N.; Iglesias, M.; Gomez-Lor, B.; Gutierrez-Puebla, E.; Monge, M. A., *Angew. Chem., Int. Ed.* **2006,** *45*, 7998-8001.

300. McIntyre, L. J.; Jackson, L. K.; Fogg, A. M., *Chem. Mater.* **2008,** *20*, 335-340.

301. Geng, F.; Matsushita, Y.; Ma, R.; Xin, H.; Tanaka, M.; Izumi, F.; Iyi, N.; Sasaki, T., *J. Am. Chem. Soc.* **2008,** *130*, 16344-16350.

302. Geng, F.; Ma, R.; Sasaki, T., *Acc. Chem. Res.* **2010,** *43*, 1177-1185.

303. Wang, S.; Alekseev, E. V.; Diwu, J. C.; W. H.; Phillips; B. L.; Depmeier, W.; Albrecht-Schmitt, T. E., *Angew. Chem. Int. Ed.* **2010,** *49*, 1057-1060.

304. Goulding, H. V.; Hulse, S. E.; Clegg, W.; Harrington, R. W.; Playford, H. Y.; Walton, R. I.; Fogg, A. M., *J. Am. Chem. Soc.* **2010,** *132*, 13618-13620.

305. Hu, M.; Jiang, J.-S.; Li, X., *Cryst. Growth Des.* **2009,** *9*, 820-824.

306. *Cambridge Crystal Structure Database*. Bond length of Cu-O: mean=2.062 Å, median=1.958 Å, standard deviation=0.204 Å. 93.4 % of the bond length is shorter than 2.4 Å.

307. Prout, C. K.; Carruthers, J. R.; Rossotti, F. J. C., *J. Chem. Soc. A* **1971**, 554-556.

308. Epstein, J. M.; Figgis, B. N.; White, A. H.; Willis, A. C., *J. Chem. Soc., Dalton Trans.* **1974**, 1954-1961.

309. Yamanaka, M.; Uekusa, H.; Ohba, S.; Saito, Y.; Iwata, S.; Kato, M.; Tokii, T.; Muto, Y.; Steward, O. W., *Acta Cryst.* **1991,** *B47*, 344-355.

310. Miller, J. H.; Powell, J. E.; Jacobson, R. A.; Kulprathipanja, S., *Inorg. Chim. Acta* **1976,** *18*, 25-28.

311. Spek, A. L., *PLATON, A Multipurpose Crystallographic Tool*. Utrecht, The Netherland, **2007**.

312. Darab, J. G.; Smith, P. A., *Chem. Mater.* **1996,** *8*, 1004-1021.

313. Darab, J. G.; Amonette, A. B.; Burke, D. S. D.; Orr, R. D.; Ponder, S. M.; Schrick, B.; Mallouk, T. M.; Lukens, W. W.; Caulder, D. L.; Shuh, D. K., *Chem. Mater.* **2007,** *19*, 5703-5713.

314. Centi, G.; Perathoner, S., *Microporous Mesoporous Mater.* **2008,** *107*, 3-15.

315. Cardoso, P. L.; Barros, J.; Valim, J., *J. Phys. Chem. Solids* **2006,** *67*, 987-993.

316. Ferreira, O. P.; Alves, O. L.; Gouveia, X.; Souza-Filho, A. G.; de Pavia, J. A. C.; Filho, J. M., *J. Solid State Chem* **2004,** *177*, 3058-3069.

Chapter 7

Anion Exchange of the Cationic Layered Material $[Pb_2F_2]^{2+}$

Abstract

We demonstrate the complete exchange of the interlamellar anions of a 2-D cationic inorganic material. The α,ω-alkanedisulfonates were exchanged for α,ω-alkanedicarboxylates, leading to two new cationic materials with the same $[Pb_2F_2]^{2+}$ layered architecture. Both were solved by single crystal X-ray diffraction and the transformation also followed by *in-situ* optical microscopy and *ex-situ* powder X-ray diffraction. This report represents a rare example of metal-organic framework displaying highly efficient and complete replacement of its anionic organic linker while retaining the original extended inorganic layer. It also opens up further possibilities for introducing other anions or abatement of problematic anions such as pharmaceuticals and their metabolites.

7.1 Introduction

Many pollutants listed as EPA (U.S. Environmental Protection Agency) priorities inherently occur as their anionic form, including metal oxo-anions (e.g. TcO_4^-, ClO_4^-, CrO_4^{2-}, etc.) and organic anions [e.g. salicylate (metabolite of Aspirin), carbamazepine, clofibrate, ibuprofen, etc.].[317,318] Recent studies have achieved successful inorganic anion pollutant trapping with high capacity and selectivity using cationic extended frameworks.[319-323] Custelcean and co-workers investigated the selectivity principles in anion separation with both metal-organic frameworks (MOFs) and hydrogen-bonded frameworks.[324-326] Solid-state anion trapping of organic pollutants, however, has been less investigated despite the growing worldwide problem of water contamination by pharmaceuticals and their metabolites, most of which are highly soluble in water and occur in anionic forms.[327] The current treatment process of chlorination often leads to even more toxic compounds such as monohalogenated and/or oxidized by-products.[328,329]

Cationic inorganic layered materials are 2-D extended topologies where positively charged layers are structure-directed by charge-balancing anions.[330] Layered double hydroxides are the most widely studied example and have general formula $[M^{2+}_{1-x}M^{3+}_{x}(OH)_2]A^{n-}_{x/n}\cdot mH_2O$, where M^{2+} and M^{3+} are a range of metals (e.g. Mg^{2+} and Al^{3+}) and A^{n-} are interlamellar anions (e.g. CO_3^{2-}).[331,332] Meanwhile, layered rare earth hydroxides are a recent series of pillared materials with eight or nine-coordinate metals as part of the positively charged architecture.[333-338] Both classes of materials display efficient equilibrium-driven anion exchange processes,

while LDHs are often subject to interference by non-toxic anions that have a higher affinity for the material (e.g. carbonate and bicarbonate).[339] Furthermore, no single-crystal structure after exchange has been reported to support that the anion has exchanged and the metal hydroxide layers remain intact. Indeed, LDHs are known to partially decompose without complete heterogeneity during exchange in aqueous media.[331,332] Similarly, our previous lower *p*-block based cationic inorganic layered materials also displayed partial to complete decomposition of the structure upon anion exchange attempts.[340-342]

Anion exchange has been observed for a few cationic MOFs, although the majority were exchange between inorganic anions of comparable size.[343-345] Postsynthetic modification — one of the most widely studied approaches to alter the organic linker — involves decoration of ligand functional groups and not altering the extended architecture.[346-348] Choe and co-workers recently reported the complete substitution of neutral N-donor organic linkers, namely tetrakis(4-carboxyphenyl) porphyrin for 4,4'-bipyridine.[349] Very recently, Cohen and co-workers reported postsynthetic exchange of anionic organic linker in MOFs.[350] However, the exchanged ligands are limited within different functionalized 1,4-benzene-dicarboxylate with the same chain length, and the exchange process is incomplete (21~97 %) with limited efficiency (5 days).

Herein, we report anion exchange within a cationic MOF to yield two new crystal structures where the 2-D inorganic topology is retained. This report is one of the rare examples of complete replacement of organic anions in a MOF and the first

exchange of an α,ω-alkanedisulfonate for an α,ω-alkanedicarboxylate. The anion exchange process is monitored by X-ray crystallography and *in-situ* optical microscopy, which supports the exchange process undergo an unconventional solvent-mediated mechanism. Unlike LDHs, the heterogeneity and high crystallinity are maintained throughout the exchange process, with intact cationic inorganic layers fully characterized by X-ray crystallography. In addition, the interlayer-spacing can be tuned by carboxylate chain length.

7.2 Experimental Section

7.2.1 Reagents

Lead fluoride (PbF_2, *ca*. 5 μm powder, 99+ %, Acros), 1,2-ethanedisulfonic acid (EDSA, $HO_3SCH_2CH_2SO_3H$, 95 %, TCI Inc.) and perchloric acid (70 % in H_2O, Acros) were used as-received for the synthesis of SLUG-6. Succinate disodium salt ($NaO_2CCH_2CH_2CO_2Na$, 99 %, TCI Inc.) and glutarate disodium salt ($NaO_2CCH_2CH_2CH_2CO_2Na$, 99 %, TCI Inc.) were used as-received for both the anion exchange reactions and hydrothermal synthesis of SLUG-32 and SLUG-33.

7.2.2 Synthesis and Anion Exchange

Synthesis of SLUG-6 follows our previously reported procedure.[351] Colorless crystals of $[Pb_2F_2][O_3SCH_2CH_2SO_3]$ (SLUG-6) can be synthesized under hydrothermal conditions. A reactant solution with a molar ratio of 1 : 2 : 2.5 : 200 for PbF_2 : EDSA : $HClO_4$: H_2O was stirred at room temperature for 15 min and then

transferred to a 15 ml Teflon lined autoclave to 2/3 filling. The autoclaves were heated at 150 °C for 48 h under autogenous pressure.

$[Pb_2F_2][O_2CCH_2CH_2CO_2]$ (which we denote as SLUG-32 for University of California, Santa Cruz, Structure No.32) can be synthesized both hydrothermally and by crystal-to-crystal anion exchange. The anion exchange process was performed by introducing 64 mg (1.0×10^{-4} mol) of as-synthesized SLUG-6 into a vial containing 20 ml of an aqueous solution of 54 mg (2.0×10^{-4} mol) sodium succinate. The vial was left sealed for up to 24 h to allow complete exchange and the colorless tetragonal crystals were isolated by filtration and rinsed with water/acetone. Hydrothermal synthesis of SLUG-32 involved heating a reactant solution of molar ratio 1 : 2 : 2 : 400 for PbF_2 : sodium succinate : perchloric acid : H_2O at 150 °C under autogenous conditions for 72 h. The average yield based on Pb was 90 % (0.05 g) using the anion exchange method and 78 % (0.29 g) using the hydrothermal method.

$[Pb_2F_2][O_2C\text{-}C_3H_6\text{-}CO_2]$ (SLUG-33) was synthesized in the same manner as for SLUG-32 but with sodium glutarate in place of sodium succinate with the same molar ratio. Again, both anion exchange and hydrothermal methods could be used. The average yield based on Pb was 87 % (0.05 g) using the anion exchange method and 91 % (0.34 g) using the hydrothermal method.

7.2.3 X-ray Crystallography

Single crystal data were recorded using a Bruker APEX II CCD area detector X-ray diffractometer and graphite monochromated Mo-Kα radiation (λ = 0.71073 Å).

The structures were solved by direct methods and expanded routinely. The models were refined by full-matrix least-squares analysis of F^2 against all reflections. All non-hydrogen atoms were refined with anisotropic thermal displacement parameters. Thermal parameters for the hydrogen atoms were tied to the isotropic thermal parameter of the atom. Programs used: APEX-II v2.1.4;[352] SHELXTL v6.14;[353] Diamond v3.2.[354]

7.2.4 Instrumental Details

Samples for powder X-ray diffraction (PXRD) were measured on a Rigaku Americas Miniflex Plus diffractometer, and were scanned from 2 to 60° (2θ) at a rate of 2° per minute and 0.04° step size under Cu-Kα radiation (λ = 1.5418 Å). Crystal structure views were obtained using Diamond v3.2[354] and rendered by POV-Ray v3.6. Fourier transform infrared (FTIR) spectroscopy of the materials was accomplished using a Perkin-Elmer Spectrum One spectrophotometer with KBr pellets. Elemental analysis was performed by Quantitative Technologies, Inc. (Whitehouse, NJ).

Table 7.1 Crystal data and structure refinement for SLUG-32.

Identification code	SLUG-32	
Empirical formula	$Pb_2F_2C_4O_4$	
Formula weight	564.42	
Temperature	296(2) K	
Wavelength	0.71073 Å	
Crystal system	Tetragonal	
Space group	I4/m	
Unit cell dimensions	a = 4.1371(7) Å	α = 90°
	b = 4.1371(7) Å	β = 90°
	c = 21.477(4) Å	γ = 90°
Volume	367.60(11) $Å^3$	
Z	4	
Density (calculated)	5.099 $g.cm^{-3}$	
Absorption coefficient (μ)	45.745 mm^{-1}	
F(000)	476	
Crystal size	0.05 × 0.05 × 0.04 mm^3	
ω range for data collection	1.90 to 26.29°	
Index ranges	$-5 \le h \le 5$, $-5 \le k \le 5$, $-26 \le l \le 26$	
Reflections collected	1828	
Independent reflections	203 [R_{int} = 0.0267]	
Completeness to θ = 26.29°	100.0 %	
Absorption correction	Empirical	
Max. and min. transmission	0.7459 and 0.3903	
Refinement method	Full-matrix least-squares on F^2	
Data / restraints / parameters	203 / 0 / 21	
Goodness-of-fit on F^2	1.245	
Final R indices [I>2σ(I)]	R_1 = 0.0176, wR_2 = 0.0506	
R indices (all data)	R_1 = 0.0178, wR_2 = 0.0508	
Largest diff. peak and hole	0.629 and –1.210 $e^{-}\cdot Å^{-3}$	

7.3 Results and Discussion

7.3.1 Crystal Structure of SLUG-6

We previously reported the hydrothermal synthesis of $[Pb_2F_2][O_3SCH_2CH_2SO_3]$ (SLUG-6).[351] This material can be synthesized with high yield and purity and is chemically stable in pH 4~10 aqueous solution. The crystal

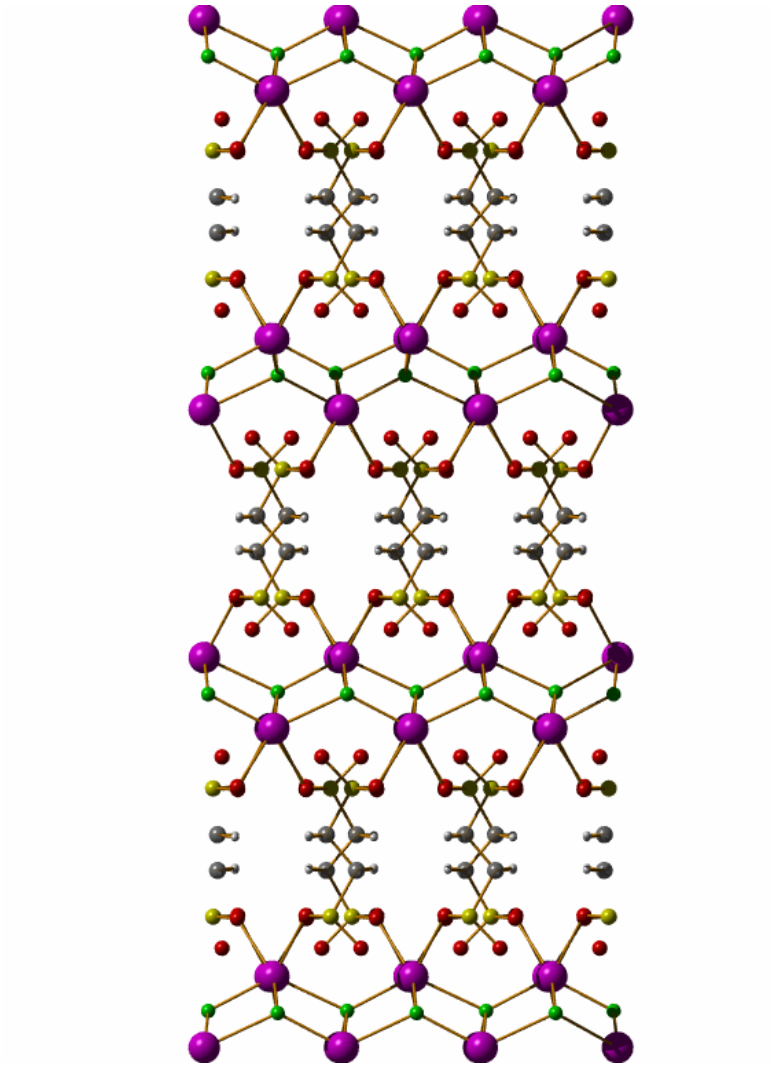

Figure 7.1 Crystallographic view of the original SLUG-6 along the *c*-axis. (Pb purple, F green, S yellow, O red, C gray, H white).

structure consists of cationic single $[Pb_2F_2]^{2+}$ layers pillared by 1,2-ethanedisulfonate (EDS) anions (Figure 7.1). The organic EDS linker is aligned perpendicular to adjacent layers with two oxygens of each sulfonate end covalently bonded to two Pb metal centers. This orientation gives rise to a large *d*-spacing between the cationic layers, while the weakly bonding nature known for organosulfonates gives rise to possible anion exchangeability and intercalation chemistry.[355, 356]

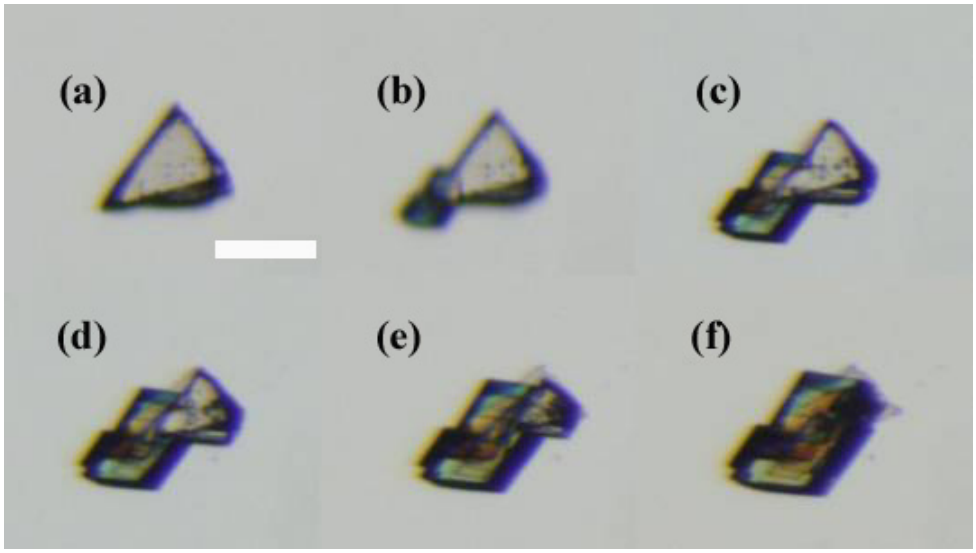

Figure 7.2 *In-situ* optical micrographs of a single crystal of SLUG-6 in sodium succinate solution for 10 min (a), 30 min (b), 60 min (c), 90 min (d), 120 min (e) and 240 min (f). Scale bar is 20 μm.

7.3.2 SLUG-32: Anion Exchange with Succinate

Succinate [$^{-}O_2C(CH_2)_2CO_2^{-}$] and glutarate [$^{-}O_2C(CH_2)_3CO_2^{-}$] were chosen as initial examples of α,ω–alkanedicarboxylate carbon chain length. Immersion of as-synthesized SLUG-6 crystals in an aqueous solution of two-fold molar excess disodium succinate under static ambient conditions afforded the highly crystalline phase $[Pb_2F_2][O_2C(CH_2)_2CO_2]$ (SLUG-32). *In-situ* optical microscopy was employed to monitor the transformation between the two crystalline phases (Figure 7.2). The

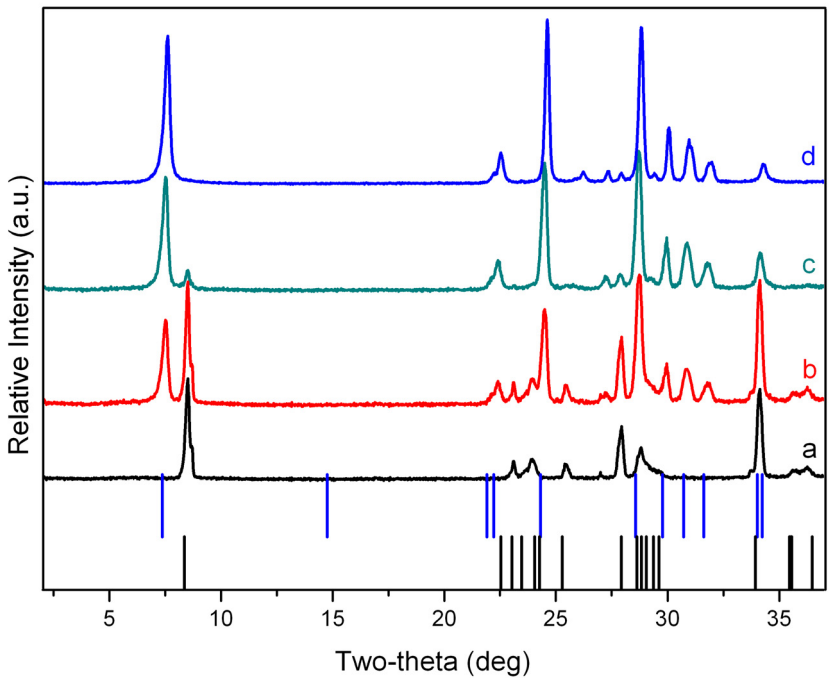

Figure 7.3 *Ex-situ* PXRD measurement of SLUG-6 anion exchange products from sodium glutarate solution after 0 h (a, black), 1 h (b, red), 2 h (c, cyan) and 24 h (d, blue). Theoretical patterns of SLUG-6 (black) and SLUG-33 (blue) are shown at the bottom as bars.

formation of SLUG-32 was observed on the surface of the SLUG-6 crystals after 30 min in the dicarboxylate solution (Figure 7.2b). The competitive crystallization allows SLUG-32 to gradually grow in expense of the original SLUG-6 crystal to form an entirely new phase and crystal morphology after 4 h. No further change in crystal morphology occurs after 4 h (Figure 7.2f), supporting the completion of the anion exchange process. Unlike solid-state equilibrium-driven anion exchange process for LDHs, this *in-situ* optical microscopy study indicates our materials undergo solvent-mediated anion exchange with a possible exfoliation and recrystallization mechanism. Figure 7.3 shows the *ex-situ* powder X-ray diffraction (PXRD) versus time for the solid from a 20 ml aqueous solution of 1.0×10^{-4} mol SLUG-6 and 0.01 M sodium glutarate. After 1 h, the new SLUG-33 phase is clearly present [e.g. (001) peak at 7.4º (2θ), Figure 3b]. Based on peak area of the majority peak, the glutarate exchange was over 90% complete after 2 h and phase-pure SLUG-33 after 24 h, with no peaks of the original SLUG-6 remaining (Figure 3c,d). Anion exchange process is also evidenced by FTIR and elemental analysis.

The crystals after anion exchange were manually separated and structurally characterized by single-crystal X-ray crystallography (Table 7.1, Figure 7.4 and 7.5) SLUG-32 crystallizes in the high-symmetry tetragonal crystal system with I4/m space group. The $[Pb_2F_2]^{2+}$ layer remains intact, with the same formula as the cationic layers in SLUG-6. The SLUG-32 cationic layer possesses slightly more condensed intralayer Pb-F connectivity in the *ab* plane (Figure 7.6) with decreasing *a* and *b* dimensions [*a* = 4.6185(2) Å and *b* = 4.4226(2) Å for SLUG-6; *a* = *b* = 4.1371(7) Å

for SLUG-32]. SLUG-32 is slightly more elongated along the *c*-axis (Figure 7.1 *vs*. Figure 7.4) since only one oxygen of each carboxylate group bonds to the layers [Pb-O bond length ranges between 2.620(20) and 2.635(19) Å] compared to two oxygens for SLUG-6. The distance between lead and the non-bonded oxygens on the carboxylates ranges from 2.814(23) to 2.826(23) Å, exceeding the accepted Pb-O

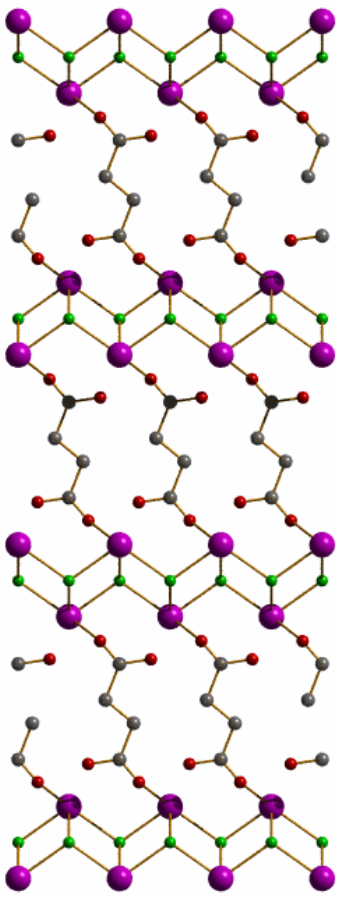

Figure 7.4 Crystallographic view of the original SLUG-32 along the *c*-axis. (Pb purple, F green, O red, C gray).

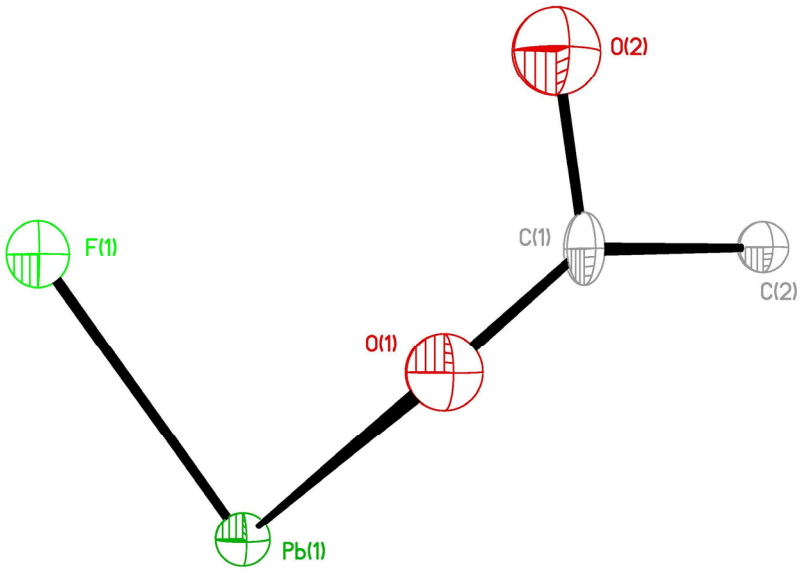

Figure 7.5 Oak Ridge Thermal Ellipsoid Plots of SLUG-32. Thermal ellipsoids are shown at 50% probability.

covalent range provided by the Cambridge Structural Database [CSD, 2.60(19) Å]. This one oxygen bonding feature for SLUG-32 is likely due to stronger coordination nature of carboxylates, which can construct extended structures with less covalent bonding. This is also supported that carboxylates attracting lead centers towards the interlamellar regions evidenced by elongated $[Pb_2F_2]^{2+}$ layers along *c* axis.

In addition to anion exchange, SLUG-32 can be synthesized by a conventional hydrothermal reaction and corresponding molar ratio, yielding a similar tetragonal crystal morphology. PXRD confirms that both synthesis methods give the identical high purity SLUG-32 phase, with experimental PXRD matching the powder pattern simulated from the crystallographic data (Figure 7.7). Interestingly, perchlorate is

necessary in the hydrothermal method to obtain the same phase as post-anion exchange, likely acting as a stabilizer.[341] Reaction without perchlorate produced α-PbF_2 (ICDD PDF# 41-1086).

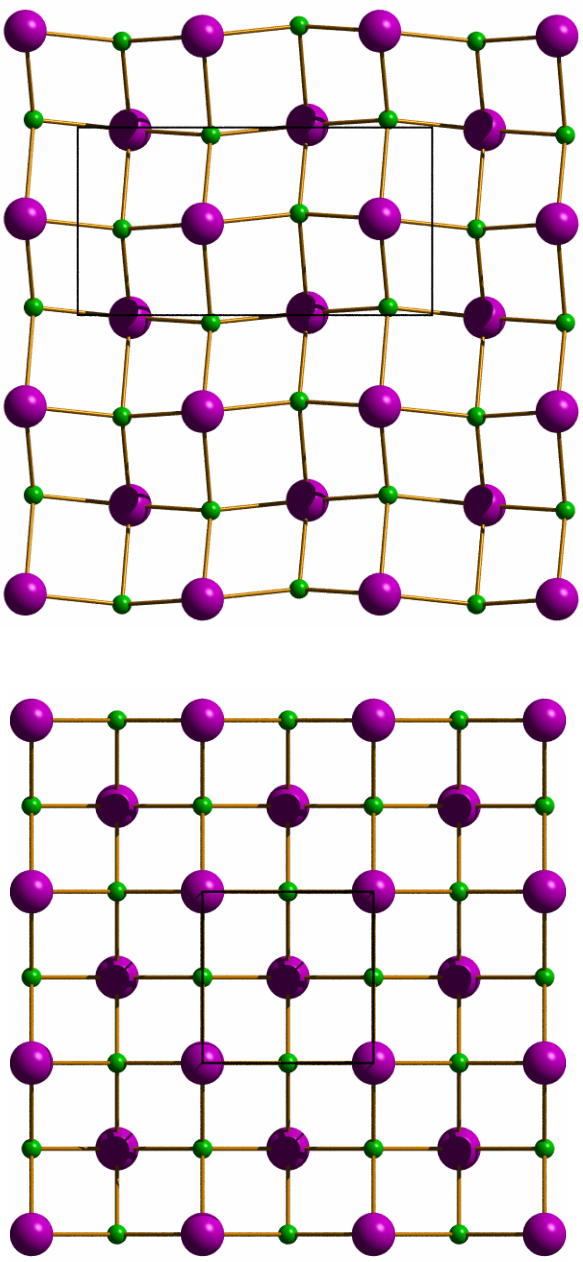

Figure 7.6 (Top) Crystallographic view of one $[Pb_2F_2]^{2+}$ layer of SLUG-6 along the crystallographic *a*-axis. (Bottom) View of one $[Pb_2F_2]^{2+}$ layer of SLUG-32 along the crystallographic *c*-axis (Pb purple, F green).

Table 7.2 Crystal data and structure refinement for SLUG-33.

Identification code	SLUG-33	
Empirical formula	$Pb_2F_2C_5O_4$	
Formula weight	576.43	
Temperature	296(2) K	
Wavelength	0.71073 Å	
Crystal system	Tetragonal	
Space group	I4/m	
Unit cell dimensions	a = 4.116(3) Å	α = 90°
	b = 4.116(3) Å	β = 90°
	c = 24.003(15) Å	γ = 90°
Volume	406.6(4) $Å^3$	
Z	2	
Density (calculated)	4.709 $g.cm^{-3}$	
Absorption coefficient (μ)	41.365 mm^{-1}	
F(000)	488	
Crystal size	0.095 × 0.045 × 0.025 mm^3	
ω range for data collection	3.39 to 27.85°	
Index ranges	$-5 \le h \le 5$, $-5 \le k \le 5$, $-31 \le l \le 31$	
Reflections collected	2168	
Independent reflections	259 [R_{int} = 0.0482]	
Completeness to θ = 27.85°	99.6 %	
Absorption correction	Empirical	
Max. and min. transmission	0.7459 and 0.3513	
Refinement method	Full-matrix least-squares on F^2	
Data / restraints / parameters	259 / 0 / 28	
Goodness-of-fit on F^2	1.163	
Final R indices [I>2σ(I)]	R_1 = 0.0190, wR_2 = 0.0461	
R indices (all data)	R_1 = 0.0200, wR_2 = 0.0476	
Largest diff. peak and hole	1.046 and -0.949 $e^- \cdot Å^{-3}$	

7.3.3 SLUG-33: Anion Exchange with Glutarate

To investigate the generality of this crystal-to-crystal anion intercalation chemistry, we employed glutarate as a longer dicarboxylate chain to intercalate between adjacent $[Pb_2F_2]^{2+}$ layers. X-ray crystallography of crystals after anion exchange confirms the formation of $[Pb_2F_2][O_2C(CH_2)_3CO_2]$ (SLUG-33) with the

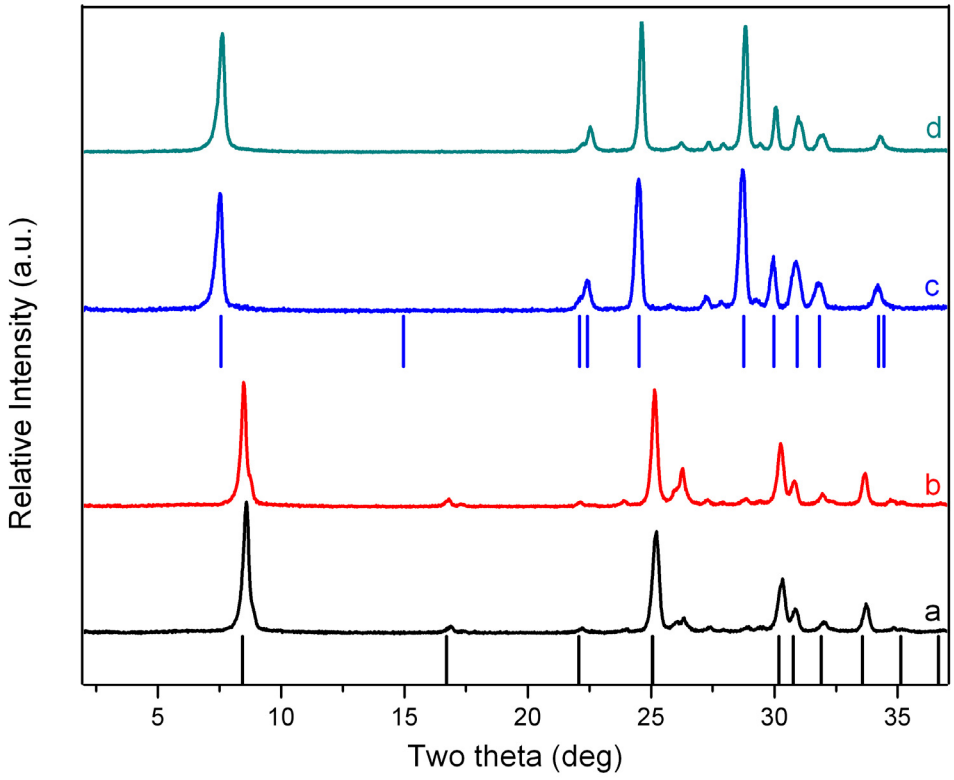

Figure 7.7 PXRD of SLUG-32 synthesized by anion exchange (a, black) and hydrothermally (b, red). PXRD of SLUG-33 synthesized by anion exchange (c, blue) and hydrothermal (d, cyan). Theoretical patterns of SLUG-32 (black) and SLUG-33 (blue) are shown as bars.

same layer topology as SLUG-32 (Table 7.2, Figure 7.8 and Figure 7.9). Both SLUG-32 and SLUG-33 share the I4/m space group and the unit cell dimensions in the *ab* plane differ by only 0.51% [SLUG-32: $a = b = 4.1371(7)$ Å; SLUG-33: $a = b = 4.116(3)$ Å]. Moreover, they afford the same feature of singly-bonded carboxylates. This feature implies that further possible anion exchangeability with other dicarboxylates and anions is possible. The cell dimension along the *c*-axis increased from 21.477(4) Å for SLUG-32 to 24.003(15) Å for SLUG-33. This 11.8 % increase agrees well with the carboxylate chain length difference of 13.9%. Again, SLUG-33 can be synthesized hydrothermally and both methods give a high purity product as evidenced by PXRD (Figure S2 c,d). Anion exchange with even longer α,ω-

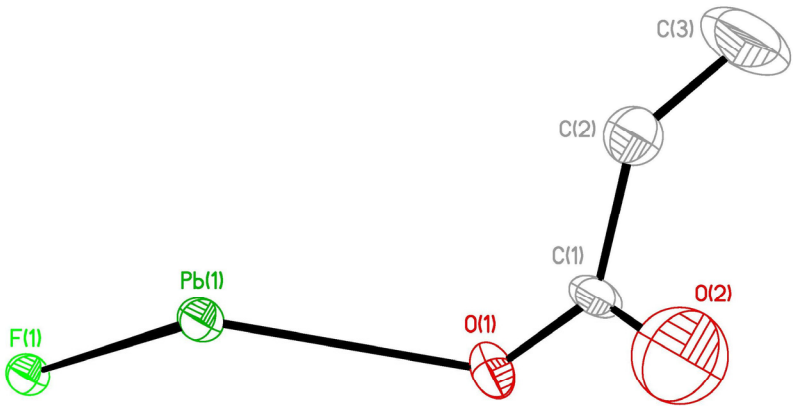

Figure 7.8 Oak Ridge Thermal Ellipsoid Plots of SLUG-33 (bottom). Thermal ellipsoids are shown at 50% probability.

alkanedicarboxylates, such as sebacate [$^{-}O_2C(CH_2)_8CO_2^{-}$] is also studied by PXRD and FTIR (Figure S4), though no success in obtaining well-diffracted crystallography data. Miller indices of (001), (002) and (003) indicate the extended structure survive to be 2-D layered with *d*-spacing increasing to ~15.93 Å.

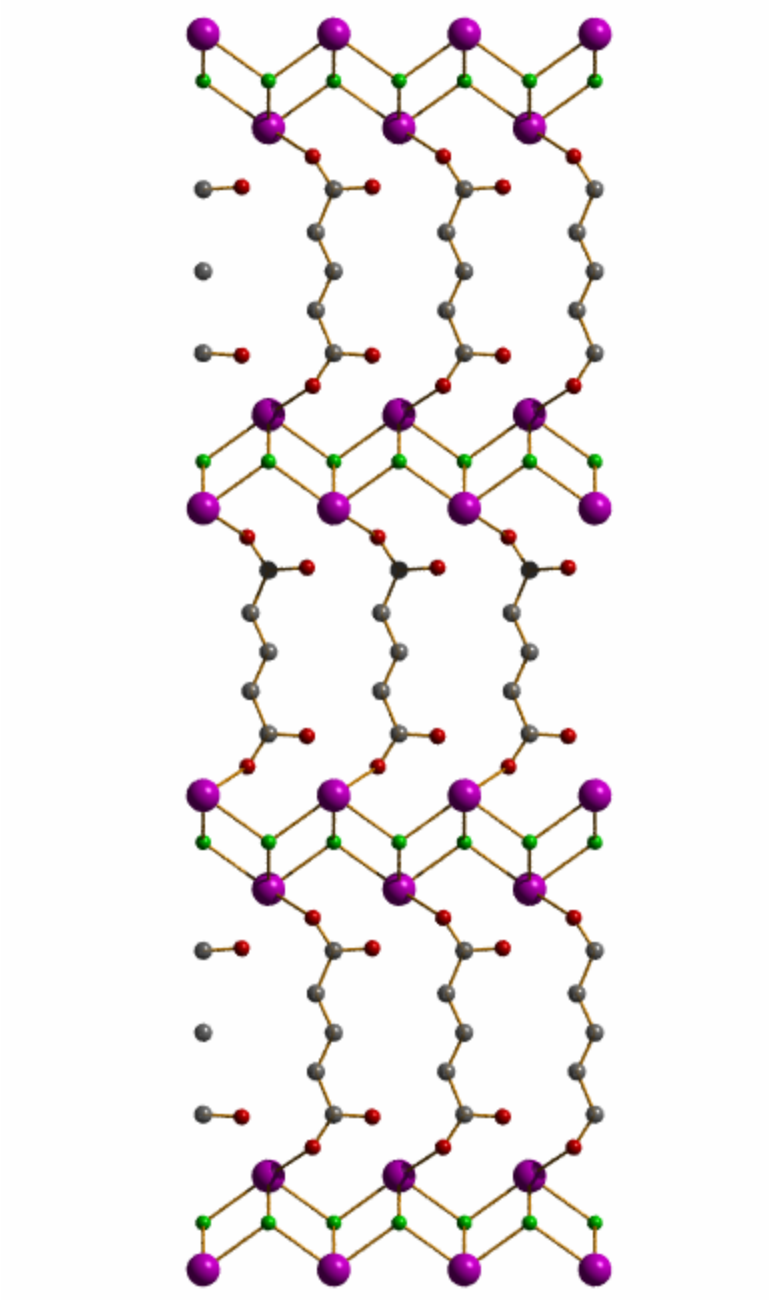

Figure 7.9 Crystallographic view of the original SLUG-33 along the *c*-axis. (Pb purple, F green, O red, C gray).

7.4 Conclusions

We have introduced the first cationic lead fluoride layered compound exhibiting high capacity anion exchange. The solvent-mediated anion exchange processes, first-time monitored by *in-situ* optical microscopy, are one of the rare examples of a MOF that completely and efficiently replaces its anionic organic linker while retaining the cationic inorganic layered structure. The post-anion exchange products were solved crystallographically and prove the survival of the cationic layers. The ability to exchange for varying length carboxylate chain indicates that rich intercalation chemistry is possible including the trapping of more complex species such as pharmaceutical or photoluminescent anions.

7.5 References

317. Keith, L. H.; Teillard, W. A., *Environ. Sci. Technol.* **1979,** *13*, 416.

318. Hogue, C., *Chemical & Engineering News* **2011,** *89*, 6.

319. Oliver, S. R. J., *Chem. Soc. Rev.* **2009,** *38*, 1868-1881.

320. Fei, H.; Rogow, D. L.; Oliver, S. R. J., *J. Am. Chem. Soc.* **2010,** *132*, 7202-7209.

321. Fei, H.; Bresler, M. R.; Oliver, S. R. J., *J. Am. Chem. Soc.* **2011,** *133*, 11110-11113.

322. Fei, H.; Oliver, S. R. J., *Angew. Chem. Int. Ed.* **2011,** *50*, 9066-9070.

323. Wang, S.; Alekseev, E. V.; Diwu, J. C.; W. H.; Phillips; B. L.; Depmeier, W.; Albrecht-Schmitt, T. E., *Angew. Chem. Int. Ed.* **2010,** *49*, 1057-1060.

324. Custelcean, R.; Moyer, B. A., *Eur. J. Inorg. Chem.* **2007**, 1321-1340.

325. Custelcean, R.; Jiang, D.; Hay, B. P.; Luo, W.; Gu, B., *Cryst. Growth Des.* **2008,** *8*, 1909-1915.

326. Custelcean, R.; Bock, A.; Moyer, B. A., *J. Am. Chem. Soc.* **2010,** *132*, 7177-7185.

327. Wu, M.; Janssen, S., *Environ. Sci. Technol.* **2011,** *45*, 366-367.

328. Mark, R.; Findley, W. N., *Polym. Eng. Sci.* **1978,** *18*, 6-15.

329. Bedner, M.; Maccrehan, W. A., *Environ Sci Technol* **2006,** *40* (2), 516-522.

330. Geng, F.; Ma, R.; Sasaki, T., *Acc. Chem. Res.* **2010,** *43*, 1177-1185.

331. Rives, V., *LDHs: Layered Double Hydroxides: Present and Future*. Nova Science Publishers Inc., Hauppauge, New York, USA: 2001.

332. Slade, D. G. E. a. R. C. T., *Layered Double Hydroxides*. X. Duan and D. G. Evans ed.; Springer-Verlag, New York, NY, USA: 2006; p 1-87.

333. Gandara, F.; Perles, J.; Snejko, N.; Iglesia, M.; Gomez-Lor, B.; Gutierrez-puebla, R.; Monge, M. A., *Angew. Chem. Int. Ed.* **2006,** *45*, 7998-8001.

334. Gandara, F.; Puebla, E. G.; Iglesia, M.; Proserpio, D. M.; Snejko, N.; Monge, M. A., *Chem. Mater.* **2009,** *21*, 655-661.

335. McIntyre, L. J.; Jackson, L. K.; Fogg, A. M., *Chem. Mater.* **2008,** *20*, 335-340.

336. Poudret, L.; Prior, T. J.; McIntyre, L. J.; Fogg, A. M., *Chem. Mater.* **2008,** *20*, 7447-7453.

337. Geng, F.; Xin, H.; Matsushida, Y.; Ma, R.; Tanaka, M.; Izumi, F.; Lyi, N.; Sasaki, T., *Chem. Eur. J.* **2008,** *14*, 9255-9260.

338. Geng, F.; Matsushida, Y.; Ma, R.; Xin, H.; Tanaka, M.; Izumi, F.; Lyi, N.; Sasaki, T., *J. Am. Chem. Soc.* **2008,** *130*, 16344-16350.

339. Goh, K. H.; Lim, T. T.; Dong, Z., *Water Res.* **2008,** *42*, 1343-1368.

340. Tran, D. T.; Zavalij, P. Y.; Oliver, S. R. J., *J. Am. Chem. Soc.* **2002,** *124*, 3966-3969.

341. Rogow, D. L.; Russell, M. P.; Wayman, L. M.; Swanson, C. H.; Oliver, A. G.; J., O. S. R., *Crystal Growth & Design* **2010,** *10*, 823-829.

342. Swanson, C. H.; Shaikh, H. A.; Rogow, D. L.; Oliver, A. G.; Campana, C. F.; Oliver, S. R. J., *J. Am. Chem. Soc.* **2008,** *130*, 11737-11741.

343. Min, K. S.; Suh, M. P., *J. Am. Chem. Soc.* **2000,** *122*, 6834-6840.

344. Du, M.; Zhao, X. J.; Guo, J. H.; Batten, S. R., *Chem. Commun.* **2005**, 4836-4838.

345. Michaelides, A.; Skoulika, S., *Cryst. Growth Des.* **2009,** *9*, 2039-2042.

346. Wang, Z.; Cohen, S. M., *Chem. Soc. Rev.* **2009,** *38*, 1315-1329.

347. Tanabe, K. K.; Cohen, S. M., *Chem. Soc. Rev.* **2011,** *40*, 498-519.

348. Cohen, S. M., *Chem. Rev.* **2012,** *112*, 970-1000.

349. Burnett, B. J.; Barron, P. M.; Hu, C.; Choe, W., *J. Am. Chem. Soc.* **2011,** *133*, 9984-9987.

350. Kim, M.; Cahill, J. F.; Su, Y.; Prather, K. A.; Cohen, S. M., *Chem. Sci.* **2012,** *3*, 126-130.

351. Rogow, D. L.; Zapata, G.; Swanson, C. H.; Fan, X.; Campana, C. F.; Oliver, A. G.; Oliver, S. R. J., *Chem. Mater.* **2007,** *19*, 4658-4662.

352. *APEX-II, 2.1.4;*. Bruker-AXS: Madison, WI, 2007.

353. *SHELXTL Crystal Structure Determination Package*. Bruker Analytical X-ray Systems Inc.: Madison, WI, 1995-99.

354. Klaus Brandenburg; H. P. Diamond; Crystal-Impact: Germany, **2007**.

355. Cote, A. P.; Shimizu, G. K. H., *Coord. Chem. Rev.* **2003,** *245*, 49-64.

356. Shimizu, G. K. H.; Vaidhyanathan, R.; Taylor, J. M., *Chem. Soc. Rev.* **2009,** *38*, 1430-1449.

Chapter 8

Synthesis and Magnetic Properties of a 3-D Nickel Hydroxide Capped by Succinate

Abstract

We have successfully synthesized a rare example of an extended nickel oxide open framework with succinate capping the channels. A honeycomb-like layer of 14-membered rings centered in the (-111) plane are connected by vertex-sharing NiO_6 octahedra and water resides in the channels. The structure is the second example of an extended hybrid containing 3-D Ni-O-Ni connectivity and was structurally characterized by single-crystal and powder X-ray diffraction. The material displays excellent chemical stability in aqueous solution from pH ~ 1 to 13 and thermal stability to ~ 375 °C as evidenced by thermogravimetic analysis coupled mass spectroscopy. The Ni^{2+} ions order ferromagnetically order below T_c = 5.1 K, and anisotropic exchange interactions lead to a field-induced metamagnetic transition and spin-glass-like dependence on cooling conditions in magnetic field.

8.1 Introduction

Hybrid inorganic-organic materials are an emerging class of materials attracting much interest due to their range of topologies and potential applications in gas absorption, catalysis, ion exchange, etc.[357-361] Unlike the purely inorganic zeolite frameworks, the hybrid inorganic-organic as well as coordination polymer groups of materials contain inorganic and organic network portions, based on the classification introduced by Cheetham and Rao.[359] Vast arrays of coordination polymers have emerged with discrete metal centers and/or clusters linked by organic ligands.[362-366] There have been relatively few efforts, however, towards extended inorganic-organic hybrids with two dimensional inorganic connectivity, i.e. extended intralayer M-L-M connectivity (L = N, O, F, S, Cl, etc.).[367-371] In most cases, this sub-group of materials possesses high thermal and chemical stability found in conventional 2-D metal oxides, but may also display magnetic properties such as modulation of magnetic thermal ordering by guest molecules and/or organic linker.[359,362,368,372]

Our research focuses on the synthesis of extended zeotype and layered inorganic frameworks with anion-based applications.[373] Our previously reported cationic layered structures $[Pb_3F_5^+][NO_3^-]$,[374] $[Pb_{4.5}F_8^+][ClO_4^-]$,[375] $[Sb_4O_4(OH)_2^{2+}][^-O_3S(CH_2)_2SO_3^-]$[376] and $[Cu_4(OH)_6^{2+}][^-O_3S(CH_2)_2SO_3^-]$[377] have positively charged extended layers with Pb-F-Pb, Sb-O-Sb and Cu-O-Cu connectivity, respectively, and potential pollutant trapping applications for both inorganic and organic anions. We have also obtained neutral 2-D inorganic copper hydroxide and lead fluoride layers pillared by 2,6-naphthalenedisulfonate and α,ω-

alkanedisulfonates, respectively.[375,378,379] There are very limited examples, however, of 3-D extended M-O-M inorganic connectivity contained within a hybrid inorganic-organic extended framework.[380-383] 3-D inorganic connectivity is known to lead to cooperative phenomena such as magnetism and conductivity.[384,385]

Nickel-based inorganic and hybrid materials have attracted increasing interest, particularly nickel phosphates for their magnetic, electronic and catalytic properties.[386-389] Two nickel phosphate networks (VSB-1 and VSB-5) are 3-D networks of NiO_6 octahedra with large 1-D channels. They exhibit zeolitic properties such as high surface area for hydrogen adsorption and size/shape selective catalysis.[386,387] Only one example of a nickel-based extended inorganic hybrid with 3-D Ni-O-Ni connectivity was previously reported by Cheetham and co-workers. Their material displayed paramagnetism down to ~ 5 K and was possibly magnetically frustrated.[380]

Herein we introduce the synthesis and structural characterization of a rare example of an extended framework with 3-D Ni-O-Ni inorganic connectivity. $Ni_7(OH)_2(H_2O)_2(O_2C\text{-}C_2H_4\text{-}CO_2)_6$ (which we denote as SLUG-31 for University of California, Santa Cruz, Structure No. 31) is only the second example of a nickel succinate 3-D inorganic hybrid material. Fourteen-membered rings of edge-sharing nickel oxide octahedra (NiO_6) define an array of unidimensional channels in a honeycomb array. Succinates bridge the rings and reduce the thermal stability of this zeotype to 375 °C, as determined by thermogravimetic analysis - coupled mass spectrometry (TGA-MS) and *ex-situ* thermodiffraction. This material also possesses

a complex low-temperature magnetic phase space in which antiferromagnetic correlations compete with the ferromagnetic mean field to produce a metamagnetic transistion. Some degree of frustration and disorder contribute to a spin glass-like irreversibility of the magnetization in field-cooled versus zero-field-cooled conditions.

8.2 Experimental Section

8.2.1 Synthesis

$Ni_7(OH)_2(H_2O)_2(O_2C\text{-}C_2H_4\text{-}CO_2)_6$ (SLUG-31) was synthesized under hydrothermal conditions. A reactant mixture of $Ni(OH)_2$ (0.12 g, 1.29 mmol, Alfa Aesar, 99 %), CH_3COOH (0.38 g, 6.32 mmol), succinic acid (0.32 g, 2.71 mmol, $HO_2C\text{-}C_2H_4\text{-}CO_2H$, TCI America, 99 %) and deionized H_2O (10.00 g, 556 mmol) was stirred at 75 °C for 15 min and then transferred to a 15 mL Teflon lined autoclave to 2/3 filling. The autoclave was heated statically at 175 °C for 10 d under autogenous pressure, followed by slow cooling to room temperature at a rate of 6 °C/h. Single-crystal colorless blocks were isolated after vacuum filtration and rinsed by water/acetone (yield: 0.78 g, 79 % based on Ni).

8.2.2 Instrumental Details

Single crystal data were collected on a Bruker APEX-II CCD area detector diffractometer under graphite monochromated Mo-Kα radiation (λ = 0.71073 Å) using a combination of ω- and φ-scans of 0.3°. An empirical absorption correction

was applied using SADABS and the structure was solved by direct methods and expanded routinely. The model was refined by full-matrix least-squares analysis of F^2 against all reflections. All non-hydrogen atoms were refined with anisotropic thermal displacement parameters. Programs used: APEX-II v2.1.4;[390] SHELXTL v6.14;[391] Diamond v3.2e.[392] Samples for powder X-ray diffraction (PXRD) were measured on a Rigaku Americas Miniflex Plus diffractometer and were scanned from 2 to 60° (2θ) at a rate of 2° per minute and 0.04° step size under Cu-Kα radiation (λ = 1.5418 Å). TGA-MS was performed using a TA Instruments 2050 TGA, heating from 25 to 600 °C under N_2 purge with a gradient of 5 °C/min. *In-situ* mass spectra coupled to the TGA were collected on a Pfeiffer Vacuum ThermoStar GSD 301 T3 mass spectrometer with a 70 eV ionization potential. Magnetic measurements were performed using a Quantum Design SQUID magnetometer. The dc magnetization *M* was measured as a function of both temperature and applied magnetic field and magnetic susceptibility χ was computed at low fields as *M/H*.

Table 8.1 Crystal data and structure refinement for SLUG-31.

Empirical formula	$C_{24}H_{24}Ni_7O_{31}$	
Formula weight	1219.40	
Temperature	100(2) K	
Wavelength	0.71073 Å	
Crystal system	Triclinic	
Space group	P-1	
Unit cell dimensions	a = 9.9900(12) Å	α = 90.790(5)°
	b = 11.2000(14) Å	β = 95.380(5)°
	c = 17.2000(16) Å	γ = 101.150(10)°
Volume	1878.8(4) $Å^3$	
Z	2	
Density (calculated)	2.155 $g.cm^{-3}$	
Absorption coefficient (μ)	3.544 mm^{-1}	
F(000)	1224	
Crystal size	0.35 × 0.11 × 0.075 mm^3	
ω range for data collection	1.19 to 30.00°	
Index ranges	$-14 \leq h \leq 14$, $-15 \leq k \leq 15$, $-24 \leq l \leq 24$	
Reflections collected	59763	
Independent reflections	10928 [R_{int} = 0.0600]	
Completeness to θ = 30.00°	99.9 %	
Absorption correction	Empirical	
Max. and min. transmission	1.0000 and 0.7178	
Refinement method	Full-matrix least-squares on F^2	
Data / restraints / parameters	10928 / 0 / 583	
Goodness-of-fit on F^2	1.251	
Final R indices [I>2σ(I)]	R_1 = 0.0477, wR_2 = 0.1055	
R indices (all data)	R_1 = 0.0501, wR_2 = 0.1066	
Extinction coefficient	0.00040(8)	
Largest diff. peak and hole	1.096 and -1.143 $e^-.Å^{-3}$	

8.3 Results and Discussion

8.3.1 Synthesis

Green prism-like crystals of SLUG-31 were isolated in high yield and pure phase after hydrothermal reaction at the optimized conditions of 175 °C and 10 d. Lower synthesis temperatures and/or synthesis time less than 7 d resulted in a mixed phase product of SLUG-31 and known nickel succinate materials, including the

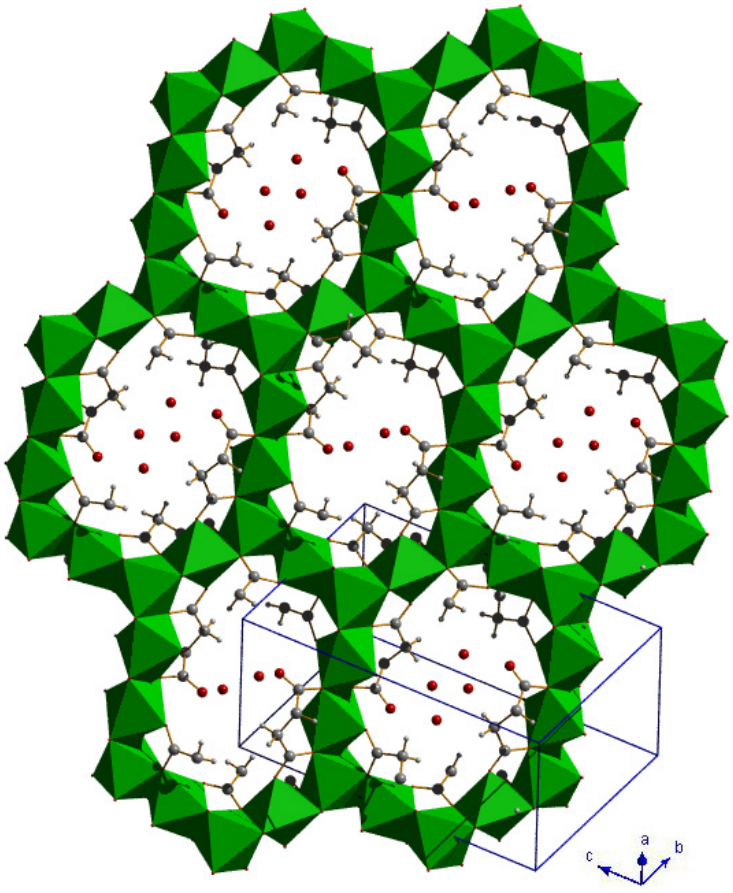

Figure 8.1 Crystallographic view of the [-1,1,1] plane showing one layer of the SLUG-31 structure containing a honeycomb array of 14-membered rings (NiO_6 polyhedra: green; carbon: gray; oxygen: red; hydrogen: white). The water hydrogens in the unidimensional channels are omitted for clarity.

layered nickel succinate $Ni_7(OH)_6(H_2O)_3(O_2C\text{-}C_2H_4\text{-}CO_2)_4\cdot 7H_2O$ and a 3-D open-framework nickel succinate $Ni_7(OH)_2(H_2O)_2(O_2C\text{-}C_2H_4\text{-}CO_2)_6\cdot 2H_2O$. The latter is the only previously reported 3-D nickel succinate, possessing 12 and 15-membered rings and a structure different to that of SLUG-31.[380,393] Indeed, nickel hydroxide and succinic acid are the necessary reagents in order to obtain SLUG-31, as other Ni-based sources or sodium succinate gave rise to either no solid product or the aforementioned nickel succinate framework.[380,381,393]

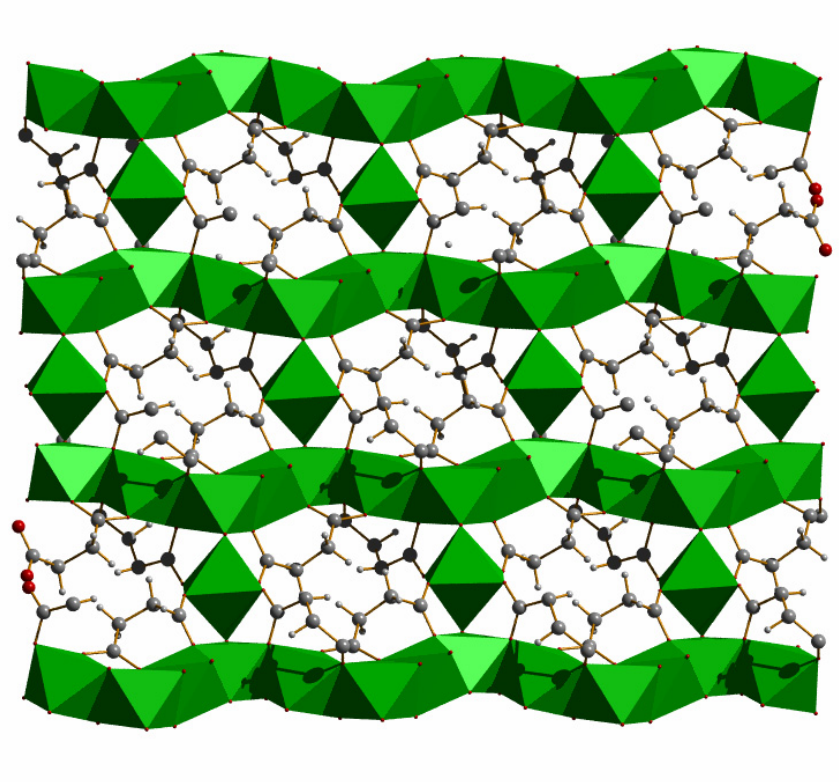

Figure 8.2 Crystallographic side view of the SLUG-31 layers, connected by isolated vertex-sharing NiO_6 octahedra.

8.3.2 Structural Characterization

Single-crystal X-ray diffraction reveals that the structure crystallized in the triclinic crystal system with P-1 space group (Table 8.1). SLUG-31 consists of edge-sharing NiO_6 octahedra in the (-111) plane that define a honeycomb array of 14-membered ring channels (Figure 8.1). Succinates bridge the nickel centers within a ring and water molecules are present in the unidimensional channels. There are two slightly different types of channels containing two versus four waters (Figure 8.1); excluding the succinates, the open apertures are *ca.* 9.6 × 5.7 $Å^2$ and 10.2 × 7.4 $Å^2$, respectively. The layers are connected by vertex-sharing NiO_6 to define 3-D Ni-O-Ni connectivity (Figure 8.2).

The 3-D inorganic hybrid $Ni_7(OH)_2(H_2O)_2(O_2C\text{-}C_2H_4\text{-}CO_2)_6$ has eight

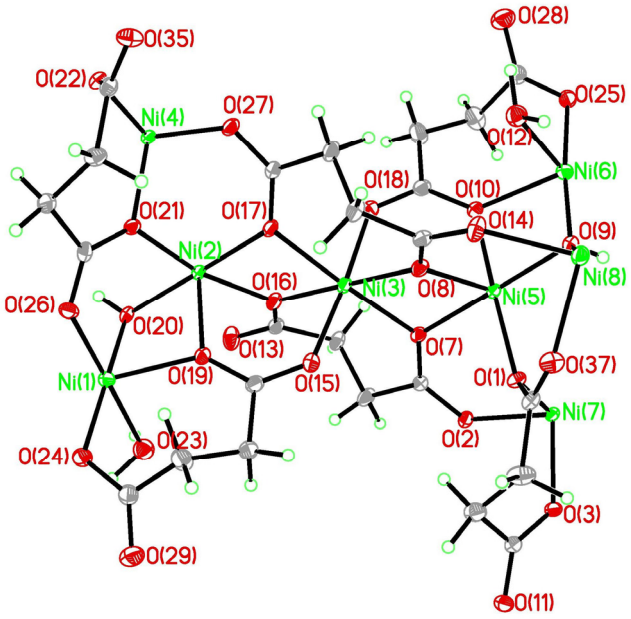

Figure 8.3 ORTEP diagram and atomic labeling of the nickel succinate structure. Thermal ellipsoids are shown at 50% probability.

crystallographically independent Ni centers with similar octahedral environment (Figure 8.3) and bond lengths [1.991(2) to 2.122(2) Å, within the accepted range of Ni-O covalent bond length]. The 14-membered rings possess four aligned Ni centers on two opposite sides while the remaining six octahedra extend outwards, defining elongated hexagons (Figure 8.1). Both central NiO_6 octahedra [Ni(1) and Ni(6)] on the aligned sides have one doubly protonated oxygen [O(12) and O(23), Figure 8.3] extending towards the center of the channel. Meanwhile, the interlayer corner-sharing octahedra [Ni(8)] have four oxygens from succinates and two oxygens [O(9) and O(20)], that are protonated and triply bridging towards three Ni centers: two from the layer and one from the interlayer vertex-sharing octahedra. All of the other oxygens in the layer are from carboxylate groups of the succinates. The distance between the adjacent vertex-sharing Ni centers is 12.426(1) Å, defining an interlayer open aperture (excluding succinates) of *ca.* 6.6 × 3.4 $Å^2$. The edge-sharing layers and vertex-sharing pillars collectively define a 3-D Ni-O-Ni framework, with succinate bridging ligands that further cross-link the Ni centers.

The overall framework charge is balanced in the formula $Ni_7(OH)_2(H_2O)_2(C_4H_4O_4)_6$, where two triply-bridging (μ_3-oxo) hydroxides are necessary to balance the +2 net charge from the seven Ni^{2+} and six divalent succinate units. The disordered solvent molecules were refined by PLATON SQUEEZE[394] and indicates the structure possesses 11.9 % solvent accessible void space [224.1 $Å^3$ of 1878.8 $Å^3$ in each unit cell], even with the pendant succinates. The high phase purity (~ 100 %) and yield (~ 80 %) are also confirmed by the close match of the experimental PXRD pattern with that simulated from the crystallographic information file (Figure 8.4 a,b).

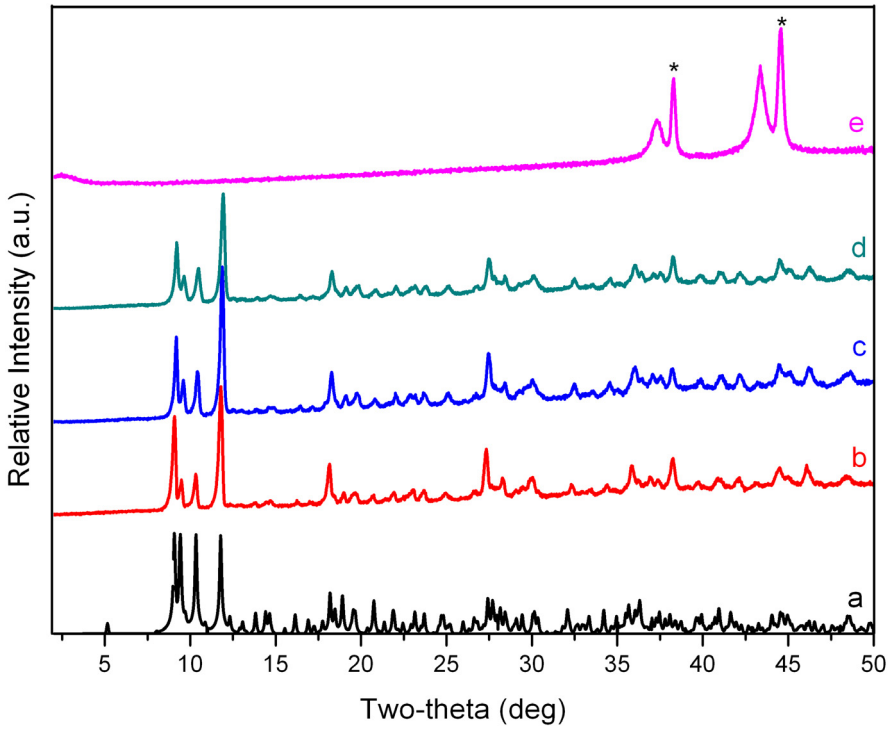

Figure 8.4 PXRD patterns of (a) theoretical data projected from the single-crystal X-ray data; (b) as-prepared material; *ex-situ* measurements after heating under N_2 flow to 200 °C (c), 350 °C (d) and 500 °C (e). Asterisks indicate diffraction peaks from the aluminum sample holder.

8.3.3 Thermal Characterization

This topology is a rare example of 3-D nickelate connectivity. In general, higher metal oxide dimensionality typically gives rise to greater thermal and chemical stability. TGA-MS indicates that SLUG-31 is thermally stable to ~ 375 °C, with two small mass loss steps present at ~ 85 °C and ~ 185 °C. The first step of ~ 2.4 % mass loss is likely due to the removal of physisorbed water, implying three water molecules in the as-synthesized material, which are disordered and removed by PLATON SQUEEZE. The second weight loss step at 185 °C is most likely the removal of the two Ni-coordinated terminal water molecules (experimental: 2.7 %; theoretical: 3.0 %). *Ex-situ* thermodiffraction also under N_2 flow indicates that no structural decomposition occurs up to the major decomposition step at 370 °C, with the mass spectra indicating removal of succinate fragments. The 44 m/z signal likely corresponds to the decomposition of the carboxylate ends to CO_2. *Ex-situ* thermodiffraction at 500 °C indicates the solid decomposed to NiO (ICDD PDF#03-065-6920). SLUG-31 is chemically stable to various organic solvents (ethanol, acetone and toluene) and aqueous solution pH 1 to 13.

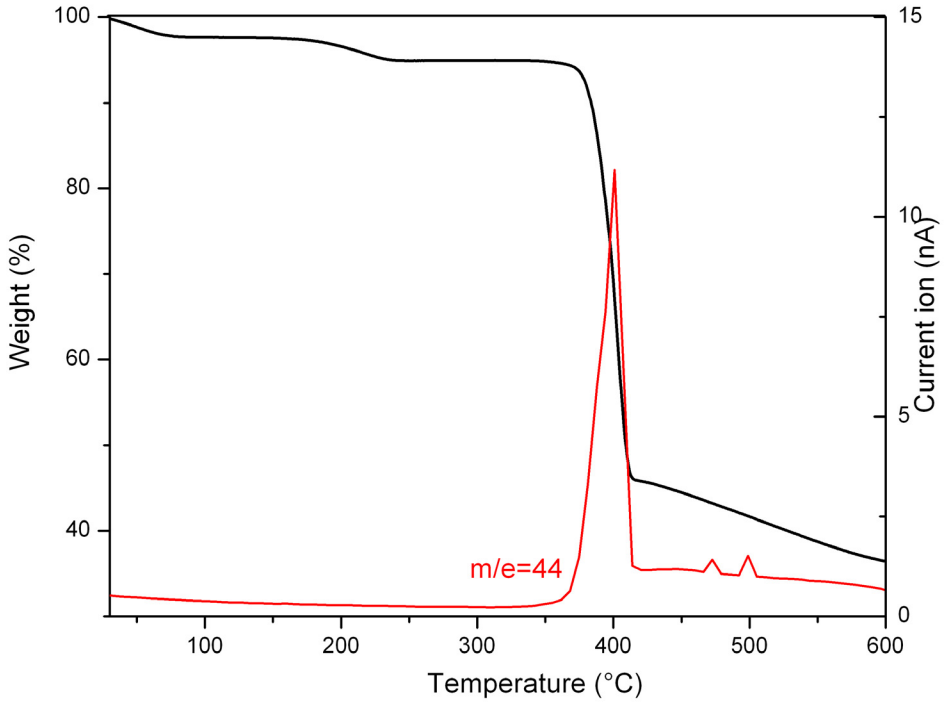

Figure 8.5 Thermogravimetric analysis trace (black) and coupled mass spectra for m/e = 44 (red).

8.3.4 Magnetic Properties

Magnetic measurements of SLUG-31 present a richly interacting system in which antiferromagnetic and ferromagnetic correlations, as well as spin-glass freezing, share a common energy scale of ~5 K. In the high-temperature paramagnetic phase the Ni^{2+} ions behave as free spins and χ is well described by the Curie-Weiss functional form $\chi = C/(T+\Theta_W)$, where C is the Curie constant and Θ_W is the Weiss temperature. This behavior is easily identifiable from the linear temperature

dependence of $1/\chi$ (see inset to Figure 8.6). A Curie-Weiss law fit in the temperature range 7 K < T < 300 K yields Θ_W = -5.45 K and C = 1.18, corresponding to an effective moment $p_{eff} = g[S(S+1)]^{1/2}$ = 3.08 μ_B/Ni. This value of p_{eff} is higher than the calculated spin-1 value of 2.83 μ_B, but within the range reported for Ni^{2+} in other compounds.[395] The negative Θ_W indicates that mean-field exchange interactions are ferromagnetic.

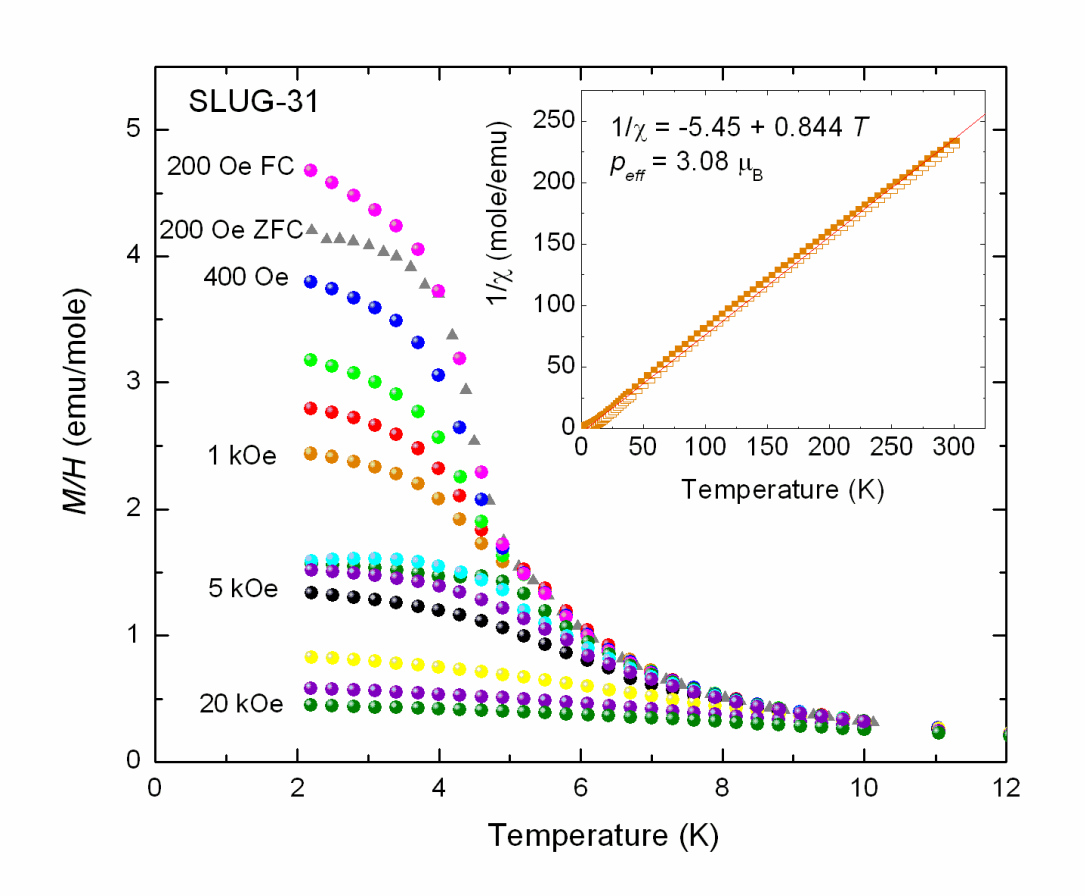

Figure 8.6 Low-temperature dc magnetization divided by magnetic field. Field increments are evenly spaced between labeled curves. All curves were measured in field-cooled conditions, except where indicated. Inset: Inverse susceptibility in applied field H = 5000 Oe with Curie-Weiss fit.

Low-temperature *M/H* data are displayed in Figure 8.6 for various magnetic fields between 200 and 20 000 Oe, Two distinct regimes of magnetic field strength are observed. For $H > H_{MM}$ = 2 kOe all curves exhibit a broad Curie tail upturn as $T \rightarrow 0$. Scans measured for H < H_{MM}, however, possess an additional ferromagnetic shoulder, and are field-independent above T = 5.1 K, Near the crossover region a broad peak is discerned near 5 K. The qualitative distinction between the high- and low-field response is suggestive of a metamagnetic transition between energetically favorable spin configurations.

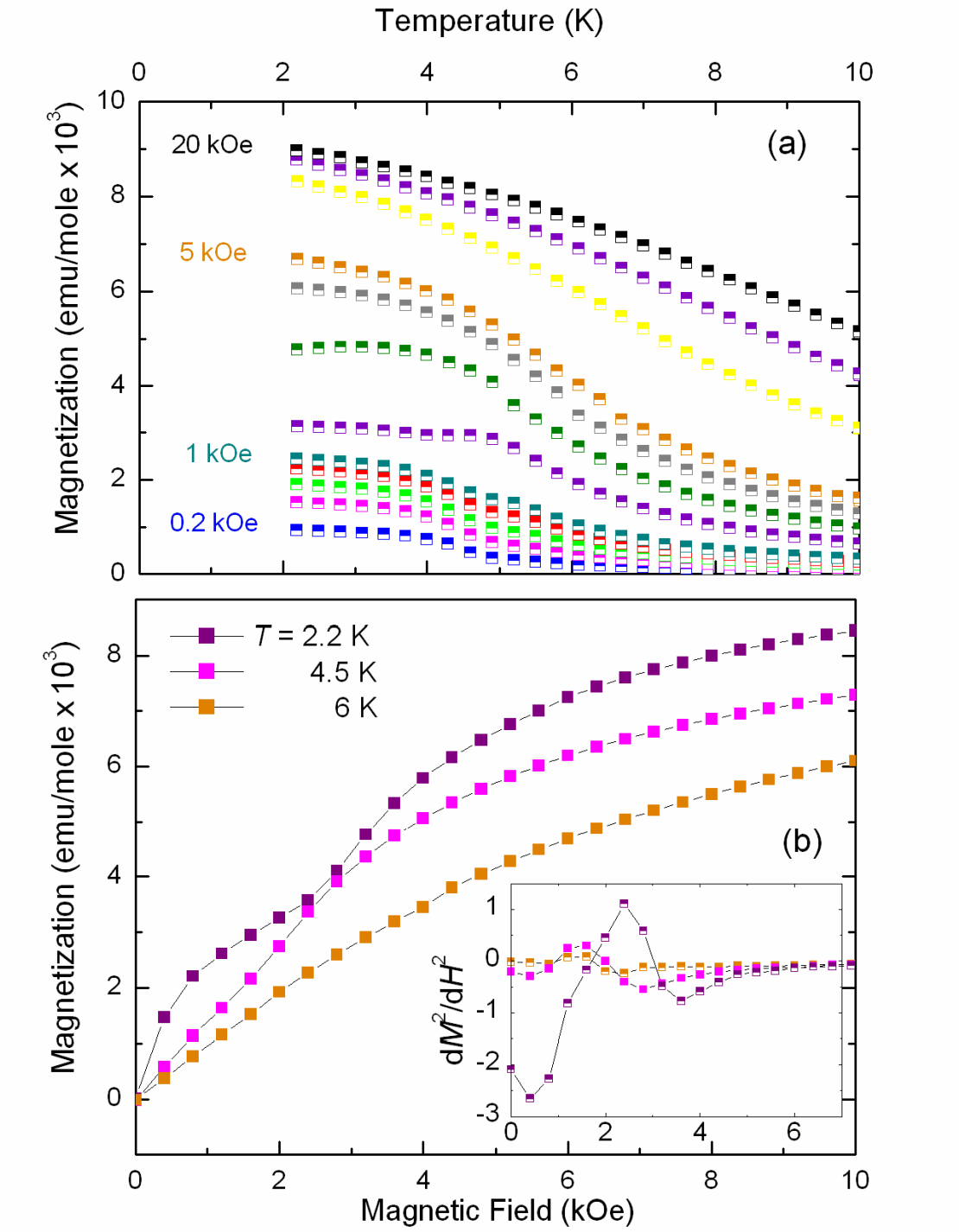

Figure 8.7: dc magnetization as a function of (a) temperature and (b) magnetic field. Field values are evenly spaced between labeled curves. Inset: second derivative of magnetization with respect to field (in emu mole^{-1} Oe^{-2} x 10^3) as a function of magnetic field (in kOe). Colors same as in main panel.

Further evidence for a metamagnetic transition is found in the M vs. H data displayed in Figure 8.7b, where similar field and temperature scales are encountered. At fields near H_{MM} the M vs. H curve has a kink and positive curvature [see dM^2/dH^2 peak in inset to Fig. 7(b)], indicating that significant antiferromagnetic interactions are present. The kink feature is most pronounced at T = 2.2 K and is visible at 4.5 K, but has mostly disappeared above T_c At higher fields M increases monotonically before saturating near 20 kOe to a value of 8940 emu/mol, accounting for 84.3% of the expected spin-1 moment. Finally, a spin-glass-like dependence of the low-temperature magnetization upon cooling conditions [field-cooled (FC) vs. zero-field-cooled (ZFC)] indicates that frustration and disorder contribute to the complexity of the magnetic response. The ZFC and FC behavior are compared for H = 200 Oe in Fig. 6, where we see a suppression of magnetization below the freezing temperature T_F = 4.0 K. This behavior likely stems not from interations between isolated atomic spins, as in a spin glass, but rather from the blocking between magnetic domains typical of a cluster glass.[396]

This material provides an important example of a framework magnet whose reduced dimensionality allows greater influence of frustration upon the magnetic properties. The significant crystal anisotropy and presence of inequivalent lattice sites promotes competition between ground state spin configurations and leads to the observed metamagnetic transition. Further details of the magnetic structure and transition will be elucidated only after the anisotropy of the magnetization can be carefully characterized, which will require larger single crystals.

8.4 Conclusions

SLUG-31 is a rare example of using succinate as a structure co-directing agent to afford a 3-D metal oxide open-framework, in this case a high dimensional inorganic-organic hybrid. The compound was synthesized by a facile one-pot hydrothermal method, with high phase purity and yield. Owing to its inorganic nature, the material displays excellent stability, and the magnetic properties exhibit a complex balance of ferromagnetic and antiferromagtic correlations which result in a metamagnetic transition. Considering its 3-D porosity and similarity to the 3-D open nickel phosphates, the heterogeneous catalytic properties are under investigation.

8.5 References

357. Ferey, G., *Chem. Soc. Rev.* **2008,** *37*, 191-214.

358. Long, J. R.; Yaghi, O. M., *Chem. Soc. Rev.* **2009,** *38*, 1213-1214.

359. Cheetham, A. K.; Rao, C. N. R.; Feller, R. K., *Chem. Commun.* **2006**, 4780-4795.

360. Meek, S. T.; Greathouse, J. A.; Allendorf, M. D., *Adv. Mater.* **2011,** *23*, 249-267.

361. Wight, A. P.; Davis, M. E., *Chem. Rev.* **2002,** *102*, 3589-3614.

362. Cheetham, A. K.; Rao, C. N. R., *Science* **2007,** *318*, 58.

363. Eddaoudi, M.; Moler, D. B.; Li, H.; Chen, B.; Reineke, T. M.; O'Keeffe, M.; Yaghi, O. M., *Acc. Chem. Res.* **2001,** *34*, 319-330.

364. Banerjee, R. P., A.; Wang, B.; Knobler, C.; Furukawa, H.; O'Keeffe, M.; Yaghi, O. M., *Science* **2008,** *319*, 939-943.

365. Kitagawa, S.; Kitaura, R.; Noro, S., *Angew. Chem. Int. Ed.* **2004,** *43*, 2334-2375.

366. Li, J.-R.; Kuppler, R. J.; Zhou, H.-C., *Chem. Soc. Rev.* **2009,** *38*, 1477-1504.

367. Clearfield, A., *Chem. Mater.* **1998,** *10,* 2801-2810.

368. Feng, P.; Bu, X.; Zheng, N., *Acc. Chem. Res.* **2005,** *38*, 293-303.

369. Falcao, E. H. L.; Naraso; Feller, R. K.; Wu, G.; Wudl, F.; Cheetham, A. K., *Inorg. Chem.* **2008,** *47*, 8336-8342.

370. Thirumurugan, A.; Sanguramath, R. A.; Rao, C. N. R., *Inorg. Chem.* **2008,** *47*, 823-831.

371. Merrill, C. A.; Cheetham, A. K., *Inorg. Chem.* **2005,** *44,* 5273-5277.

372. Rao, C. N. R.; Cheetham, A. K.; Thirumurugan, R., *J. Phys. Condens. Matter* **2008,** *20*, 083202.

373. Oliver, S. R. J., *Chem. Soc. Rev.* **2009,** *38*, 1868-1881.

374. Tran, D. T.; Zavalij, P. Y.; Oliver, S. R. J., *J. Am. Chem. Soc.* **2002,** *124*, 3966-3969.

375. Rogow, D. L.; Russell, M. P.; Wayman, L. M.; Swanson, C. H.; Oliver, A. G.; J., O. S. R., *Crystal Growth & Design* **2010,** *10*, 823-829.

376. Swanson, C. H.; Shaikh, H. A.; Rogow, D. L.; Oliver, A. G.; Campana, C. F.; Oliver, S. R. J., *J. Am. Chem. Soc.* **2008,** *130*, 11737-11741.

377. Fei, H.; Oliver, S. R. J., *Angew. Chem. Int. Ed.* **2011,** *50*, 9066-9070.

378. Rogow, D. L.; Zapata, G.; Swanson, C. H.; Fan, X.; Campana, C. F.; Oliver, A. G.; Oliver, S. R. J., *Chem. Mater.* **2007,** *19*, 4658-4662.

379. Tran, D. T.; Chernova, N. A.; Chu, D.; Oliver, A. G.; Oliver, S. R. J., *Crystal Growth & Design* **2010,** *10*, 874-879.

380. Forster, P. M.; Cheetham, A. K., *Angew. Chem. Int. Ed.* **2002,** *41*, 457-461.

381. Guillou, N.; Livage, C.; Drillon, M.; Ferey, G., *Angew. Chem. Int. Ed.* **2003,** *42*, 5314-5318.

382. Zhang, J.; Chen, S.; Valle, H.; Wong, M.; Austria, C.; Cruz, M.; Bu, X., *J. Am. Chem. Soc.* **2007,** *129*, 14168-14169.

383. Zhang, L.; Li, Z.-J.; Lin, Q.-P.; Qin, Y.-Y.; Zhang, J.; Yin, P.-X.; Cheng, J.-K.; Yao, Y.-G., *Inorg. Chem.* **2009,** *48*, 6517-6525.

384. Ferey, G.; Millange, F.; Morcrette, M.; Serre, C.; Doublet, M. L.; Greneche, J. M.; Tarascon, J. M., *Angew. Chem. Int. Ed.* **2007,** *46*, 3259-3264.

385. Livage, C.; Egger, C.; Ferey, G., *Chem. Mater.* **2001,** *13*, 410-414.

386. Guillou, N.; Gao, Q. M.; Nogues, M.; Morris, R. E.; Hervieu, M.; Ferey, G.; Cheetham, A. K., *C. R. Acad. Sci. Paris* **1999,** *2*, 387.

387. Guillou, N.; Gao, Q. M.; Forster, P. M.; Chang, J. S.; Park, S. E.; Ferey, G.; Cheetham, A. K., *Angew. Chem. Int. Ed.* **2001,** *40*, 2831-2835.

388. Forster, P. M.; Eckert, J.; Chang, J. S.; Park, S. E.; Ferey, G.; Cheetham, A. K., *J. Am. Chem. Soc.* **2003,** *125*, 1309-1312.

389. Liu, S. J.; Cheng, H. Y.; Zhao, F. Y.; Gong, J. Y.; Yu, S. H., *Chem. Eur. J.* **2008,** *14*, 4074-4081.

390. *APEX-II, 2.1.4;*. Bruker-AXS: Madison, WI, 2007.

391. *SHELXTL Crystal Structure Determination Package*. Bruker Analytical X-ray Systems Inc.: Madison, WI, 1995-99.

392. Klaus Brandenburg; H. P. Diamond; Crystal-Impact: Germany, **2007**.

393. Guillou, N.; Livage, C.; van Beek, W.; Nogues, M.; Ferey, G., *Angew. Chem. Int. Ed.* **2003,** *42*, 643-647.

394. Spek, A. L., *PLATON, A Multipurpose Crystallographic Tool*. Utrecht, The Netherland, 2007.

395. Berger, K., *Coordination Chemistry: Experimental Methods*. Butterworth, London, 1973.

396. P. Nozar; V. Sechovský; V. Kamberský, *Journal of Magnetism and Magnetic Materials* **1987,** *69*, 71-78.

Chapter 9

Synthesis and Characterization of A Cationic Antimonite Chain Templated by Sulfate: $[Sb_6O_7^{4+}][(SO_4^{2-})_2]$

Abstract

A new example of extended metal oxide possessing a cationic charge on the host has been successfully synthesized hydrothermally. $[Sb_6O_7][(SO_4)_2]$ (SLUG-34) consists of a very unusual 1-D antimony oxide chain four Sb atoms wide, with unprotonated sulfate between the chains. The material can be synthesized in high yield and pure phase and was characterized by both powder and single-crystal X-ray diffraction. The entirely inorganic nature of SLUG-34 along with infinite 1-D Sb-O-Sb connectivity results in high thermal stability and chemical resistance. SLUG-34 is thermally stable to *ca.* 500 °C as evidenced by *in-situ* variable temperature thermodiffraction as well as thermogravimetric analysis. Unlike the basic nature of layered double hydroxides (which are the only well-studied class of cationic inorganic materials), SLUG-34 is chemically stable in aqueous acidic conditions. This opens up the possibility for synthesis of other non-LDH type cationic inorganic materials with potential host-guest applications based on their extraframework anions.

9.1 Introduction

Research on open framework metal oxides has steadily increased following the discovery of zeolites, which are a family of aluminosilicates having enormous applications in catalysis, molecular separation and water purification.[397-400] The overall neutral or anionic charge on the framework, however, limits their importance in anion-based applications. Meanwhile, many of the metals listed as EPA priority pollutants are in the oxo-hydroxo anion form.[401,402] The trapping, immobilization and recognition of both inorganic and organic anionic species (e.g. DNA polyanions, pharmaceutical pollutants and their metabolites) are important in both biological and environmental systems.[403,404]

Cationic inorganic materials are a family of extended architectures where positively charged extended frameworks are held together with charge-balancing anions residing in 0-D capsules, 1-D channels or 2-D interlamellar regions. Layered double hydroxides (LDHs) are the most widely studied examples, with general formula of $[M^{2+}_{1-x}M^{3+}_{x}(OH)_2][A^{n-}_{x/n}\cdot mH_2O]$, where M^{2+} and M^{3+} are a range of metals (e.g. Mg^{2+} and Al^{3+}), x is the ratio of $M^{3+}/(M^{2+}+M^{3+})$ and A^{n-} is the n-valent counter anion (e.g. CO_3^{2-}, n = 2).[405,406] They demonstrate reversible anion exchange process, though displaying lack of heterogeneity and thus difficulty in recovery and reusability. Indeed, the Bronsted basicity of their hydroxyl groups limits their chemical stability in acidic conditions and thus application in corrosive wastewater.[407] Recently, layered rare earth hydroxides are another emerging series of cationic

inorganic layered materials with halide, nitrate, sulfate and organosulfonate as interlamellar anions, though with intrinsic basicity as for LDHs.[408-414]

Our group has reported a class of cationic inorganic frameworks based on lower *p*-block metals, which commonly have inert electron pairs pointing away from the inorganic connectivity and capping the layers.[415] Usually this group of materials has some or no hydroxyl groups, unlike the fully hydroxylated metals of LDHs that are necessary to stabilize its positively charge.[416-420] One example is lead fluoride $[Pb_2F_2]^{2+}$ materials showing complete anion exchange with α,ω-alkanedicarboxylates.[421] Antimony oxide are used as fire retardants and catalysts, including our previously reported $[Sb_4O_4(OH)_2][O_3S\text{-}C_2H_4\text{-}SO_3]$.[418] Two examples of antimony oxide chains were reported with one anionic $[Sb_2O_4]^{2-}$ and one cationic $[Sb(OH)]^{2+}$, though the latter with single Sb atom wide is zigzag and covalently bridging to oxalate.[422,423] Two 3-D zeotype cationic inorganic materials were also reported based on thorium and ytterbium, with borate clusters and chloride residing in 1-D channels, respectively.[424,425]

Herein, we report the synthesis and crystallographic characterization of a new cationic 1-D antimony oxide $[Sb_6O_7^{4+}][(SO_4)_2^{4-}]$ (which we denote as SLUG-34, University of California, Santa Cruz, Structure No. 34). The array of 1-D $[Sb_6O_7]^{4+}$ chains interact electrostatically with the sulfates. Though initial anion-based host-guest experiments were not successful, this rare example of an entirely inorganic cationic framework along with 1-D M-O-M connectivity gives rise to high thermal stability to ~ 500 °C and chemical resistance in aqueous acidic conditions.

9.2 Experimental Section

9.2.1 Synthesis

Antimony acetate [$Sb(OOCCH_3)_3$, Alfa Aesar, 97%] and sulfuric acid (H_2SO_4, Fisher, 96%) were used as-received for the synthesis. Colorless crystals of $[Sb_6O_7][(SO_4)_2]$ (SLUG-34) can be synthesized under hydrothermal conditions. A reactant solution with a molar ratio of 1:5:200 for $Sb(OOCCH_3)_3$:H_2SO_4:H_2O was stirred at room temperature for 15 min and then transferred to a 15 ml Teflon lined autoclave to 2/3 filling. The autoclaves were heated at 150 °C for 72 hours under autogenous pressure. Colorless needle-like crystals were collected by vacuum filtration and rinsing with deionized water and acetone. Yield was 0.33 g and 86.8 % based on antimony(III).

9.2.2 Instrumental Details

Samples for powder X-ray diffraction (PXRD) were measured on a Rigaku Americas Miniflex Plus diffractometer, and were scanned from 2 to 50° (2θ) at a rate of 2° per minute and 0.04° step size under Cu-Kα radiation (λ = 1.5418 Å). Thermogravimetric analysis (TGA) was measured on a TA Instruments 2050 TGA under air or nitrogen purge, heating from 25 to 800 °C at 5 °C/min. Samples for *in-situ* variable temperature PXRD were measured on a Rigaku Americas SmartLab diffractometer. Patterns were taken from 5 to 60° 2θ, with a step rate of 0.05° 2θ/s. The mounted sample was heated from 25 to 400 °C with an interval of 50 °C from room temperature to 100 °C and an interval of 100 °C from 100 °C to 400 °C.

Crystal structure views were obtained using Diamond v3.2 and rendered by POV-Ray v3.6. Fourier transform infrared (FTIR) spectroscopy of the materials was collected on a Perkin-Elmer Spectrum One spectrophotometer with KBr pellets.

9.2.3 Crystallography

Single crystal data were recorded using a Bruker APEX II CCD area detector X-ray diffractometer using graphite monochromated Mo-Kα radiation (λ = 0.71073 Å). The structures were solved by direct methods and expanded routinely. The models were refined by full-matrix least-squares analysis of F^2 against all reflections. All non-hydrogen atoms were refined with anisotropic thermal displacement parameters. Thermal parameters for the hydrogen atoms were tied to the isotropic thermal parameter of the atom to which they are bound. Programs used: APEX-II v2.1.4;[426] SHELXTL v6.14;[427] Diamond v3.2.[428]

Table 9.1 Crystal data and structure refinement for SLUG-34

Empirical formula	$[Sb_6O_7][SO_4]_2$	
Formula weight	1034.62	
Temperature	296(2) K	
Wavelength	0.71073 Å	
Crystal system	orthorhombic	
Space group	Ccc2	
Unit cell dimensions	a = 12.0329(6) Å	α = 90°
	b = 18.9371(10) Å	β = 90°
	c = 5.8595(3) Å	γ = 90°
Volume	1335.19(12) $Å^3$	
Z	4	
Density (calculated)	5.147 $g.cm^{-3}$	
Absorption coefficient (μ)	12.364 mm^{-1}	
F(000)	1832	
Crystal size	0.245 × 0.035 × 0.030 mm^3	
ω range for data collection	2.01 to 27.08°	
Index ranges	$-15 \le h \le 15$, $-24 \le k \le 24$, $-7 \le l \le 7$	
Reflections collected	6647	
Independent reflections	1479 [R_{int} = 0.0263]	
Completeness to θ = 27.08°	100.0 %	
Refinement method	Full-matrix least-squares on F^2	
Data / restraints / parameters	1479 / 1 / 107	
Goodness-of-fit on F^2	1.098	
Final R indices [I>2σ(I)]	R_1 = 0.0115, wR_2 = 0.0278	
R indices (all data)	R_1 = 0.0116, wR_2 = 0.0279	
Absolute structure parameter	0.04(2)	
Extinction coefficient	0.00164(5)	
Largest diff. peak and hole	0.682 and -0.463 $e^{-}·Å^{-3}$	

9.3 Results and Discussion

9.3.1 Synthesis

Colorless needle-like crystals of SLUG-34 were synthesized under acidic hydrothermal conditions with high yield and phase purity at 150 °C, as supported by the match of experimental powder X-ray diffraction (PXRD) pattern to the theoretical pattern simulated from single-crystal data. Hydrothermal synthesis conditions higher than 150 °C produced a mixed phase with SLUG-34 and SbO_2 (ICDD PDF# 01-074-0127). Lower temperature (125 °C) resulted in lower crystallinity, as evidenced by lower intensity and broadening of the X-ray diffraction peaks. More concentrated hydrothermal aqueous solution and/or higher molar ratio of metal sources to sulfuric acid gave rise to Sb_2O_3 (ICDD PDF# 99-000-3357).

9.3.2 Structural Characterization

SLUG-34 crystallizes in a high symmetry Ccc2 space group of the orthorhombic crystal system (Table 9.1). Single-crystal X-ray crystallography reveals that the structure contains isolated 1-D cationic antimony oxide chains with charge-balancing sulfate anions between adjacent chains (Figure 9.1).[429] Each $[Sb_6O_7]^{4+}$ chain propagates along the *c*-axis and is surrounded by sulfate anions in the *ab*-plane. The $[Sb_6O_7]^{4+}$ chains consist of three crystallographically independent Sb centers, all with a similar trigonal pyramidal coordination environment. The inert pair effect of lower *p*-block metals allows umbrella-like coordination, with the inert pair of the outer animony centers (Sb1 and Sb3, Figures 9.1 and 9.2) pointing outwards and

capping the chains. All of the oxygens in the antimonite chains are unprotonated, supported by both charge balance and X-ray crystallography (R_1=0.0115,

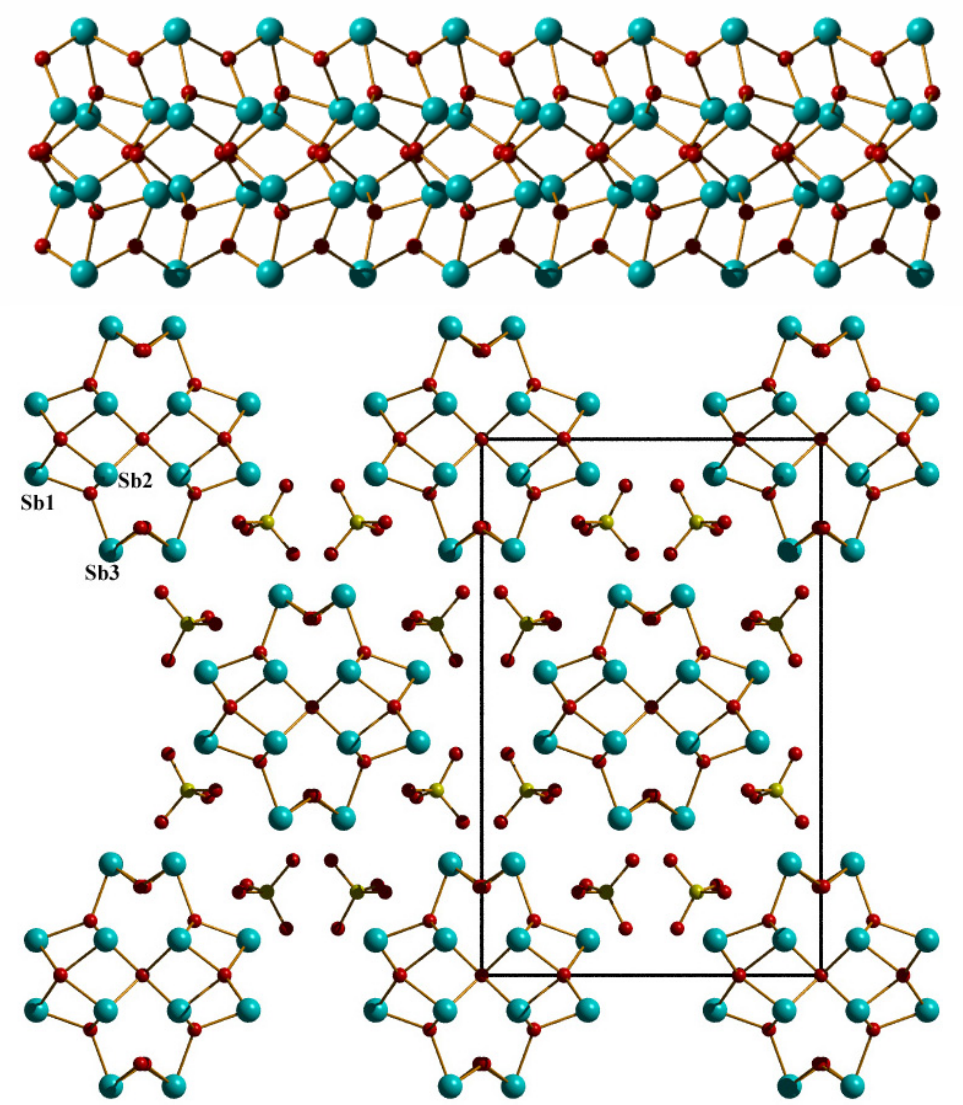

Figure 9.1 Top: *b*-projection of one cationic $[Sb_6O_7]^{4+}$ chain of SLUG-34; Bottom: *c*-projection of SLUG-34 showing the chains end-on and interchain sulfates (Sb: turquoise, S: yellow, O: red).

wR_2=0.0278) and attributable to the semi-metal nature of Sb. Two of four crystallographically independent intra-chain oxygens [O(2) and O(4)] triply bridge to metal centers as for LDHs, while two other oxygens [O(3) and O(5)] doubly bridge to antimony. The positive charge feature of this 1-D extended structure is contributed by both trivalent Sb centers and μ_3-oxygen.

The cationic topology is further defined by electrostatic interaction between sulfates and positively charged chains. The sulfate oxygens coordinate to antimony by a weak interaction [~ 2.290(3) to 2.376(3) Å] (Table 9.2). These contact distances are not only significantly longer than the intrachain Sb-O bonds [~ 1.982(2) to 2.149(2) Å] but are well outside the accepted distance for a covalent Sb-O bond [2.061±0.116 Å] from the Cambridge Structural Database (CSD).[430] These numbers

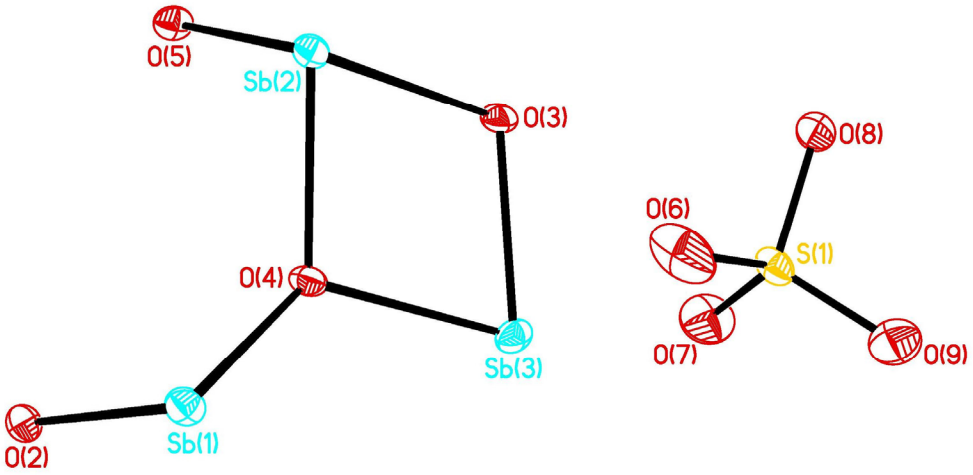

Figure 9.2 Oak Ridge thermal ellipsoid plot (shown as 50% probability) and atom labeling scheme of SLUG-34.

indicate the sulfates are not covalently bonded to the antimony oxide chains, supporting that this material is indeed a cationic 1-D extended inorganic structure. Initial attempts to exchange sulfate with other anions [e.g. chromate (CrO_4^{2-}), permanganate (MnO_4^-), perchlorate (ClO_4^-) and selenite (SeO_3^{2-})], however, were unsuccessful. Likely the divalent nature of the sulfates gives rise to strong electrostatic bonding with the cationic chains.

Table 9.2 Selected bond lengths [Å] and bond angles (°) for SLUG-34

Sb(1)-O(2)	2.002(3)	Sb(1)-O(4)	2.067(2)
Sb(1)-O(2)^{i}	2.199(3)	Sb(2)-O(5)	1.997(2)
Sb(2)-O(4)	2.082(2)	Sb(2)-O(2)^{i}	2.130(2)
Sb(3)-O(3)^{ii}	1.982(2)	Sb(3)-O(3)	2.035(2)
Sb(3)-O(4)	2.149(2)		
O(2)-Sb(1)-O(4)	86.18(9)	O(2)-Sb(1)-O(2)^{i}	88.31(4)
O(4)-Sb(1)-O(2)^{i}	71.91(8)	O(5)-Sb(2)-O(4)	89.12(14)
O(5)-Sb(2)-O(2)^{i}	89.79(8)	O(4)-Sb(2)-O(2)^{i}	73.05(10)
O(3)^{ii}-Sb(3)-O(3)	93.80(4)	O(3)^{ii}-Sb(3)-O(4)	85.45(8)
O(3)-Sb(3)-O(4)	73.34(8)		

Symmetry transformations used to generate equivalent atoms:
^{i}x,-y+1,z+1/2 ^{ii}-x+1,y,z-1/2

9.3.3 Thermal Characterization

Thermal behavior of this rare cationic 1-D antimonite topology was probed by *in-situ* powder X-ray thermodiffraction in air, and by thermogravimetric analysis (TGA) under both N_2 and air purge. The TGA traces indicates SLUG-34 is thermally stable to *ca*. 500 °C, which was also observed by *in-situ* thermodiffraction, with no structural rearrangement after annealing the crystals to 400 °C (Figure 9.3 and 9.4).

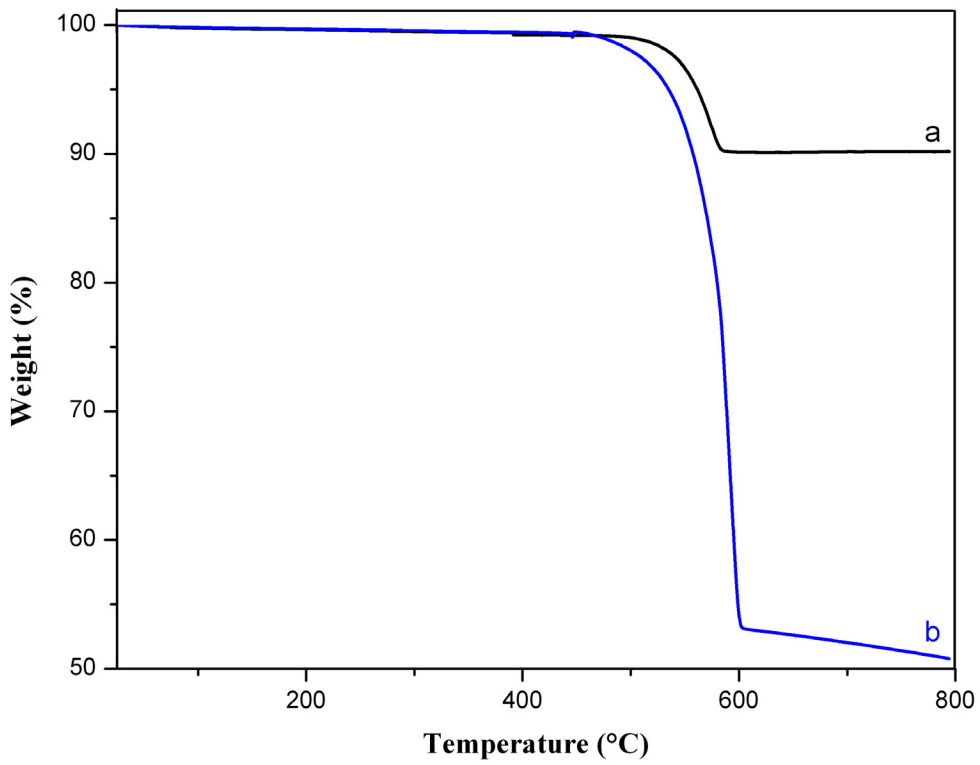

Figure 9.3 TGA trace of SLUG-34 from 25 °C to 800 °C under air (a, black) and N_2(b, blue) purge.

This thermal stability of SLUG-34 is significantly higher than both metal-organic frameworks and layered rare-earth hydroxides.[409,414,431-434] No apparent peak broadening in the *in-situ* thermodiffraction confirms negligible loss of crystallanity upon heating. The major decomposition step occurred in the temperature range 450 to 600 °C, presumably condensing the structure to antimony oxide under air with over 9.90 % weight loss (theoretical 10.83 %). *Ex-situ* thermal treatment of SLUG-34 evidenced producing SbO_2 after annealing at 600 °C (ICDD PDF# 01-074-0127).

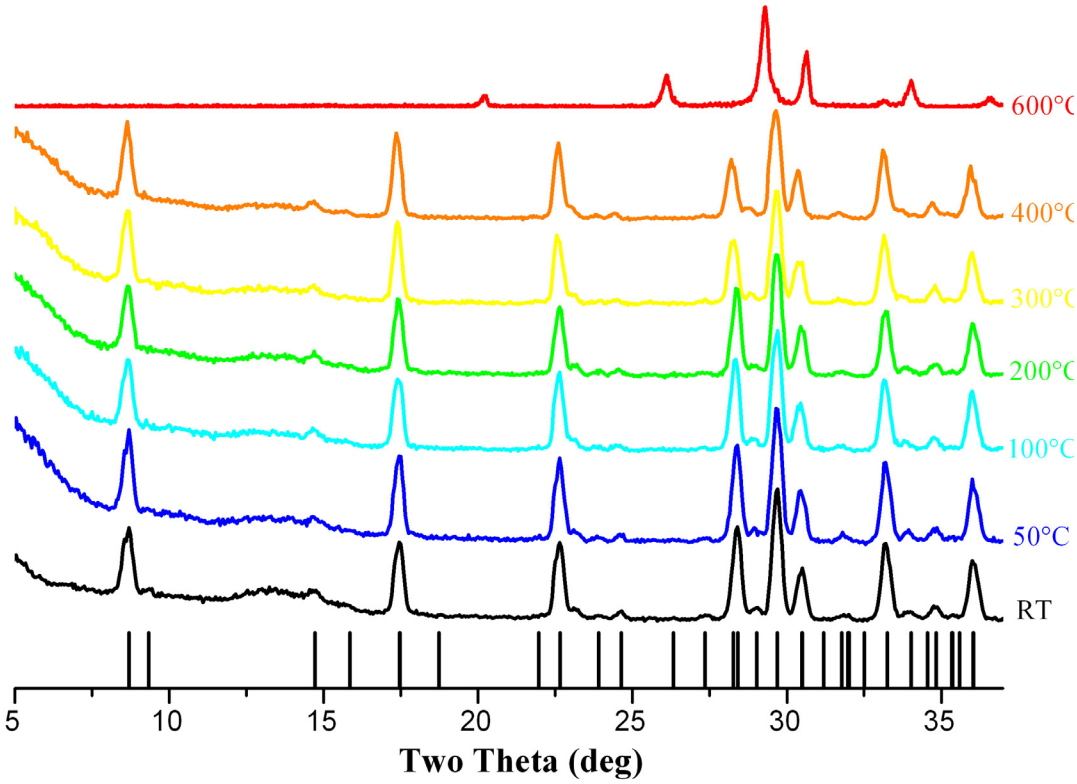

Figure 9.4 *In-situ* variable temperature PXRD of SLUG-34 from room temperature to 400 °C and *ex-situ* thermodiffraction of SLUG-34 after heating to 600 °C. Theoretical pattern is shown at the bottom as bars.

9.3.4 Chemical Stability

The basic nature of layered double hydroxides and layered rare earth hydroxides does not allow chemical stability in acidic conditions, which is often the operation parameter in environmental hazardous waste. The chemical resistance of SLUG-34 to acidic aqueous solution was examined by suspending samples of crystals (*ca.* 100 mg) in Milli-Q water, buffered solution at pH 4 and aqueous HCl, HNO_3 or H_2SO_4 solution at pH 2. PXRD before and after acidic solution treatment for 12 h

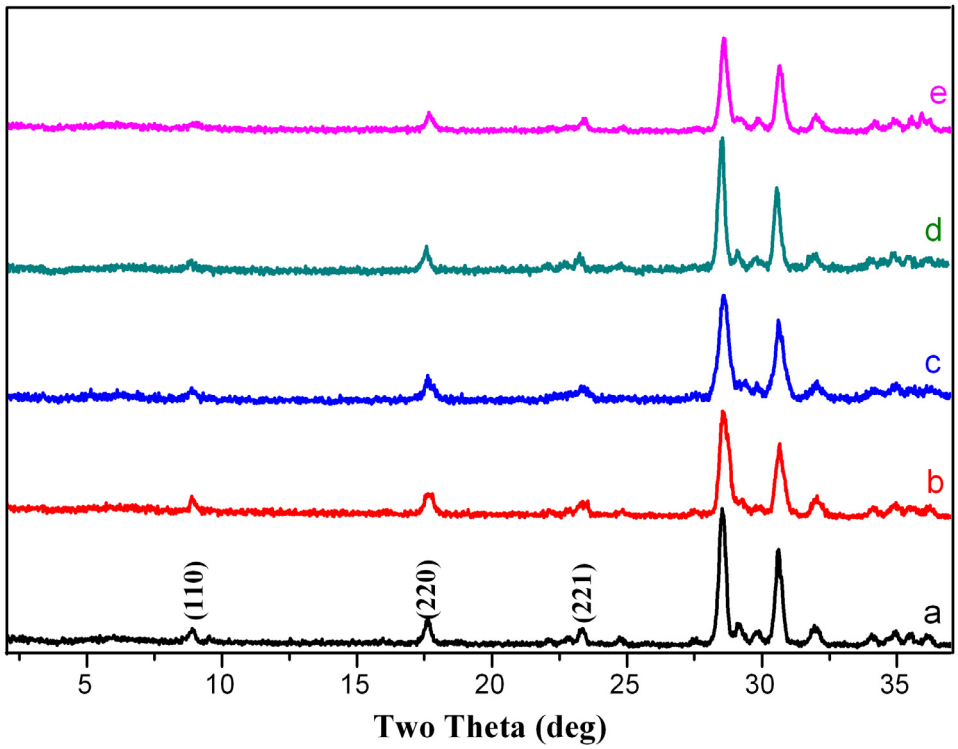

Figure 9.5 PXRD of SLUG-34 after treatment for 12 h in Milli-Q water (a), buffer at pH 4 (b), HCl aqueous solution at pH 2 (c), HNO_3 aqueous solution at pH 2 (d) and H_2SO_4 aqueous solution at pH 2 (e).

confirms the integrity of the SLUG-34 extended 1-D structure (Figure 9.5). Though crystallanity reduced after acid treatment as judged by the lower diffraction peak intensity, the survival of three low 2θ angle diffraction peaks with miller indices (110), (220) and (221) indicates chemical stability in acidic condition. Indeed, there is no phase transition and no diffraction peaks for SbO_2, Sb_2O_3 or other antimony oxides are observed.

9.4 Conclusions

SLUG-34 is a new cationic antimony oxide and entirely inorganic with 1-D Sb-O-Sb inorganic connectivity. The strong sulfate divalent anions give rise to stability to ~ 500 °C and chemical resistance to acidic condition. Although initial attempts for host-guest applications were unsuccessful, this breakthrough in both new cationic inorganic topology and sulfate templating opens up the possibility of cationic extended metalates with stability superior to that of LDHs for anion-based applications.

9.5 References

397. Thomas, J. M., *Sci. Am.* **1992,** *1992*, 112-115.

398. Wight, A. P.; Davis, M. E., *Chem. Rev.* **2002,** *102*, 3589-3614.

399. Davis, M. E., *Nature* **2002,** *417*, 813-821.

400. Corma, A., *J. Catal.* **2003,** *216*, 298-312.

401. Keith, L. H.; Teillard, W. A., *Environ. Sci. Technol.* **1979,** *13*, 416.

402. Hogue, C., *Chemical & Engineering News* **2011,** *89*, 6.

403. Weitkamp, J., *Solid State Ionics* **2000,** *131*, 175-188.

404. Wu, M.; Janssen, S., *Environ. Sci. Technol.* **2011,** *45*, 366-367.

405. Rives, V., *LDHs: Layered Double Hydroxides: Present and Future*. Nova Science Publishers Inc., Hauppauge, New York, USA: **2001**.

406. Slade, D. G. E. a. R. C. T., *Layered Double Hydroxides*. X. Duan and D. G. Evans ed.; Springer-Verlag, New York, NY, USA: **2006**; pp 1-87.

407. Rao, K. K.; Gravelle, M.; Valente, J. S.; Figueras, F., *J. Catal.* **1997,** *173*, 115-121.

408. Geng, F.; Ma, R.; Sasaki, T., *Acc. Chem. Res.* **2010,** *43*, 1177-1185.

409. Geng, F.; Matsushida, Y.; Ma, R.; Xin, H.; Tanaka, M.; Izumi, F.; Lyi, N.; Sasaki, T., *J. Am. Chem. Soc.* **2008,** *130*, 16344-16350.

410. Liu, Z.; Ma, R.; Osada, M.; Iyi, N.; Ebina, Y.; Takada, K.; Sasaki, T., *J. Am. Chem. Soc.* **2006,** *128*, 4872-4880.

411. Poudret, L.; Prior, T. J.; McIntyre, L. J.; Fogg, A. M., *Chem. Mater.* **2008,** *20*, 7447-7453.

412. McIntyre, L. J.; Jackson, L. K.; Fogg, A. M., *Chem. Mater.* **2008,** *20*, 335-340.

413. Gandara, F.; Perles, J.; Snejko, N.; Iglesia, M.; Gomez-Lor, B.; Gutierrez-puebla, R.; Monge, M. A., *Angew. Chem. Int. Ed.* **2006,** *45*, 7998-8001.

414. Liang, J.; Ma, R.; Geng, F.; Ebina, Y.; Sasaki, T., *Chem. Mater.* **2010,** *22*, 6001-6007.

415. Oliver, S. R. J., *Chem. Soc. Rev.* **2009,** *38*, 1868-1881.

416. Tran, D. T.; Zavalij, P. Y.; Oliver, S. R. J., *J. Am. Chem. Soc.* **2002,** *124*, 3966-3969.

417. Rogow, D. L.; Russell, M. P.; Wayman, L. M.; Swanson, C. H.; Oliver, A. G.; J., O. S. R., *Crystal Growth & Design* **2010,** *10*, 823-829.

418. Swanson, C. H.; Shaikh, H. A.; Rogow, D. L.; Oliver, A. G.; Campana, C. F.; Oliver, S. R. J., *J. Am. Chem. Soc.* **2008,** *130*, 11737-11741.

419. Fei, H.; Oliver, S. R. J., *Angew. Chem. Int. Ed.* **2011,** *50*, 9066-9070.

420. Rogow, D. L.; Fei, H.; Brennan, D. P.; Ikehata, M.; Zavalij, P. Y.; Oliver, A. G.; Oliver, S. R. J., *Inorg. Chem.* **2010,** *49*, 5619-5624.

421. Fei, H.; Pham, C. H.; Oliver, S. R. J., *J. Am. Chem. Soc.* **2012,** *134*, DOI: 10.1021/ja3017686.

422. Kaduk, J. A.; Toft, M. A.; Golab, J. T., *Powder Diffraction* **2009,** *25*, 19-24.

423. Sykora, R. E.; King, J. E.; Illies, A. J.; Albrecht-Schmitt, T. E., *J. Solid State Chem* **2004,** *177*, 1717-1722.

424. Wang, S.; Alekseev, E. V.; Diwu, J. C.; W. H.; Phillips; B. L.; Depmeier, W.; Albrecht-Schmitt, T. E., *Angew. Chem. Int. Ed.* **2010,** *49*, 1057-1060.

425. Goulding, H. V.; Hulse, S. E.; Clegg, W.; Harrington, R. W.; Playford, H. Y.; Walton, R. I.; Fogg, A. M., *J. Am. Chem. Soc.* **2010,** *132*, 13618-13620.

426. *APEX-II, 2.1.4;*. Bruker-AXS: Madison, WI, 2007.

427. *SHELXTL Crystal Structure Determination Package*. Bruker Analytical X-ray Systems Inc.: Madison, WI, 1995-99.

428. Klaus Brandenburg; H. P. Diamond; Crystal-Impact: Germany, **2007**.

429. $[Sb_6O_7][(SO_4)_2]$ (SLUG-34): colorless needle-like crystal dimensions 0.245 × 0.035 × 0.030 mm; orthorhombic; space group Ccc2; a=12.0329(6); b=18.9371(10); c=5.8595(3); V=1335.19(12); Z=4; T=296(2) K; λ(Mo-Kα) = 0.71073 Å; μ(Mo-Kα) = 12.364 mm-1; 7481 reflections collected; 6647 reflections collected;1479 unique (Rint = 0.0263); giving R_1 = 0.0115, wR_2 = 0.0278 for 1471 data with [I>2σ(I)]; and R_1 = 0.0116, wR_2 = 0.0279 for all 1479 data.

430. *Cambridge Structural Database*. A covalent Sb-O bond length is generally between 1.9 Å and 2.1 Å, while 90.8% Sb-O bonds with a bond length less than 2.27 Å.

431. Fei, H.; Paw, L. U.; Rogow, D. L.; Bresler, M. R.; Abdollahian, Y. A.; Oliver, S. R. J., *Chem. Mater.* **2010,** *22*, 2027-2032.

432. Fei, H.; Rogow, D. L.; Oliver, S. R. J., *J. Am. Chem. Soc.* **2010,** *132*, 7202-7209.

433. Zhao, X.; Wu, T.; Zheng, S. T.; Wang, L.; Bu, X.; Feng, P., *Chem. Commun.* **2011,** *47*, 5536-5538.

434. Choi, H. J.; Dinca, M.; Long, J. R., *J. Am. Chem. Soc.* **2008,** *130*, 7848-7849.

Chapter 10

Polymer Templated Nanospider TiO_2 Thin Films for Efficient Photoelectrochemical Water Splitting

Abstract

We have discovered a facile and inexpensive approach to fabricate "nanospider" TiO_2 thin films with not only an amazing morphology but highly efficient water splitting to produce hydrogen. Our method employs benzene-swollen poly(ethylene glycol) as a sacrificial organic polymer to template the semiconductor thin film. The synthesized TiO_2 thin films are highly crystalline with optimized particle and channel size to enhance the liquid-semiconductor junction interaction. This enhanced contact area leads to more than twice the water splitting performance than conventional P25 thin films. In addition, the nanospider thin films also outperform P25 films in the photodegradation of toxic organics.

10.1 Introduction

TiO_2 is a wide band-gap semiconductor attracting much attention since the discovery of Gratzel type dye-sensitized solar cells and the Honda–Fujishima effect of photoelectrochemical (PEC) cells.[435,436] Various nanostructures based on TiO_2 and their properties have been studied in detail, including nanowires, nanotubes, nanorods, nanodisks, nanoflowers and nanotrees.[437-440] Considering the extreme environmental need for clean energy systems, recent effort has focused on using these nanomaterials for water splitting to produce hydrogen as well as the photodegradation of toxic organic dyes.[441,442]

The use of H_2 as an efficient and environmentally clean energy carrier is an essential part of future energy production. A clean source of H_2 is also required if CO_2 recycling is to be realized.[443,444] Semiconductor/liquid junction PEC cells are an emerging solar energy conversion system to produce hydrogen. They often utilize TiO_2 as photocatalyst, which is non-toxic, low-cost and biocompatible.[436] This configuration is capable of continuously producing H_2 based on water splitting, $2H_2O + h\nu \rightarrow 2H_2 + O_2$, as long as the cell is illuminated. With the discovery of various nano-morphologies of TiO_2,[445-448] the light-to-hydrogen efficiency has been effectively advanced over bulk titania. Despite the low-cost, convenient synthesis, highly-crystallinity, small particle size and large semiconductor-liquid contact area, TiO_2 or ZnO photoelectrode PECs for water splitting are still limited due to low overall light-to-hydrogen conversion efficiency, typically 0.15 % or lower.[448-450]

Polymer templating of porous metal oxides is a well-established method and has been used to template ordered/quasi-ordered/disordered mesoporous metal oxides.[451] Our group and others (most notably, Caruso and co-workers) have used ethanol and/or water solvated polymers to obtain porous metal oxides, owing to the evaporation of the solvent and/or thermal decomposition of the polymer template.[452-456] Meanwhile, we have also investigated organic solvent swollen polymers, with promising performance as dye-sensitized solar cells.[457,458]

Herein, we report a convenient and low-cost method to synthesize high-crystalline TiO2 thin films displaying a "nanospider" morphology over the entire substrate. The method utilizes benzene-swollen polyethylene glycol (PEG) as a structure-directing template to support the nanospider growth, and the unprecedented nanochannel morphology greatly increases contact with a surrounding solvent. The films show over double the photocatalytic performance compared to P25 type films, for both PEC water splitting and organic dye degradation.

10.2 Experimental Section

10.2.1 Preparation of the TiO_2 nanospider thin film

5 wt.% polyethylene glycol (Alfa Aesar) was stirred and dissolved in 10 ml benzene (Aldrich), followed by titanium isopropoxide (Acros Organic). The viscous mixture was stirred mechanically in a closed vial for 3 hours. The resultant transparent solution was spin-coated at 1000 rpm for 30 seconds on F-doped SnO_2 (FTO) glass (Hartford Glass Co.). The FTO had been pre-cleaned with ethanol and

deionized water under sonication, followed by drying under an N_2 stream, and edge area defined by applying tape. The thin film was heated in a tube furnace at a rate of 2 °C/min to the desired annealing temperature and soaked for 2 hours. The P25 thin film was deposited by spin-coating the P25 paste in ethanol on FTO glass and then heated in an oven set to 110 °C. For the P25 thin film only, the procedure of spin-coating was repeated until the film thickness was ca. 1 μm (monitored by cross-sectional SEM). The 15 nm nanoparticle thin film was grown by hydrolysis of titanium n-butoxide under acidic medium (diluted HNO_3 with pH = 1.2). The deposition procedure was the same as for P25, then the film was annealed at 450 °C for 2 hours.

10.2.2 Photoelectrochemical Measurements

The nanospider thin film anode was prepared by connecting a copper wire to a bare portion of the FTO glass after tape removal and secured with high-purity silver conducting paint (Alfa Aesar). The cell was then sealed on all edges with epoxy resin except for a working electrode surface area of ~ 0.10 cm^2. An electrolyte solution of 0.1 M NaOH and an Ag/AgCl reference electrode (+0.198 V vs. NHE) was employed, along with a coiled Pt wire counter electrode during all testing. All PEC measurements were carried out on a Solartron 1280B Workstation coupled to an infrared water-filled filter (Oriel no. 6127), aligned in a monochromator (Oriel Cornerstone 130 1/8m). A 1000W Xe lamp was utilized as a white-light source and irradiance was measured with a power meter.

10.2.3 Methylene Blue (MB) Degradation Photocatalysis

A 6W compact UV lamp (UVL-56, UVP Inc., intensity 1.35 mW/cm2 at 365 nm) was used as the light source, with the sample holder placed on its side to maximize exposure. For a typical experiment, a TiO_2 thin film was suspended in the MB solution for 10 min under dark conditions to achieve absorption equilibrium before carrying out the photocatalysis reaction. A UV-Vis spectrometer (model 8452A, Hewlett-Packard) was used to determine the concentration of MB solution versus UV exposure time.

10.3 Results and Discussion

10.3.1 Fabrication and Characterizations

A non-polar organic solvent is required during the deposition; attempts to carry out the reaction in ethanol, dichloromethane or acetonitrile were unsuccessful. Stirring in a closed environment to avoid overly rapid hydrolysis of the TiO_2 precursor is also essential to reach a homogeneous morphology. The substrate has no impact on forming the nanospider: the thin film can be grown on bare glass, F-doped tin oxide (FTO) glass, indium tin oxide (ITO) coated glass or bare silicon wafer.

Top-view optical and SEM micrographs (Figure 10.1, 10.2a and 10.2b) of as-prepared TiO_2 nanospider thin films show a homogeneous morphology of interconnected nanochannels over the entire surface (2 cm × 2 cm). These nanochannels are all a similar width of ~ 1 μm and occupy *ca*. 20 % the area of the

film; the remaining area is raised domains of TiO_2. Cross-sectional scanning electron microscope (SEM) images (Figure 10.2) of the TiO_2 nanospider on FTO glass show that the nanochannels are defined by the TiO_2 coated area, with a depth of around 1.2 μm. Slightly increasing the PEG ratio from 5 wt.% to 6 wt.% greatly changed the thin film morphology by increasing the nanochannel width, reducing the titania coverage on the substrate (Figure 10.1).

Irregular or discontinuous cracks usually lead to less coverage of titania on the substrate, and in turn reduced light absorption and photocatalytic performance. In our case, however, the presence of controlled narrow-width channels leads to larger semiconductor-liquid contact area at the channel walls as well as small cracks in the island regions (Figure 10.2). We are thus balancing these two effects of larger semiconductor-liquid contact (*via* channels and island cracks) while maximizing TiO_2

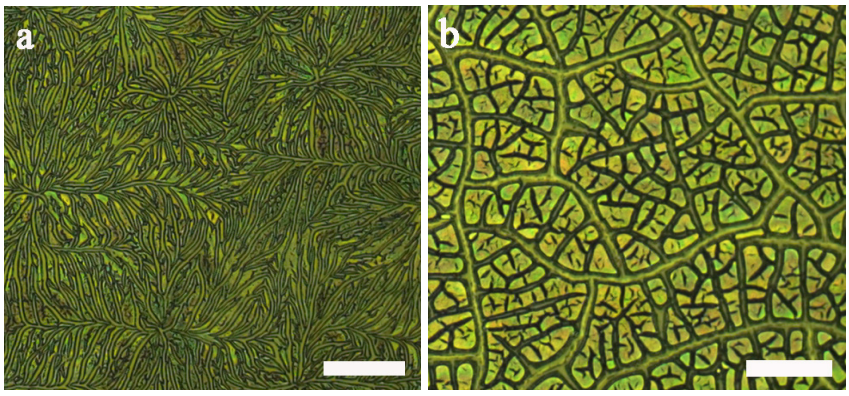

Figure 10.1 Optical micrograph of (a) the $TiOB_{2B}$ nanospider morphology synthesized by 5% wt. PEG; (b) $TiOB_{2B}$ morphology synthesized by 6% wt. PEG (scale bar: 50 μm)

coverage. Considering the greater homogeneity and semiconductor coverage of the thin film synthesized from 5 wt.% PEG over 6 wt.% PEG (Figure 10.1), we employed the former for photocatalytic investigation.

A possible formation mechanism for this nanostructure is self-assembled phase separation of the solvent-swollen PEG and titania precursor. PEG is a hydrophilic long-chain polymer, while titanium(IV) isopropoxide [$Ti(O^iPr)_4$] is a hydrophobic titanium precursor with bulky organic side chains surrounding the metal centers. Hydrophilicity/hydrophobicity could lead to phase separation of the PEG and $Ti(O^iPr)_4$. In addition, $Ti(O^iPr)_4$ hydrolyzes more rapidly than titanium (IV) n-butoxide [$Ti(O^nBu)_4$] and titanium(IV) n-propoxide [$Ti(O^nPr)_4$].[459] This observation accounts for the lack of any homogeneous nanospider film in the case of $Ti(O^nBu)_4$ and $Ti(O^nPr)_4$, with the presence of irregular, cracks and widely varying channel width. Compared with intriguing nanospider morphology (Figure 10.1a), the formation of broad width channels (Figure 10.1b) with higher PEG concentration can also be reasonably explained by this phase separation mechanism.

We further investigated the effect of annealing temperature on the crystallinity, phase and PEC performance of the TiO_2 nanospider thin film. Figure 3 presents the powder X-ray diffraction (PXRD) patterns of titania films annealed to various temperatures. As polyethylene glycol is known to decompose after 430 °C and FTO degrades (in terms of optical and transport properties) above 600 °C, annealing temperatures between 450 °C and 600 °C were investigated. If a TiO_2

sample is a mixture of anatase and rutile, the weight fraction of both can be calculated from eq 10.1:[460]

$$\text{wt.\% (Rutile)} = A_R/(0.884\ A_A + A_R) \times 100\% \qquad (10.1)$$

where A_A represents the integrated intensity of the anatase (101) peak positioned at 25.28° and A_R is that of the rutile (110) peak located at 27.36°. There is a gradual phase transition from anatase to rutile above 500 °C. Pure anatase can only be obtained at 450 °C (Table 10.1). The crystal size of the annealed film can also be estimated by the Scherrer equation:

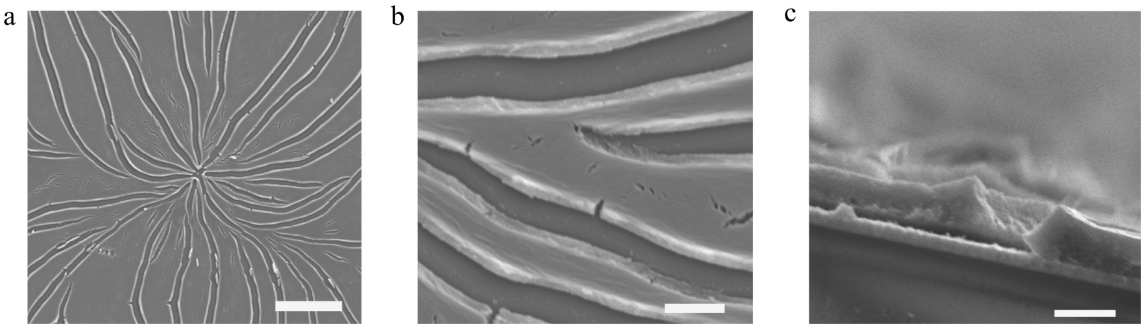

Figure 10.2 (a, b) Top-view SEM images of the TiO_2 nanospider film grown on FTO glass (scale bars: 20 μm and 2 μm, respectively); (c) Cross-sectional SEM image of a wall edge in the nanospider thin film (scale bar: 2 μm).

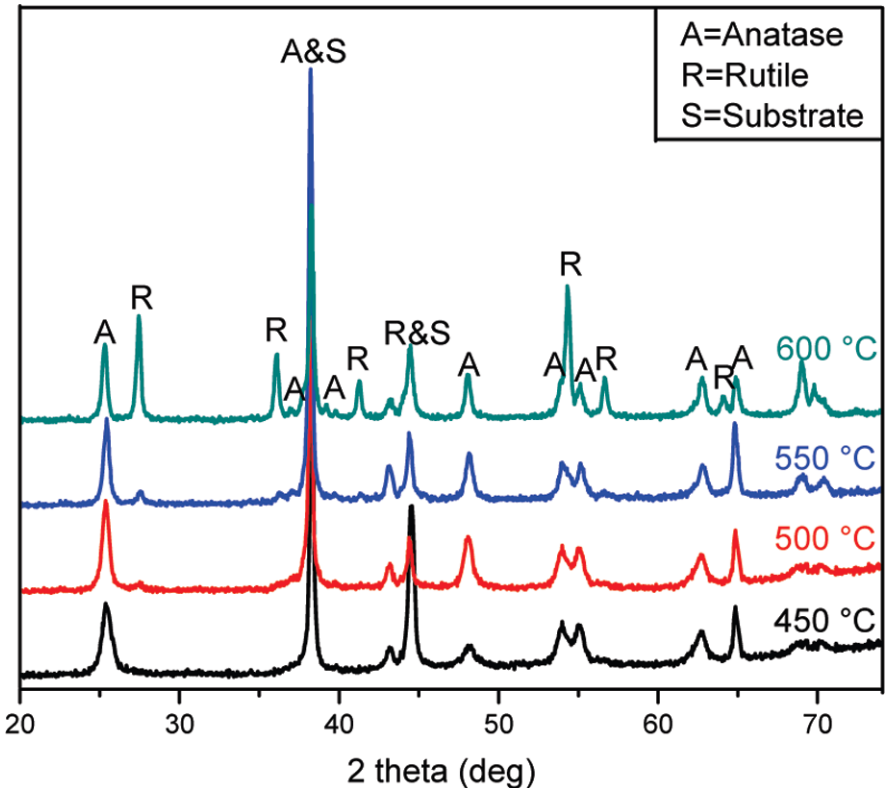

Figure 10.3 PXRD of the nanospider thin film annealed to specified temperatures (A: anatase phase; R: rutile phase; S: substrate).

$$D = 0.9\,\lambda/\beta\cos\theta \qquad (10.2)$$

where D is crystal size, λ is PXRD wavelength, β is the line broadening factor and θ is the Bragg angle. From this calculation, the crystal size gradually increases with annealing temperature from *ca*. 10 to 30 nm (Table 10.1). The TEM image after 500 °C annealing shows average TiO_2 particle size ~16 nm, which agrees well with the Scherrer calculation and confirms that the films are highly nanocrystalline in nature.

10.3.2 Methylene Blue Photocatalysis Degradation

A standard method to establish the efficiency of a semiconductor photocatalyst is to test the photodegradation of methylene blue (MB). This benchmark reaction requires that the catalyst have large surface area and effective dye adsorptive capability. The mechanistic details of organic photodecomposition have been discussed elsewhere,[442,461,462] and a simplified scheme is described as follows:

$$TiO_2 + \text{dye} \leftrightarrow TiO_2\text{-dye} \tag{10.3}$$

$$TiO_2\text{-dye} + h\nu \rightarrow TiO_2(e^-, h^+)\text{-dye} \tag{10.4}$$

$$TiO_2(h^+) + H_2O \rightarrow TiO_2(OH\cdot) + H^+ \tag{10.5}$$

$$TiO_2(h^+) + OH^- \rightarrow TiO_2(OH\cdot) \tag{10.6}$$

$$TiO_2(e^-) + O_2 \rightarrow TiO_2(O_2^-\cdot) \tag{10.7}$$

$$TiO_2(OH\cdot) + TiO_2(O_2^-\cdot) + \text{dye} \rightarrow \text{degradation products} + TiO_2 \tag{10.8}$$

The first dye adsorption step is the rate determining step and prefers a large surface area TiO_2 nano/mesostructure. Photocatalytic efficiency can thus be enhanced with higher TiO_2 semiconductor-liquid contact. We employed a 1 cm × 1

Table 10.1 Average crystal size and weight fraction of the $TiOB_{2B}$ nanospider thin films versus annealing temperature, as calculated from equations 10.1 and 10.2.

Annealing temp (°C)	450	500	550	600
Anatase crystal size (nm)	11.0	16.7	20.4	25.1
Rutile crystal size (nm)	N/A	N/A	N/A	27.9
Anatase weight fraction (%)	100	91.2	82.4	36.4
Rutile weight fraction (%)	0	8.8	17.6	63.6

cm area nanospider thin film (< 0.01 g) to photodegrade 5 ml of a 1×10^{-5} M MB aqueous solution under illumination by a 6 W compact UV lamp at a fixed distance of 10 cm. Before photocatalysis, absorption/desorption equilibrium was achieved by immersing the thin film into the MB solution for 10 min under dark conditions. Our nanospider thin films are free-standing and chemically stable in the dye solution unlike commercial P25 powders. Thus, centrifuging or other particle suspension methods are not required after the catalytic reaction. During the photodegradation step, the concentration of MB solution decreased incrementally for all samples of nanospider thin films (Figures 10.4). The most efficient sample was the nanospider annealed at 500 °C, with turnover decreasing for the 550 °C annealed film. Notably, the former outperforms the P25 thin film, with over 20 % higher efficiency.

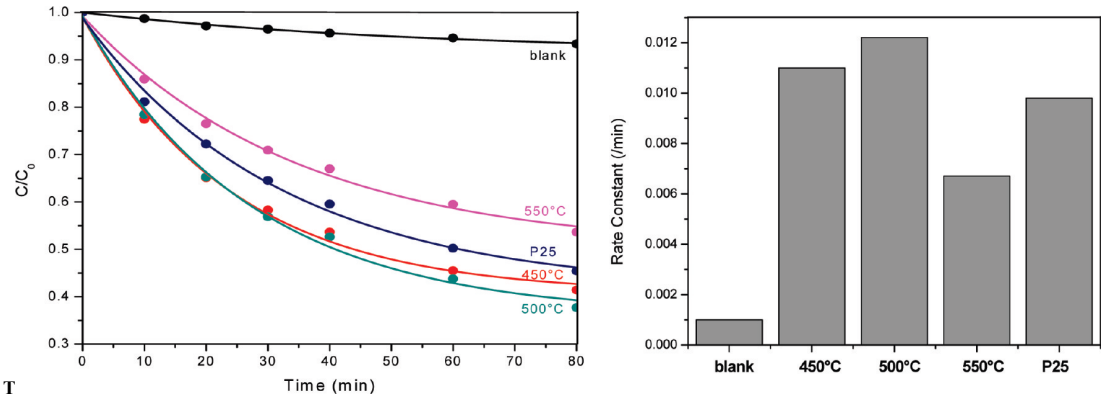

Figure 10.4 Concentration vs time plots (left) and reaction rate constants (right) for MB photolysis under UV light (blank is without UV light).

Photodegradation of MB has previously been shown by others to obey pseudo-first-order kinetics. Hence, the rate of MB degradation was obtained from a first-order plot:[27]

$$\ln (c/c_0) = kt \tag{10.9}$$

where c_0 is the initial concentration of MB, c is the concentration of MB after time t of photolysis, and k is the rate constant. The highest rate constant amongst our nanospider samples was 0.012 min^{-1}, which is 22% higher than the commercial

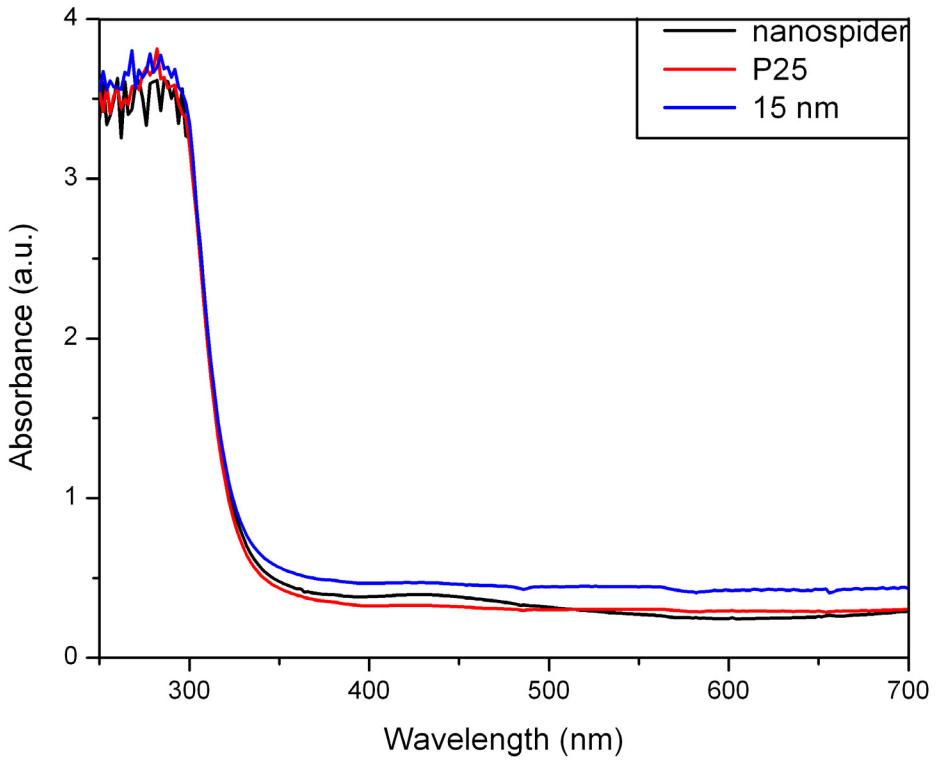

Figure 10.5 UV-Vis absorption spectra of the nanospider thin film (black), P25 thin film (red), and the thin film with 15 nm nanoparticle size (blue). All three films were deposited on an FTO glass substrate.

photocatalyst P25 film (Figure 10.4). The open channel system and high crystallinity of the nanospider film facilitates MB adsorption onto the spider surface, achieving higher photocatalytic efficiency with less semiconductor material.

10.3.3 Photoelectrochemical Water Splitting

Owing to the above superior photodecomposition performance over current titania thin films, we further investigated application of the nanospider as a PEC cell for water splitting to produce hydrogen. Surface area, crystallinity and particle size are well known to strongly affect the photoelectrochemical properties of the semiconductor. High crystallinity reduces defects that serve as recombination trapping sites and decrease photocatalytic ability. At the same time, smaller particle size is also preferred for shorter path distance between electron-hole and surface active sites. Considering the 500 °C annealed sample had the highest MB photodegradation performance, systematic measurements were carried out on this sample, as well as a P25 thin film and a TiO_2 thin film with nanoparticle size ~15 nm for reference. All three TiO_2 samples have similar band gaps and therefore UV-Vis absorption spectra (Figure 10.5). During the photoelectrochemical test, all three samples had a pronounced photocurrent beginning from ~ −0.6 V (vs. Ag/AgCl), with a saturated photocurrent at −0.1 V (Figure 10.6a). The nanospider thin film reached 230 $\mu A/cm^2$ at 0 V and 272 $\mu A/cm^2$ at +1.1 V. In stark contrast, the P25 thin film reaches only 110 $\mu A/cm^2$ with no applied potential and 125 $\mu A/cm^2$ at +1.1 V. A thin

film with particle diameter of ~15 nm of pure anatase phase prepared by acid hydrolysis was also tested. Despite having the same particle size, the lack of nanochannels led to a much lower saturated photocurrent density of around 130 $\mu A/cm^2$, just over half that of the nanospider sample.

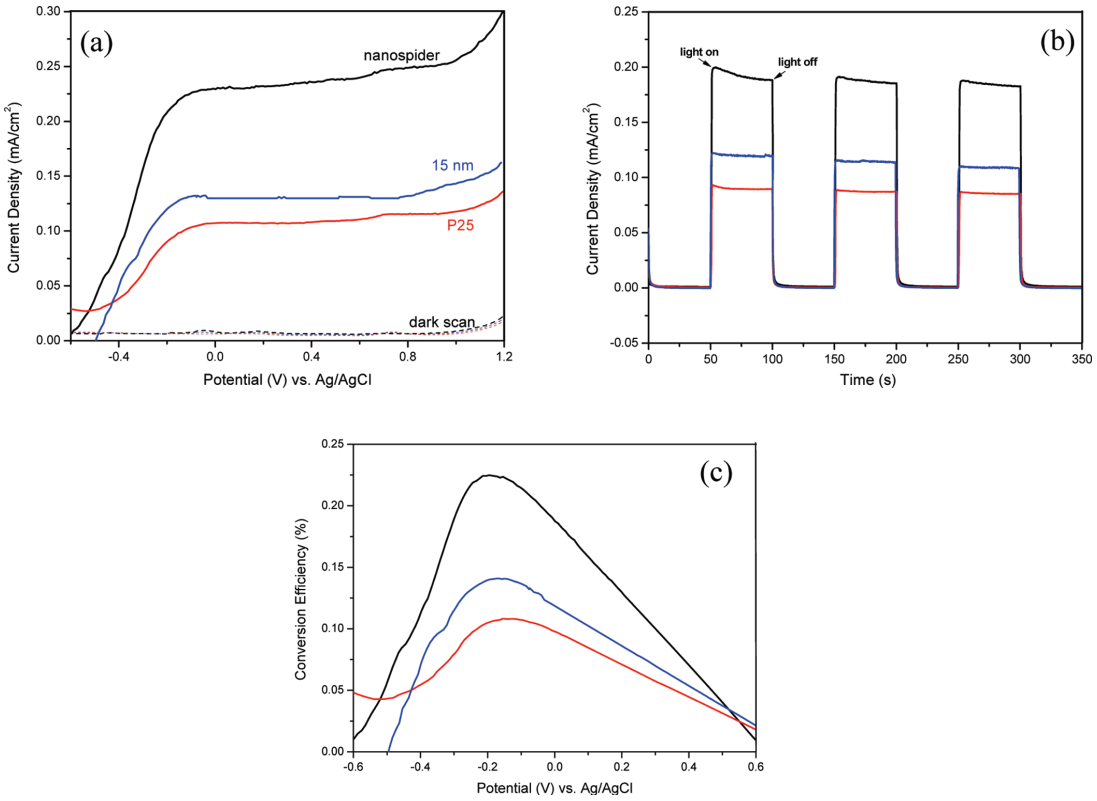

Figure 10.6 (a) Linear sweep voltammograms, collected at a scan rate of 10 mV/s from -0.6 to +1.2 V for the nanospider (black), P25 (red), and 15 nm (blue) films. Solid curves are for 100 mV/cm_2 illumination, whereas dark conditions are shown as dashed curves; (b) amperometric *I-t* curves of the nanospider (black), P25 (red), and 15 nm (blue) films at an applied voltage of +0.2 V and 100 mW/cm_2 illumination with 50 s light on/off cycles; (c) photoconversion efficiency of PEC cells for the nanospider (black), P25 (red) and 15 nm (blue) electrodes as a function of potential vs Ag/AgCl.

We also collected amperometric I-t curves to study the photoresponse of the nanospider, P25 and 15 nm films; three light on/off cycles were examined. All three electrodes displayed similar low dark currents of less than 10^{-7} A/cm^2. With illumination, however, the nanospider photocurrent is around twice than that of the P25 and 15 nm film (Figure 10.6b). The nanospider is also highly stable chemically and photolytically in solution under sunlight illumination, with only a very small decay with light on/off cycles. The efficiency of incident photon to chemical energy can be expressed by the following equation:[28]

$$\eta = j_p (1.23 - |E_{app}|) / J_{light} \quad (10.10)$$

where η is the overall efficiency, j_p (A) is the photocurrent density, J_{light} (W) is the sunlight illumination intensity and $|E_{app}|$ is the absolute value of the applied potential E_{app}, which is obtained as:

$$E_{app} = E_{meas} - E_{aoc} \quad (10.11)$$

where E_{meas} is the electrode potential at which j_p was measured and E_{aoc} is the open circuit potential in the same electrolyte solution and illumination conditions at which j_p was measured. E_{aoc} = –0.6 V (*vs*. Ag/AgCl) for nanospider, E_{aoc} for P25 is estimated to be –0.7 V and E_{aoc}= –0.5 V for 15 nm film. The small variation is due to the difference in flat band potential caused by either nanochannels leading to less coverage of substrate or larger particle size leading to exposure of the substrate to electrolyte.[29] With correction for optical loss in the equipment setup (25%), the TiO_2 nanospider thin film reaches 0.23 % overall light-to-hydrogen efficiency at –0.15 V (*vs*. Ag/AgCl) (Figure 10.6c). The overall efficiency of the P25 thin film is only 0.08

%, and 0.11 % for the 15 nm film. Although our result is less than the highest reported 0.75 % achieved by a single-crystal nanowire array,[446] the efficiency of the nanospider is among the highest value for a conventionally deposited TiO_2 thin film, as compared with other 0D and 1D TiO_2 nanostructures.[447,448,463,464] In order to further illustrate our nanospider PEC efficiency, a sacrificial electrolyte of Na_2S and Na_2SO_3 was also tested. In this case, the nanospider displayed over five times larger photocurrent than Degussa P25. This supports our conclusion that controllable nanochannels is a favorable morphology for photoelectrochemical water splitting applications.

10.4 Conclusions

We report a facile and low cost method to template titania thin films with a nanospider morphology of large area and homogeneity. This material displayed both intriguing morphology and efficient application in methylene blue degradation and photoelectrochemical water splitting. The PEC photocurrent density of the nanospider working electrode was two times larger than that of the thin film with same particle size but no nanospider morphology. In future work, we aim to dope/incorporate other metal/metal oxide nanostructures into the nanochannels with controllable width throughout the film to possibly further enhance the photocatalytic efficiency.

10.5 References

435. Oregan, B.; Gratzel, M., *Nature* **1991,** *353*, 737-740.

436. Fujishima, A.; Honda, K., *Nature* **1972,** *238*, 37-40.

437. Law, M.; Greene, L. E.; Johnson, J. C.; Saykally, R.; Yang, P. D., *Nature Materials* **2005,** *4*, 455-459.

438. Brammer, K. S.; Oh, S. H.; Gallagher, J. O.; Jin, S. H., *Nano Letters* **2008,** *8*, 786-793.

439. Casavola, M.; Grillo, V.; Carlino, E.; Giannini, C.; Gozzo, F.; Pinel, E. F.; Garcia, M. A.; Manna, L.; Cingolani, R.; Cozzoli, P. D., *Nano Letters* **2007,** *7*, 1386-1395.

440. Pan, Y.-X.; Liu, C.-J.; Wiltoski, T. S.; Ge, Q., *Catal. Today* **2009,** *147*, 68-76.

441. Cai, Y. Q.; Shi, Y. L.; Zhang, P.; Mou, S. F.; Jiang, G. B., *Progress in Chemistry* **2006,** *18*, 1554-1564.

442. Wu, C. H.; Chern, J. M., *Ind. Eng. Chem. Res.* **2006,** *45*, 6450-6457.

443. Olah, G. A.; Goeppert, A.; Prakash, G. K. S., *J. Org. Chem.* **2009,** *74*, 487-498.

444. Dai, W. L.; Luo, S. L.; Yin, S. F.; Au, C. T., *Appl. Catal. A-General* **2009,** *366*, 2-12.

445. Grimes, C. A., *J. Mater. Chem.* **2007,** *17*, 1451-1457.

446. Feng, X. J.; Shankar, K.; Varghese, O. K.; Paulose, M.; Latempa, T. J.; Grimes, C. A., *Nano Letters* **2008,** *8*, 3781-3786.

447. Wu, G. S.; Wang, J. P.; Thomas, D. F.; Chen, A. C., *Langmuir* **2008,** *24*, 3503-3509.

448. Wolcott, A.; Smith, W. A.; Kuykendall, T. R.; Zhao, Y. P.; Zhang, J. Z., *Small* **2009,** *5*, 104-111.

449. Yang, X.; Wolcottt, A.; Wang, G.; Sobo, A.; Fitzmorris, R. C.; Qian, F.; Zhang, J. Z.; Li, Y., *Nano Letters* **2009,** *9*, 2331-2336.

450. Ahn, K. S.; Yan, Y.; Shet, S.; Deutsch, T.; Turner, J.; Al-Jassim, M., *Appl. Phys. Lett.* **2007,** *91*.

451. Tian, B. Z.; Liu, X. Y.; Tu, B.; Yu, C. Z.; Fan, J.; Wang, L. M.; Xie, S. H.; Stucky, G. D.; Zhao, D. Y., *Nature Materials* **2003,** *2*, 159-163.

452. Yue, W. B.; Xu, X. X.; Irvine, J. T. S.; Attidekou, P. S.; Liu, C.; He, H. Y.; Zhao, D. Y.; Zhou, W. Z., *Chem. Mater.* **2009,** *21*, 2540-2546.

453. Deshpande, A. S.; Shchukin, D. G.; Ustinovich, E.; Antonietti, M.; Caruso, R. A., *Adv. Funct. Mater.* **2005,** *15* (2), 239-245.

454. Fan, X.; Fei, H.; Demaree, D. H.; Brennan, D. P.; John, J. M. S.; Oliver, S. R. J., *Langmuir* **2009,** *25*, 5835-5839.

455. Liang, C. D.; Li, Z. J.; Dai, S., *Angew. Che* **2008,** *47*, 3696-3717.

456. Drisko, G. L.; Luca, V.; Sizgek, E.; Scales, N.; Caruso, R. A., *Langmuir* **2009,** *25*, 5286-5293.

457. Fan, X. J.; Demaree, D. P.; John, J. M. S.; Tripathi, A.; Oliver, S. R. J., *Appl. Phys. Lett.* **2008,** *92*.

458. Tran, D. T.; Fan, X. J.; Brennan, D. P.; Zavalij, P. Y.; Oliver, S. R. J., *Inorg. Chem.* **2005,** *44*, 6192-6196.

459. Hakim, S. H.; Shanks, B. H., *Chem. Mater.* **2009,** *21*, 2027-2038.

460. Zhang, H. Z.; Banfield, J. F., *J. Phys. Chem. B* **2000,** *104*, 3481-3487.

461. Testino, A.; Bellobono, I. R.; Buscaglia, V.; Canevali, C.; D'Arienzo, M.; Polizzi, S.; Scotti, R.; Morazzoni, F., *J. Am. Chem. Soc.* **2007,** *129*, 3564-3575.

462. Ryu, Y. H.; Kim, M. J.; Lee, J. D.; Yoon, C. S.; Kim, J. H.; Kim, J. H., *J. Nuclear Medicine* **2002,** *43*, 347-348.

463. Lin, C. J.; Lu, Y. T.; Hsieh, C. H.; Chien, S. H., *Appl. Phys. Lett.* **2009,** *94*.

464. Oliva, F. Y.; Avalle, L. B.; Santos, E.; Camara, O. R., *J. Photochem. Photobiol. A.* **2002,** *146*, 175-188.

Chapter 11

Solid-State Dye-Sensitized Solar Cells from Polymer Templated TiO_2 Bilayer Thin Films

Abstract

We report an inexpensive method using solvent-swollen poly(methyl methacrylate) as a sacrificial template for mesoporous titanium oxide thin films with tunable meso/nano morphology. The conversion efficiency reaches 4.2 % despite using a solid state electrolyte, which circumvents the longevity issues of liquid electrolytes. The cells show a large short-circuit photocurrent density of 7.98 mA, open-circuit voltage of 0.78 V and maximum conversion efficiency of 4.2 % under air-mass 1.5 global illumination. At higher titania precursor ratios, nanodisk particles are formed, increasing light scattering and doubling the efficiency over our previous reports. The tunability of the semiconductor morphology and all solid-state nature of the cells makes the method a viable alternative to existing solar cell technology.

11.1 Introduction

Since O'Regan and Gratzel's significant breakthrough in 1991, extensive studies have been devoted to the development of dye-sensitized solar cells (DSSCs).[465-469] The cells have the potential to replace conventional silicon based solar cells due to their lower cost. They also employ, however, liquid electrolyte usually in the form of an I^-/I_3^- redox couple dissolved in an organic solvent such as acetonitrile. This configuration causes long-term practical problems including flammability, reduced stability and evaporation and/or leakage of electrolyte. Recent efforts have led to the development of solid-state electrolytes using room-temperature ionic liquids or iodide-containing polymers to achieve photovoltaic performance comparable to the record of 11% for liquid electrolyte based DSSCs.[470-472]

TiO_2 semiconductor thin film anodes serve as the electron carrier and require sensitization by an adsorbed dye that can be excited in the visible region. While most research has focused on the nature of the dye,[473-475] electrolyte and redox couple,[476-478] it is becoming evident that the TiO_2 morphology is equally important to determining cell properties.[479-482] Unlike the high-vacuum chemical vapor deposition (CVD) or solvothermal method,[483-485] polymer templating of inorganic materials approach is facile, inexpensive and is not substrate specific.[486-488] There have been several reports where the TiO_2 thin film anode of DSSCs was prepared by polymer templating.[480,489,490] Caruso and coworkers reported the synthesis of mesoporous TiO_2 beads with hexadecylamine as a template to achieve high-performance DSSCs of 7.20 % with liquid electrolyte.[16] Wang *et al*. developed a method based on

octadecylamine as a structure directing agent for a single-layer TiO_2 nanostructure.[489] Their maximum conversion efficiency was 1.5 %, comparatively low with respect to DSSCs but used a solid state electrolyte.

Although polymer swelling by organic solvents is a common phenomenon, combining this swelling with templating effects occurred only in recent years.[482,488,491-494] Caruso's group first reported use of agarose gels to template high-crystalline macroporous metal oxide monoliths.[27-28] Our group had independently been employing polymer templates to achieve a variety of titania morphologies including monoliths,[492,493] networks,[494] beads,[480,481] and thin films.[482,488] The advantage of this method is that the resultant morphology can, to some degree, be controlled through choice of polymer, its concentration, degree of swelling and/or crosslinking. Studies on optimizing the swollen polymer templating method for DSSCs, however, are limited. Indeed, the detailed mechanisms were not investigated regarding the synthetic procedures and conditions.

The photoanode of DSSCs is the electrode that collects sunlight, where the light traverses from the conductive working electrode towards the sensitized semiconductor layer. Multilayer TiO_2 thin films with increasing particle size and porosity from the bottom layer to the top layer leads to ~ 23 to 48 % higher conversion efficiency than the typical non-porous single layers of nanoparticles.[490,495-497] Stathatos *et al.* reported the synergistic effect with two distinct nanoparticle layers that increased the efficiency from 4.8 % to 6.9 %.[494] In theory, the enhancement is due to light scattering (i.e. Mie, Rayleigh and Raman scattering) by the top layer,

which enhances the absorption of red light by the surface layer and in turn light harvesting.[496] Previous studies have created a DSSC multilayer photoanode with sub-micrometer size Al_2O_3 and SiO_2 top layer to light scatter and facilitate light energy capture by the 400 nm particle-size TiO_2 bottom layer.[496] Cao and coworkers developed hierarchically structured ZnO aggregates 100 to 400 nm in size to provide both large surface area and efficient light scattering.[498-500] They achieved an impressive enhancement of conversion efficiency from 2.4 % to 5.4 % in DSSC performance compared with conventional ZnO nanoparticle thin films.[498-500] These light scattering layers based on TiO_2 and ZnO lead to higher open-circuit voltage (V_{oc}),[495,497] short-circuit current density (J_{sc})[479,490] or both.[498-501]

Herein, we describe an inexpensive, one-step method to synthesize a double-layer porous anatase thin film using methyl ethyl ketone (MEK) swollen poly(methyl methacrylate) (PMMA) as a sacrificial structure directing agent. The ratio of nanodisks to nanospheres in the composite film scales with titanium precursor concentration. The nanodisks, coupled with an improved solid state electrolyte and sensitizing dye, leads to a much higher J_{sc} and conversion efficiency over our previous reports.

11.2 Experimental Section

11.2.1 Materials

Titanium n-butoxide (Alfa Aesar) and PMMA (MW 350,000, Aldrich) were used as-purchased. Methyl ethyl ketoneT (MEK, Acros Organics) was used as solvent. 4,4'-dicarboxylate-2.2'-dipyridyl (98 %, Alfa-Aesar), ruthenium(III) chloride hydrate (35-40 % Ru, Acros) and ammonium thiocyanate (≥ 98 %, Fisher) were used as received to synthesize the N3 dye according to literature methods.[502] The polymer electrolyte components were also used as-purchased without further modification: LiI (MP Biomedicals), I_2 (>99.9 %, Alfa-Aesar), poly(ethylene oxide) (PEO, MW 5,000,000, Polysciences, Inc.).

11.2.2 Preparation of TiO_2 thin films

PMMA was first stirred in 20 mL MEK at a concentration of 10 % (w/v). After stirring at 40 °C for 4 to 8 hours, the PMMA was completely dissolved and a clear transparent solution was formed. Titanium n-butoxide [4 %, 6 % or 8 % (w/v)] was then introduced quickly, the solution sealed with parafilm and stirred at room temperature for 2 to 4 hours. The yellow transparent solution was spin-coated on F-doped SnO_2 (FTO) glass (Hartford Glass Co.) which had been first cleaned with ethanol and deionized water and sonicated and dried under an N_2 stream. The thin film was heated in a tube furnace to 450 °C at a rate of 1 °C/min, then soaked for 2 hours. Annealing removed the PMMA and resulted in the final double-layer pure-

phase anatase thin film anode. Sonication of the thin film in deionized water removed the top layer, leaving only the transparent bottom layer on the substrate.

11.2.3 Fabrication of solar cells

The N3 dye was used to sensitize the TiO_2 electrode by immersing the above thin film in a 0.5 mM dye solution in absolute ethanol for at least 48 hours. The film was then washed with ethanol and dried thoroughly. The electrolyte solution was prepared using reported methods[503] with slight modification: 0.01 M LiI, 1 mM I_2, 6 mM PEO and 0.011 mM (0.0220 g) TiO_2 (Degussa P25) dissolved in 25 mL acetonitrile. The electrolyte solution was cast drop-wise on the film at a temperature of 70°C using a hot plate. The electrolyte deposition was repeated several times and the thin film became dark red in color. Finally, another FTO glass plate sputter-coated with gold was placed on top of the surface with no applied pressure. This sandwich configuration was compressed with alligator clips to facilitate penetration of the electrolyte into the TiO_2 nanostructure. The edge area of the solar cell was then sealed with epoxy to avoid contact of the electrolyte with air, thus ensuring long-term stability. Photovoltaic performance and characterization were carried out 6 hours after preparation of the cell.

11.2.4 Instrumentational Details

Scanning electron micrographs (SEMs) were collected on a Hitachi S-2700 SEM. Samples for powder X-ray diffraction (PXRD) were obtained by manually

removing material from the FTO glass using a razor blade. A Rigaku Americas Miniflex Plus diffractometer was scanned from 10 to 80°(2θ) at a scan rate of 2°(2θ) per minute and 0.04° step size, under Cu-Kα radiation (λ = 1.5418 Å). The solid state DSSCs (SDSSCs) were illuminated using a calibrated Xe lamp (660W, Leviton Manufacturing Co.). Current-voltage (I-V) measurements were carried out with a CHI 440 electrochemical workstation. UV-Vis spectroscopic studies were performed with a Hewlett-Packard Model 8452A spectrophotometer. Tapping-mode atomic force microscope (AFM) images were collected with a PicoLE SPM instrument (Molecular Imaging Inc.) to acquire the bottom layer morphology. Thermogravimetric analysis (TGA) was performed using a TA Instruments 2050 TGA by heating from 25 to 800°C in air at a rate of 15°C/min. Fourier transform infrared (FTIR) spectroscopy of the materials was collected on a Perkin-Elmer Spectrum One spectrophotometer with KBr pellets. ^{1}H NMR spectra were collected with a Varian Oxford 600 MHz spectrometer by dissolving the sample in 700μL of deuterated choloroform with tetramethylsilane as internal standard.

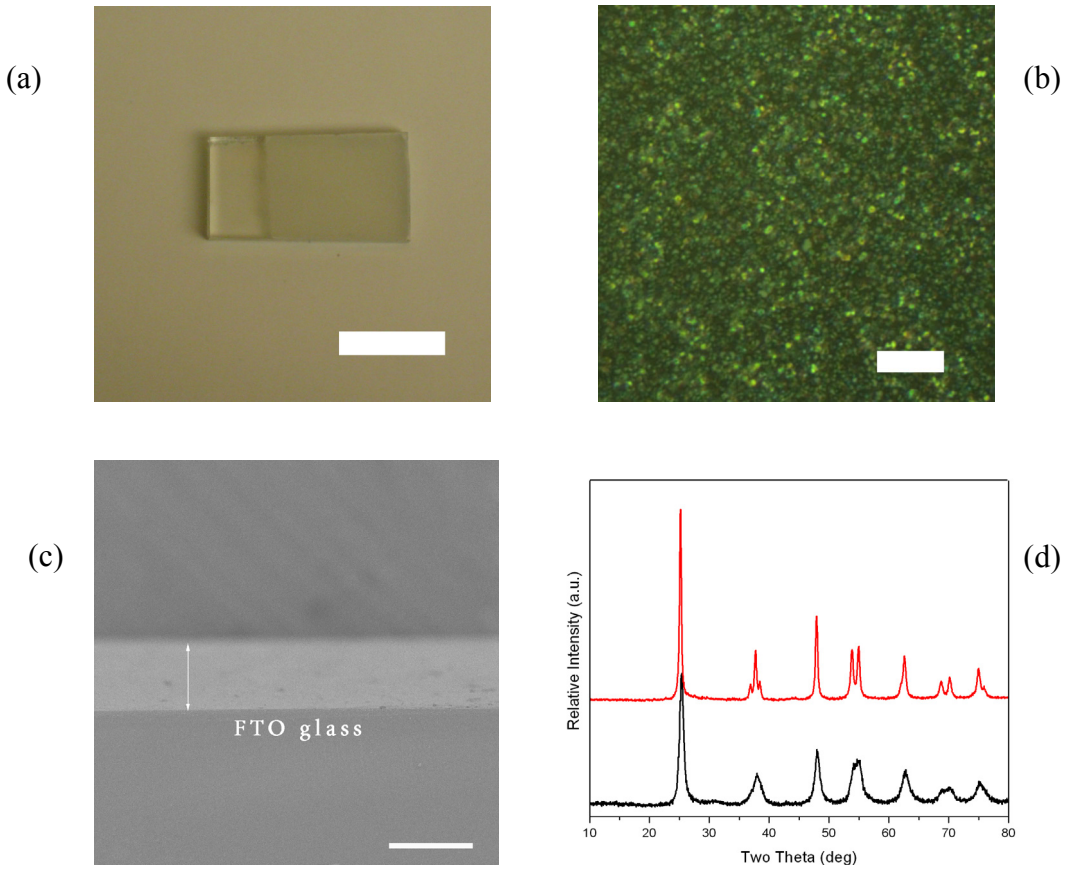

Figure 11.1 (a) Optical image of the as-synthesized $TiOB_{2B}$ thin film on FTO glass (scale bar: 1 cm); (b) Top-view optical micrograph of the $TiOB_{2B}$ thin film (scale bar: 10 µm); (c) Cross-sectional SEM of the $TiOB_{2B}$ film (scale bar: 10 µm); (d) PXRD pattern of the $TiOB_{2B}$ product calcination (red: top layer; black: bottom layer).

11.3 Results and Discussion

11.3.1 Synthesis

The optimum concentration of PMMA in MEK was determined to be 10 % (w/v). Lower ratios did not give rise to a nanodisk morphology, which facilitates light scattering (*vide infra*). Ratios higher than 15 % resulted in overly viscous mixtures and inhomogeneous films after spin coating as well as cracks occur after annealing. The powder X-ray diffraction (PXRD) pattern of both top-layer and bottom-layer thin films after annealing at 450°C for 2 hours indicated pure-phase anatase (Figure 11.1d). This form of titania has been shown to have better photoelectrochemical properties than rutile.[468] The FTIR and TGA trace of the titania before dye sensitization and pure PMMA clearly demonstrates that the annealing removed almost all of the original polymer (Figure 11.2 a,b). The ~ 10% decrease in mass of TGA for the calcined sample is likely due to phsyisorbed water in the porous thin film. The FTIR of titania after calcination further indicates only negligible amount of organics in the calcined thin film, with disapearence of bands at ~ 3000 cm^{-1} and ~ 1750 cm^{-1}, characteristic of C-H and C=O bands, respectively. Two weak, broad bands located at 3500 cm^{-1} and 700 cm^{-1} are possibly due to O-H from physisorbed water and Ti-O stretching, respectively.[504]

A possible mode of formation of the pure anatase phase thin film is self-condesation of 2-butanone (Scheme 11.1). Yatluk *et al*. reacted titanium alkoxide with carbonyl compounds to form titanoxane, while methyl ethyl ketone self-

condensed into 3,4-dimethyl-3-hexene-2-one.[505] Titanoxane is known to crystallize into anatase or rutile by annealing under air.[506,507] This pathway would explain the observed colour change of solution, from colourless to yellow after introducing the titanium precursor into 2-butanone, the intensity increasing with stirring time. ^{1}H NMR of neat titanium n-butoxide and MEK solution after introduction of the titanium precursor also support an aldol condensation reaction. Though the products provided small intergrated peak area due to the MEK solvent as well as ketone precursor, the bands (δ 0.82, m, 2H; δ 1.10, m, 2H; δ 2.25, m, 3H and δ 2.47, m, 3H) are characteristic of the self-condensed product of either β-hydroxycarbonyl or dehydrated self-condensed ketone. The pure titanium precursor (δ 0.92, m, 3H; δ 1.22, m, 2H; δ 1.39, m, 2H; and δ 1.52, m, 2H;) have no replicate peaks in the condensation product but provide comparable intergrated area, indicating the completeness of the reaction. In addition, spin coating neat titanium precursor in an attempt to obtain a TiO_2 thin film was unsuccessful; instead amorphous organic residues were present after calcination.

Scheme 11.1 Self-condensation of 2-butanone *via* titanium n-butoxide into 5-methyl-4-hepten-3-one, 1-butanol and titanoxane.

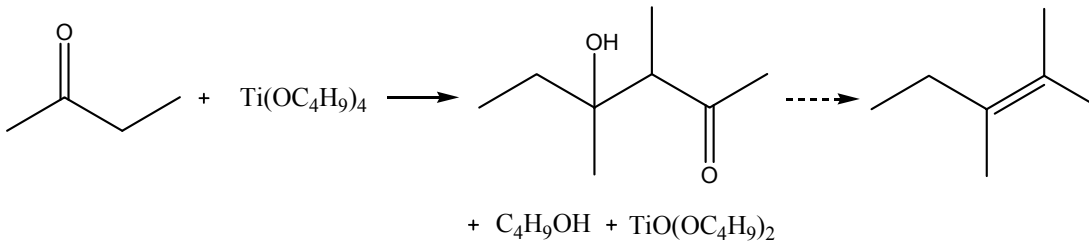

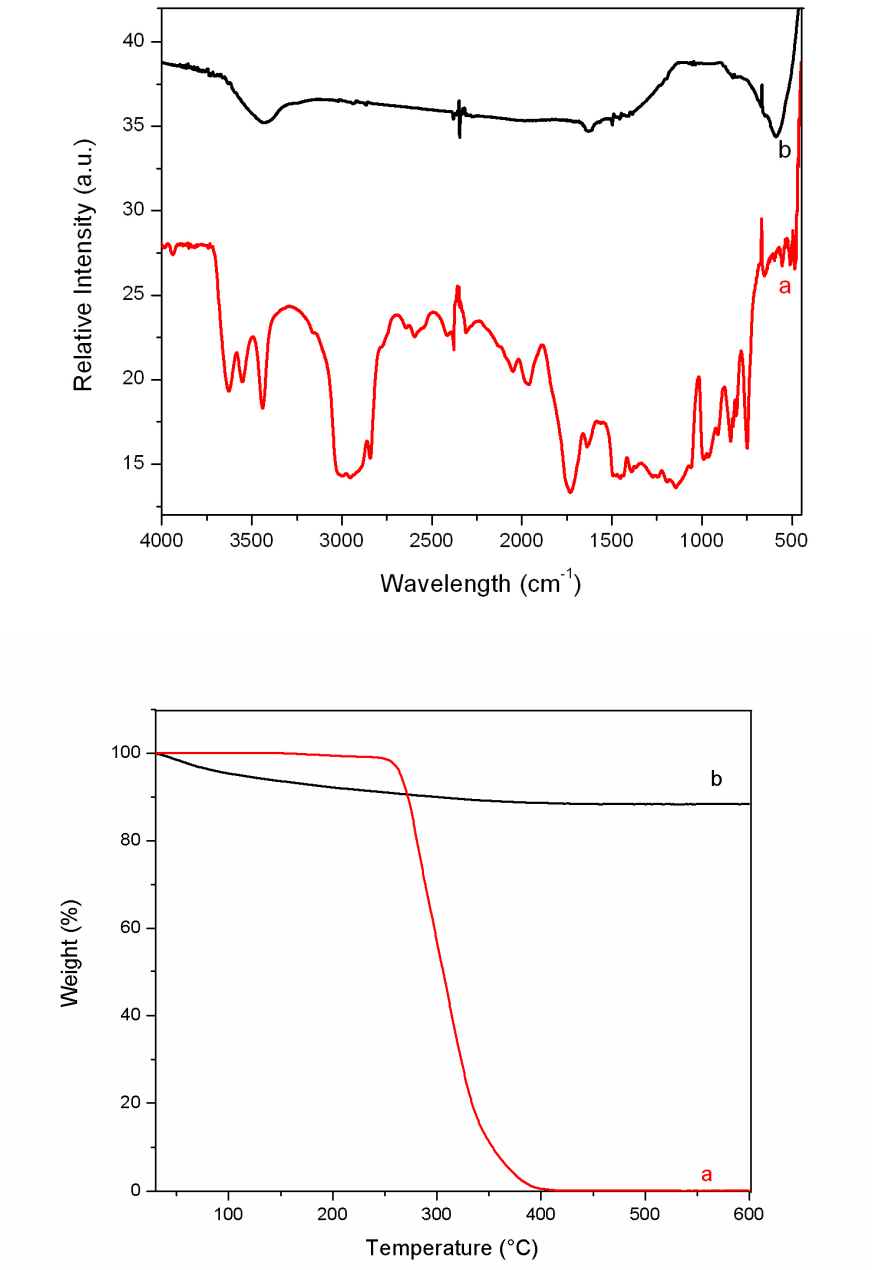

Figure 11.2 FTIR (top) and TGA curves (bottom) in the range of 25 to 800°C for: (a) pure PMMA powder; (b) powder removed from a thin film prepared from 8 % (m/v) titanium precursor and 10 % (w/v) PMMA in MEK followed by annealing at 450°C for 2 hours.

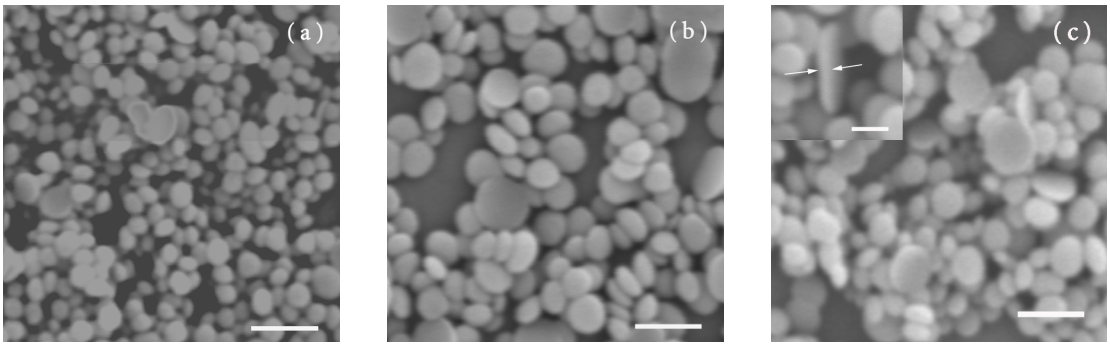

Figure 11.3 SEM images of the top $TTiOB_{2B}$ layer Tsynthesized by 10% (w/v) PMMA and: (a) 4% (w/v) titanium n-butoxide; (b) 6% (w/v) titanium n-butoxide; (c) 8% (w/v) titanium n-butoxide in MEK (scale bars: 1 μm) The inset of (c) is a closer nanodisk side image (scale bar: 500 nm).

11.3.2 Characterization

Optical images and micrographs of the thin film after sintering (Figure 11.1a,b) indicates that the surface is homogeneous and crack-free over the long range (2 cm × 1 cm). Most calcined nanoparticle TiO_2 thin films in the literature lack such long-range homogeneity and often have cracks.[508] SEM images of porous thin films made from 10 % (w/v) PMMA and 4 %, 6 %, 8 % (w/v) titania precursor are shown in Figure 3. The top layer is composed of multilayered particles and is likely responsible for enhancing the light-scattering effect. The films from higher percentages of titanium n-butoxide have the identical underlayer. A cross-sectional SEM image (Figure 11.1c) indicates that the thickness of thin film is ~ 7 μm. Though slightly thinner than the conventional P25 deposition method, this thickness is within the optimized range shown for liquid-based DSSCs cells.[465,502]

A nanodisk morphology is observed for the samples using higher concentration of titania precursor (6 %, Figure 11.3b and 8 %, Figure 11.3c). This new morphology not observed before for DSSCs is in higher concentration for the 8 % sample. The nanodisks all show a similar thickness of ~ 50 nm and a round shape with an average diamter of ~ 500 nm. The nanosphere morphology, however, is still present and mixed with the nanodisks. Though the percentage of

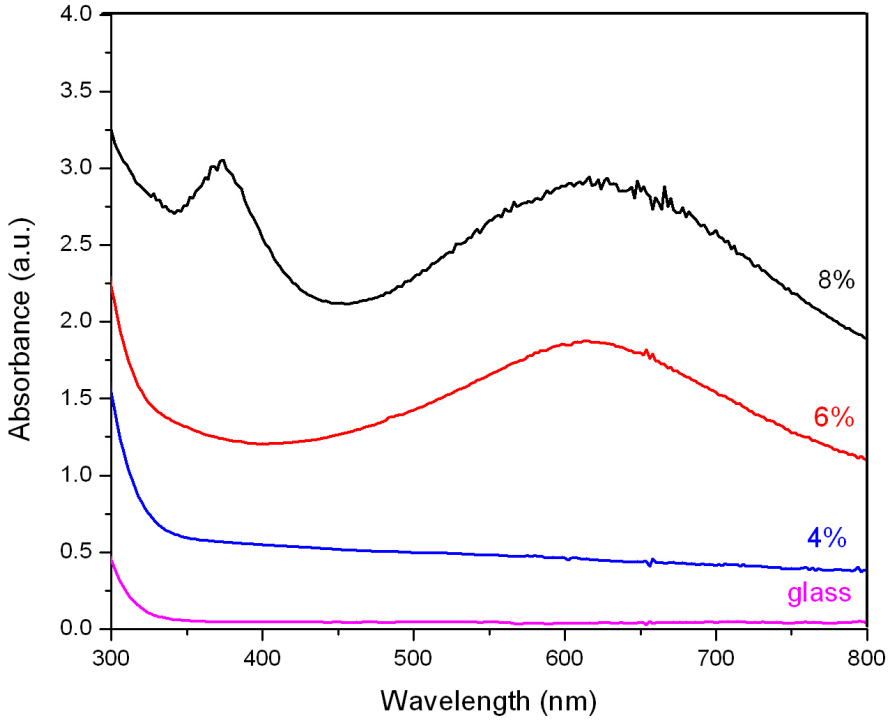

Figure 11.4 UV-Vis spectra of $TTiOB_{2B}$ thin films synthesized by 10% (w/v) PMMA and the shown percentage (w/v) of titanium n-butoxide in MEK. The spectrum for bare glass is shown for comparison.T

nanodisks increases with Ti n-butoxide concentration, the nanosphere particle size shows little change, with an average size of ~ 150 nm. One possible explanation for this new type of nanodisk morphology is that our system uses swollen PMMA with limited interior channels or pores for the growth of the metal oxide. Higher concentration of titania precursor leads to a more complete filling and replica of the original channel space of the swollen PMMA. This would also account for the lack of nanodisk formation in our previously reported experiments with 2 % to 8 % PMMA, which gave only nanospheres due to the larger swollen volume.

The nanodisks likely possess distinct optical properties versus typical nanospheres. Specifically, increased light scattering is possible, which would lead to enhanced photoelectrochemical performance.[496,497] UV-Vis spectra of the three above calcined TiO_2 thin films before dye loading are shown in Figure 4. The energy difference between the TiO_2 valence and conduction bands is well known to lie between 3.0 and 3.3 eV, corresponding to a wavelength range of 375 to 400 nm. Therefore, no absorption occurs in the visible region above 400 nm and dye sensitization is required. Increased absorption is observed in the 500 to 750 nm wavelength range as the titanium n-butoxide concentration is increased. Ferber *et al*. used Mie theory to account for the light scattering ability of the top layer of bilayer DSSCs. The surface particles enhance the photon absorption mainly in the 500 to 750 nm region, contributing to the higher photocurrent density.[508] The stronger light scattering effect of nanodisks has already been studied for WO_3, where the absorption profile from 400 to 500 nm is enhanced over that of a WO_3

nanosphere thin film. Moreover, ultrathin WO_3 nanodisks extend the absorption to the near-infrared region of 500 to 780 nm.[509, 510] Therefore, it is reasonable to ascribe our increased TiO_2 thin film red light adsorption to the presence of the nanodisk morphology. The absorption band occurring from 350 to 400 nm at 8 % Ti n-butoxide is due to an interband transition, as discussed earlier.[511]

The bottom nanostructure layer was analyzed by tapping-mode AFM (Figure 11.5). The top layer was first removed by sonication in deionized water, leaving only the transparent bottom layer on the substrate. The bottom layer image indicates an average nanoparticle size of ~ 20 nm. Average size of the nanoparticles

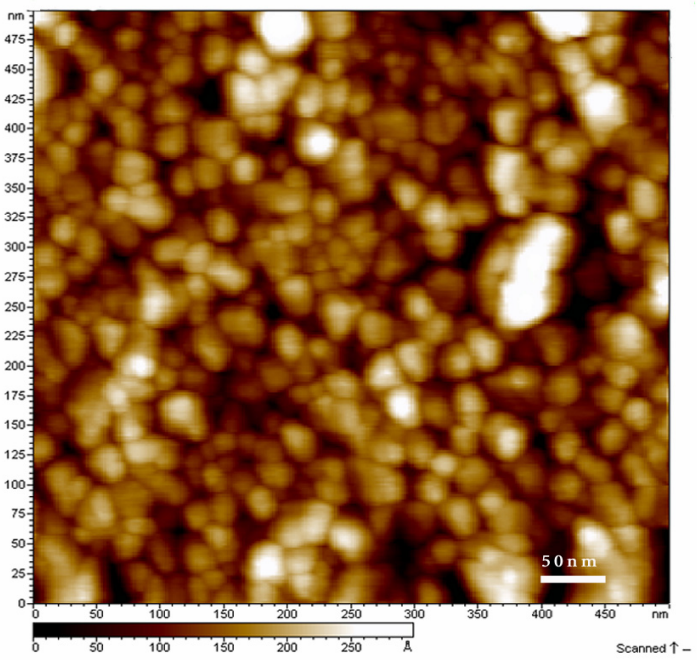

Figure 11.5 Tapping-mode AFM of the bottom layer of the porous $TTiOB_{2B}$ thin film from 8% Ti-butoxide (scale bar: 50 nm).T

in top and bottom layer as determined by the Scherrer equation [$0.9\lambda/(\beta\cos\theta)$, where λ is X-ray wavelength, β is peak width at half height and θ is Bragg angle] of the strongest powder XRD peak was 145.2 nm and 22.0 nm, respectively (Figure 11.1d, red and black). Both the top and bottom layers are therefore crystalline, with the calculated particle size matching well with the observed particle size (Figures 11.3 and 11.5). The nanocrystalline TiO_2 bottom layer with ~ 20 nm particle size increases the surface area up to 1000 fold over that of the top layer, for greater adsorption of dye.[468, 508] The more compact array of the underlayer serves to also minimize contact of the electrolyte with the anode conductive glass. This separation likely retards the back transfer of electrons, which is known to be the main pathway for electron-hole recombination and low conversion efficiency for DSSCs.[512-514]

11.3.3 Photovoltaic Performances

Considering the higher ratio of nanodisks and increased homogeneity, the optimized sample from 10 % PMMA and 8 % titanium n-butoxide was tested for I-V measurements and a sample with 4% titanium n-butoxide was tested for comparison (Figure 11.6). Under an illumination of AM 1.5 (100mW/cm^2), the

T

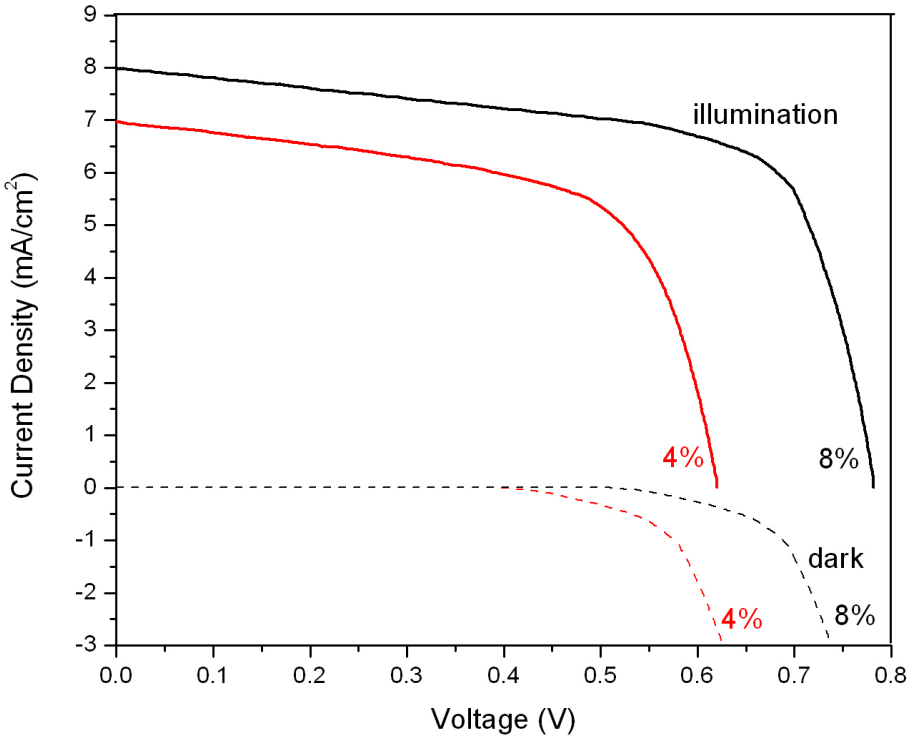

Figure 11.6. Photocurrent density-voltage curves for the $TiOB_{2B}$ thin film (solid lines) prepared from 4% (w/v) and 8 % (w/v) Ti n-butoxide, sensitized by N3 dye and coated with polymer electrolyte composed of PEO, P25, LiI and IB_{2B} under 100W/cmP^{2P} (AM 1.5 illumination). Dark conditions (dashed lines) are

nanodisk cell from 8 % titanium precursor exhibits a V_{oc} of 0.78V, J_{sc} of 7.98 mA/cm^2, fill factor of 67.2 % and the overall light-to-electricity efficiency reaches 4.2 %. The corresponding cell from 4 % titania, however, reaches a V_{oc} of 0.62V, J_{sc} of 6.99 mA/cm^2, fill factor of 61.9 % and overall conversion efficiency of only 2.7%. The cell with higher ratio titanium precusor exhibits 25% higher open-circuit voltage performance, likely due to longer electron residence time in the larger distinct particle sizes, further increasing the Fermi level of the photoelectrode semiconductor. Usually, electron trapping would also occur and lower current density. It seems the better light harvesting ability of our nanodisk morphology overcomes this disadvantage, for a slightly enhanced current. The improved current density might be also ascribed to the higher absorption of dye due to a more homogeneous structure and pore space versus that of the thin film made from 4 % titanium precursor.

Our previous report used a lower ratio of 8 % PMMA and 6 % Ti n-butoxide, a meso-tetra(4-carboxyphenyl)-porphyrin dye and electrolyte containing polyethylene glycol, KI and I_2 without P25 inorganic nanoparticle filler.[495] The I-V curve for the present report shows an increase in J_{sc} from 3.02 mA/cm^2 to 7.98 mA/cm^2 but a decrease of V_{oc} from 1.18V to 0.78V. The increase in current density is likely due to several factors: (i) the nanodisk morphology leads to more effective light scattering, thereby enhancing light harvesting and limiting the back transfer of electrons; (ii) the P25 TiO_2 nanoparticles reduces the crystallinity of the poly(ethylene oxide) (PEO) electrolyte and a more effective charge

transport;[503] (iii) the N3 dye has a stronger absorption ability in the 350 to 650 nm region, with absorbance greater than 0.5 in 0.5 mM ethanol solution. The latter two points are also backed up by the current improvement from 4 % titanium precursor compared with our previous cells. Our previous meso-tetra(4-carboxyphenyl)-porphyrin dye has weaker absorption from 350 to 500 nm. The N3 dye therefore also contributes to this effective optimization for light harvesting efficiency by an SDSSC.[495,502,514]

The open-circuit voltage arises from the difference between the Fermi level of the TiO_2 semiconductor and the electrolyte redox potential. The lower V_{oc} for the current data is likely due to the smaller particle size of the top layer, which is ~ 150 nm compared with ~ 500 nm in our earlier report.[495] The closer match of the two layers for the current report likely increases the lifetime of charge carriers and raises the Fermi level.[497] Despite the relatively slight decrease in V_{oc}, the short-circuit current density significantly increases from 3.02 mA/cm^2 to 7.98 mA/cm^2. This enhancement was achieved by the optimization of the film morphology, particle size and improvement in the dye and electrolyte, greatly increasing light-to-electricity conversion efficiency.

11.4 Conclusions

A simple swollen polymer method has been developed to fabricate an inexpensive, large area SDSSCs with a new record efficiency of 4.2 %. This test was carried out under large sensitizing area (2 cm^2) and only requires the commercially available polymer PEO to achieve efficient photovoltaic performance. Our approach could therefore potentially replace the conventional P25 deposition method. We are currently working on further optimizing the porosity and thus performance of the thin films through choice and concentration of both inorganic precursor and polymer.

11.5 References

465. Oregan, B.; Gratzel, M., *Nature* **1991,** *353*, 737-740.

466. Bach, U.; Lupo, D. C., P.; Moser, J. E.; Weissortel, F. J.; Salbeck, J.; Spreitzer, H.; Gratzel, M.;, *Nature* **1998,** *395*, 583-585.

467. Hagfeldt, A.; Gratzel, M., *Acc. Chem. Res.* **2000,** *33*, 269-277.

468. Gratzel, M., *Inorganic Chemistry* **2005,** *44*, 6841-6851.

469. Gratzel, M., *Nature* **2001,** *414*, 338-342.

470. Bai, Y.; Cao, Y. M.; Zhang, J.; Wang, M.; Li, R. Z.; Wang, P.; Zakeeruddin, S. M.; Gratzel, M., *Nature Materials* **2008,** *7*, 626-630.

471. Bai, Y.; He, G. Z., Y.; Duan, C.; Dang, D.; Meng, Q.;, *Chem. Commun.* **2006**, 1530-1533.

472. Wu, J.; Hao, S. Z., L.; Lin, J.; Huang, M.; Huang, Y.; Li, P.; Yin, S.; Sato, T.;, *J. Am. Chem. Soc.* **2008,** *130*, 11568-11569.

473. Chen, C. Y.; Chen, J. G. W., S. J.; Li, J. Y.; Wi, C. G.; Ho, K. C.;, *Angew. Chem. Int. Ed.* **2008,** *47*, 7342-7345.

474. Hardin, B. E.; Hoke, E. T. A., P. B.; Yum, J. H.; Comte, P.; Torres, T.; Frechet, J. M. J.; Nazeeruddin, M. K.; Gratzel, M.; McGehee, M. D.;, *Nat. Photonics* **2009,** *3*, 406-411.

475. Bessho, T.; Yoneda, E. Y., J. H.; Guglielmi, M.; Tavernelli, I.; Imai, H.; Rothlisberger, U.; Nazeeruddin, M. K.; Gratzel, M.;, *J. Am. Chem. Soc.* **2009,** *131*, 5930-5934.

476. Li, T. C. S., A. M.; She, C.; Farha, O. K.; Mirkin, C. A.; Marks, T. J.; Hupp, J. T., *J. Am. Chem. Soc.* **2010,** *132*, 4580-4582.

477. Cameron, P. J.; Peter, L. M. Z., S. M.; Gratzel, M.;, *Coord. Chem. Rev.* **2004,** *248*, 1447-1453.

478. Yanagida, S.; Yu, Y. M., K.;, *Acc. Chem. Res.* **2009,** *42*, 1827-1838.

479. Palomares, E.; Clifford, J. N.; Haque, S. A.; Lutz, T.; Durrant, J. R., *Journal of the American Chemical Society* **2003,** *125* (2), 475-482.

480. Chen, D. H., F.; Cheng, Y.; Caruso, R. A.;, *Adv. Mater.* **2009,** *21*, 2206-2210.

481. Chen, D. C., L.; Huang, F.; Imperia, P.; Cheng, Y.; Caruso, R. A.;, *J. Am. Chem. Soc.* **2010,** *132*, 4438-4444.

482. Fan, X. D., D. P.; St. John, J. M.; Tripathi, A.; Oliver, S. R. J.;, *App. Phys. Let.* **2008,** *92*, 193108.

483. Feng, X. S., K.; Varghese, O. K.; Paulose, M.; Latempa, T. J.; Grimes, C. A.;, *Nano Lett.* **2008,** *8*, 3781-3786.

484. Yu, H.; Quan, X. C., S.; Zhao, H.; Zhang, Y.;, *Journal of Photochemistry and Photobiology, A: Chemistry* **2008,** *200*, 301-306.

485. Boyd, D. A.; Greengard, L. B., M.; El-Naggar, M. Y.; Goodwin, D. G.;, *Nano Lett.* **2006,** *6*, 2592-2597.

486. Zhao, D.; Feng, J. H., Q.; Melosh, N.; Fredrickson, G. H.; Chmelka, B. F.; Stucky, G. D.;, *Science* **1998,** *279*, 548-552.

487. Liang, C. L., Z.; Dai, S.;, *Angew. Chem. Int. Ed.* **2008,** *47*, 3696-3717.

488. Fei, H.; Yang, Y.; Rogow, D. L.; Fan, X.; Oliver, S. R. J., *ACS Appl. Mater. Interfaces* **2010,** *2*, 974–979.

489. Wang, Y. Q.; Chen, S. G.; Tang, X. H.; Palchik, O.; Zaban, A.; Koltypin, Y.; Gedanken, A., *J. Mater. Chem.* **2001,** *11*, 521-526.

490. Tian, Z. P.; Tian, H. M.; Wang, X. Y.; Yuan, S. K.; Zhang, J. Y.; Zhang, X. B.; Yu, T.; Zou, Z. G., *Applied Physics Letters* **2009,** *94*.

491. Deshpande, A. S.; Shchukin, D. G. U., E.; Antonietti, M,; Caruso, R. A.;, *Adv. Funct. Mater.* **2005,** *25*, 239-245.

492. Zhou, J. Z., J.; Zhou, M.; Caruso, R. A.;, *Langmuir* **2006,** *22*, 3332-3336.

493. Fan, X.; Fei, H. D., D. H.; Brennan, D. P.; St, John, J. M.; Oliver, S. R. J.;, *Langmuir* **2009,** *25*, 5835-5839.

494. Brennan, D. P.; Dobley, A.; Sideris, P. J.; Oliver, S. R. J., *Langmuir* **2005,** *21*, 11994-11998.

495. Xue, M.; Zhu, G. Z., Y.; Fang, Q.; Hewitt, I. J.; Qiu, S.;, *Crystal Growth & Design* **2008,** *8*, 427-434.

496. Wang, M.-S.; Guo, G.-C.; Chen, W.; Xu, G.; Zhou, W. W.; Wu, K.; Huang, J.-S., *Angew. Chem. Int. Ed.* **2007,** *46*, 3909-3911.

497. Stathatos, E.; Lianos, P., *Advanced Materials* **2007,** *19*, 3338-3340.

498. Zhang, Q. F. C., T. P.; Russo, N.; Cao, G., *Angew. Chem. Int. Ed.* **2008,** *47*, 2402-2406.

499. Zhang, Q. F.; Chou, T. P. R., S. A.; Jenekhe, S. A.; Cao, G., *Adv. Funct. Mater.* **2008,** *18*, 1654-1660.

500. Zhang, Q.; Dandeneau, C. S.; Zhou, X.; Cao, G., *Adv. Mater.* **2009,** *21*, 4087-4108.

501. Wang, L. S. Z., J. F.; Yang, S. P., *Acta Cryst. Sect. E* **2004,** *E60*, m1484-m1486.

502. Nazeeruddin, M. K.; Kay, A.; Rodicio, I.; Humphrybaker, R.; Muller, E.; Liska, P.; Vlachopoulos, N.; Gratzel, M., *J. Am. Chem. Soc.* **1993,** *115*, 6382-6390.

503. Stergiopoulos, T.; Arabatzis, I. M.; Katsaros, G.; Falaras, P., *Nano Letters* **2002,** *2*, 1259-1261.

504. Peng, G.-W.; Chen, S.-K.; Liu, H.-S., *Appl. Spectroscopy* **1995,** *49*, 1995.

505. Yatlik, Y. G.; Sosnovskikh, V. Y.; Suvorov, A. L., *Russian J. Org. Chem.* **2004,** *40*, 763-765.

506. Haoudi, A.; Dhamelincourt, P.; Mazzah, A.; Drache, M.; Conflant, P.; Lazraq, M., *J. Mater. Chem.* **2000,** *10*, 1001-1005.

507. Gunji, T.; Nagao, Y.; Misono, T.; Abe, Y., *J. Non-crystalline Solids* **1989,** *107*, 149-154.

508. Ferber, J.; Luther, J., *Solar Energy Materials and Solar Cells* **1998,** *54* (1-4), 265-275.

509. Wolcott, A.; Kuykendall, T. R.; Chen, W.; Chen, S. W.; Zhang, J. Z., *J. Phys. Chem. B* **2006,** *110*, 25288-25296.

510. Gu, B. X.; Wang, L. M.; Ewing, R. C., *Journal of Nuclear Materials* **2000,** *278*, 64-72.

511. Yoon, M.; Seo, M.; Jeong, C.; Jang, J. H.; Jeon, K. S., *Chem. Mater.* **2005,** *17*, 6069-6079.

512. Nakade, S.; Saito, Y.; Kubo, W.; Kitamura, T.; Wada, Y.; Yanagida, S., *J. Phys. Chem. B* **2003,** *107*, 8607-8611.

513. Huang, S. Y.; Schlichthorl, G.; Nozik, A. J.; Gratzel, M.; Frank, A. J., *J. Phys. Chem. B* **1997,** *101*, 2576-2582.

514. Khairutdinov, R. F.; Hurst, J. K., *J. Phys. Chem. B* **1999,** *103*, 3682-3686.

Chapter 12

Conclusions and Future Work

12.1 Conclusions

The work in this thesis presented significant progress in the synthesis of cationic inorganic materials and cationic hybrid inorganic-organic frameworks. This class of cationic materials shows superior performance on efficient and selective anion pollutant trapping over the extensively studied LDHs and anion exchange resins. SLUG-21 has the potential to selectively trap pertechnetate in high capacity for the treatment of radioactive waste (*cf*. 292 mg/g and 602 mg/g for permanganate and perrhenate, respectively). With the formation of a new crystal structure driving the reaction, the anions would be permanently trapped. Re-use of the material would in fact be undesirable for a highly problematic radionuclide. Under the same experimental conditions, the calcined form of hydrotalcites only reaches 41 mg/g for permangnate and 134 mg/g for perrhenate. Our cationic material therefore overcomes both the low capacity and retention problems of hydrotalcites. It also displays high selectivity towards group 7 oxo-anions over other non-radioactive and non-toxic

anions such as nitrate and carbonate, even in 100-fold excess. Other advantageous properties include complete heterogeneity and no need for pre-treatment.

SLUG-26 is a rare example of a cationic layered inorganic metalate based on a 3d metal, with high thermal stability and excellent anion exchange properties. Despite the structural similarities with LDHs, SLUG-26 demonstrated five time higher adsorption capacity for permanganate with a value over 200 mg/g. In addition to metal oxo-anion exchange, the material displays flexibility for variable-length α,ω-alkanedicarboxylates, which may be a pathway to adsorbing other problematic anions and/or increasing capacity.

SLUG-32 and SLUG-33 are the first cationic lead fluoride layered compounds exhibiting high capacity anion exchange. The solvent-mediated anion exchange processes, first-time monitored by *in-situ* optical microscopy, are one of the rare examples of a MOF that completely and efficiently replaces its anionic organic linker while retaining the cationic inorganic layered structure. The post-anion exchange products were solved crystallographically and prove the survival of the cationic layers.

SLUG-31 is a rare example of using succinate as a structure co-directing agent to afford a 3-D metal oxide open-framework, in this case a high dimensional inorganic-organic hybrid. The compound was synthesized by a facile one-pot hydrothermal method, with high phase purity and yield. Owing to its inorganic nature, the material displays excellent stability, and the magnetic properties exhibit a

complex balance of ferromagnetic and antiferromagtic correlations which result in a metamagnetic transition.

SLUG-34 is a new cationic antimony oxide and entirely inorganic with 1-D Sb-O-Sb inorganic connectivity. The material can be synthesized in high yield and pure phase and was characterized by both powder and single-crystal X-ray diffraction. The strong sulfate divalent anions give rise to stability to ~ 500 °C and chemical resistance to acidic condition. Unlike the basic nature of layered double hydroxides (which are the only well-studied class of cationic inorganic materials), SLUG-34 is chemically stable in aqueous acidic conditions.

Swollen polymer templating of titania thin films is a facile and low cost method to achieve a nanospider morphology of large area and homogeneity. This material displayed both intriguing morphology and efficient application in methylene blue degradation and photoelectrochemical water splitting. The PEC photocurrent density of the nanospider working electrode was two times larger than that of the thin film with same particle size but no nanospider morphology. In future work, we aim to dope/incorporate other metal/metal oxide nanostructures into the nanochannels with controllable width throughout the film to possibly further enhance the photocatalytic efficiency.

This simple method has also been developed to fabricate an inexpensive, large area SDSSCs with a new record efficiency of 4.2 %. This test was carried out under large sensitizing area (2 cm^2) and only requires the commercially available polymer PEO to achieve efficient photovoltaic performance. Our approach could therefore

potentially replace the conventional P25 deposition method. We are currently working on further optimizing the porosity and thus performance of the thin films through choice and concentration of both inorganic precursor and polymer.

12.2 Future Work

The future work of SLUG-21 needs to focus on the kinetics of its anion exchange. Further investigation of this and related cationic extended frameworks are underway to evaluate and exploit their anion trapping properties. Variable conditions, including temperature and solvents, are necessary to be applied in anion exchange. Initial attempts with higher temperature (e.g. 50 ºC) indicate a slower rate of anion exchange for permanganate and chromate. These results possibly indicate that the anion pollutant trapping for SLUG-21 undergoes a thermodynamic mechanism. Transmission electron microscopy (TEM), atomic force microscopy (AFM) and electron diffraction for samples after anion exchange are necessary to determine if the exchange process is a solvent-mediated pathway. Synchrotron *in-situ* X-ray diffraction for anion exchange is also on going in cooperation with Professor Andrew Fogg and his research group at the University of Liverpool.

The majority of future work for SLUG-26 is to study its exfoliation behavior and possible application in catalysis. The layered feature of SLUG-26 allow the possibility to delaminate the 3-D extended structure into $[Cu_4(OH)_6]^{2+}$ positively

charged nanosheets. One of the synthetic approaches is to exchange a longer sulfonate or carboxylate ending organic linker into the interlamellar regions. Then following the conventional LDH delamination pathways, it may be possible to exfoliate the copper hydroxide nanosheets. The other part of future work for SLUG-26 is to study its anion exchange properties. The ideal scenario is to introduce non-toxic carbonate or bicarbonate into the interlamellar regions. The post-anion exchange products will have potential applications in anion trapping of environmental pollutants.

SLUG-32 and SLUG-33 can further be studied for their anion exchange properties. The single-bonding feature for interlamellar carboxylates allows the possibility to be exchanged for other anionic pollutants. The ability to exchange for varying length carboxylate chain for SLUG-6 indicates that rich intercalation chemistry is possible including the trapping of more complex species such as pharmaceutical or photoluminescent anions. Luminescent anion-intercalated cationic layered inorganic materials have potential applications as ion sensors.

SLUG-34 opens up the possibility for synthesis of other non-LDH type cationic inorganic materials with potential host-guest applications based on their extraframework anions. Sulfate as anionic template can be used for other metals, including lower *p*-block metals, *f*-block metals and *d*-block metals. Tuning to a higher pH for synthetic hydrothermal solution is possible to give bisulfate, which may have lower affinity to the cationic host and in turn higher exchangeability. SLUG-34 can also be applied for anion exchange with elevated temperature and different solvents.

Future work for polymer templating semiconductor thin films is to employ both nanospider and PMMA-templated titania to fabricate a multilayer TiO_2 photoanode for dye-sensitized solar cells. A nanospider TiO_2 thin film as the bottom layer for efficient dye absorption with small particle size ~15 nm, while a PMMA-templated TiO_2 top layer serveing as a light scattering layer to facilitate light harvesting by bottom layer. This assembly scheme might contribute to higher efficiency in solar cells. Liquid electrolyte as well as laser ablation could further enhance its photovoltaic performance. Another direction is to fabricate compact-layer TiO_2 thin film and filling the channels of nanospider films, such as TiO_2 nanowire and/or nanorod growth by hydrothermal synthesis.

Appendix

Solvothermal Synthesis

sample	date	compound	ratio(n)	wt. Used(g)	actual ratio	T ©C	time(hrs)
HF001	12.10.07	CrF3	1	0.3	0.991797413	150	72
		HNO3	2	0.185	1.05808254		
		H2O	200	8	160		
HF002	12.10.07	CrF3	1	0.3	0.991797413	175	72
		HNO3	2	0.185	1.05808254		
		H2O	200	8	160		
HF003	12.10.07	CrF3	1	0.3	0.991797413	200	72
		HNO3	2	0.185	1.05808254		
		H2O	200	8	160		
HF004	12.11.07	CrF3	1	0.402	1.329008533	200	72
		EDSA	2	0.84	1.591318612		
		H2O	200	8	160		
HF005	12.11.07	CrF3	1	0.402	1.329008533	150	72
		EDSA	2	0.84	1.591318612		
		H2O	200	8	160		
HF006	12.10.07	CrF3	1	0.3	0.991797413	200	72
		HNO3	3	0.52	2.974069841		
		H2O	200	8	160		
HF007	12.13.07	CrF3	1	0.3	0.991797413	200	72
		HNO3	4	0.7	4.003555556		
		H2O	200	8	160		
HF008	12.20.07	CrF3	1	0.3	0.991797413	200	72
		HNO3	3	0.52	2.974069841		
		1,3-Benzenedisu	1	0.78	0.996629787		
		H2O	200	10	200		
HF009	12.20.07	CrF3	1	0.3	0.991797413	200	72
		HNO3	4	0.7	4.003555556		
		1,3-Benzenedisu	1	0.78	0.996629787		
		H2O	200	10	200		

HF010	12.20.07	CrF3	1	0.3	0.991797413	200	72
		HNO3	5	0.87	4.975847619		
		1,3-Benzenedisu	1	0.78	0.996629787		
		H2O	200	10	200		
HF011	12.20.07	CrF3	1	0.3	0.991797413	200	72
		HNO3	6	1.05	6.005333333		
		1,3-Benzenedisu	1	0.78	0.996629787		
		H2O	200	10	200		
HF012	12.20.07	CrF3	0.5	0.15	0.495898706	200	72
		HNO3	4	0.87	4.975847619		
		1,3-Benzenedisu	1	0.78	0.996629787		
		H2O	200	10	200		
HF013	12.20.07	CrF3	0.75	0.22	0.727318103	200	72
		HNO3	4	0.87	4.975847619		
		1,3-Benzenedisu	1	0.78	0.996629787		
		H2O	200	10	200		
HF014	12.20.07	CrF3	1	0.3	0.991797413	200	72
		HNO3	4.5	0.78	4.461104762		
		1,3-Benzenedisu	1	0.78	0.996629787		
		H2O	200	10	200		
HF015	12.20.07	CrF3	1.25	0.39	1.289336636	200	72
		HNO3	4	0.87	4.975847619		
		1,3-Benzenedisu	1	0.78	0.996629787		
		H2O	200	10	200		
HF016	01.18.08	CrF3	1	0.3	0.991797413	200	72
		HNO3	5	0.87	4.975847619		
		1,3-Benzenedisu	1	0.78	0.996629787		
		H2O	200	10	200		
HF017	01.18.08	CrF3	1	0.3	0.991797413	200	72
		HNO3	6	1.05	6.005333333		
		1,3-Benzenedisu	1	0.78	0.996629787		
		H2O	200	10	200		
HF018	01.18.08	CrF3	1	0.39	1.289336636	200	72
		HNO3	7	1.22	6.977625397		
		1,3-Benzenedisu	1	0.78	0.996629787		
		H2O	200	10	200		
HF019	01.24.08	CrF3	2	0.72	2.38031379	150	72
		HClO4	1	0.2	0.717054726		
		H2O	200	8	160		

HF020	01.24.08	CrF3	1	0.36	1.190156895	150	72
		HClO4	1	0.25	0.896318408		
		H2O	200	8	160		
HF021	01.24.08	CrF3	1	0.36	1.190156895	150	72
		HClO4	2	0.5	1.792636816		
		H2O	200	8	160		
HF022	01.31.08	Cr(NO3)hydrate	1	0.89	1.00214	175	72
		EDSA	1	0.43	1.018254469		
		HF(40%)	1	0.07	1.5764		
		H2O	250	10	250		
HF023	01.31.08	Cr(NO3)hydrate	1	0.88	0.99088	175	72
		EDSA	1.5	0.63	1.491861199		
		HF(40%)	1	0.07	1.5764		
		H2O	250	10	250		
HF024	01.31.08	Cr(NO3)hydrate	1	0.88	0.99088	175	72
		succinic acid	1	0.26	0.99240678		
		HF(40%)	1	0.07	1.5764		
		H2O	250	10	250		
HF025	01.31.08	Cr(NO3)hydrate	1	0.88	0.99088	175	72
		succinic acid	1	0.26	0.99240678		
		HF(40%)	1	0.07	1.5764		
		H2O	250	10	250		
HF026	01.31.08	Cr(NO3)hydrate	1	0.88	0.99088	175	72
		succinic acid	1	0.26	0.99240678		
		HF(40%)	1	0.07	1.5764		
		H2O	250	10	250		
HF027	02.05.08	Cr(NO3)hydrate	1	0.88	0.99088	175	72
		succinic acid	1	0.26	0.99240678		
		H2O	250	10	250		
HF028	02.05.08	Cr(NO3)hydrate	1	0.88	0.99088	175	72
		succinic acid	2.5	0.65	2.481016949		
		H2O	250	10	250		
HF029	02.05.08	Cr(NO3)hydrate	1	0.88	0.99088	175	72
		succinic acid	3	0.63	2.404677966		
		H2O	250	10	250		
HF030	02.05.08	Cr(NO3)hydrate	1	0.89	1.00214	175	72
		succinic acid	2	0.52	1.984813559		
		HF(40%)	1	0.07	1.5764		
		H2O	250	10	250		

HF031	02.05.08	Cr(NO3)hydrate	1	0.88	0.99088	200	72
		succinic acid	2	0.52	1.984813559		
		HF(40%)	1	0.07	1.5764		
		H2O	250	10	250		
HF032	02.05.08	Cr(NO3)hydrate	1	0.88	0.99088	175	72
		succinic acid	2	0.52	1.984813559		
		H2O	250	10	250		
HF033	02.05.08	Cr(NO3)hydrate	1	0.88	0.99088	200	72
		succinic acid	2	0.52	1.984813559		
		H2O	250	10	250		
HF034	02.05.08	Cr(NO3)hydrate	1	0.88	0.99088	175	72
		toluenesulfonate	2	0.76	1.990139535		
		H2O	250	10	250		
HF035	03.04.08	Cr(NO3)hydrate	1	0.88	0.99088	200	72
		toluenesulfonate	2	0.76	1.990139535		
		H2O	250	10	250		
HF036	03.04.08	Cr(NO3)hydrate	1	0.88	0.99088	175	72
		toluenesulfonate	2	0.76	1.990139535		
		HF(40%)	1	0.07	1.5764		
		H2O	250	10	250		
HF037	03.04.08	Cr(NO3)hydrate	1	0.88	0.99088	200	72
		toluenesulfonate	2	0.76	1.990139535		
		HF(40%)	1	0.07	1.5764		
		H2O	250	10	250		
HF038	03.17.08	Cr(NO3)hydrate	1	0.88	0.99088	200	72
		1,3-benzenedisul	1	0.63	1.006212766		
		HNO3	4	0.56	4.003555556		
		H2O	250	10	250		
HF039	03.17.08	Cr(NO3)hydrate	1	0.88	0.99088	200	72
		1,3-benzenedisul	1	0.63	1.006212766		
		HNO3	5	0.7	5.004444444		
		H2O	250	10	250		
HF040	03.17.08	Cr(NO3)hydrate	1	0.88	0.99088	200	72
		1,3-benzenedisul	1.5	0.94	1.501333333		
		HNO3	4	0.56	4.003555556		
		H2O	250	10	250		
HF041	03.17.08	Cr(NO3)hydrate	1	0.88	0.99088	200	72
		1,3-benzenedisul	1.5	0.93	1.485361702		

		HNO3	5	0.7	5.004444444		
		H2O	250	10	250		
HF042	03.20.08	Cr(NO3)hydrate	1	0.88	0.99088	200	72
		1,3-benzenedisul	1	0.61	0.974269504		
		HF	2	0.12	2.7024		
		HNO3	3	0.42	3.002666667		
		H2O	250	10	250		
HF043	03.20.08	Cr(NO3)hydrate	1	0.88	0.99088	200	72
		1,3-benzenedisul	1	0.62	0.990241135		
		HF	3	0.2	4.504		
		HNO3	2	0.27	1.930285714		
		H2O	250	10	250		
HF044	03.26.08	MnF2	1	0.21	1.017688832	175	72
		EDSA	1	0.42	0.994574132		
		H2O	200	8	200		
HF045	03.26.08	MnF2	1	0.402	1.948147192	175	72
		EDSA	0.5	0.21	0.497287066		
		H2O	200	8	200		
HF046	03.26.08	MnF2	1	0.402	1.948147192	175	72
		EDSA	2	0.84	1.989148265		
		H2O	200	8	200		
HF047	04.01.08	MnF2	1	0.21	1.017688832	150	72
		terephthalic acid	2	0.74	2.007807229		
		n-butanol		4	#DIV/0!		
		H2O	100	4	100		
HF048	04.01.08	MnF2	1	0.21	1.017688832	150	72
		terephthalic acid	1	0.74	2.007807229		
		n-butanol		4	#DIV/0!		
		H2O	100	4	100		
HF049	04.01.08	MnF2	1	0.21	1.017688832	150	72
		terephthalic acid	1	0.37	1.003903614		
		H2O	200	8	200		
HF050	04.04.08	NiF2 hydrate	1	0.37	0.987894955	150	72
		EDSA	1	0.42	0.994574132		
		cyclohexanol		4	#DIV/0!		
		H2O	100	4	100		
HF051	04.04.08	NiF2 hydrate	1	0.21	0.560697137	150	72
		EDSA	1	0.74	1.7523449		
		cyclohexanol		4	#DIV/0!		

		H2O	100	4	100		
HF052	04.04.08	NiF2 hydrate	1	0.37	0.987894955	175	72
		EDSA	1	0.63	1.491861199		
		H2O	200	8	200		
HF053	04.08.08	Cr(NO3)hydrate	1	0.89	1.00214	150	72
		succinic acid	2	0.52	1.984813559		
		toluene		4	#DIV/0!		
		H2O	100	4	100		
HF054	04.08.08	MnF2	1	0.21	1.017688832	200	72
		terephthalic acid	1	0.37	1.003903614		
		cyclohexanol		4	#DIV/0!		
		H2O	100	4	100		
HF055	04.08.08	MnF2	1	0.21	1.017688832	200	72
		terephthalic acid	1	0.37	1.003903614		
		cyclohexanol		4	#DIV/0!		
		H2O	100	4	100		
HF056	04.11.08	MnF2	1	0.21	1.017688832	200	72
		terephthalic acid	1	0.37	1.003903614		
		H2O	200	8	200		
HF057	04.11.08	MnF2	1	0.21	1.017688832	175	72
		terephthalic acid	1	0.37	1.003903614		
		H2O	200	8	200		
HF058	04.11.08	MnF2	1	0.21	1.017688832	200	72
		terephthalic acid	0.5	0.19	0.515518072		
		H2O	200	8	200		
HF059	04.11.08	MnF2	1	0.21	1.017688832	175	72
		terephthalic acid	0.5	0.19	0.515518072		
		H2O	200	8	200		
HF060	04.15.08	MnF2	1	0.21	1.017688832	200	72
		EDSA	0.25	0.11	0.260483701		
		HClO4	0.75	0.17	0.761870647		
		H2O	200	8	200		
HF061	04.15.08	MnF2	1	0.21	1.017688832	200	72
		EDSA	0.125	0.05	0.118401682		
		HClO4	0.375	0.08	0.358527363		
		H2O	200	8	200		
HF062	04.15.08	MnF2	1	0.21	1.017688832	150	72
		terephthalic acid	1	0.37	1.003903614		

		n-butanol		3.5	#DIV/0!		
		H2O	100	4	100		
HF063	04.24.08	MnF2	1	0.21	1.017688832	200	72
		POPSO	0.5	0.44	0.497429719		
		HClO4	0.5	0.12	0.537791045		
		H2O	200	8	200		
HF064	04.24.08	MnF2	1	0.21	1.017688832	200	72
		POPSO	0.5	0.44	0.497429719		
		HClO4	1.5	0.42	1.882268657		
		H2O	200	8	200		
HF065	04.24.08	MnF2	1	0.21	1.017688832	200	72
		POPSO	0.5	0.44	0.497429719		
		NaOH	1	0.08	0.9008		
		H2O	200	8	200		
HF066	04.24.08	MnF2	1	0.21	1.017688832	200	72
		POPSO	1	0.88	0.994859438		
		NaOH	2	0.16	1.8016		
		H2O	200	8	200		
HF067	04.24.08	MnF2	1	0.21	1.017688832	200	72
		POPSO	1	0.88	0.994859438		
		NaOH	3	0.24	2.7024		
		H2O	200	8	200		
HF068	04.28.08	MnF2	1	0.21	1.017688832	200	72
		EDSA	0.5	0.21	0.497287066		
		NaOH	1	0.08	0.9008		
		H2O	200	8	200		
HF069	04.28.08	MnF2	1	0.21	1.017688832	200	72
		EDSA	0.5	0.21	0.497287066		
		cyclohexanol		4	#DIV/0!		
		NaOH	1	0.08	0.9008		
		H2O	100	4	100		
HF070	04.28.08	MnF2	1	0.21	1.017688832	175	72
		EDSA	0.5	0.21	0.497287066		
		NaOH	1	0.08	0.9008		
		H2O	200	8	200		
HF071	04.28.08	MnF2	1	0.21	1.017688832	175	72
		EDSA	0.5	0.21	0.497287066		
		cyclohexanol		4	#DIV/0!		
		NaOH	1	0.08	0.9008		
		H2O	100	4	100		

HF072	05.05.08	Mc(Ac)2hydrate	1	0.54	1.017725333	200	72
		EDSA	1	0.42	0.994574132		
		cyclohexanol		4	#DIV/0!		
		NaOH	1.5	0.13	1.4638		
		H2O	100	4	100		
HF073	05.05.08	Mc(Ac)2hydrate	1	0.54	1.017725333	200	72
		EDSA	1	0.42	0.994574132		
		cyclohexanol		4	#DIV/0!		
		NaOH	2	0.18	2.0268		
		H2O	100	4	100		
HF074	05.05.08	Mc(Ac)2hydrate	1	0.54	1.017725333	200	72
		EDSA	1	0.42	0.994574132		
		cyclohexanol		4	#DIV/0!		
		NaOH	3	0.27	3.0402		
		H2O	100	4	100		
HF075	05.05.08	Mc(Ac)2hydrate	1	0.54	1.017725333	200	72
		EDSA	1	0.42	0.994574132		
		cyclohexanol		4	#DIV/0!		
		NaOH	4	0.36	4.0536		
		H2O	100	4	100		
HF076	05.05.08	Mc(Ac)2hydrate	1	0.54	1.017725333	200	72
		EDSA	1	0.42	0.994574132		
		cyclohexanol		4	#DIV/0!		
		NaOH	5	0.44	4.9544		
		H2O	100	4	100		
HF077	05.05.08	Mc(Ac)2hydrate	1	0.54	1.017725333	200	72
		EDSA	1.5	0.63	1.491861199		
		cyclohexanol		4	#DIV/0!		
		NaOH	6	0.54	6.0804		
		H2O	100	4	100		
HF078	05.21.08	MnF2	1	0.21	1.017688832	200	72
		terephthalic acid	1	0.37	1.003903614		
		cyclohexanol		4	#DIV/0!		
		NaOH	4	0.35	3.941		
		H2O	100	4	100		
HF079	05.21.08	MnF2	1	0.21	1.017688832	200	72
		terephthalic acid	1	0.37	1.003903614		
		cyclohexanol		4	#DIV/0!		
		NaOH	6	0.53	5.9678		
		H2O	100	4	100		

HF080	05.25.08	MnF2	1	0.21	1.017688832	150	72
		citric acid	1	0.43	1.003897989		
		cyclohexanol		4	#DIV/0!		
		NaOH	3	0.27	3.0402		
		H2O	100	4	100		
HF081	05.25.08	MnF2	1	0.21	1.017688832	175	72
		citric acid	1	0.43	1.003897989		
		cyclohexanol		4	#DIV/0!		
		NaOH	3	0.27	3.0402		
		H2O	100	4	100		
HF082	05.25.08	MnF2	1	0.21	1.017688832	200	72
		citric acid	1	0.43	1.003897989		
		cyclohexanol		4	#DIV/0!		
		NaOH	3	0.27	3.0402		
		H2O	100	4	100		
HF083	05.28.08	NiF2 hydrate	1	0.37	0.987894955	175	72
		HNO3	2	0.28	2.001777778		
		H2O	200	8	200		
HF084	05.28.08	NiF2 hydrate	1	0.21	0.560697137	175	72
		HNO3	2	0.88	6.291301587		
		NaOH	2	0.18	2.0268		
		H2O	200	8	200		
HF085	05.28.08	NiF2 hydrate	1	0.21	0.560697137	175	72
		HNO3	2	0.88	6.291301587		
		NaOH	4	0.36	4.0536		
		H2O	200	8	200		
HF086	05.28.08	NiF2 hydrate	1	0.21	0.560697137	175	72
		HNO3	2	0.88	6.291301587		
		NaOH	6	0.53	5.9678		
		H2O	200	8	200		
HF087	06.03.08	NiF2 hydrate	1	0.37	0.987894955	150	72
		PDSNa	1	0.55	0.998066076		
		H2O	200	8	200		
HF088	06.03.08	NiF2 hydrate	1	0.37	0.987894955	150	72
		PDSNa	1	0.55	0.998066076		
		HClO4	1	0.22	0.985950249		
		H2O	200	8	200		
HF089	06.03.08	NiF2 hydrate	1	0.37	0.987894955	150	72
		PDSNa	1	0.55	0.998066076		
		HClO4	2	0.45	2.016716418		

		H2O	200	8	200		
HF090	06.03.08	NiF2 hydrate	1	0.37	0.987894955	150	72
		PDSNa	1	0.55	0.998066076		
		HClO4	3	0.67	3.002666667		
		H2O	200	8	200		
HF091	06.03.08	NiF2 hydrate	1	0.37	0.987894955	150	72
		Sb(Ac)3	1	0.67	1.002884679		
		EDSA	0.5	0.21	0.497287066		
		H2O	200	8	200		
HF092	06.10.08	NiF2 hydrate	1	0.37	0.987894955	150	72
		Sb(Ac)3	1	0.67	1.002884679		
		EDSA	1	0.42	0.994574132		
		H2O	200	8	200		
HF093	06.10.08	NiF2 hydrate	1	0.37	0.987894955	150	72
		Sb(Ac)3	1	0.67	1.002884679		
		NaOH	1	0.08	0.9008		
		EDSA	0.5	0.21	0.497287066		
		H2O	200	8	200		
HF094	06.10.08	NiF2 hydrate	1	0.37	0.987894955	150	72
		Sb(Ac)3	1	0.67	1.002884679		
		NaOH	1	0.08	0.9008		
		EDSA	1	0.42	0.994574132		
		H2O	200	8	200		
HF095	06.10.08	NiF2 hydrate	1	0.37	0.987894955	150	72
		Sb(Ac)3	1	0.67	1.002884679		
		NaOH	2	0.17	1.9142		
		EDSA	0.5	0.21	0.497287066		
		H2O	200	8	200		
HF096	06.10.08	NiF2 hydrate	1	0.37	0.987894955	150	72
		Sb(Ac)3	1	0.67	1.002884679		
		NaOH	2	0.18	2.0268		
		EDSA	1	0.42	0.994574132		
		H2O	200	8	200		
HF097	06.13.08	NiF2 hydrate	1	0.37	0.987894955	150	72
		Sb(Ac)3	1	0.67	1.002884679		
		EDSA	0.25	0.1	0.236803365		
		HClO4	1.75	0.4	1.792636816		
		H2O	200	8	200		
HF098	06.13.08	NiF2 hydrate	1	0.37	0.987894955	150	72
		Sb(Ac)3	1	0.67	1.002884679		

		EDSA	0.25	0.1	0.236803365		
		HClO4	2	0.45	2.016716418		
		H2O	200	8	200		
HF099	06.13.08	NiF2 hydrate	1	0.37	0.987894955	150	72
		Sb(Ac)3	1	0.67	1.002884679		
		EDSA	0.25	0.1	0.236803365		
		HClO4	2.25	0.5	2.24079602		
		H2O	200	8	200		
HF100	06.24.08	NiF2 hydrate	0	0.37	0.987894955	150	72
		Sb(Ac)3	1	0.67	1.002884679		
		EDSA	1	0.42	0.994574132		
		H2O	200	8	200		
HF101	06.24.08	NiF2 hydrate	0.25	0.09	0.240298773	150	72
		Sb(Ac)3	0.75	0.5	0.748421402		
		EDSA	1	0.42	0.994574132		
		H2O	200	8	200		
HF102	06.24.08	NiF2 hydrate	0.75	0.28	0.747596182	150	72
		Sb(Ac)3	0.25	0.17	0.254463277		
		EDSA	1	0.42	0.994574132		
		H2O	200	8	200		
HF105	07.02.08	Mc(Ac)2hydrate	1	0.67	1.010186626	150	72
		citric acid	1	0.52	0.987334141		
		Et3N	1	0.28	1.0256135		
		H2O	200	10	200		
HF106	07.02.08	Mc(Ac)2hydrate	1	0.67	1.010186626	150	72
		EDSA	1	0.52	0.985101998		
		Et3N	2.5	0.68	2.490775643		
		H2O	200	10	200		
HF107	07.02.08	Mc(Ac)2hydrate	1	0.67	1.010186626	150	72
		citric acid	1	0.52	0.987334141		
		Et3N	2.5	0.68	2.490775643		
		H2O	200	10	200		
HF108	07.02.08	Mc(Ac)2hydrate	1	0.67	1.010186626	150	72
		EDSA	1	0.52	0.985101998		
		Et3N	1	0.28	1.0256135		
		H2O	200	10	200		
HF109	08.04.08	NiO	1	0.17	1.025143928	150	72
		HNO3	3	0.42	3.002666667		
		ethanol		5.1	#DIV/0!		
		Et3N	1	0.21	0.961512656		

		H2O	50	2	50		
HF110	08.04.08	NiO	1	0.17	1.025143928	175	72
		HNO3	3	0.42	3.002666667		
		ethanol		5.1	#DIV/0!		
		Et3N	0	0	0		
		H2O	50	2	50		
HF111	08.04.08	NiO	1	0.17	1.025143928	150	72
		HNO3	3	0.42	3.002666667		
		ethanol		5.1	#DIV/0!		
		Et3N	1	0.21	0.961512656		
		H2O	50	2	50		
HF112	08.04.08	NiO	1	0.17	1.025143928	175	72
		HNO3	3	0.42	3.002666667		
		ethanol		5.1	#DIV/0!		
		Et3N	0	0	0		
		H2O	50	2	50		
HF113	10.03.08	NiO	1	0.17	1.025143928	100	72
		HNO3	1	0.14	1.000888889		
		H2O	200	8	200		
HF114	10.03.08	NiO	1	0.17	1.025143928	100	72
		HNO3	2	0.28	2.001777778		
		H2O	200	8	200		
HF115	10.03.08	NiO	1	0.17	1.025143928	100	72
		HNO3	5	0.7	5.004444444		
		H2O	200	8	200		
HF116	10.03.08	NiF2 hydrate	1	0.37	0.987894955	100	72
		HNO3	1	0.14	1.000888889		
		H2O	200	8	200		
HF117	10.03.08	NiF2 hydrate	1	0.37	0.987894955	100	72
		HNO3	2	0.28	2.001777778		
		H2O	200	8	200		
HF118	10.03.08	NiF2 hydrate	1	0.37	0.987894955	100	72
		HNO3	5	0.7	5.004444444		
		H2O	200	8	200		
HF119	10.16.08	NiF2 hydrate	1	0.37	0.987894955	100	72
		HNO3	2	0.28	2.001777778		
		pyridine	200	8	200		
HF120	10.16.08	NiF2 hydrate	1	0.37	0.987894955	100	72

		HNO3	5	0.7	5.004444444		
		pyridine	200	8	200		
HF121	10.22.08	Mc(Ac)2hydrate	1	1.32	0.995109214	200	72
		EDS disodium sa	1	1.3	1.000034159		
		NaOH	2	0.44	1.98176		
		H2O	80	8	80		
HF122	10.22.08	Mc(Ac)2hydrate	1	1.32	0.995109214	200	72
		EDS disodium sa	1	1.3	1.000034159		
		NaOH	0	0	0		
		H2O	80	8	80		
HF123	10.22.08	Mc(Ac)2hydrate	1	1.32	0.995109214	200	72
		EDS disodium sa	1	1.3	1.000034159		
		HNO3	2	0.7	2.001777778		
		H2O	80	8	80		
HF124	10.23.08	NiO	1	0.39	0.978480129	200	72
		EDS disodium sa	1	1.3	1.040035525		
		NaOH	2	0.43	2.0141888		
		H2O	52	5	52		
HF125	10.23.08	NiO	1	0.39	0.978480129	200	72
		EDS disodium sa	1	1.3	1.040035525		
		H2O	52	5	52		
HF126	10.23.08	NiO	1	0.39	0.978480129	200	72
		EDS disodium sa	1	1.3	1.040035525		
		HNO3	2	0.7	2.081848889		
		H2O	52	5	52		
HF127	10.28.08	NiO	1	0.39	0.978480129	200	72
		EDS disodium sa	1	1.02	1.004804038		
		H2O	52	5	52		
HF128	10.28.08	NiF2 hydrate	1	0.9	0.999642895	200	72
		EDS disodium sa	1	1.02	1.004804038		
		H2O	52	5	52		
HF129	10.28.08	NiF2 hydrate	1	0.9	0.999642895	200	72
		EDS disodium sa	1	1.3	1.040035525		
		HNO3	2	0.7	2.081848889		
		H2O	52	5	52		
HF130	10.28.08	NiF2 hydrate	1	0.9	0.999642895	200	72
		EDS disodium sa	1	1.3	1.040035525		
		HNO3	2	0.7	2.081848889		
		H2O	52	5	52		

HF131	10.29.08	Cr(NO3)3 hydrat	0.75	0.67	0.75442	150	72
		K2Cr2O7	1	0.65	0.995173023		
		H2O	200	8	200		
HF132	10.29.08	Cr(NO3)3 hydrat	1	2.13	0.99772608	200	72
		EDSA	1	1.02	1.004804038		
		NaOH	2	0.43	2.0141888		
		H2O	52	5	52		
HF133	10.29.08	CrF3	1	0.58	0.997086999	200	72
		EDSA	1	1.02	1.004804038		
		NaOH	2	0.43	2.0141888		
		H2O	52	5	52		
HF134	11.03.08	NiF2 hydrate	1	0.9	0.999642895	175	72
		EDS disodium sa	1	1.3	1.040035525		
		HNO3	2	0.7	2.081848889		
		H2O	52	5	52		
HF135	11.03.08	NiO	1	0.4	1.003434998	200	72
		EDS disodium sa	1	1.3	1.040035525		
		NaOH	2	0.43	2.0141888		
		H2O	52	5	52		
HF136	11.07.08	NiO	1	0.4	1.003434998	200	72
		2,6-NDSNa	1	1.77	0.998911229		
		HNO3	2	0.67	1.992626794		
		H2O	52	5	52		
HF137	11.07.08	NiF2 hydrate	1	0.9	0.999642895	200	72
		2,6-NDSNa	1	1.77	0.998911229		
		HNO3	2	0.67	1.992626794		
		H2O	52	5	52		
HF138	11.10.08	NiF2 hydrate	1	0.9	0.925150276	150	72
		2,6-NDSNa	1	1.91	0.997595301		
		HNO3	2	0.67	1.844137778		
		H2O	77	5	48.125		
HF139	11.10.08	NiF2 hydrate	1	0.9	0.925150276	175	72
		2,6-NDSNa	1	1.91	0.997595301		
		HNO3	2	0.67	1.844137778		
		H2O	77	5	48.125		
HF140	11.13.08	Cr(NO3)3 hydrat	1	2.31	1.0014081	175	72
		EDSA	1	1.1	1.00286225		
		NaOH	1	0.23	0.997073		
		H2O	77	5	48.125		

HF141	11.13.08	CrF3	1	0.63	1.00233526	175	72
		EDSA	1	1.1	1.00286225		
		NaOH	1	0.23	0.997073		
		H2O	77	5	48.125		
HF142	11.13.08	NiF2 hydrate	1	0.9	0.999642895	200	72
		2,6-NDSNa	1	1.78	1.004554795		
		H2O	52	5	52		
HF143	11.17.08	Ni(OH)2	1	0.5	1.010715288	200	72
		EDSA	1	1.02	1.004804038		
		H2O	52	5	52		
HF144	11.18.08	Ni(OH)2	1	0.5	1.010715288	200	72
		EDSNa	1	1.24	1.001441103		
		H2O	52	5	52		
HF145	11.18.08	NiF2 hydrate	1	0.9	0.999642895	200	72
		1,3-BDSNa	1	1.5	0.996629787		
		H2SO4	1	0.52	0.994189061		
		H2O	52	5	52		
HF146	11.18.08	NiF2 hydrate	1	0.9	0.925150276	175	72
		2,6-NDSNa	1	1.91	0.997595301		
		H2SO4	1	0.67	1.185517143		
		H2O	77	5	48.125		
HF147	11.20.08	Ni(OH)2	1	0.5	1.010715288	200	72
		EDSA	2	2.03	1.999757056		
		H2O	52	5	52		
HF148	11.20.08	Ni(OH)2	1	0.5	1.010715288	200	72
		2,6-NDSNa	1	1.77	0.998911229		
		HF	4	0.43	4.0283776		
		H2O	52	5	52		
HF149	11.20.08	Ni(OH)2	1	0.5	1.010715288	200	72
		HNO3	2	0.67	1.992626794		
		H2O	52	5	52		
HF150	11.26.08	NiF2 hydrate	1	0.9	0.999642895	150	72
		1,3-BDSNa	1	1.5	0.996629787		
		H2SO4	1	0.52	0.994189061		
		H2O	52	5	52		
HF151	11.26.08	NiF2 hydrate	1	0.9	0.999642895	175	72
		1,3-BDSNa	1	1.5	0.996629787		
		H2SO4	1	0.52	0.994189061		

		H2O	52	5	52		
HF152	11.30.08	NiF2 hydrate	1	0.72	0.999642895	100	72
		1,3-BDSNa	1	1.2	0.996629787		
		H2SO4	1	0.42	1.003748571		
		H2O	104	8	104		
HF153	11.30.08	NiF2 hydrate	1	0.72	0.999642895	125	72
		1,3-BDSNa	1	1.2	0.996629787		
		H2SO4	1	0.42	1.003748571		
		H2O	104	8	104		
HF154	11.30.08	NiF2 hydrate	1	0.72	0.999642895	150	72
		1,3-BDSNa	1	1.2	0.996629787		
		H2SO4	1	0.42	1.003748571		
		H2O	104	8	104		
HF155	12.04.08	Ni(OH)2	1	0.5	1.010715288	200	72
		EDSA	1	1.77	1.743630536		
		HF	2	0.21	1.9673472		
		H2O	52	5	52		
HF156	12.04.08	Ni(OH)2	1	0.4	1.010715288	200	72
		EDSA	1	0.81	0.997415773		
		HF	2	0.17	1.990768		
		H2O	104	5	65		
HF157	12.08.08	Ni(OH)2	1	0.5	1.010715288	150	72
		HClO4	2	1.52	2.833800279		
		H2O	52	5	52		
HF158	12.08.08	Ni(OH)2	1	0.5	1.010715288	175	72
		HClO4	2	1.52	2.833800279		
		H2O	52	5	52		
HF159	12.08.08	Ni(OH)2	1	0.5	1.010715288	200	72
		HClO4	2	1.52	2.833800279		
		H2O	52	5	52		
HF160	12.09.08	Ni(OH)2	1	0.5	1.010715288	200	72
		1,3-BDSNa	1	1.5	0.996629787		
		H2O	52	5	52		
HF161	12.09.08	Ni(OH)2	1	0.5	1.010715288	150	72
		1,3-BDSNa	1	1.5	0.996629787		
		H2O	52	5	52		
HF162	12.12.08	Ni(OH)2	1	0.5	1.010715288	200	72
		1,3-BDSNa	2	3.01	1.999903773		

		H2O	52	5	52		
HF163	12.12.08	Ni(OH)2	1	0.5	1.010715288	150	72
		1,3-BDSNa	2	3.01	1.999903773		
		H2O	52	5	52		
HF164	12.12.08	Ni(OH)2	1	0.5	1.010715288	150	72
		EDSA	5	5.08	5.004318149		
		H2O	52	5	52		
HF165	01.15.09	Ni(OH)2	1	0.21	1.020433704	150	72
		1,3-BDSNa	1	0.61	0.974269504		
		cyclohexanal		4			
		H2O	100	4	100		
HF166	01.15.09	Ni(OH)2	1	0.21	1.020433704	150	72
		2,6-NDSNa	1	0.73	0.990337349		
		cyclohexanal		4			
		H2O	100	4	100		
HF167	01.13.09	Ni(OH)2	1	0.25	1.010715288	200	72
		POPSO	0.5	0.35	0.492791584		
		HCl	2	0.2	2.053330411		
		H2O	104	5	104		
HF168	01.13.09	Ni(OH)2	1	0.5	1.013491978	125	72
		1,3-BDSNa	0.25	0.37	0.246510719		
		H2SO4	1	0.52	0.99692035		
		H2O	73	5	52.14285714		
HF169	01.13.09	Ni(OH)2	1	0.5	1.013491978	150	72
		1,3-BDSNa	0.25	0.37	0.246510719		
		H2SO4	1	0.52	0.99692035		
		H2O	73	5	52.14285714		
HF170	01.13.09	Ni(OH)2	1	0.5	1.013491978	125	72
		1,3-BDSNa	1	1.5	0.999367781		
		H2SO4	1	0.52	0.99692035		
		H2O	73	5	52.14285714		
HF171	01.21.09	Ni(OH)2	1	0.5	1.010715288	125	72
		2,6-NDSNa	0.25	0.44	0.248316916		
		HCl	1	0.2	1.026665205		
		H2O	52	5	52		
HF172	01.21.09	Ni(OH)2	1	0.5	1.010715288	150	72
		2,6-NDSNa	0.25	0.44	0.248316916		
		HCl	1	0.2	1.026665205		
		H2O	52	5	52		

HF173	01.23.09	Ni(OH)2	1	0.5	1.020433704	150	72
		1,3-BDSNa	1	1.5	1.006212766		
		HCl	1	0.2	1.036536986		
		H2O	63	5	52.5		
HF174	01.23.09	Ni(OH)2	1	0.5	1.020433704	150	72
		1,3-BDSNa	2	3	2.012425532		
		HCl	1	0.2	1.036536986		
		H2O	63	5	52.5		
HF175	01.28.09	Ni(OH)2	1	0.09	0.969120466	175	72
		EDSA	2	0.38	1.994073775		
		H2SO4	1	0.09	0.916609959		
		H2O	277	5	277		
HF176	01.28.09	Ni(OH)2	1	0.09	0.969120466	200	72
		EDSA	2	0.38	1.994073775		
		H2SO4	1	0.09	0.916609959		
		H2O	277	5	277		
HF242	09.17.09	Cu(CH3COO)2 h	1	0.27	0.975077426	200	72
		triazole	2	0.2	1.970203996		
		EDSA	2	0.52	1.970203996		
		H2O	400	9.5	380		
HF243	09.29.09	Cu(CH3COO)2 h	1	0.27	0.975077426	175	120
pxrd		4,4'-bipy	1	0.21	0.968912222		
		EDSA	1	0.26	0.985101998		
		H2O	400	9.91	396.4		
HF244	10.02.09	Cu(CH3COO)2 h	1	0.27	0.975077426	175	120
		4,4'-bipy	2	0.42	1.937824445		
		EDSA	2	0.52	1.970203996		
		H2O	400	9	360		
HF245	10.02.09	Cu(CH3COO)2 h	1	0.27	0.975077426	150	160
pxrd	12.07.09	4,4'-bipy	1	0.21	0.968912222		
synchrochon cr	12.08.09	EDSA	1	0.29	1.098767613		
		H2O	400	9	360		
HF246	10.14.09	Co(NO3)2 hydrat	1	0.4	0.990808786	200	72
		triazole	1	0.11	1.147848248		
		EDSNa	1	0.32	0.9763116		
		H2O	400	10	400		
HF247	10.14.09	Co(NO3)2 hydrat	1	0.41	1.015579005	175	72
pxrd	10.19.09	4,4'-bipy	1	0.21	0.968912222		
crystallgraphy	10.21.09	EDSNa	1	0.32	0.9763116		

		H2O	400	10	400		
HF248	11.14.09	Cu(CH3COO)2 h	1	0.3	1.083419362	175	
		4,4'-bipy	1	0.21	0.968912222		
		EDSNa	1	0.3	1.136656151		
		H2O	400	10	400		
HF249	10.19.09	Co(NO3)2 hydrat	1	0.4	0.990808786	150	120
		4,4'-bipy	1	0.21	0.968912222		
		1,3-benzene disu	1	0.38	0.971075177		
		H2O	400	10	400		
HF250	10.19.09	Co(NO3)2 hydrat	1	0.4	0.990808786	150	120
		4,4'-bipy	1	0.21	0.968912222		
		2,6-naphthalene	1	0.45	0.976006742		
		H2O	400	10	400		
HF251	10.19.09	Co(NO3)2 hydrat	1	0.4	0.990808786	150	120
pxrd	10.28.09	4,4'-bipy	1	0.21	0.968912222		
		1,3-propanedisul	1	0.34	0.987217857		
		H2O	400	10	400		
HF252	10.19.09	Co(NO3)2 hydrat	1	0.4	0.990808786	150	120
pxrd	10.28.09	4,4'-bipy	1	0.21	0.968912222		
		p-Styrenesulfonic	1	0.3	1.048457808		
		H2O	400	10	400		
HF253	11.02.09	Cd(NO3)2 hydrat	1	0.42	0.981193633	125	144
filtration	11.08.09	4,4'-bipy	1	0.21	0.968912222		
pxrd	11.10.09	EDSNa	1	0.31	0.945801863		
		H2O	400	10	400		
HF254	11.02.09	Cd(NO3)2 hydrat	1	0.4	0.934470127	150	144
filtration	11.08.09	4,4'-bipy	1	0.21	0.968912222		
pxrd	11.10.09	EDSNa	1	0.31	0.945801863		
		H2O	400	10	400		
HF255	11.02.09	Cd(NO3)2 hydrat	1	0.4	0.934470127	175	144
filtration	11.08.09	4,4'-bipy	1	0.21	0.968912222		
pxrd	11.10.09	EDSNa	1	0.31	0.945801863		
		H2O	400	10	400		
HF256	12.13.09	Cu(NO3)2 hydrat	2	0.1	1.936454706	200	120
		boric acid	50	0.67	48.80608119	Parr autoclave	
		EDSNa	2	0.1	1.906858594		
		H2O	25	0.1	25		
HF257	12.13.09	Cu(NO3)2 hydrat	2	0.1	1.3167892	200	120
		boric acid	34	0.47	23.28122918	normal autoclave	

		EDSNa	2	0.1	1.296663844		
		H2O	17	0.06	10.2		
HF257	12.21.09	bismuth nitrate p	1	1.34	0.995379636	200	120
		boric acid	10	1.7	9.906906033	Parr autoclave	
		H2O	2	0.12	2.4		
HF258	12.21.09	bismuth nitrate p	1	1.34	0.995379636	200	120
		boric acid	10	1.7	9.906906033	Parr autoclave	
		triflate acid	2	0.8	1.920810289		
		H2O	2	0.12	2.4		
HF259	01.06.10	bismuth nitrate p	1	0.54	1.002807842	200	120
		boric acid	10	0.68	9.906906033	Parr autoclave	
		EDSA	1	0.21	0.994574132		
		H2O	30	0.6	30		
HF260	01.06.10	antimony acetate	1	0.33	0.994593148	200	120
		boric acid	10	0.68	9.906906033	Parr autoclave	
		EDSA	3	0.63	2.983722397		
		H2O	30	0.6	30		
HF261	01.07.10	Cu(NO3)2 hydrat	1	0.13	1.031843644	150	96
		triazole	2	0.07	1.871255309		
		EDSNa	2	0.25	1.953987112		
		2-butanol	200	8	199.252802		
HF262	01.07.10	Cu(NO3)2 hydrat	1	0.15	0.998656616	150	96
		triazole	2	0.08	1.793822125		
		EDSNa	2	0.3	1.96678698		
		DMF	200	9.44	200		
HF263	01.25.10	AgNO3	1	0.05	0.859882353	150	120
		4,4'-bipyridine	1	0.05	0.937051282		
		H2O	200	5	200		
HF264	01.25.10	AgNO3	1	0.18	1.048235294	180	120
		boric acid	3	0.189	3.026200873		
		urea	5	0.29	4.78021978		
		pyridine	54	4.3	53.81795196		
		H2O	33	0.6	33		
HF265	01.25.10	Cd(NO3)2 hydrat	1	0.3	0.962816481	180	120
		boric acid	3	0.18	2.88209607		
		urea	5	0.3	4.945054945		
		pyridine	54	4.3	53.81795196		
		H2O	33	0.6	33		
HF266	02.02.10	MoO3	1	0.54	0.999416424	175	120

		Mo	0.13	0.05	0.138836773		
		boric acid	3	0.7	3.016011645		
		imidazole	3	0.77	3.013486117		
		EDSA	3	0.75	2.525916561		
		H2O	74	5.5	81.4		
HF267	03.09.10	Cd(NO3)2 hydrat	1	0.42	0.981193633	180	120
		4,4'-bipy	1	0.21	0.968912222	slow cooling	
		PDSNa	1	0.34	0.987178082		
		H2O	400	10	400		
HF268	03.09.10	Ni(NO3)2 hydrate	1	0.4	0.991285808	180	120
		4,4'-bipy	1	0.22	1.0150509	slow cooling	
		EDSA	1	0.26	0.985101998		
		H2O	400	10	400		
HF269	03.09.10	Ni(NO3)2 hydrate	1	0.4	0.991285808	180	120
		4,4'-bipy	1	0.22	1.0150509	slow cooling	
		EDSNa	1	0.33	1.006821338		
		H2O	400	10	400		
HF270	03.15.10	Cd(NO3)2 hydrat	1	0.42	0.981193633	180	120
		4,4'-bipy	1	0.26	1.199605609	slow cooling	
		BDSNa	1	0.36	0.989437071		
		H2O	400	10	400		
HF271	03.15.10	Cd(NO3)2 hydrat	1	0.42	0.981193633	180	120
		4,4'-bipy	1	0.27	1.245744286	slow cooling	
		2,6-NDSNa	0.5	0.24	0.520536929		
		H2O	400	10	400		
HF272	03.15.10	Cd(NO3)2 hydrat	1	0.42	0.981193633	180	120
		2,6-NDSNa	0.5	0.23	0.49884789	slow cooling	
		H2O	400	10	400		
HF273	03.16.10	Zn(NO3)2 hydrat	1	0.41	0.993251084	180	120
		4,4'-bipy	1	0.22	1.0150509	slow cooling	
		EDSNa	1	0.32	0.9763116		
		H2O	400	10	400		
HF274	03.28.10	Zn(NO3)2 hydrat	1	0.42	1.01747672	180	120
		4,4'-bipy	1	0.22	1.0150509	slow cooling	
		PDSNa	1	0.35	1.016212732		
		H2O	400	10	400		
HF275	03.28.10	Zn(NO3)2 hydrat	1	0.42	1.01747672	180	120
		4,4'-bipy	1	0.22	1.0150509	slow cooling	
		BDSNa	1	0.36	0.989437071		
		H2O	400	10	400		

HF276	04.18.10	MoO3	1	0.54	9.003751563	200	120
		boric acid	26	0.67	26.00679282	slow cooling	
		H2O	12	0.09	12		
HF277	04.18.10	MoO3	1	0.06	1.00041684	200	120
		Mo	0.13	0.005	0.125078174	slow cooling	
		boric acid	26	0.67	26.00679282		
		H2O	12	0.09	12		
HF278	05.11.10	Ni(OH)2	1	0.51	0.990398101	150	120
		1,3-benzene disu	1	1.57	1.00212766	slow cooling	
		H2SO4	1	0.54	0.991027732		
		CTAB	0.02	0.06	0.029633695		
		H2O	100	10	100		
HF279	05.04.10	Ni(Ac)2tetrahydra	1	0.69	0.998191682	150	120
		1,3-benzene disu	1	0.78	0.995744681	slow cooling	
		CTAB	0.02	0.02	0.019755796		
		H2O	200	10	200		
HF280	05.11.10	Ni(OH)2	1	0.26	1.009817672	150	120
		1,3-benzene disu	1	0.78	0.995744681	slow cooling	
		H2SO4	1	0.27	0.991027732		
		CTAB	0.02	0.02	0.019755796		
		H2O	200	10	200		
HF281	05.04.10	NiSO4hydrate	1	1.46	0.999847816	150	120
		1,3-benzene disu	1	1.57	1.00212766	slow cooling	
		CTAB	0.02	0.04	0.019755796		
		H2O	100	10	100		
HF282	05.11.10	Ni(OH)2	1	0.26	0.340813464	150	120
		1,3-benzene disu	1	0.78	0.33606383	slow cooling	
		H2SO4	1	0.27	0.33447186		
		CTAB	0.02	0.02	0.006667581		
		H2O	54	10	67.5		
HF283	05.18.10	Co(NO3)2 hydrat	0.5	0.2	0.495404393	175	72
		Zn(NO3)2 hydrat	0.5	0.21	0.50873836		
		4,4'-bipy	1	0.22	1.0150509		
		1,2-ethanedisulfo	1	0.33	1.006863965		
		H2O	400	10	400		
HF284	05.18.10	Cu(NO3)2 hydrat	1	0.32	0.991464809	175	72
		4,4'-bipy	1	0.22	1.0150509		
		1,3-propanedisul	1	0.34	0.987217857		
		H2O	400	10	400		

HF285	05.18.10	Cu(NO3)2 hydrat	1	0.32	0.991464809	175	72
		4,4'-bipy	1	0.22	1.0150509		
		1,4-butanedisulfo	1	0.36	0.997080595		
		H2O	400	10	400		
HF286	05.18.10	Cu(NO3)2 hydrat	1	0.32	0.991464809	175	72
		1,2-di(4-pyridyl)e	1	0.27	0.982690909		
		1,2-ethanedisulfo	1	0.32	0.993172833		
		H2O	400	10	400		
HF287	07.15.10	Cu(NO3)2 hydrat	1	0.32	0.991464809	100	96
		4,4'-bipy	1	0.22	1.0150509		
		2,6-Naphthalene	1	0.46	0.99769578		
		H2O	400	10	400		
HF288	07.19.10	Cu(NO3)2 hydrat	1	0.16	0.993886238	100	48
		1,2-di(4-pyridyl)e	1	0.14	1.021575758		
		1,2-ethanedisulfo	1	0.16	0.995598432		
		H2O	400	5	400		
HF289	07.15.10	Cd(NO3)2 *4H2O	1	0.1	0.9477745	100	96
		4.4--bipy	1	0.05	0.93591139		
		1,2-ethanedisulfo	1	0.07	0.881398854		
		DMF	400	10	400		
HF290	07.15.10	Cd(NO3)2 *4H2O	1	0.1	0.9477745	100	96
		1,2-ethanedisulfo	1	0.07	0.881398854		
		DMF	400	10	400		
HF291	07.19.10	Cu(NO3)2 hydrat	1	0.08	1.005580635	100	96
		4.4--bipy	1	0.05	0.93591139		
		1,2-ethanedisulfo	1	0.08	1.007312976		
		DMF	200	5	200		
HF292	07.19.10	Cu(NO3)2 hydrat	1	0.08	1.005580635	100	96
		4.4--bipy	1	0.07	1.310275946		
		1,3-propanedisul	1	0.08	0.950030464		
		DMF	200	5	200		
HF293	07.23.10	CdCl2 hydrate	1	0.08	1.024297101	80	48
		4.4--bipy	1	0.05	0.93591139		
		1,2-ethanedisulfo	1	0.08	1.007312976		
		DMF	400	10	400		
HF294	07.23.10	Cd(Ac)2hydrate	1	0.09	0.987257992	80	48
		4.4--bipy	1	0.05	0.93591139		
		1,2-ethanedisulfo	1	0.08	1.007312976		
		DMF	400	10	400		

HF295	07.23.10	Cd(Ac)2hydrate	1	0.37	1.000438241	150	
		4.4--bipy	1	0.22	1.0150509		
		1,2-ethanedisulfo	1	0.32	0.993172833		
		H2O	400	10	400		
HF296		Cd(Ac)2hydrate	1		0		
		1,2-ethanedisulfo	5		0		
		H2O	800		0		
HF297	07.23.10	Cd(Ac)2hydrate	1	0.04	0.43878133	80	48
xsc1032		1,2-ethanedisulfo	5	0.2	2.518282441		
		DMF	400	10	400		
HF298	07.28.10	sodium hydroxide	1	0.05	0.913853463	100	120
filtration	08.02.10	1,2-ethanedisulfo	1	0.26	0.999127234		
		DMF	100	10	100		
HF299	07.28.10	lithium perchlorat	5	0.37	5.05671279	100	120
filtration	08.02.10	sodium hydroxide	1	0.02	1.096624156		
		1,2-ethanedisulfo	1	0.09	1.037555205		
		DMF	300	10	300		
HF300	07.28.10	hydrofluoric acid	1	0.05	1.82725	100	120
filtration	08.02.10	1,2-ethanedisulfo	1	0.32	0.990211685		
		DMF	100	10	100		
HF301	08.07.10	Cu(NO3)2 hydrat	1	0.13	1.00941571	100	48
		1,2-di(4-pyridyl)e	1	0.11	1.003333333		
		1,2-ethanedisulfo	1	0.13	1.011154658		
		H2O	400	5	500		
HF302	08.07.10	Cd(NO3)2 hydrat	1	0.21	0.983589976	100	48
		1,2-di(4-pyridyl)e	1	0.14	1.021575758		
		1,2-ethanedisulfo	1	0.16	0.995598432		
		H2O	400	5	400		
HF303	08.07.10	Cd(NO3)2 hydrat	1	0.21	0.983589976	100	48
		1,2-di(4-pyridyl)e	1	0.14	1.021575758		
		1,3-propanedisul	1	0.16	0.938982087		
		H2O	400	5	400		
HF304	08.07.10	Cadmium fluoride	1	0.21	1.008603151	150	48
		1,2-ethanedisulfo	1	0.32	0.995598432		
		H2O	400	5	200		
HF305	08.07.10	1,2-ethanedisulfo	1	0.16	2.014625953	100	48
		DMF	400	10	400		
HF306	08.11.10	Cd(NO3)2 hydrat	1	0.21	0.983589976	100	48

		1,2-di(4-pyridyl)e	1	0.14	1.021575758		
		1,4-butanedisulfo	1	0.16	0.888492582		
		H2O	400	5	400		
HF307	08.11.10	Cadmium fluoride	1	0.21	1.008603151	175	48
		1,2-ethanedisulfo	3	0.96	2.986795297		
		H2O	400	5	200		
HF308	08.11.10	Cadmium fluoride	1	0.21	1.008603151	200	48
		1,2-ethanedisulfo	3	0.96	2.986795297		
		H2O	400	5	200		
HF309	08.17.10	Cadmium fluoride	1	0.13	0.936560069	150	48
		1,2-ethanedisulfo	2	0.4	2.278864353		
		H2O	600	5	300		
HF310	08.17.10	Cadmium fluoride	1	0.21	1.008603151	150	48
		1,2-ethanedisulfo	0.25	0.03	0.113943218		
		NaClO4	1.75	0.37	1.902947458		
		H2O	400	10	400		
HF311	08.17.10	Cd(NO3)2 hydrat	1	0.21	0.983589976	125	120
		1,2-di(4-pyridyl)e	1	0.14	1.021575758		
		1,2-propanedisul	1	0.16	0.995727085		
		H2O	400	5	400		
HF312	08.17.10	Cd(NO3)2 hydrat	1	0.21	0.983589976	150	48
		1,2-di(4-pyridyl)e	1	0.14	1.021575758		
		1,2-propanedisul	1	0.16	0.995727085		
		H2O	400	5	400		
HF313	08.29.10	V2O5	1	0.49	0.998939641	175	72
		EDSNa	0.25	0.16	0.251170253		
		HClO4 (70 %)	1.75	1.11	2.867903964		
		H2O	200	9.71	206.696538		
HF314	08.29.10	V2O5	1	0.49	0.998939641	200	72
		EDSNa	0.25	0.16	0.251170253		
		HClO4 (70 %)	1.75	0.67	1.731077167		
		H2O	200	9.71	203.9798255		
HF315	08.29.10	V2O5	1	0.23	0.986957795	175	72
		EDSNa	1	0.295	1.000166693		
		HF(48wt%)	10	0.51	6.965686359		
		H2O	400	9.23	406.4798617		
HF316	08.29.10	V2O5	1	0.23	0.986957795	200	72
		EDSNa	1	0.298	1.010337879		
		HF(48wt%)	10	0.513	7.006660985		

		H2O	400	9.23	406.5188505		
HF317	08.29.10	Nb2O5	1	0.23	1.503421279	150	72
		EDSNa	5	0.295	2.226593152		
		HF(48wt%)	10	0.51	22.15309231		
		ethylene glycol	100		0		
		H2O	400	9.23	890.1588218		
HF318	08.29.10	Nb2O5	1	0.23	1.503421279	175	72
		EDSNa	5	0.295	2.226593152		
		HF(48wt%)	10	0.51	22.15309231		
		ethylene glycol	100		0		
		H2O	400	9.23	890.1588218		
HF319	08.29.10	Nb2O5	1	0.23	1.503421279	200	72
		EDSNa	5	0.295	2.226593152		
		HF(48wt%)	10	0.51	22.15309231		
		ethylene glycol	100		0		
		H2O	400	9.23	890.1588218		
HF320	08.29.10	Nb2O5	1	0.23	1.503421279	150	72
		2,6-Naphthalene	3	0.295	1.542652572		
		HF(48wt%)	10	0.51	22.15309231		
		ethylene glycol	100		0		
		H2O	400	9.23	890.1588218		
HF321	11.01.10	Zn(NO3)2 hydrat	1	0.41	0.993251084	150	72
		4,4'-bipy	1	0.21	0.968912222		
		1,2-ethanedisulfo	1	0.33	1.006863965		
		H2O	400	10	400		
HF322	11.01.10	Co(NO3)2 hydrat	0.05	0.03	0.049540439	150	72
		Zn(NO3)2 hydrat	0.95	0.59	0.952875024		
		4,4'-bipy	1	0.32	0.984291781		
		1,2-ethanedisulfo	1	0.49	0.996693622		
		H2O	400	12	320		
HF323	11.01.10	Co(NO3)2 hydrat	0.1	0.06	0.099080879	150	72
		Zn(NO3)2 hydrat	0.9	0.55	0.888273327		
		4,4'-bipy	1	0.33	1.0150509		
		1,2-ethanedisulfo	1	0.49	0.996693622		
		H2O	400	12	320		
HF324	11.01.10	Co(NO3)2 hydrat	0.25	0.15	0.247702196	150	72
		Zn(NO3)2 hydrat	0.75	0.46	0.74291951		
		4,4'-bipy	1	0.32	0.984291781		
		1,2-ethanedisulfo	1	0.49	0.996693622		
		H2O	400	12	320		

HF325	11.01.10	Co(NO3)2 hydrat	0.5	0.3	0.928883237	150	72
		Zn(NO3)2 hydrat	0.5	0.31	0.938743403		
		4,4'-bipy	1	0.32	1.84554709		
		1,2-ethanedisulfc	1	0.49	1.868800542		
		H2O	400	12	600		
HF326	11.01.10	Co(NO3)2 hydrat	0.75	0.45	0.743106589	150	72
		Zn(NO3)2 hydrat	0.25	0.15	0.242256362		
		4,4'-bipy	1	0.32	0.984291781		
		1,2-ethanedisulfc	1	0.49	0.996693622		
		H2O	400	12	320		
HF327	11.05.10	Co(NO3)2 hydrat	0.9	0.18	0.445863954	150	72
		Zn(NO3)2 hydrat	0.1	0.02	0.048451272		
		4,4'-bipy	1	0.11	0.50752545		
		1,2-ethanedisulfc	1	0.16	0.488176468		
		H2O	400	10	400		
HF328	11.05.10	Co(NO3)2 hydrat	0.95	0.19	0.470634173	150	72
		Zn(NO3)2 hydrat	0.05	0.01	0.024225636		
		4,4'-bipy	1	0.1	0.461386773		
		1,2-ethanedisulfc	1	0.16	0.488176468		
		H2O	400	10	400		
HF329	11.05.10	Co(NO3)2 hydrat	0.025	0.01	0.018577665	150	72
		Zn(NO3)2 hydrat	0.975	0.54	0.981138266		
		4,4'-bipy	1	0.29	1.00351623		
		1,2-ethanedisulfc	1	0.44	1.006863965		
		H2O	300	10	300		
HF330	11.05.10	Co(NO3)2 hydrat	1	0.2	0.495404393	150	72
		4,4'-bipy	1	0.1	0.461386773		
		1,2-ethanedisulfc	1	0.16	0.488176468		
		H2O	400	12	480		
HF331	11.11.10	Ni(Ac)2 hydrate	1	0.44	0.995419111	150	72
		1,3-benzenedisul	1	0.5	0.99822695		
		CTAB	0.03	0.02	0.032500144		
		H2O	250	8	250		
HF332	11.11.10	Ni(NO3)2 hydrate	1	0.51	0.98734569	150	72
		1,3-benzenedisul	1	0.5	0.99822695		
		CTAB	0.03	0.02	0.032500144		
		H2O	250	8	250		
HF333	11.11.10	NiSO4 hydrate	1	0.46	0.985239291	150	72
		1,3-benzenedisul	1	0.5	0.99822695		
		CTAB	0.03	0.02	0.032500144		
		H2O	250	8	250		

HF334	11.11.10	Ni(OH)2	1	0.16	0.971631971	150	72
		1,3-benzenedisul	1	0.5	0.99822695		
		CTAB	0.03	0.02	0.032500144		
		H2SO4	1	0.17	0.976632653		
		H2O	250	8	250		
HF335	11.12.10	PbF2	1	0.78	0.994862034	150	72
		EDSA	2	1.44	1.990860822		
		HClO4 (70 %)	2.5	1.14	2.484216102		
		H2O	200	11.52	205.9067365		
HF336	11.16.10	Sb(Ac)3	1	0.78	0.940720311	150	72
		EDSA	5	1.44	2.727974763		
		H2O	200	11.52	230.4		
HF337	11.16.10	SbF3	1	0.78	3.27514704	150	72
		HClO4 (70 %)	5	1.14	5.962118645		
		H2O	400	11.52	494.1761675		
HF338	11.16.10	SbF3	1	0.78	3.27514704	150	72
		EDSA	2	1.44	4.778065973		
		HClO4 (70 %)	5	1.14	5.962118645		
		H2O	400	11.52	494.1761675		
HF339	11.23.10	Sb(Ac)3	1	0.67	1.004324834	150	72
		HClO4 (70 %)	5	1.59	4.961722672		
		H2O	200	8.5	223.148875		
HF340	11.23.10	PbF2	1	0.59	1.007364198	150	72
		HClO4 (70 %)	2.75	0.87	2.53787378		
		H2O	200	8.8	210.5498862		
HF341	11.23.10	PbF2	1	0.81	0.991949101	150	72
		HNO3	2	0.42	2.001777778		
		H2O	200	12	202.1		
HF342	11.23.10	Ni(OH)2	1	0.23	1.010879956	150	72
		1,3-benzenedisul	1	0.69	0.997007242		
		CTAB	0.03	0.02	0.023522053		
		H2SO4	1	0.274	1.139259917		
		ethanol	32	3.6	31.88915413		
		H2O	100	4.4	99.51593639		
HF343	11.23.10	Ni(OH)2	1	0.23	1.010879956	150	72
		1,3-benzenedisul	1	0.7	1.011456622		
		H2SO4	1	0.24	0.997891898		
		ethanol	32	3.61	31.97773511		
		H2O	100	4.42	99.96828155		

HF344	11.23.10	Ni(OH)2	1	0.22	0.97260175	150	72
		1,3-benzenedisul	1	0.69	1.002856813		
		CTAB	0.03	0.02	0.02366006		
		H2SO4	1	0.24	1.003746659		
		ethanol	54	6.06	53.9950241		
		H2O	30	1.3	29.57494366		
HF345	11.29.10	Ni(Ac)2 hydrate	1	0.48	0.999572839	150	72
		1,3-benzenedisul	0.5	0.27	0.496184235		
		ethanol	80	7.1	79.98873398		
HF346	11.29.10	Ni(NO3)2 hydrate	1	0.56	0.997945896	150	72
		1,3-benzenedisul	0.5	0.27	0.496184235		
		ethanol	80	7.1	79.98873398		
HF347	11.29.10	NiSO4 hydrate	1	0.5	0.985765936	150	72
		1,3-benzenedisul	0.5	0.27	0.496184235		
		ethanol	80	7.1	79.98873398		
HF348	11.29.10	Ni(OH)2	1	0.18	1.00617664	150	72
		1,3-benzenedisul	0.5	0.27	0.496184235		
		H2SO4	1	0.19	1.004744948		
		ethanol	80	7.1	79.98873398		
HF345i	11.29.10	Ni(Ac)2 hydrate	1	0.09	1.054236978	150	72
		1,3-benzenedisul	1	0.1	1.033717157		
		ethanol	600	9.5	602.0278834		
HF346i	11.29.10	Ni(NO3)2 hydrate	1	0.1	1.002401012	150	72
		1,3-benzenedisul	1	0.1	1.033717157		
		ethanol	600	9.5	602.0278834		
HF348H2O	11.29.10	Ni(OH)2	1	0.16	0.993941648	150	72
		1,3-benzenedisul	1	0.49	1.000724331		
		H2SO4	1	0.17	0.999057151		
		ethanol	100	8.1	101.4132438		
		H2O	60	1.88	60.09896092		
HF348i	11.29.10	Ni(OH)2	1	0.19	0.995695633	150	72
		1,3-benzenedisul	1	0.58	0.999259918		
		H2SO4	1	0.2	0.99152462		
		ethanol	100	9.5	100.3379806		
HF348ii	12.04.10	Ni(OH)2	1	0.057	0.993473919	150	72
		1,3-benzenedisul	0.1	0.017	0.097411002		
		H2SO4	1	0.06	0.989312213		
		ethanol	200	5.69	199.8769117		
		H2O	160	1.78	159.6503316		

HF348iii	12.04.10	Ni(OH)2	1	0.05	0.971631971	150	72
		1,3-benzenedisul	0.1	0.015	0.095829787		
		H2SO4	1	0.054	0.992718367		
		H2O	900	9	900		
HF348iv	12.04.10	Ni(OH)2	1	0.053	0.987729513	150	72
		1,3-benzenedisul	0.1	0.016	0.098030139		
		H2SO4	1	0.056	0.987303538		
		ethanol	100	2.66	99.91082541		
		H2O	60	0.63	60.41863624		
HF348v	12.04.10	Ni(OH)2	1	0.02	0.874468774	150	72
		1,3-benzenedisul	0.1	0.007	0.100621277		
		H2SO4	1	0.02	0.827265306		
		H2O	900	4	900		
HF348vi	12.04.10	Ni(OH)2	1	0.46	0.993223792	150	72
		1,3-benzenedisul	0.1	0.14	0.099379039		
		H2SO4	1	0.49	1.000888889		
		H2O	100	9	100		
HF348vii	12.04.10	Ni(OH)2	1	0.206	1.00078093	150	72
		1,3-benzenedisul	0.1	0.06	0.095829787		
		H2SO4	1	0.21	0.965142857		
		H2O	100	4	100		
HF348viii	12.04.10	Ni(OH)2	1	0.205	0.99592277	150	72
		1,3-benzenedisul	0.1	0.06	0.095829787		
		H2SO4	1	0.2	0.919183673		
		H2O	100	4	100		
HF348ix	12.04.10	Ni(OH)2	1	0.205	0.99592277	150	72
		1,3-benzenedisul	0.5	0.31	0.495120567		
		H2SO4	1	0.217	0.997314286		
		H2O	100	4	100		
HF349i	12.15.10	Ni(OH)2	1	0.21	1.020213569	180	72
		1,3-benzenedisul	0.5	0.32	0.511092199		
		H2SO4	1	0.22	1.011102041		
		H2O	100	4	100		
HF349ii	12.15.10	Ni(OH)2	1	0.21	1.020213569	180	72
		1,3-benzenedisul	0.25	0.16	0.255546099		
		H2SO4	1	0.22	1.011102041		
		H2O	100	4	100		
HF349iii	12.15.10	Ni(OH)2	1	0.21	1.020213569	180	72
		1,3-benzenedisul	0.1	0.06	0.095829787		

		H2SO4	1	0.22	1.011102041		
		H2O	100	4	100		
HF349iv	12.15.10	Ni(OH)2	1	0.21	1.020213569	200	72
		1,3-benzenedisul	0.5	0.32	0.511092199		
		H2SO4	1	0.22	1.011102041		
		H2O	100	4	100		
HF349v	12.15.10	Ni(OH)2	1	0.21	1.020213569	200	72
		1,3-benzenedisul	0.25	0.16	0.255546099		
		H2SO4	1	0.22	1.011102041		
		H2O	100	4	100		
HF349vi	12.15.10	Ni(OH)2	1	0.21	1.020213569	200	72
		1,3-benzenedisul	0.1	0.06	0.095829787		
		H2SO4	1	0.22	1.011102041		
		H2O	100	4	100		
HF350	12.21.10	Cu(NO3)2hydrate	1	0.65	1.006290173	150	72
		1,3-benzenedisul	0.25	0.16	0.255546099		
		H2O	200	8	200		
HF351	12.21.10	Cu(NO3)2hydrate	1	0.65	1.006290173	180	72
		1,3-benzenedisul	0.25	0.16	0.255546099		
		H2O	200	8	200		
HF352	12.21.10	Cu(NO3)2hydrate	1	0.65	1.006290173	150	72
pxrd	01.03.11	EDSNa	0.25	0.11	0.260483701		
		H2O	200	8	200		
HF353	12.21.10	Cu(NO3)2hydrate	1	0.65	1.006290173	180	72
		EDSNa	0.25	0.11	0.260483701		
		H2O	200	8	200		
HF354	12.21.10	Cu(NO3)2hydrate	1	0.65	1.006290173	150	72
pxrd	01.03.11	EDSNa	2	0.84	1.61571575		
		H2O	200	8	200		
HF355	12.21.10	Cu(NO3)2hydrate	1	0.65	1.006290173	180	72
		EDSNa	2	0.8	1.894426919		
		H2O	200	8	200		
HF356	12.26.10	Cu(NO3)2hydrate	1	0.65	1.006290173	150	72
pxrd	01.03.11	EDSNa	4	0.8	1.894426919		
		H2O	200	8	200		
HF357	12.26.10	Cu(NO3)2hydrate	1	0.65	1.006290173	150	72
		PDSNa	2	0.86	1.639898391		
		H2O	200	8	200		

HF358	12.26.10	Cu(NO3)2hydrate	1	0.65	1.006290173	150	72
		1,3-benzenedisul	1	0.62	0.990241135		
		H2O	200	8	200		
HF359	01.03.11	Ni(OH)2	1	0.21	1.020213569	150	72
		1,3-benzenedisul	1	0.63	1.006212766		
		H2SO4	1	0.22	1.011102041		
		H2O	200	8.5	212.5		
HF360	01.03.11	Ni(OH)2	1	0.29	1.408866357	150	72
		EDSNa	2	1.03	1.997984409		
		H2SO4	1	0.3	1.37877551		
		H2O	200	8.5	212.5		
HF361	01.03.11	Ni(NO3)2 hydrate	1	0.64	0.993638458	150	72
		1,2-ethanedisulfo	2	1.03	2.002864034		
		H2O	200	8	200		
HF362	01.03.11	Cadmium fluoride	1	0.33	0.990592381	150	72
		1,2-ethanedisulfo	2	1.03	2.002864034		
		H2O	200	8	200		
HF363	01.10.11	Cu(NO3)2hydrate	1	0.65	1.006290173	150	72
		EDSNa	4	2.11	4.058524086		
		H2O	200	8	200		
HF364	01.10.11	Cu(NO3)2hydrate	1	0.16	0.990808786	150	72
		EDSNa	2	0.26	2.000409976		
		H2O	800	8	800		
HF365	01.10.11	Cu(NO3)2hydrate	1	0.65	1.006290173	150	72
		NaClO4	5	1.56	5.002306707		
		H2O	200	8	200		
HF367	01.12.11	CuCl2hydrate	1	0.38	1.003941811	150	72
		EDSNa	4	2.08	4.000819952		
		H2O	200	8	200		
HF368	01.12.11	Cu(Ac)2monohyd	1	0.44	0.993114508	150	72
		EDSNa	4	2.07	3.981585241		
		H2O	200	8	200		
HF369	01.12.11	CuO	1	0.38	2.151772693	150	72
		EDSNa	4	2.08	4.000819952		
		H2O	200	8	200		
HF370	01.12.11	Cu(NO3)2 hydrat	1	0.13	1.00941571	125	72
		1,2-di(4-pyridyl)e	1	0.11	1.003333333		

		1,2-ethanedisulfo	1	0.13	1.011154658		
		H2O	400	4	400		
HF371	01.19.11	Cu(NO3)2hydrate	1	0.65	1.006290173	150	72
		PDSNa	4	2.15	3.933864153		
		H2O	200	8	200		
HF372	01.24.11	Nickel acetate	1	0.55	0.995419111	175	72
		succinate acid di	2	0.72	2.001160136		
		H2O	200	8	200		
HF373	01.24.11	Nickel acetate	1	0.55	0.995419111	175	72
		succinate acid	2	0.72	2.7461089		
		H2O	200	8	200		
HF374	01.24.11	nickel hydroxide	1	0.12	1.036742915	175	72
		acetic acid	2	0.15	2.000111019		
		succinate acid	2	0.31	2.101959899		
		H2O	400	9	400		
HF375	01.24.11	nickel hydroxide	1	0.12	1.036742915	175	120
		acetic acid	2	0.15	2.000111019		
		succinate acid	2	0.31	2.101959899		
		H2O	400	9	400		
HF376	04.13.11	Zn(NO3)2 hydrat	1	0.44	0.999307493	150	72
		EDSNa	4	1.4	4.039289375		
		H2O	300	8	300		
HF377	04.13.11	Zn(NO3)2 hydrat	1	0.44	0.999307493	150	72
		EDSA	4	1.11	3.943605385		
		H2O	300	8	300		
HF378	08.15.11	Cu(NO3)2 hydrat	1	0.135	1.045685541	150	72
		tetraethylammon	17	1.54	16.99935053		
		H2O	800	7.5	750		
HF379	08.15.11	Cu(NO3)2 hydrat	1	0.132	1.022448085	175	72
		tetraethylammon	17	1.54	16.99935053		
		H2O	800	7.6	760		
HF380	08.15.11	Cu(NO3)2 hydrat	1	0.131	1.014702266	150	72
		urea	17	0.54	16.1982018		
		H2O	800	8.5	850		
HF381	08.31.11	PbF2	1	0.53	1.005911132	175	120
		succinate disodiu	2	1.16	1.999312694		
		HClO4 (70 %)	2	0.61	2.825737439		
		H2O	200	7.74	199.925912		

HF382	08.31.11	PbF2	1	0.53	1.005911132	175	120
		glutarate disodiu	2	0.76	2.008584288		
		HClO4 (70 %)	2	0.61	2.825737439		
		H2O	200	7.74	199.925912		
HF383i	10.06.11	PbF2	1	0.27	1.008419844	125	72
		disodium sabaca	2	0.54	2.010198874		
		HClO4 (70 %)	2	0.31	2.825904877		
		H2O	400	7.74	393.425912		
HF383ii	10.06.11	PbF2	1	0.27	1.008419844	150	72
		disodium sabaca	2	0.54	2.010198874		
		HClO4 (70 %)	2	0.31	2.825904877		
		H2O	400	7.74	393.425912		
HF384	10.06.11	PbF2	1	0.27	1.01253753	150	72
		EDSA	2	0.54	2.018407129		
		HClO4 (70 %)	2.5	0.39	3.569687498		
		H2O	400	7.74	395.03239		
HF385	10.06.11	PbF2	1	0.27	0.991949101	150	72
		disodium sabaca	2	0.54	1.977365854		
		H2O	400	7.74	387		

Bibliography

1. Cheetham, A. K.; Rao, C. N. R.; Feller, R. K., *Chem. Commun.* **2006**, 4780-4795.

2. Davis, M. E., *Nature* **2002,** *417*, 813-821.

3. Weitkamp, J., *Solid State Ionics* **2000,** *131*, 175-188.

4. Thomas, J. M., *Sci. Am.* **1992,** *1992*, 112-115.

5. Corma, A., *J. Catal.* **2003,** *216*, 298-312.

6. Oliver, S. R. J., *Chem. Soc. Rev.* **2009,** *38*, 1868-1881.

7. Rives, V., *LDHs: Layered Double Hydroxides: Present and Future*. Nova Science Publishers Inc., Hauppauge, New York, USA: 2001.

8. Slade, D. G. E. a. R. C. T., *Layered Double Hydroxides*. X. Duan and D. G. Evans ed.; Springer-Verlag, New York, NY, USA: 2006; p 1-87.

9. Boclair, J. W.; Braterman, P. S.; Brister, B. D.; Yarberry, F., *Chem. Mater.* **1999,** *11*, 2199-2204.

10. Liu, Z.; Ma, R.; Ebina, Y.; Iyi, N.; Takada, K.; Sasaki, T., *Langmuir* **2007,** *23*, 861-867.

11. Cho, S.; Jung, S. H.; Jang, J. W.; Oh, E.; Lee, K. H., *Cryst. Growth Des.* **2008,** *8*, 4553-4558.

12. Valente, J. S.; Lima, E.; Toledo-Antonio, J. A.; Cortes-Jacome, M. A.; Lartundo-Rojas, L.; Montiel, R.; Prince, J., *J. Phys. Chem. C* **2010,** *114*, 2089-2099.

13. Liang, J.; Ma, R.; Iyi, N.; Ebina, Y.; Takada, K.; Sasaki, T., *Chem. Mater.* **2010,** *22*, 371-378.

14. Ma, R.; Liu, Z.; Takada, K.; Iyi, N.; Bando, Y.; Sasaki, T., *J. Am. Chem. Soc.* **2007,** *129*, 5257-5263.

15. Meyn, M.; Beneke, K.; Lagaly, G., *Inorg. Chem.* **1990,** *29*, 5201-5207.

16. Li, B.; He, J.; Evans, D. G.; Duan, X., *App. Caly Sci.* **2004,** *27*, 199-207.

17. Choudary, B. M.; Jaya, V. S.; Reddy, B. R.; Kantam, M. L.; Rao, M. M.; Madhavendra, S. S., *Chem. Mater.* **2005,** *17*, 2740-1743.

18. Jin, L.; Liu, Q.; Sun, Z.; Ni, X.; Wei, M., *Ind. Eng. Chem. Res* **2010,** *49*, 11176-11181.

19. Depege, C.; Metoui, F. E.; Forano, C.; Roy, A.; Dupuis, J.; Besse, J. P., *Chem. Mater.* **1996,** *8*, 952-960.

20. Keith, L. H.; Teillard, W. A., *Environ. Sci. Technol.* **1979,** *13*, 416.

21. Hogue, C., *Chemical & Engineering News* **2011,** *89*, 6.

22. *Perchlorate environmental contamination: toxicological review and risk characterization*. Second external review draft, NCEA-1-0503; U.S. EPA, Office of Research and Development, National Center for Environmental Assessment, U.S. Government Printing Office: Washington, DC, 2002.

23. Darab, J. G.; Amonette, A. B.; Burke, D. S. D.; Orr, R. D.; Ponder, S. M.; Schrick, B.; Mallouk, T. M.; Lukens, W. W.; Caulder, D. L.; Shuh, D. K., *Chem. Mater.* **2007,** *19* (5703-5713).

24. Darab, J. G.; Smith, P. A., *Chem. Mater.* **1996,** *8*, 1004-1021.

25. Wang, Y.; Bryan, C.; Gao, H.; Phol, P. I.; Brinker, C. J.; Yu, K.; Xu, H.; Yang, Y.; Braterman, P. S.; Xu, Z., *Sandia Report (Potential Applications of Nanostructured Materials in Nuclear Waste Management* **2003,** *SAND2003-3313*, 1-95.

26. Wu, M.; Janssen, S., *Environ. Sci. Technol.* **2011,** *45*, 366-367.

27. Mark, R.; Findley, W. N., *Polym. Eng. Sci.* **1978,** *18*, 6-15.

28. Bedner, M.; Maccrehan, W. A., *Environ. Sci. Technol.* **2006,** *40*, 516-522.

29. Taviot-Gueho, C.; Feng, Y.; Faour, A.; Leroux, F., *Dalton Trans.* **2010,** *39*, 5994-6005.

30. Prasanna, S. V.; Kamath, P. V., *Solid State Sci.* **2007,** *10*, 260-266.

31. Hu, G. J.; Wang, H. X.; Yan, L. L.; Pu, M.; He, J.; Evans, D. G., *J. Phys. Chem. Solids* **2010,** *71*, 1290-1294.

32. Yang, L.; Shahrivari, Z.; Liu, P. K. T.; Sahimi, M.; Tsotsis, T. T., *Ind. Eng. Chem. Res* **2005,** *44*, 6804-6815.

33. Das, J.; Patra, B. S.; Baliarsingh, N.; Parida, K. M., *App. Caly Sci.* **2006,** *32*, 252-260.

34. Das, J.; Das, D.; Dash, G. P.; Das, D. P.; Parida, K. M., *Int. J. Environ. Stud.* **2004,** *61* 605-616.

35. You, Y. W.; Vance, G. F.; Zhao, H. T., *App. Caly Sci.* **2001,** *20*, 13-25.

36. Goswamee, R. L.; Sengupta, P.; Bhattacharyya, K. G.; Dutta, D. K., *Appl. Clay Sci.* **1998,** *13*, 21-34.

37. You, Y. W.; Zhao, H. T.; Vance, G. F., *Environ. Technol.* **2001,** *22*, 1447-1457.

38. Miyata, S., *Clays Clay Miner.* **1983,** *31*, 305-311.

39. Goh, K. H.; Lim, T. T.; Dong, Z., *Water Res.* **2008,** *42*, 1343-1368.

40. Li, F.; Duan, X., *Struct. Bond.* **2005,** *119*, 193-223.

41. Iyi, N.; Matsumoto, T.; Kaneko, Y.; Kitamura, K., *Chem. Lett.* **2004,** *33*, 1122-1123.

42. Liu, Z.; Ma, R.; Osada, M.; Iyi, N.; Ebina, Y.; Takada, K.; Sasaki, T., *J. Am. Chem. Soc.* **2006,** *128*, 4872-4880.

43. Constantino, V. R. L.; Pinnavaia, T. J., *Inorg. Chem.* **1995,** *34*, 883-892.

44. Awaleh, M. O.; Badia, A.; Brisse, F., *Cryst. Growth Des.* **2006,** *6*, 2674-2685.

45. Custelcean, R., *Chem. Soc. Rev.* **2010,** *39*, 3675-3685.

46. Noro, S.; Kitaura, R.; Kondo, M.; Kitagawa, S.; Ishii, T.; Matsuzaka, H.; Yamashita, M., *J. Am. Chem. Soc.* **2002,** *124*, 2568-2583.

47. Custelcean, R.; Gorbunova, M. G., *J. Am. Chem. Soc.* **2005,** *127*, 16362-16363.

48. Geng, F.; Ma, R.; Sasaki, T., *Acc. Chem. Res.* **2010,** *43*, 1177-1185.

49. Rogow, D. L.; Russell, M. P.; Wayman, L. M.; Swanson, C. H.; Oliver, A. G.; J., O. S. R., *Crystal Growth & Design* **2010,** *10*, 823-829.

50. Perles, J.; Snejko, N.; Iglesia, M.; Monge, M. A., *J. Mater. Chem.* **2009,** *19*, 6504-6511.

51. Li, H.; Eddaoudi, M.; O'Keeffe, M.; Yaghi, O. M., *Nature* **1999,** *402*, 276-279.

52. Ferey, G.; Mellot, C. D.; Serre, C.; Millange, F.; Dutour, J.; Surble, S.; Margiolaki, I., *Science* **2005,** *309*, 2040-2042.

53. Gandara, F.; Perles, J.; Snejko, N.; Iglesia, M.; Gomez-Lor, B.; Gutierrez-puebla, R.; Monge, M. A., *Angew. Chem. Int. Ed.* **2006,** *45*, 7998-8001.

54. Gandara, F.; Puebla, E. G.; Iglesia, M.; Proserpio, D. M.; Snejko, N.; Monge, M. A., *Chem. Mater.* **2009,** *21*, 655-661.

55. Poudret, L.; Prior, T. J.; McIntyre, L. J.; Fogg, A. M., *Chem. Mater.* **2008,** *20*, 7447-7453.

56. Geng, F.; Matsushida, Y.; Ma, R.; Xin, H.; Tanaka, M.; Izumi, F.; Lyi, N.; Sasaki, T., *J. Am. Chem. Soc.* **2008,** *130*, 16344-16350.

57. Geng, F.; Ma, R.; Matsushida, Y.; Liang, J.; Michiue, Y.; Sasaki, T., *Inorg. Chem.* **2011,** *50*, 6667-6672.

58. Lee, K. H.; Byeon, S. H., *Eur. J. Inorg. Chem.* **2009**, 926-936.

59. McIntyre, L. J.; Jackson, L. K.; Fogg, A. M., *J. Phys. Chem. Solids* **2008,** *69*, 1070-1074.

60. McIntyre, L. J.; Jackson, L. K.; Fogg, A. M., *Chem. Mater.* **2008,** *20*, 335-340.

61. Hindocha, S. A.; McIntyre, L. J.; Fogg, A. M., *Inorg. Chem.* **2009,** *48*, 6724-6730.

62. Geng, F.; Xin, H.; Matsushida, Y.; Ma, R.; Tanaka, M.; Izumi, F.; Lyi, N.; Sasaki, T., *Chem. Eur. J.* **2008,** *14*, 9255-9260.

63. Geng, F.; Matsushida, Y.; Ma, R.; Xin, H.; Tanaka, M.; Iyi, N.; Sasaki, T., *Inorg. Chem.* **2009,** *48*, 6724-6730.

64. Liang, J.; Ma, R.; Geng, F.; Ebina, Y.; Sasaki, T., *Chem. Mater.* **2010,** *22*, 6001-6007.

65. Tran, D. T.; Zavalij, P. Y.; Oliver, S. R. J., *J. Am. Chem. Soc.* **2002,** *124*, 3966-3969.

66. Rogow, D. L.; Zapata, G.; Swanson, C. H.; Fan, X.; Campana, C. F.; Oliver, A. G.; Oliver, S. R. J., *Chem. Mater.* **2007,** *19*, 4658-4662.

67. Swanson, C. H.; Shaikh, H. A.; Rogow, D. L.; Oliver, A. G.; Campana, C. F.; Oliver, S. R. J., *J. Am. Chem. Soc.* **2008,** *130*, 11737-11741.

68. Rogow, D. L.; Fei, H.; Brennan, D. P.; Ikehata, M.; Zavalij, P. Y.; Oliver, A. G.; Oliver, S. R. J., *Inorg. Chem.* **2010,** *49*, 5619-5624.

69. Meyn, M.; Beneke, K.; Lagaly, G., *Inorg. Chem.* **1993,** *32*, 1209-1215.

70. Newman, S. P.; Jones, W., *J. Solid State Chem* **1999,** *148*, 26-40.

71. Stahlin, W.; Oswald, H. R., *Acta Cryst. B* **1970,** *26*, 860-861.

72. Nowacki, W.; Scheidegger, R., *Helv. Chim. Acta.* **1952**, 375-376.

73. Louer, M.; Louer, D.; Delgado, A. L.; Martinez, O. G., *Eur. J. Solid State Inorg. Chem.* **1989,** *26*, 241-245.

74. Forster, P. M.; Tafoya, M. M.; Cheetham, A. K., *J. Phys. Chem. Solids* **2004,** *65*, 11-15.

75. Feller, R. K.; Melot, B. C.; Forster, P. M.; Cheetham, A. K., *J. Mater. Chem.* **2009,** *19* 2604-2609.

76. Nicholls, J. L.; Hulse, S. E.; Callear, S. K.; Tizzard, G. J.; Stephenson, R. A.; Hursthouse, M. B.; Clegg, W.; Harrington, R. W.; Fogg, A. M., *Inorg. Chem.* **2010,** *49*, 8545-8551.

77. Besserguenev, A. V.; Fogg, A. M.; Francis, R. J.; Price, S. J.; O'Hare, D.; Isupov, V. P.; Tolochko, B. P., *Chem. Mater.* **1997,** *9*, 241-247.

78. Salami, T. O.; Patterson, S. N.; Jones, V. D.; Masello, A.; Abboud, K. A., *Inorg. Chem. Comm.* **2009,** *12*, 1150-1153.

79. Millet, P.; Bastide, B.; Pashchenko, V.; Gnatchenko, S.; Gapon, V.; Ksari, Y.; Stepanov, A., *J. Mater. Chem.* **2001,** *11*, 1152.

80. Wang, S.; Alekseev, E. V.; Diwu, J. C.; W. H.; Phillips; B. L.; Depmeier, W.; Albrecht-Schmitt, T. E., *Angew. Chem. Int. Ed.* **2010,** *49*, 1057-1060.

81. Goulding, H. V.; Hulse, S. E.; Clegg, W.; Harrington, R. W.; Playford, H. Y.; Walton, R. I.; Fogg, A. M., *J. Am. Chem. Soc.* **2010,** *132*, 13618-13620.

82. Hindocha, S. A.; McIntyre, L. J.; Fogg, A. M., *J. Solid State Chem* **2009,** *182*, 1070-1074.

83. Long, J. R.; Yaghi, O. M., *Chem. Soc. Rev.* **2009,** *38*, 1213-1214.

84. Ni, Z.; O'Keeffe; M.; Yaghi, O. M., *Angew. Chem. Int. Ed.* **2008,** *47*, 5136-5147.

85. Ferey, G., *Chem. Soc. Rev.* **2008,** *37*, 191-214.

86. Kitagawa, S.; Kitaura, R.; Noro, S., *Angew. Chem. Int. Ed.* **2004,** *43*, 2334-2375.

87. Horike, S.; Dinca, M.; Tamaki, K.; Long, J. R., *J. Am. Chem. Soc.* **2008,** *130*, 5854-5855.

88. Wan, C.; Zhao, L.; Mak, T. C. W., *Inorg. Chem.* **2010,** *49*, 97-107.

89. Black, C. A.; Hanton, L. R.; Spicer, M. D., *Inorg. Chem.* **2007,** *46*, 3669-3679.

90. Balamurugan, V.; Mukherjee, R., *Inorg. Chim. Acta* **2006,** *359*, 1376-1382.

91. Custelcean, R.; Moyer, B. A., *Eur. J. Inorg. Chem.* **2007**, 1321-1340.

92. Dalrymple, S. A.; Shimizu, G. K. H., *Chem. Eur. J.* **2002,** *8*, 3010-3015.

93. Sudik, A. C.; Cote, A. P.; Yaghi, O. M., *Inorg. Chem.* **2005,** *44*, 2998-3000.

94. Mulfort, K. L.; Farha, O. K.; Stern, C. L.; Sarjeant, A. A.; Hupp, J. T., *J. Am. Chem. Soc.* **2009,** *131*, 3866-3868.

95. Yuan, G.; Zhu, C.; Liu, Y.; Xuan, W.; Cui, Y., *J. Am. Chem. Soc.* **2009,** *131*, 10452-10460.

96. Vilar, R., *Eur. J. Inorg. Chem.* **2008,** *3*, 357-367.

97. Tang, J.; Costa, J. S.; Pevec, A.; Kozlevcar, B.; Massera, C.; Roubeau, O.; Mutikainen, I.; Turpeinen, U.; Gamez, P.; Reedijk, J., *Cryst. Growth Des.* **2008,** *8*, 1005-1012.

98. Mondal, R.; Basu, T.; Sadhukhan, D.; Chattopadhyay, T.; Bhunia, M. K., *Cryst. Growth Des.* **2009,** *9*, 1095-1105.

99. Diaz, P.; Buchholz, J. B.; Vilar, R.; White, A. J. P., *Inorg. Chem.* **2006,** *45*, 1617-1626.

100. Reichert, W. M.; Holbrey, J. D.; Vigour, K. B.; Morgan, T. D.; Broker, G. A.; Rogers, R. D., *Chem. Commun.* **2006**, 4767-4779.

101. Jin, K.; Huang, X.; Pang, L.; Li, J.; Appel, A.; Wherland, S., *Chem. Commun.* **2002**, 2872-2873.

102. Dybtsev, D. N.; Chun, H.; Kim, K., *Chem. Commun.* **2004**, 1594-1595.

103. Blake, A. J.; Baum, G.; Champness, N. R.; Chung, S. S. M.; Cooke, P. A.; Fenske, D.; Khlobystov, A. N.; Lemenovskii, D. A.; Li, W. S.; Schroder, M., *J. Chem. Soc. Dalton Trans.* **2000**, 4285-4291.

104. Sharma, C. V. K.; Griffin, S. T.; Rogers, R. D., *Chem. Commun.* **1998**, 215-216.

105. Demessence, A.; D'Alessandro, D. M.; Foo, M. L.; Long, J. R., *J. Am. Chem. Soc.* **2009,** *131*, 8784-8786.

106. Hofmeister, F., *Arch. Exp. Pathol. Pharmakol.* **1888,** *24*, 247-250.

107. Khlobystov, A. N.; Champness, N. R.; Roberts, C.; Tendler, S. J. B.; Thompson, C.; Schroder, M., *CrystEngComm* **2002,** *4*, 426-431.

108. Marcus, Y., *J. Chem. Soc., Faraday Trans.* **1991,** *87*, 2995-2999.

109. Roobottom, H. K.; Jenkins, H. D. B.; Passmore, J.; Glasser, L., *J. Chem. Educ.* **1999,** *76*, 1570-1573.

110. Levitskaia, T. G.; Maya, L.; Van Berkel, G. J.; Moyer, B. A., *Inorg. Chem.* **2006,** *46*, 261-272.

111. Fei, H.; Paw, L. U.; Rogow, D. L.; Bresler, M. R.; Abdollahian, Y. A.; Oliver, S. R. J., *Chem. Mater.* **2010,** *22*, 2027-2032.

112. Fei, H.; Rogow, D. L.; Oliver, S. R. J., *J. Am. Chem. Soc.* **2010,** *132*, 7202-7209.

113. Fei, H.; Bresler, M. R.; Oliver, S. R. J., *J. Am. Chem. Soc.* **2011,** *133*, 11110-11113.

114. Hay, B. P.; Firman, T. K.; Moyer, B. A., *J. Am. Chem. Soc.* **2005,** *127*, 1810-1819.

115. Custelcean, R.; Haverlock, T. J.; Moyer, B. A., *Inorg. Chem.* **2006,** *45*, 6446-6452.

116. Feng, J.; Dong, Y.; Salamat-Miller, N.; Middaugh, C. R., *Nucleic Acids Res.* **2008,** *36*, D303-D306.

117. Chen, B.; Wang, L.; Zapata, F.; Qian, G.; Lobkovsky, E. B., *J. Am. Chem. Soc.* **2008,** *130*, 6718-6719.

118. Wong, K. L.; Law, G. L.; Yang, Y. Y.; Wong, W. T., *Adv. Mater.* **2006,** *18*, 1051-1054.

119. Cheetham, A. K.; Rao, C. N. R.; Feller, R. K. *Chem. Commun.* **2006**, 4780–4795.

120. Wu, C. D.; Hu, A.; Zhang, L.; Lin, W. B., *J. Am. Chem. Soc.* **2005,** *127*, 8940-8941.

121. Horike, S.; Dinca, M.; Tamaki, K.; Long, J. R., *J. Am. Chem. Soc.* **2008,** *130*, 5854-5855.

122. Lee, J.; Farha, O. K.; Roberts, J.; Scheidt, K. A.; Nguyen, S. T.; Hupp, J. T., *Chem. Soc. Rev.* **2009,** *38*, 1450-1459.

123. Service, R. F., *Science* **2004,** *305*, 958-961.

124. Murray, L. J.; Dinca, M.; Long, J. R., *Chem. Soc. Rev.* **2009,** *38*, 1294-1314.

125. Kondo, A.; Noguchi, H.; Ohnishi, S.; Kajiro, H.; Tohdoh, A.; Hattori, Y.; Xu, W. C.; Tanaka, H.; Kanoh, H.; Kaneko, K., *Nano Letters* **2006,** *6*, 2581-2584.

126. McIntyre, L. J.; Jackson, L. K.; Fogg, A. M., *Chem. Mater.* **2008,** *20*, 335-340.

127. Vallet-Regi, M.; Balas, F.; Arcos, D., *Angew. Chem. Int. Ed.* **2007,** *46*, 7548-7558.

128. Wight, A. P.; Davis, M. E., *Chem. Rev.* **2002,** *102* (10), 3589-3613.

129. Wang, Z.; Chen, G.; Ding, K. L., *Chem. Rev.* **2009,** *109* (2), 322-359.

130. Henschel, A.; Gedrich, K.; Kraehnert, R.; Kaskel, S., *Chem. Commun.* **2008,** 4192-4194.

131. Alaerts, L.; Seguin, E.; Poelman, H.; Thibault-Starzyk, F.; Jacobs, P. A.; De Vos, D. E., *Chem. Eur. J.* **2006,** *12*, 7353-7363.

132. Sudik, A. C.; Cote, A. P.; Yaghi, O. M., *Inorg. Chem.* **2005,** *44*, 2998-3000.

133. Chen, X. D.; Wan, C. Q.; Sung, H. H. Y.; Williams, I. D.; Mak, T. C. W., *Chem. Eur. J.* **2009,** *15*, 6518-6528.

134. Custelcean, R.; Gorbunova, M. G., *J. Am. Chem. Soc.* **2005,** *127*, 16362-16363.

135. Swanson, C. H.; Shaikh, H. A.; Rogow, D. L.; Oliver, A. G.; Campana, C. F.; Oliver, S. R. J., *J. Am. Chem. Soc.* **2008,** *130*, 11737-11741.

136. Rogow, D. L.; Zapeda, G.; Swanson, C. H.; Fan, X.; Campana, C. F.; Oliver, A. G.; Oliver, S. R. J., *Chem. Mater.* **2007,** *19*, 4658-4662.

137. Tran, D. T.; Zavalij, P. Y.; Oliver, S. R. J., *J. Am. Chem. Soc.* **2002,** *124*, 3966-3969.

138. Gandara, F.; Puebla, E. G.; Iglesias, M.; Proserpio, D. M.; Snejko, N.; Monge, M. A., *Chem. Mater.* **2009,** *21*, 655-661.

139. Oliver, S. R. J., *Chem. Soc. Rev.* **2009,** *38*, 1868-1881.

140. Forster, P. M.; Tafoya, M. M.; Cheetham, A. K., *J. Phys. Chem. Solids* **2004,** *65*, 11-16.

141. Hu, S.; He, K. H.; Zeng, M. H.; Zou, H. H.; Jiang, Y. M., *Inorg. Chem.* **2008,** *47*, 5218-5224.

142. Makinen, S. K.; Melcer, N. J.; Parvez, M.; Shimizu, G. K. H., *Chem. Eur. J.* **2001,** *7*, 5176-5182.

143. Hoffart, D. J.; Dalrymple, S. A.; Shimizu, G. K. H., *Inorg. Chem.* **2005,** *44*, 8868-8875.

144. Ma, J. F.; Yang, J.; Li, S. L.; Song, S. Y., *Cryst. Growth Des.* **2005,** *5*, 807-812.

145. Cote, A. P.; Ferguson, M. J.; Khan, K. A.; Enright, G. D.; Kulynych, A. D.; Dalrymple, S. A.; Shimizu, G. K. H., *Inorg. Chem.* **2002,** *41*, 287-292.

146. Fan, X. J.; Demaree, D. P.; John, J. M. S.; Tripathi, A.; Oliver, S. R. J., *Appl. Phy. Lett.* **2008,** *92*.

147. Nakade, S.; Saito, Y.; Kubo, W.; Kitamura, T.; Wada, Y.; Yanagida, S., *J. Phys. Chem. B* **2003,** *107*, 8607-8611.

148. Seward, C.; Chan, J. L.; Song, D. T.; Wang, S. N., *Inorg. Chem.* **2003,** *42*, 1112-1120.

149. Budka, J.; Lhotak, P.; Stibor, I.; Sykora, J.; Cisarova, I., *Supramolecular Chemistry* **2003,** *15*, 353-357.

150. Aguado, J. E.; Canales, S.; Gimeno, M. C.; Jones, P. G.; Laguna, A.; Villacampa, M. D., *Dalton Trans.* **2005,** 18, 3005-3015.

151. Gu, X. J.; Xue, D. F., *Crys Growth Des.* **2006,** *6*, 2551-2557.

152. Yaghi, O. M.; Li, H. L., *J. Am. Chem. Soc.* **1996,** *118*, 295-296.

153. Gu, X. J.; Xue, D. F., *Inorg. Chem.* **2006,** *45*, 9257-9261.

154. Tsuchiya, T.; Ohmuro, S., *Tetra. Lett.* **2002,** *43*, 611-615.

155. Patel, M. V.; Bell, R.; Majest, S.; Henry, R.; Kolasa, T., *J. Org. Chem.* **2004,** *69*, 7058-7065.

156. Gopinath, R.; Haque, S. J.; Patel, B. K., *J. Org. Chem.* **2002,** *67*, 5842-5845.

157. Wang, B.; Gu, Y. L.; Song, G. Y.; Yang, T.; Yang, L. M.; Suo, J. S., *J. Mol. Catal. A-Chemistry* **2005,** *233*, 121-126.

158. Ren, Y. M.; Cai, C., *Tetra. Lett.* **2008,** *49*, 7110-7112.

159. Wu, J. H.; Hao, S.; Lan, Z.; Lin, J. M.; Huang, M. L.; Huang, Y. F.; Li, P. J.; Yin, S.; Satot, T., *J. Am. Chem. Soc.* **2008,** *130*, 11568-11569.

160. *Perchlorate environmental contamination: toxicological review and risk characterization*. Second external review draft, NCEA-1-0503; U.S. EPA, Office of Research and Development, National Center for Environmental Assessment, U.S. Government Printing Office: Washington, DC, 2002.

161. Urbansky, E. T., *Environ. Sci. Pollut. Res. Int.* **2002,** *9*, 187-192.

162. Castiglioni, S.; Bagnati, R.; Fanelli, R.; Pomati, F.; Calamari, D.; Zuccato, E., *Environ. Sci. Technology* **2006,** *40*, 357-363.

163. Praharaj, S.; Nath, S.; Panigrahi, S.; Ghosh, S. K.; Basu, S.; Pande, S.; Jana, S.; Pal, T., *Inorg. Chem.* **2006,** *45*, 1439-1441.

164. Jana, S.; Praharaj, S.; Panigrahi, S.; Basu, S.; Pande, S.; Chang, C. H.; Pal, T., *Org. Lett.* **2007,** *9*, 2191-2193.

165. Mark, R.; Findley, W. N., *Polymer Eng. Sci.* **1978,** *18*, 6-15.

166. Slade, D. G. E. a. R. C. T., *Layered Double Hydroxides*. X. Duan and D. G. Evans ed.; Springer-Verlag, New York, NY, USA: **2006**; pp. 1-87.

167. Prasanna, S. V.; Kamath, P. V., *Solid State Sci* **2008,** *10*, 260-266.

168. Ma, R. Z.; Liu, Z. P.; Li, L.; Iyi, N.; Sasaki, T., *J. Mater. Chem.* **2006,** *16*, 3809-3813.

169. Goh, K. H.; Lim, T. T.; Dong, Z. L., *Environ. Sci. Technology* **2009,** *43*, 2537-2543.

170. Chibwe, K.; Jones, W., *J. Chem. Soc. Chem. Commun.* **1989,** 14, 926-927.

171. Mackenzie, K. J. D.; Meinhold, R. H.; Sherriff, B. L.; Xu, Z., *Journal of Materials Chemistry* **1993,** *3*, 1263-1269.

172. Hibino, T.; Tsunashima, A., *Chemistry of Materials* **1998,** *10*, 4055-4061.

173. Stanimirova, T. S.; Kirov, G.; Dinolova, E., *Journal of Materials Science Letters* **2001,** *20*, 453-455.

174. Lima, E.; Lasperas, M.; de Menorval, L. C.; Tichit, D.; Fajula, F., *Journal of Catalysis* **2004,** *223*, 28-35.

175. Wang, S.; Alekseev, E. V.; Diwu, J. C.; W. H.; Phillips; B. L.; Depmeier, W.; Albrecht-Schmitt, T. E., *Angew. Chem. Int. Ed.* **2010,** *49*, 1057-1060.

176. Joo, S. H. C., S. J.; Oh, I.; Kwak, J.; Liu, Z.; Terasaki, O.; Ryoo, R., *Nature* **2001,** *412*, 169-172.

177. Lee, J. F., O. K.; Roberts, J.; Scheidt, K. A.; Nguyen, S. T.; Hupp, J. T. , *Chem. Soc. Rev.* **2009,** *38*, 1450-1464.

178. Swanson, C. H.; Shaikh, H. A.; Rogow, D. L.; Oliver, A. G.; Campana, C. F.; Oliver, S. R. J., *J. Am. Chem. Soc.* **2008,** *130*, 11737-11741.

179. Horike, S.; Dinca, M.; Tamaki, K.; Long, J. R., *J. Am. Chem. Soc.* **2008,** *130*, 5854-5855.

180. Chae, H. K.; Siberio-Perez, D. Y.; Kim, J.; Go, Y.; Eddaoudi, M.; Matzger, A. J.; O'Keeffe, M.; Yaghi, O. M., *Nature* **2004,** *427*, 523-527.

181. Murray, L. J.; Dinca, M. L., J. R., *Chem. Soc. Rev.* **2009,** *38*, 1294-1314.

182. Wang, B. C., A. P.; Furukawa, H.; O'Keeffe, M.; Yaghi, O. M., *Nature* **2008,** *453*, 207-211.

183. Banerjee, R. P., A.; Wang, B.; Knobler, C.; Furukawa, H.; O'Keeffe, M.; Yaghi, O. M., *Science* **2008,** *319*, 939-943.

184. Oliver, S. R. J., *Chem. Soc. Rev.* **2009,** *38*, 1868-1881.

185. Custelcean, R.; Moyer, B. A., *Eur. J. Inorg. Chem.* **2007,** 10, 1321-1340.

186. Yaghi, O. M.; Li, H. L.; Groy, T. L., *Inorg. Chem.* **1997,** *36*, 4292-4293.

187. Min, K. S.; Suh, M. P., *J. Am. Chem. Soc.* **2000,** *122*, 6834-6840.

188. Sudik, A. C.; Cote, A. P.; Yaghi, O. M., *Inorg. Chem.* **2005,** *44*, 2998-3000.

189. Du, M.; Zhao, X. J.; Guo, J. H.; Batten, S. R., *Chem. Commun.* **2005,** 4836-4838.

190. Bao, S. S.; Ma, L. F.; Wang, Y.; Fang, L.; Zhu, C. J.; Li, Y. Z.; Zheng, L. M., *Chem. Eur. J.* **2007,** *13*, 2333-2343.

191. Michaelides, A.; Skoulika, S., *Cryst. Growth Des.* **2009,** *9*, 2039-2042.

192. Chen, X. D.; Wan, C. Q.; Sung, H. H. Y.; Williams, I. D.; Mak, T. C. W., *Chem. Eur. J.* **2009,** *15*, 6518-6528.

193. Fei, H.; Paw, L. U.; Rogow, D. L.; Bresler, M. R.; Abdollahian, Y. A.; Oliver, S. R. J., *Chem. Mater.* **2010,** *22*, 2027-2032.

194. Wang, Y. F. G., H. Z., *J. Colloid. Interface Sci.* **2006,** *301*, 19-26.

195. *SHELXTL Crystal Structure Determination Package*. Bruker Analytical X-ray Systems Inc.: Madison, WI, 1995-99.

196. Lucassen, A. C. B. K., A.; Leitus, G.; Shimon, L. J. W.; Martin, J. M. L.; van der Boon, M. E., *Crys. Growth Des.* **2007,** *7*, 386-392.

197. *Cambridge Structural Database*. A covalent Sb-O bond length is generally between 1.9 Å and 2.1 Å, while 90.8% Sb-O bonds with a bond length less than 2.27 Å.

198. Wu, M. Y.; Yuan, D. Q.; Han, L.; Wu, B. L.; Xu, Y. Q.; Hong, M. C., *Eur. J. Inorg. Chem.* **2006,** 526-530.

199. Ju, J.; Lin, J. H.; Li, G. B.; Yang, T.; Li, H. M.; Liao, F. H.; Loong, C. K.; You, L. P., *Angew. Chem. Int. Ed.* **2003,** *42*, 5607-5610.

200. Liu, S. X.; Xie, L. H.; Gao, B.; Zhang, C. D.; Sun, C. Y.; Li, D. H.; Su, Z. M., *Chem. Commun.* **2005,** *40*, 5023-5025.

201. Yu, J. H.; Xu, R. R.; Chen, J. S.; Yue, Y., *J. Mater. Chem.* **1996,** *6*, 465-468.

202. Ok, K. M. H., P. S., *Inorg. Chem.* **2002,** *41*, 3805-3807.

203. Tran, D. T.; Zavalij, P. Y.; Oliver, S. R. J., *J. Am. Chem. Soc.* **2002,** *124*, 3966-3969.

204. Rogow, D. L.; Russell, M. P.; Wayman, L. M.; Swanson, C. H.; Oliver, A. G.; J., O. S. R., *Cryst. Growth Des.* **2010,** *10*, 823-829.

205. Yaghi, O. M.; Li, H. L., *J. Am. Chem. Soc.* **1996,** *118*, 295-296.

206. Wang, L. S.; Zhang, J. F.; Yang, S. P., *Acta Cryst. Sect. E* **2004,** *E60*, m1484-m1486.

207. Yaghi, O. M.; Li, H., *J. Am. Chem. Soc.* **1995,** *117*, 10401-10402.

208. Zhang, J. K., Y.; Wen, Y.; Li, Z.; Qin, Y.; Cheng, J.; Yao, Y.;, *Acta Cryst. Sect. E* **2004,** *E60*, m504-m505.

209. Banik, B. K. C., M.; Marquez, J.; Cardona, M., *Tetra. Lett.* **2005,** *46*, 2341-2343.

210. Ren, Y. M. C., C., *Tetra. Lett.* **2008,** *49*, 7110-7112.

211. Spek, A. L., *PLATON, A Multipurpose Crystallographic Tool*. Utrecht, The Netherland, 2007.

234. Cheetham, A. K.; Rao, C. N. R.; Feller, R. K., *Chem. Commun.* **2006**, 4780-4795.

235. Ni, Z.; O'Keeffe; M.; Yaghi, O. M., *Angew. Chem. Int. Ed.* **2008,** *47*, 5136-5147.

236. Ferey, G., *Chem. Soc. Rev.* **2008,** *37*, 191-214.

237. Eddaoudi, M.; Moler, D. B.; Li, H.; Chen, B.; Reineke, T. M.; O'Keeffe, M.; Yaghi, O. M., *Acc. Chem. Res.* **2001,** *34*, 319-330.

238. Kitagawa, S.; Kitaura, R.; Noro, S., *Angew. Chem. Int. Ed.* **2004,** *43*, 2334-2375.

239. Morris, R. E.; Wheatley, P. S., *Angew. Chem. Int. Ed.* **2008,** *47*, 4966.

240. Murray, L. J.; Dinca, M.; Long, J. R., *Chem. Soc. Rev.* **2009,** *38*, 1294-1314.

241. Banerjee, R. P., A.; Wang, B.; Knobler, C.; Furukawa, H.; O'Keeffe, M.; Yaghi, O. M., *Science* **2008,** *319*, 939-943.

242. Matsuda, R.; Kitaura, R.; Kitagawa, S.; Kawazoe, Y.; Mita, Y., *Nature* **2005,** *436*, 238-241.

243. Dybtsev, D. N.; Chun, H.; Yoon, S. H.; Kim, D.; Kim, K., *J. Am. Chem. Soc.* **2004,** *126*, 32-33.

244. Li, J.-R.; Kuppler, R. J.; Zhou, H.-C., *Chem. Soc. Rev.* **2009,** *38*, 1477-1504.

245. Hwang, Y. K.; Hong, D. Y.; Chang, J. S.; H.;, J. S.; Seo, Y. K.; Kim, J.; Vimont, A.; Daturi, M.; Serre, C.; Ferey, G., *Angew. Chem. Int. Ed.* **2008,** *47*, 4144-4148.

246. Lee, J. F., O. K.; Roberts, J.; Scheidt, K. A.; Nguyen, S. T.; Hupp, J. T. , *Chem. Soc. Rev.* **2009,** *38*, 1450.

247. Horike, S.; Dinca, M.; Tamaki, K.; Long, J. R., *J. Am. Chem. Soc.* **2008,** *130*, 5854-5855.

248. Seo, J. S.; Whang, D.; Lee, H.; Jun, S. I.; Oh, J.; Jeon, Y. J.; Kim, K., *Nature* **2000,** *404*, 982-986.

249. Cho, S. H.; Ma, B.; Nguyen, S. T.; Hupp, J. T.; Albrecht-Schmitt, T. E., *Chem. Commun.* **2006**, 2563-2565.

250. Allendorf, M. D. H., R. J. T.; Andruszkiewicz, L.; Talin, A. A.; Pikarsky, J.; Choudhury, A.; Gall, K. A.; Hesketh, P. J., *J. Am. Chem. Soc.* **2008,** *130*, 14404-14405.

251. Albrecht, M.; Lutz, M.; Spek, A. L.; van Koten, G., *Nature* **2000,** *406*, 970.

252. Chen, B.; Yang, Y.; Zapata, F.; Lin, G.; Qian, G.; Lobkovsky, E. B., *Adv. Mater.* **2007,** *19*, 1693-1696.

253. Wang, Z.; Cohen, S. M., *Chem. Soc. Rev.* **2009,** *38*, 1315-1329.

254. Chui, S. S.; Lo, S. M.; Charmant, J. P.; Orpen, A. G.; Williams, I. D., *Science* **1999,** *283*, 1148-1150.

255. Song, Y. F.; Cronin, L., *Angew. Chem. Int. Ed.* **2008,** *47*, 4635-4637.

256. Ingleson, M. J.; Barrio, J. P.; Bacsa, J.; Dickinson, C.; Park, H.; Rosseinsky, M. J., *Chem. Commun.* **2008**, 1287-1289.

257. Vimont, A.; Goupil, J.-M.; Lavalley, J.-C.; Daturi, M.; Surble, S.; Serre, C.; Millange, F.; Ferey, G.; Audebrand, N., *J. Am. Chem. Soc.* **2006,** *128*, 3218-3227.

258. Oliver, S. R. J., *Chem. Soc. Rev.* **2009,** *38*, 1868-1881.

259. Fei, H.; Rogow, D. L.; Oliver, S. R. J., *J. Am. Chem. Soc.* **2010,** *132*, 7202-7209.

260. Fei, H.; Paw, L. U.; Rogow, D. L.; Bresler, M. R.; Abdollahian, Y. A.; Oliver, S. R. J., *Chem. Mater.* **2010,** *22*, 2027-2032.

261. Swanson, C. H.; Shaikh, H. A.; Rogow, D. L.; Oliver, A. G.; Campana, C. F.; Oliver, S. R. J., *J. Am. Chem. Soc.* **2008,** *130*, 11737-11741.

262. Tran, D. T.; Zavalij, P. Y.; Oliver, S. R. J., *J. Am. Chem. Soc.* **2002,** *124*, 3966-3969.

263. Rogow, D. L.; Russell, M. P.; Wayman, L. M.; Swanson, C. H.; Oliver, A. G.; J., O. S. R., *Crystal Growth & Design* **2010,** *10*, 823-829.

264. Tran, D. T.; Chernova, N. A.; Chu, D.; Oliver, A. G.; Oliver, S. R. J., *Crystal Growth & Design* **2010,** *10*, 874-879.

265. Allendorf, M. D.; Bauer, C. A.; Bhakta, R. K.; Houk, R. J. T., *Chem. Soc. Rev.* **2008,** *38*, 1330-1352.

266. Bauer, C. A.; Timofeeva, T. V. S., T. B.; Patterson, B. D.; Liu, V. H.; Simmons, B. A.; Allendorf, M. D., *J. Am. Chem. Soc.* **2007,** *129*, 7136-7144.

267. Xue, M.; Zhu, G. Z., Y.; Fang, Q.; Hewitt, I. J.; Qiu, S.;, *Crystal Growth & Design* **2008,** *8*, 427-434.

268. Bordiga, S.; Lamberti, C.; Ricchiardi, G.; Regli, L.; Bonino, F.; Damin, A.; Lillerud, K. P.; Bjorgen, M.; Zecchina, A., *Chem. Commun.* **2004**, 2300-2301.

269. Fang, Q.; Zhu, G. Z., Y.; Fang, Q.; Hewitt, I. J.; Qiu, S.;; Xue, M.; Sun, J.; Sun, F.; Qiu, S., *Inorg. Chem.* **2006,** *45*, 3582-3587.

270. Wang, M.; Guo, S. L., Y.; Cai, L.; Zou, J.; Xu, G.; Zhou, W.; Zheng, F.; Guo, G.;, *J. Am. Chem. Soc.* **2009,** *131*, 13572-23573.

271. Liao, Y.-C.; Lin, C.-H.; Wang, S.-L., *J. Am. Chem. Soc.* **2005,** *127*, 9986-9987.

272. Wang, M.-S.; Guo, G.-C.; Chen, W.; Xu, G.; Zhou, W. W.; Wu, K.; Huang, J.-S., *Angew. Chem. Int. Ed.* **2007,** *46*, 3909-3911.

273. Chen, B.; Wang, L.; Zapata, F.; Qian, G.; Lobkovsky, E. B., *J. Am. Chem. Soc.* **2008,** *130*, 6718-6719.

274. McGarrah, J. E.; Kim, Y. J. H., M.; Eisenberg, R., *Inorg. Chem.* **2001,** *40*, 4510-4511.

275. Bai, Y.; He, G. Z., Y.; Duan, C.; Dang, D.; Meng, Q.;, *Chem. Commun.* **2006**, 1530-1533.

276. Wu, Q.; Esteghamatian, M. H., N.; Popovic, Z.; Enright, G.; Tao, Y.; D'lorio, M.; Wang, S.;, *Chem. Mater.* **2000,** *12*, 79-83.

277. *APEX-II, 2.1.4;*. Bruker-AXS: Madison, WI, 2007.

278. *SHELXTL Crystal Structure Determination Package*. Bruker Analytical X-ray Systems Inc.: Madison, WI, 1995-99.

279. Klaus Brandenburg; H. P. Diamond; Crystal-Impact: Germany, **2007**.

280. *Cambridge Crystal Structure Database*. Bond length of Cu-O: mean=2.062 Å, median=1.958 Å, standard deviation=0.204 Å. 93.4 % of the bond length is shorter than 2.4 Å.

281. Rogow, D. L.; Zapata, G.; Swanson, C. H.; Fan, X.; Campana, C. F.; Oliver, A. G.; Oliver, S. R. J., *Chem. Mater.* **2007,** *19*, 4658-4662.

282. Wang, S.; Alekseev, E. V.; Diwu, J. C.; W. H.; Phillips; B. L.; Depmeier, W.; Albrecht-Schmitt, T. E., *Angew. Chem. Int. Ed.* **2010,** *49* (6), 1057-1060.

283. Doty, F. P.; Bauer, C. A. S., A. J.; Grant, P. G.; Allendorf, M. D.;, *Adv. Mater.* **2008,** *20*, 1-7.

284. de Lill, D. T.; de Bettencourt-Dias, A.; Cahill, C. L., *Inorg. Chem.* **2007,** *46*, 3960-3965.

285. Lu, W.-G.; Jiang, L.; Feng, X.-L.; Lu, T.-B., *Crystal Growth & Design* **2006,** *6*, 564-571.

286. Keith, L. H.; Teillard, W. A., *Environ. Sci. Technol.* **1979,** *13*, 416.

287. Hogue, C., *Chemical & Engineering News* **2011,** *89*, 6.

288. Wang, Y.; Bryan, C.; Gao, H.; Phol, P. I.; Brinker, C. J.; Yu, K.; Xu, H.; Yang, Y.; Braterman, P. S.; Xu, Z., *Sandia Report (Potential Applications of Nanostructured Materials in Nuclear Waste Management* **2003,** *SAND2003-3313*, 1-95.

289. Izak, P.; Hrma, P.; Arey, B. W.; Plaisted, T. J., *J. Non-Cryst. Solids* **2001,** *289*, 17-29.

290. Wu, M.; Janssen, S., *Environ. Sci. Technol.* **2011,** *45*, 366-367.

291. Mark, R.; Findley, W. N., *Polym. Eng. Sci.* **1978,** *18*, 6-15.

292. Rives, V., *LDHs: Layered Double Hydroxides: Present and Future*. Nova Science Publishers Inc., Hauppauge, New York, USA: **2001**.

293. Slade, D. G. E. a. R. C. T., *Layered Double Hydroxides*. X. Duan and D. G. Evans ed.; Springer-Verlag, New York, NY, USA: **2006**; pp 1-87.

294. Goh, K. H.; Lim, T. T.; Dong, Z., *Water Res.* **2008,** *42*, 1343-1368.

295. Tran, D. T.; Zavalij, P. Y.; Oliver, S. R. J., *J. Am. Chem. Soc.* **2002,** *124*, 3966-3969.

296. Swanson, C. H.; Shaikh, H. A.; Rogow, D. L.; Oliver, A. G.; Campana, C. F.; Oliver, S. R. J., *J. Am. Chem. Soc.* **2008,** *130*, 11737-11741.

297. Rogow, D. L.; Russell, M. P.; Wayman, L. M.; Swanson, C. H.; Oliver, A. G.; J., O. S. R., *Crystal Growth & Design* **2010,** *10*, 823-829.

298. Oliver, S. R. J., *Chem. Soc. Rev.* **2009,** *38*, 1868-1881.

299. Gandara, F.; Perles, J.; Snejko, N.; Iglesias, M.; Gomez-Lor, B.; Gutierrez-Puebla, E.; Monge, M. A., *Angew. Chem., Int. Ed.* **2006,** *45*, 7998-8001.

300. McIntyre, L. J.; Jackson, L. K.; Fogg, A. M., *Chem. Mater.* **2008,** *20*, 335-340.

301. Geng, F.; Matsushita, Y.; Ma, R.; Xin, H.; Tanaka, M.; Izumi, F.; Iyi, N.; Sasaki, T., *J. Am. Chem. Soc.* **2008,** *130*, 16344-16350.

302. Geng, F.; Ma, R.; Sasaki, T., *Acc. Chem. Res.* **2010,** *43*, 1177-1185.

303. Wang, S.; Alekseev, E. V.; Diwu, J. C.; W. H.; Phillips; B. L.; Depmeier, W.; Albrecht-Schmitt, T. E., *Angew. Chem. Int. Ed.* **2010,** *49*, 1057-1060.

304. Goulding, H. V.; Hulse, S. E.; Clegg, W.; Harrington, R. W.; Playford, H. Y.; Walton, R. I.; Fogg, A. M., *J. Am. Chem. Soc.* **2010,** *132*, 13618-13620.

305. Hu, M.; Jiang, J.-S.; Li, X., *Cryst. Growth Des.* **2009,** *9*, 820-824.

306. *Cambridge Crystal Structure Database*. Bond length of Cu-O: mean=2.062 Å, median=1.958 Å, standard deviation=0.204 Å. 93.4 % of the bond length is shorter than 2.4 Å.

307. Prout, C. K.; Carruthers, J. R.; Rossotti, F. J. C., *J. Chem. Soc. A* **1971**, 554-556.

308. Epstein, J. M.; Figgis, B. N.; White, A. H.; Willis, A. C., *J. Chem. Soc., Dalton Trans.* **1974**, 1954-1961.

309. Yamanaka, M.; Uekusa, H.; Ohba, S.; Saito, Y.; Iwata, S.; Kato, M.; Tokii, T.; Muto, Y.; Steward, O. W., *Acta Cryst.* **1991,** *B47*, 344-355.

310. Miller, J. H.; Powell, J. E.; Jacobson, R. A.; Kulprathipanja, S., *Inorg. Chim. Acta* **1976,** *18*, 25-28.

311. Spek, A. L., *PLATON, A Multipurpose Crystallographic Tool*. Utrecht, The Netherland, **2007**.

312. Darab, J. G.; Smith, P. A., *Chem. Mater.* **1996,** *8*, 1004-1021.

313. Darab, J. G.; Amonette, A. B.; Burke, D. S. D.; Orr, R. D.; Ponder, S. M.; Schrick, B.; Mallouk, T. M.; Lukens, W. W.; Caulder, D. L.; Shuh, D. K., *Chem. Mater.* **2007,** *19*, 5703-5713.

314. Centi, G.; Perathoner, S., *Microporous Mesoporous Mater.* **2008,** *107*, 3-15.

315. Cardoso, P. L.; Barros, J.; Valim, J., *J. Phys. Chem. Solids* **2006,** *67*, 987-993.

316. Ferreira, O. P.; Alves, O. L.; Gouveia, X.; Souza-Filho, A. G.; de Pavia, J. A. C.; Filho, J. M., *J. Solid State Chem* **2004,** *177*, 3058-3069.

317. Keith, L. H.; Teillard, W. A., *Environ. Sci. Technol.* **1979,** *13*, 416.

318. Hogue, C., *Chemical & Engineering News* **2011,** *89*, 6.

319. Oliver, S. R. J., *Chem. Soc. Rev.* **2009,** *38*, 1868-1881.

320. Fei, H.; Rogow, D. L.; Oliver, S. R. J., *J. Am. Chem. Soc.* **2010,** *132*, 7202-7209.

321. Fei, H.; Bresler, M. R.; Oliver, S. R. J., *J. Am. Chem. Soc.* **2011,** *133*, 11110-11113.

322. Fei, H.; Oliver, S. R. J., *Angew. Chem. Int. Ed.* **2011,** *50*, 9066-9070.

323. Wang, S.; Alekseev, E. V.; Diwu, J. C.; W. H.; Phillips; B. L.; Depmeier, W.; Albrecht-Schmitt, T. E., *Angew. Chem. Int. Ed.* **2010,** *49*, 1057-1060.

324. Custelcean, R.; Moyer, B. A., *Eur. J. Inorg. Chem.* **2007**, 1321-1340.

325. Custelcean, R.; Jiang, D.; Hay, B. P.; Luo, W.; Gu, B., *Cryst. Growth Des.* **2008,** *8*, 1909-1915.

326. Custelcean, R.; Bock, A.; Moyer, B. A., *J. Am. Chem. Soc.* **2010,** *132*, 7177-7185.

327. Wu, M.; Janssen, S., *Environ. Sci. Technol.* **2011,** *45*, 366-367.

328. Mark, R.; Findley, W. N., *Polym. Eng. Sci.* **1978,** *18*, 6-15.

329. Bedner, M.; Maccrehan, W. A., *Environ Sci Technol* **2006,** *40* (2), 516-522.

330. Geng, F.; Ma, R.; Sasaki, T., *Acc. Chem. Res.* **2010,** *43*, 1177-1185.

331. Rives, V., *LDHs: Layered Double Hydroxides: Present and Future*. Nova Science Publishers Inc., Hauppauge, New York, USA: 2001.

332. Slade, D. G. E. a. R. C. T., *Layered Double Hydroxides*. X. Duan and D. G. Evans ed.; Springer-Verlag, New York, NY, USA: 2006; p 1-87.

333. Gandara, F.; Perles, J.; Snejko, N.; Iglesia, M.; Gomez-Lor, B.; Gutierrez-puebla, R.; Monge, M. A., *Angew. Chem. Int. Ed.* **2006,** *45*, 7998-8001.

334. Gandara, F.; Puebla, E. G.; Iglesia, M.; Proserpio, D. M.; Snejko, N.; Monge, M. A., *Chem. Mater.* **2009,** *21*, 655-661.

335. McIntyre, L. J.; Jackson, L. K.; Fogg, A. M., *Chem. Mater.* **2008,** *20*, 335-340.

336. Poudret, L.; Prior, T. J.; McIntyre, L. J.; Fogg, A. M., *Chem. Mater.* **2008,** *20*, 7447-7453.

337. Geng, F.; Xin, H.; Matsushida, Y.; Ma, R.; Tanaka, M.; Izumi, F.; Lyi, N.; Sasaki, T., *Chem. Eur. J.* **2008,** *14*, 9255-9260.

338. Geng, F.; Matsushida, Y.; Ma, R.; Xin, H.; Tanaka, M.; Izumi, F.; Lyi, N.; Sasaki, T., *J. Am. Chem. Soc.* **2008,** *130*, 16344-16350.

339. Goh, K. H.; Lim, T. T.; Dong, Z., *Water Res.* **2008,** *42*, 1343-1368.

340. Tran, D. T.; Zavalij, P. Y.; Oliver, S. R. J., *J. Am. Chem. Soc.* **2002,** *124*, 3966-3969.

341. Rogow, D. L.; Russell, M. P.; Wayman, L. M.; Swanson, C. H.; Oliver, A. G.; J., O. S. R., *Crystal Growth & Design* **2010,** *10*, 823-829.

342. Swanson, C. H.; Shaikh, H. A.; Rogow, D. L.; Oliver, A. G.; Campana, C. F.; Oliver, S. R. J., *J. Am. Chem. Soc.* **2008,** *130*, 11737-11741.

343. Min, K. S.; Suh, M. P., *J. Am. Chem. Soc.* **2000,** *122*, 6834-6840.

344. Du, M.; Zhao, X. J.; Guo, J. H.; Batten, S. R., *Chem. Commun.* **2005**, 4836-4838.

345. Michaelides, A.; Skoulika, S., *Cryst. Growth Des.* **2009,** *9*, 2039-2042.

346. Wang, Z.; Cohen, S. M., *Chem. Soc. Rev.* **2009,** *38*, 1315-1329.

347. Tanabe, K. K.; Cohen, S. M., *Chem. Soc. Rev.* **2011,** *40*, 498-519.

348. Cohen, S. M., *Chem. Rev.* **2012,** *112*, 970-1000.

349. Burnett, B. J.; Barron, P. M.; Hu, C.; Choe, W., *J. Am. Chem. Soc.* **2011,** *133*, 9984-9987.

350. Kim, M.; Cahill, J. F.; Su, Y.; Prather, K. A.; Cohen, S. M., *Chem. Sci.* **2012,** *3*, 126-130.

351. Rogow, D. L.; Zapata, G.; Swanson, C. H.; Fan, X.; Campana, C. F.; Oliver, A. G.; Oliver, S. R. J., *Chem. Mater.* **2007,** *19*, 4658-4662.

352. *APEX-II, 2.1.4;*. Bruker-AXS: Madison, WI, 2007.

353. *SHELXTL Crystal Structure Determination Package*. Bruker Analytical X-ray Systems Inc.: Madison, WI, 1995-99.

354. Klaus Brandenburg; H. P. Diamond; Crystal-Impact: Germany, **2007**.

355. Cote, A. P.; Shimizu, G. K. H., *Coord. Chem. Rev.* **2003,** *245*, 49-64.

356. Shimizu, G. K. H.; Vaidhyanathan, R.; Taylor, J. M., *Chem. Soc. Rev.* **2009,** *38*, 1430-1449.

357. Ferey, G., *Chem. Soc. Rev.* **2008,** *37*, 191-214.

358. Long, J. R.; Yaghi, O. M., *Chem. Soc. Rev.* **2009,** *38*, 1213-1214.

359. Cheetham, A. K.; Rao, C. N. R.; Feller, R. K., *Chem. Commun.* **2006**, 4780-4795.

360. Meek, S. T.; Greathouse, J. A.; Allendorf, M. D., *Adv. Mater.* **2011,** *23*, 249-267.

361. Wight, A. P.; Davis, M. E., *Chem. Rev.* **2002,** *102*, 3589-3614.

362. Cheetham, A. K.; Rao, C. N. R., *Science* **2007,** *318*, 58.

363. Eddaoudi, M.; Moler, D. B.; Li, H.; Chen, B.; Reineke, T. M.; O'Keeffe, M.; Yaghi, O. M., *Acc. Chem. Res.* **2001,** *34*, 319-330.

364. Banerjee, R. P., A.; Wang, B.; Knobler, C.; Furukawa, H.; O'Keeffe, M.; Yaghi, O. M., *Science* **2008,** *319*, 939-943.

365. Kitagawa, S.; Kitaura, R.; Noro, S., *Angew. Chem. Int. Ed.* **2004,** *43*, 2334-2375.

366. Li, J.-R.; Kuppler, R. J.; Zhou, H.-C., *Chem. Soc. Rev.* **2009,** *38*, 1477-1504.

367. Clearfield, A., *Chem. Mater.* **1998,** *10,* 2801-2810.

368. Feng, P.; Bu, X.; Zheng, N., *Acc. Chem. Res.* **2005,** *38*, 293-303.

369. Falcao, E. H. L.; Naraso; Feller, R. K.; Wu, G.; Wudl, F.; Cheetham, A. K., *Inorg. Chem.* **2008,** *47*, 8336-8342.

370. Thirumurugan, A.; Sanguramath, R. A.; Rao, C. N. R., *Inorg. Chem.* **2008,** *47*, 823-831.

371. Merrill, C. A.; Cheetham, A. K., *Inorg. Chem.* **2005,** *44,* 5273-5277.

372. Rao, C. N. R.; Cheetham, A. K.; Thirumurugan, R., *J. Phys. Condens. Matter* **2008,** *20*, 083202.

373. Oliver, S. R. J., *Chem. Soc. Rev.* **2009,** *38*, 1868-1881.

374. Tran, D. T.; Zavalij, P. Y.; Oliver, S. R. J., *J. Am. Chem. Soc.* **2002,** *124*, 3966-3969.

375. Rogow, D. L.; Russell, M. P.; Wayman, L. M.; Swanson, C. H.; Oliver, A. G.; J., O. S. R., *Crystal Growth & Design* **2010,** *10*, 823-829.

376. Swanson, C. H.; Shaikh, H. A.; Rogow, D. L.; Oliver, A. G.; Campana, C. F.; Oliver, S. R. J., *J. Am. Chem. Soc.* **2008,** *130*, 11737-11741.

377. Fei, H.; Oliver, S. R. J., *Angew. Chem. Int. Ed.* **2011,** *50*, 9066-9070.

378. Rogow, D. L.; Zapata, G.; Swanson, C. H.; Fan, X.; Campana, C. F.; Oliver, A. G.; Oliver, S. R. J., *Chem. Mater.* **2007,** *19*, 4658-4662.

379. Tran, D. T.; Chernova, N. A.; Chu, D.; Oliver, A. G.; Oliver, S. R. J., *Crystal Growth & Design* **2010,** *10*, 874-879.

380. Forster, P. M.; Cheetham, A. K., *Angew. Chem. Int. Ed.* **2002,** *41*, 457-461.

381. Guillou, N.; Livage, C.; Drillon, M.; Ferey, G., *Angew. Chem. Int. Ed.* **2003,** *42*, 5314-5318.

382. Zhang, J.; Chen, S.; Valle, H.; Wong, M.; Austria, C.; Cruz, M.; Bu, X., *J. Am. Chem. Soc.* **2007,** *129*, 14168-14169.

383. Zhang, L.; Li, Z.-J.; Lin, Q.-P.; Qin, Y.-Y.; Zhang, J.; Yin, P.-X.; Cheng, J.-K.; Yao, Y.-G., *Inorg. Chem.* **2009,** *48*, 6517-6525.

384. Ferey, G.; Millange, F.; Morcrette, M.; Serre, C.; Doublet, M. L.; Greneche, J. M.; Tarascon, J. M., *Angew. Chem. Int. Ed.* **2007,** *46*, 3259-3264.

385. Livage, C.; Egger, C.; Ferey, G., *Chem. Mater.* **2001,** *13*, 410-414.

386. Guillou, N.; Gao, Q. M.; Nogues, M.; Morris, R. E.; Hervieu, M.; Ferey, G.; Cheetham, A. K., *C. R. Acad. Sci. Paris* **1999,** *2*, 387.

387. Guillou, N.; Gao, Q. M.; Forster, P. M.; Chang, J. S.; Park, S. E.; Ferey, G.; Cheetham, A. K., *Angew. Chem. Int. Ed.* **2001,** *40*, 2831-2835.

388. Forster, P. M.; Eckert, J.; Chang, J. S.; Park, S. E.; Ferey, G.; Cheetham, A. K., *J. Am. Chem. Soc.* **2003,** *125*, 1309-1312.

389. Liu, S. J.; Cheng, H. Y.; Zhao, F. Y.; Gong, J. Y.; Yu, S. H., *Chem. Eur. J.* **2008,** *14*, 4074-4081.

390. *APEX-II, 2.1.4;*. Bruker-AXS: Madison, WI, 2007.

391. *SHELXTL Crystal Structure Determination Package*. Bruker Analytical X-ray Systems Inc.: Madison, WI, 1995-99.

392. Klaus Brandenburg; H. P. Diamond; Crystal-Impact: Germany, **2007**.

393. Guillou, N.; Livage, C.; van Beek, W.; Nogues, M.; Ferey, G., *Angew. Chem. Int. Ed.* **2003,** *42*, 643-647.

394. Spek, A. L., *PLATON, A Multipurpose Crystallographic Tool*. Utrecht, The Netherland, 2007.

395. Berger, K., *Coordination Chemistry: Experimental Methods*. Butterworth, London, 1973.

396. P. Nozar; V. Sechovský; V. Kamberský, *Journal of Magnetism and Magnetic Materials* **1987,** *69*, 71-78.

397. Thomas, J. M., *Sci. Am.* **1992,** *1992*, 112-115.

398. Wight, A. P.; Davis, M. E., *Chem. Rev.* **2002,** *102*, 3589-3614.

399. Davis, M. E., *Nature* **2002,** *417*, 813-821.

400. Corma, A., *J. Catal.* **2003,** *216*, 298-312.

401. Keith, L. H.; Teillard, W. A., *Environ. Sci. Technol.* **1979,** *13*, 416.

402. Hogue, C., *Chemical & Engineering News* **2011,** *89*, 6.

403. Weitkamp, J., *Solid State Ionics* **2000,** *131*, 175-188.

404. Wu, M.; Janssen, S., *Environ. Sci. Technol.* **2011,** *45*, 366-367.

405. Rives, V., *LDHs: Layered Double Hydroxides: Present and Future*. Nova Science Publishers Inc., Hauppauge, New York, USA: **2001**.

406. Slade, D. G. E. a. R. C. T., *Layered Double Hydroxides*. X. Duan and D. G. Evans ed.; Springer-Verlag, New York, NY, USA: **2006**; pp 1-87.

407. Rao, K. K.; Gravelle, M.; Valente, J. S.; Figueras, F., *J. Catal.* **1997,** *173*, 115-121.

408. Geng, F.; Ma, R.; Sasaki, T., *Acc. Chem. Res.* **2010,** *43*, 1177-1185.

409. Geng, F.; Matsushida, Y.; Ma, R.; Xin, H.; Tanaka, M.; Izumi, F.; Lyi, N.; Sasaki, T., *J. Am. Chem. Soc.* **2008,** *130*, 16344-16350.

410. Liu, Z.; Ma, R.; Osada, M.; Iyi, N.; Ebina, Y.; Takada, K.; Sasaki, T., *J. Am. Chem. Soc.* **2006,** *128*, 4872-4880.

411. Poudret, L.; Prior, T. J.; McIntyre, L. J.; Fogg, A. M., *Chem. Mater.* **2008,** *20*, 7447-7453.

412. McIntyre, L. J.; Jackson, L. K.; Fogg, A. M., *Chem. Mater.* **2008,** *20*, 335-340.

413. Gandara, F.; Perles, J.; Snejko, N.; Iglesia, M.; Gomez-Lor, B.; Gutierrez-puebla, R.; Monge, M. A., *Angew. Chem. Int. Ed.* **2006,** *45*, 7998-8001.

414. Liang, J.; Ma, R.; Geng, F.; Ebina, Y.; Sasaki, T., *Chem. Mater.* **2010,** *22*, 6001-6007.

415. Oliver, S. R. J., *Chem. Soc. Rev.* **2009,** *38*, 1868-1881.

416. Tran, D. T.; Zavalij, P. Y.; Oliver, S. R. J., *J. Am. Chem. Soc.* **2002,** *124*, 3966-3969.

417. Rogow, D. L.; Russell, M. P.; Wayman, L. M.; Swanson, C. H.; Oliver, A. G.; J., O. S. R., *Crystal Growth & Design* **2010,** *10*, 823-829.

418. Swanson, C. H.; Shaikh, H. A.; Rogow, D. L.; Oliver, A. G.; Campana, C. F.; Oliver, S. R. J., *J. Am. Chem. Soc.* **2008,** *130*, 11737-11741.

419. Fei, H.; Oliver, S. R. J., *Angew. Chem. Int. Ed.* **2011,** *50*, 9066-9070.

420. Rogow, D. L.; Fei, H.; Brennan, D. P.; Ikehata, M.; Zavalij, P. Y.; Oliver, A. G.; Oliver, S. R. J., *Inorg. Chem.* **2010,** *49*, 5619-5624.

421. Fei, H.; Pham, C. H.; Oliver, S. R. J., *J. Am. Chem. Soc.* **2012,** *134*, DOI: 10.1021/ja3017686.

422. Kaduk, J. A.; Toft, M. A.; Golab, J. T., *Powder Diffraction* **2009,** *25*, 19-24.

423. Sykora, R. E.; King, J. E.; Illies, A. J.; Albrecht-Schmitt, T. E., *J. Solid State Chem* **2004,** *177*, 1717-1722.

424. Wang, S.; Alekseev, E. V.; Diwu, J. C.; W. H.; Phillips; B. L.; Depmeier, W.; Albrecht-Schmitt, T. E., *Angew. Chem. Int. Ed.* **2010,** *49*, 1057-1060.

425. Goulding, H. V.; Hulse, S. E.; Clegg, W.; Harrington, R. W.; Playford, H. Y.; Walton, R. I.; Fogg, A. M., *J. Am. Chem. Soc.* **2010,** *132*, 13618-13620.

426. *APEX-II, 2.1.4;*. Bruker-AXS: Madison, WI, 2007.

427. *SHELXTL Crystal Structure Determination Package*. Bruker Analytical X-ray Systems Inc.: Madison, WI, 1995-99.

428. Klaus Brandenburg; H. P. Diamond; Crystal-Impact: Germany, **2007**.

429. $[Sb_6O_7][(SO_4)_2]$ (SLUG-34): colorless needle-like crystal dimensions 0.245 × 0.035 × 0.030 mm; orthorhombic; space group Ccc2; a=12.0329(6); b=18.9371(10); c=5.8595(3); V=1335.19(12); Z=4; T=296(2) K; λ(Mo-Kα) = 0.71073 Å; μ(Mo-Kα) = 12.364 mm-1; 7481 reflections collected; 6647 reflections collected;1479 unique (Rint = 0.0263); giving R_1 = 0.0115, wR_2 = 0.0278 for 1471 data with [I>2σ(I)]; and R_1 = 0.0116, wR_2 = 0.0279 for all 1479 data.

430. *Cambridge Structural Database*. A covalent Sb-O bond length is generally between 1.9 Å and 2.1 Å, while 90.8% Sb-O bonds with a bond length less than 2.27 Å.

431. Fei, H.; Paw, L. U.; Rogow, D. L.; Bresler, M. R.; Abdollahian, Y. A.; Oliver, S. R. J., *Chem. Mater.* **2010,** *22*, 2027-2032.

432. Fei, H.; Rogow, D. L.; Oliver, S. R. J., *J. Am. Chem. Soc.* **2010,** *132*, 7202-7209.

433. Zhao, X.; Wu, T.; Zheng, S. T.; Wang, L.; Bu, X.; Feng, P., *Chem. Commun.* **2011,** *47*, 5536-5538.

434. Choi, H. J.; Dinca, M.; Long, J. R., *J. Am. Chem. Soc.* **2008,** *130*, 7848-7849.

435. Oregan, B.; Gratzel, M., *Nature* **1991,** *353*, 737-740.

436. Fujishima, A.; Honda, K., *Nature* **1972,** *238*, 37-40.

437. Law, M.; Greene, L. E.; Johnson, J. C.; Saykally, R.; Yang, P. D., *Nature Materials* **2005,** *4*, 455-459.

438. Brammer, K. S.; Oh, S. H.; Gallagher, J. O.; Jin, S. H., *Nano Letters* **2008,** *8*, 786-793.

439. Casavola, M.; Grillo, V.; Carlino, E.; Giannini, C.; Gozzo, F.; Pinel, E. F.; Garcia, M. A.; Manna, L.; Cingolani, R.; Cozzoli, P. D., *Nano Letters* **2007,** *7*, 1386-1395.

440. Pan, Y.-X.; Liu, C.-J.; Wiltoski, T. S.; Ge, Q., *Catal. Today* **2009,** *147*, 68-76.

441. Cai, Y. Q.; Shi, Y. L.; Zhang, P.; Mou, S. F.; Jiang, G. B., *Progress in Chemistry* **2006,** *18*, 1554-1564.

442. Wu, C. H.; Chern, J. M., *Ind. Eng. Chem. Res.* **2006,** *45*, 6450-6457.

443. Olah, G. A.; Goeppert, A.; Prakash, G. K. S., *J. Org. Chem.* **2009,** *74*, 487-498.

444. Dai, W. L.; Luo, S. L.; Yin, S. F.; Au, C. T., *Appl. Catal. A-General* **2009,** *366*, 2-12.

445. Grimes, C. A., *J. Mater. Chem.* **2007,** *17*, 1451-1457.

446. Feng, X. J.; Shankar, K.; Varghese, O. K.; Paulose, M.; Latempa, T. J.; Grimes, C. A., *Nano Letters* **2008,** *8*, 3781-3786.

447. Wu, G. S.; Wang, J. P.; Thomas, D. F.; Chen, A. C., *Langmuir* **2008,** *24*, 3503-3509.

448. Wolcott, A.; Smith, W. A.; Kuykendall, T. R.; Zhao, Y. P.; Zhang, J. Z., *Small* **2009,** *5*, 104-111.

449. Yang, X.; Wolcottt, A.; Wang, G.; Sobo, A.; Fitzmorris, R. C.; Qian, F.; Zhang, J. Z.; Li, Y., *Nano Letters* **2009,** *9*, 2331-2336.

450. Ahn, K. S.; Yan, Y.; Shet, S.; Deutsch, T.; Turner, J.; Al-Jassim, M., *Appl. Phys. Lett.* **2007,** *91*.

451. Tian, B. Z.; Liu, X. Y.; Tu, B.; Yu, C. Z.; Fan, J.; Wang, L. M.; Xie, S. H.; Stucky, G. D.; Zhao, D. Y., *Nature Materials* **2003,** *2*, 159-163.

452. Yue, W. B.; Xu, X. X.; Irvine, J. T. S.; Attidekou, P. S.; Liu, C.; He, H. Y.; Zhao, D. Y.; Zhou, W. Z., *Chem. Mater.* **2009,** *21*, 2540-2546.

453. Deshpande, A. S.; Shchukin, D. G.; Ustinovich, E.; Antonietti, M.; Caruso, R. A., *Adv. Funct. Mater.* **2005,** *15* (2), 239-245.

454. Fan, X.; Fei, H.; Demaree, D. H.; Brennan, D. P.; John, J. M. S.; Oliver, S. R. J., *Langmuir* **2009,** *25*, 5835-5839.

455. Liang, C. D.; Li, Z. J.; Dai, S., *Angew. Che* **2008,** *47*, 3696-3717.

456. Drisko, G. L.; Luca, V.; Sizgek, E.; Scales, N.; Caruso, R. A., *Langmuir* **2009,** *25*, 5286-5293.

457. Fan, X. J.; Demaree, D. P.; John, J. M. S.; Tripathi, A.; Oliver, S. R. J., *Appl. Phys. Lett.* **2008,** *92*.

458. Tran, D. T.; Fan, X. J.; Brennan, D. P.; Zavalij, P. Y.; Oliver, S. R. J., *Inorg. Chem.* **2005,** *44*, 6192-6196.

459. Hakim, S. H.; Shanks, B. H., *Chem. Mater.* **2009,** *21*, 2027-2038.

460. Zhang, H. Z.; Banfield, J. F., *J. Phys. Chem. B* **2000,** *104*, 3481-3487.

461. Testino, A.; Bellobono, I. R.; Buscaglia, V.; Canevali, C.; D'Arienzo, M.; Polizzi, S.; Scotti, R.; Morazzoni, F., *J. Am. Chem. Soc.* **2007,** *129*, 3564-3575.

462. Ryu, Y. H.; Kim, M. J.; Lee, J. D.; Yoon, C. S.; Kim, J. H.; Kim, J. H., *J. Nuclear Medicine* **2002,** *43*, 347-348.

463. Lin, C. J.; Lu, Y. T.; Hsieh, C. H.; Chien, S. H., *Appl. Phys. Lett.* **2009,** *94*.

464. Oliva, F. Y.; Avalle, L. B.; Santos, E.; Camara, O. R., *J. Photochem. Photobiol. A.* **2002,** *146*, 175-188.

465. Oregan, B.; Gratzel, M., *Nature* **1991,** *353*, 737-740.

466. Bach, U.; Lupo, D. C., P.; Moser, J. E.; Weissortel, F. J.; Salbeck, J.; Spreitzer, H.; Gratzel, M.;, *Nature* **1998,** *395*, 583-585.

467. Hagfeldt, A.; Gratzel, M., *Acc. Chem. Res.* **2000,** *33*, 269-277.

468. Gratzel, M., *Inorganic Chemistry* **2005,** *44*, 6841-6851.

469. Gratzel, M., *Nature* **2001,** *414*, 338-342.

470. Bai, Y.; Cao, Y. M.; Zhang, J.; Wang, M.; Li, R. Z.; Wang, P.; Zakeeruddin, S. M.; Gratzel, M., *Nature Materials* **2008,** *7*, 626-630.

471. Bai, Y.; He, G. Z., Y.; Duan, C.; Dang, D.; Meng, Q.;, *Chem. Commun.* **2006**, 1530-1533.

472. Wu, J.; Hao, S. Z., L.; Lin, J.; Huang, M.; Huang, Y.; Li, P.; Yin, S.; Sato, T.;, *J. Am. Chem. Soc.* **2008,** *130*, 11568-11569.

473. Chen, C. Y.; Chen, J. G. W., S. J.; Li, J. Y.; Wi, C. G.; Ho, K. C.;, *Angew. Chem. Int. Ed.* **2008,** *47*, 7342-7345.

474. Hardin, B. E.; Hoke, E. T. A., P. B.; Yum, J. H.; Comte, P.; Torres, T.; Frechet, J. M. J.; Nazeeruddin, M. K.; Gratzel, M.; McGehee, M. D.;, *Nat. Photonics* **2009,** *3*, 406-411.

475. Bessho, T.; Yoneda, E. Y., J. H.; Guglielmi, M.; Tavernelli, I.; Imai, H.; Rothlisberger, U.; Nazeeruddin, M. K.; Gratzel, M.;, *J. Am. Chem. Soc.* **2009,** *131*, 5930-5934.

476. Li, T. C. S., A. M.; She, C.; Farha, O. K.; Mirkin, C. A.; Marks, T. J.; Hupp, J. T., *J. Am. Chem. Soc.* **2010,** *132*, 4580-4582.

477. Cameron, P. J.; Peter, L. M. Z., S. M.; Gratzel, M.;, *Coord. Chem. Rev.* **2004,** *248*, 1447-1453.

478. Yanagida, S.; Yu, Y. M., K.;, *Acc. Chem. Res.* **2009,** *42*, 1827-1838.

479. Palomares, E.; Clifford, J. N.; Haque, S. A.; Lutz, T.; Durrant, J. R., *Journal of the American Chemical Society* **2003,** *125* (2), 475-482.

480. Chen, D. H., F.; Cheng, Y.; Caruso, R. A.;, *Adv. Mater.* **2009,** *21*, 2206-2210.

481. Chen, D. C., L.; Huang, F.; Imperia, P.; Cheng, Y.; Caruso, R. A.;, *J. Am. Chem. Soc.* **2010,** *132*, 4438-4444.

482. Fan, X. D., D. P.; St. John, J. M.; Tripathi, A.; Oliver, S. R. J.;, *App. Phys. Let.* **2008,** *92*, 193108.

483. Feng, X. S., K.; Varghese, O. K.; Paulose, M.; Latempa, T. J.; Grimes, C. A.;, *Nano Lett.* **2008,** *8*, 3781-3786.

484. Yu, H.; Quan, X. C., S.; Zhao, H.; Zhang, Y.;, *Journal of Photochemistry and Photobiology, A: Chemistry* **2008,** *200*, 301-306.

485. Boyd, D. A.; Greengard, L. B., M.; El-Naggar, M. Y.; Goodwin, D. G.;, *Nano Lett.* **2006,** *6*, 2592-2597.

486. Zhao, D.; Feng, J. H., Q.; Melosh, N.; Fredrickson, G. H.; Chmelka, B. F.; Stucky, G. D.;, *Science* **1998,** *279*, 548-552.

487. Liang, C. L., Z.; Dai, S.;, *Angew. Chem. Int. Ed.* **2008,** *47*, 3696-3717.

488. Fei, H.; Yang, Y.; Rogow, D. L.; Fan, X.; Oliver, S. R. J., *ACS Appl. Mater. Interfaces* **2010,** *2*, 974–979.

489. Wang, Y. Q.; Chen, S. G.; Tang, X. H.; Palchik, O.; Zaban, A.; Koltypin, Y.; Gedanken, A., *J. Mater. Chem.* **2001,** *11*, 521-526.

490. Tian, Z. P.; Tian, H. M.; Wang, X. Y.; Yuan, S. K.; Zhang, J. Y.; Zhang, X. B.; Yu, T.; Zou, Z. G., *Applied Physics Letters* **2009,** *94*.

491. Deshpande, A. S.; Shchukin, D. G. U., E.; Antonietti, M,; Caruso, R. A.;, *Adv. Funct. Mater.* **2005,** *25*, 239-245.

492. Zhou, J. Z., J.; Zhou, M.; Caruso, R. A.;, *Langmuir* **2006,** *22*, 3332-3336.

493. Fan, X.; Fei, H. D., D. H.; Brennan, D. P.; St, John, J. M.; Oliver, S. R. J.;, *Langmuir* **2009,** *25*, 5835-5839.

494. Brennan, D. P.; Dobley, A.; Sideris, P. J.; Oliver, S. R. J., *Langmuir* **2005,** *21*, 11994-11998.

495. Xue, M.; Zhu, G. Z., Y.; Fang, Q.; Hewitt, I. J.; Qiu, S.;, *Crystal Growth & Design* **2008,** *8*, 427-434.

496. Wang, M.-S.; Guo, G.-C.; Chen, W.; Xu, G.; Zhou, W. W.; Wu, K.; Huang, J.-S., *Angew. Chem. Int. Ed.* **2007,** *46*, 3909-3911.

497. Stathatos, E.; Lianos, P., *Advanced Materials* **2007,** *19*, 3338-3340.

498. Zhang, Q. F. C., T. P.; Russo, N.; Cao, G., *Angew. Chem. Int. Ed.* **2008,** *47*, 2402-2406.

499. Zhang, Q. F.; Chou, T. P. R., S. A.; Jenekhe, S. A.; Cao, G., *Adv. Funct. Mater.* **2008,** *18*, 1654-1660.

500. Zhang, Q.; Dandeneau, C. S.; Zhou, X.; Cao, G., *Adv. Mater.* **2009,** *21*, 4087-4108.

501. Wang, L. S. Z., J. F.; Yang, S. P., *Acta Cryst. Sect. E* **2004,** *E60*, m1484-m1486.

502. Nazeeruddin, M. K.; Kay, A.; Rodicio, I.; Humphrybaker, R.; Muller, E.; Liska, P.; Vlachopoulos, N.; Gratzel, M., *J. Am. Chem. Soc.* **1993,** *115*, 6382-6390.

503. Stergiopoulos, T.; Arabatzis, I. M.; Katsaros, G.; Falaras, P., *Nano Letters* **2002,** *2*, 1259-1261.

504. Peng, G.-W.; Chen, S.-K.; Liu, H.-S., *Appl. Spectroscopy* **1995,** *49*, 1995.

505. Yatlik, Y. G.; Sosnovskikh, V. Y.; Suvorov, A. L., *Russian J. Org. Chem.* **2004,** *40*, 763-765.

506. Haoudi, A.; Dhamelincourt, P.; Mazzah, A.; Drache, M.; Conflant, P.; Lazraq, M., *J. Mater. Chem.* **2000,** *10*, 1001-1005.

507. Gunji, T.; Nagao, Y.; Misono, T.; Abe, Y., *J. Non-crystalline Solids* **1989,** *107*, 149-154.

508. Ferber, J.; Luther, J., *Solar Energy Materials and Solar Cells* **1998,** *54* (1-4), 265-275.

509. Wolcott, A.; Kuykendall, T. R.; Chen, W.; Chen, S. W.; Zhang, J. Z., *J. Phys. Chem. B* **2006,** *110*, 25288-25296.

510. Gu, B. X.; Wang, L. M.; Ewing, R. C., *Journal of Nuclear Materials* **2000,** *278*, 64-72.

511. Yoon, M.; Seo, M.; Jeong, C.; Jang, J. H.; Jeon, K. S., *Chem. Mater.* **2005,** *17*, 6069-6079.

512. Nakade, S.; Saito, Y.; Kubo, W.; Kitamura, T.; Wada, Y.; Yanagida, S., *J. Phys. Chem. B* **2003,** *107*, 8607-8611.

513. Huang, S. Y.; Schlichthorl, G.; Nozik, A. J.; Gratzel, M.; Frank, A. J., *J. Phys. Chem. B* **1997,** *101*, 2576-2582.

514. Khairutdinov, R. F.; Hurst, J. K., *J. Phys. Chem. B* **1999,** *103*, 3682-3686.